frontiers | Research Topics

Insights of important mammalian viruses: Infection, pathogenesis and drugs

Edited by
Lingbao Kong, Lin Deng, Douglas Paul Gladue, Sha Li, Patricia V. Aguilar and Chao Shen

Published in
Frontiers in Microbiology

ISSN 1664-8714
ISBN 978-2-83251-836-6
DOI 10.3389/978-2-83251-836-6

About Frontiers

Frontiers is more than just an open access publisher of scholarly articles: it is a pioneering approach to the world of academia, radically improving the way scholarly research is managed. The grand vision of Frontiers is a world where all people have an equal opportunity to seek, share and generate knowledge. Frontiers provides immediate and permanent online open access to all its publications, but this alone is not enough to realize our grand goals.

Frontiers journal series

The Frontiers journal series is a multi-tier and interdisciplinary set of open-access, online journals, promising a paradigm shift from the current review, selection and dissemination processes in academic publishing. All Frontiers journals are driven by researchers for researchers; therefore, they constitute a service to the scholarly community. At the same time, the *Frontiers journal series* operates on a revolutionary invention, the tiered publishing system, initially addressing specific communities of scholars, and gradually climbing up to broader public understanding, thus serving the interests of the lay society, too.

Dedication to quality

Each Frontiers article is a landmark of the highest quality, thanks to genuinely collaborative interactions between authors and review editors, who include some of the world's best academicians. Research must be certified by peers before entering a stream of knowledge that may eventually reach the public - and shape society; therefore, Frontiers only applies the most rigorous and unbiased reviews. Frontiers revolutionizes research publishing by freely delivering the most outstanding research, evaluated with no bias from both the academic and social point of view. By applying the most advanced information technologies, Frontiers is catapulting scholarly publishing into a new generation.

What are Frontiers Research Topics?

Frontiers Research Topics are very popular trademarks of the *Frontiers journals series*: they are collections of at least ten articles, all centered on a particular subject. With their unique mix of varied contributions from Original Research to Review Articles, Frontiers Research Topics unify the most influential researchers, the latest key findings and historical advances in a hot research area.

Find out more on how to host your own Frontiers Research Topic or contribute to one as an author by contacting the Frontiers editorial office: frontiersin.org/about/contact

Insights of important mammalian viruses: Infection, pathogenesis and drugs

Topic editors

Lingbao Kong — Jiangxi Agricultural University, China
Lin Deng — Kobe University, Japan
Douglas Paul Gladue — Plum Island Animal Disease Center, Agricultural Research Service (USDA), United States
Sha Li — Jiangxi Agricultural University, China
Patricia V. Aguilar — University of Texas Medical Branch at Galveston, United States
Chao Shen — Wuhan University, China

Topic coordinator

Yihan Li — Jiangxi Agricultural University, China
Ting Wang — Jiangxi Agricultural University, China

Citation

Kong, L., Deng, L., Gladue, D. P., Li, S., Aguilar, P. V., Shen, C., eds. (2023). *Insights of important mammalian viruses: Infection, pathogenesis and drugs*.
Lausanne: Frontiers Media SA. doi: 10.3389/978-2-83251-836-6

Table of contents

frontiers | Frontiers in Microbiology

TYPE Editorial
PUBLISHED 21 February 2023
DOI 10.3389/fmicb.2023.1147109

OPEN ACCESS

EDITED AND REVIEWED BY
Anna Kramvis,
University of the Witwatersrand, South Africa

*CORRESPONDENCE
Lingbao Kong
✉ lingbaok@mail.jxau.edu.cn

SPECIALTY SECTION
This article was submitted to Virology, a section of the journal Frontiers in Microbiology

RECEIVED 18 January 2023
ACCEPTED 08 February 2023
PUBLISHED 21 February 2023

CITATION
Li Y, Gladue DP, Li S, Deng L, Shen C, Aguilar PV, Wang T and Kong L (2023) Editorial: Insights of important mammalian viruses: Infection, pathogenesis and drugs. *Front. Microbiol.* 14:1147109. doi: 10.3389/fmicb.2023.1147109

Editorial: Insights of important mammalian viruses: Infection, pathogenesis and drugs

Yihan Li[1], Douglas Paul Gladue[2], Sha Li[1], Lin Deng[3], Chao Shen[4], Patricia V. Aguilar[5], Ting Wang[1] and Lingbao Kong[1]*

[1]Institute of Pathogenic Microorganism and College of Bioscience and Engineering, Jiangxi Agricultural University, Nanchang, China, [2]Plum Island Animal Disease Center, Agricultural Research Service, United States Department of Agriculture Greenport, Greenport, NY, United States, [3]Division of Infectious Disease Control, Center for Infectious Diseases, Kobe University Graduate School of Medicine, Kobe, Japan, [4]College of Life Sciences, Wuhan University, Wuhan, China, [5]Department of Pathology, University of Texas Medical Branch, Galveston, TX, United States

KEYWORDS

mammalian viruses, pathogenesis, virus-host interaction, animal models, epidemiological surveillance

Editorial on the Research Topic
Insights of important mammalian viruses: Infection, pathogenesis and drugs

COVID-19, has brought new attention to the importance of new or emerging pathogenic viruses as a major threat to global health. Viruses have evolved multiple mechanisms to counteract host immunity that can be similar or drastically different for various viruses, making it difficult to control viruses using a single countermeasure. To further increase the complexity of controlling viruses, during replication viruses can vary genetically providing the viruses with the ability to overcome a countermeasure. As has been demonstrated by SARS-CoV-2, the viruses can evolve changing from the original target strains. Understanding the molecular mechanisms involved in how different viruses evade the immune system, or how different mutations could cause species shift is of great importance, especially for mammalian viruses. Evasion of immune system and/or genetic evolution can influence the virulence of the viral species, with the potential to cause pandemics. This collection of articles and reviews updates information on the research into the pathogenesis, diagnostic methods and vaccine development for a number of important mammalian viruses, which could be exploited to control the spread of existing viral diseases and prevent future potential virus epidemics.

Viruses are obligate intracellular pathogens and rely on host biological machinery for their own survival. Though different viruses have distinct infection characteristics and pathogenesis characteristics, a deeper understanding of how the virus interacts with the host and in particular virus-host protein-protein interactions can facilitate the control of viral infections. Ruan et al. observed that Enterovirus 71 (EV71) infection caused a significant increase of cellular exosome secretion. They further demonstrated the interaction between EV71 3A and vacuolar protein sorting 25 (VPS25) facilitates exosome biogenesis through the endosomal sorting complex required for transport (ESCRT) pathway, which favors virus replication. Xie et al. studied the underlying mechanism of pseudorabies virus (PRV) infection. They highlighted that porcine DDX56 promotes IFN-β expression through cGAS-STING signaling pathway to inhibit PRV proliferation. Viral infection in pregnancy and

vertical transmission that can result in fetal abortions and malformations is an important focus of animal viral research. Trinh et al. found low glucose-induced endoplasmic reticulum (ER) stress may play a key role in increasing rubella virus (RuV) infection and the risk of congenital rubella syndrome (CRS) in early pregnancy.

Animal models have made outstanding contributions to the elucidation of the pathogenesis and transmission mechanisms of human viral diseases. To mimic the symptoms in humans, different animal models have been applied in COVID-19 research, of which the major strengths and weaknesses were comparatively evaluated by Zhao et al. They noted that animal models have shown a great utility in viral studies, yet a credible and reasonable animal model that encompasses all aspects of human COVID-19 has not been found. Depression is a common mental disorder that is gaining increasing interest, but its pathogenesis is poorly understood. Analyzing the core symptoms of depression manifested by specific animal models is an important approach to reveal the underlying mechanisms of depression. Based on viral metagenomics and metabolomics analyses, Duan et al. established a chronic restraint stress (CRS)-induced mouse model of depression to study the relationship between gut virome and depression. Gut virome dyregulation was observed in the CRS mouse model and further investigation revealed that the differential gut virome was strongly associated with neurotransmitter metabolites. Meanwhile this study also pointed out the existing deficiencies of current research, such as lack of clinical data, small sample size and no examination of gut bacteria.

Investigating the occurrence and prevalence of infectious diseases is necessary to control the spread of epidemics and prevent the outbreak of newly emerging viruses. Therefore, the development of rapid, accurate and cost-effective methods to identify viruses is important for epidemiological investigations. In this collection, optimized epidemiologic methods were proposed. Wu et al. accurately classified human adenoviruses (HadVs) by polymerase chain reaction with specially designed primers that target the variable regions of the three major capsid genes span the genome. Hu et al. conducted a detailed seroepidemiological survey of porcine circovirus 4 (PCV4) in Jiangxi Province of China based on an indirect immunosorbent assay (ELISA) with purified His-Cap or His-Rep proteins as the coating antigens.

However, there are certain limitations for standard epidemiological surveillance in predicting the behavior of infectious diseases, as modern transportation has been recognized as the predominant driver of global spread of viruses. To clarify the origin and dispersal routes of bovine leukemia virus (BLV), Nishikaku et al. used phylogenetic and Bayesian phylogeographic analyses. In their study, it was demonstrated that the original BLV came from Asia and zebu cattle were the source of introducing BLV into the taurine cattle. Interestingly, several Asian indigenous bat species shares endogenous delta-retrovirus sequences closely related to BLV lineage II, which further supports the origin of BLV virus in Asia. Ruiz-Saenz et al. raised a warning that African swine fever (ASF) is posing a potential threat to the swine industry in the Americas. With the difficulty of diagnosing ASF and the absence of effective vaccines, there is an urgent need to improve precautionary methods and establish international cooperation for the prevention of ASF spread globally.

In a conclusion, the collection of articles highlights some important advances in virology, that will aid in the understanding of mammalian viruses and potentially be useful in prevention of the next virus pandemic.

Author contributions

YL: writing—original draft. DG, SL, LD, CS, PA, and TW: writing—review and editing. LK: supervision. All authors contributed to the article and approved the submitted version.

Conflict of interest

The authors declare that the research was conducted in the absence of any commercial or financial relationships that could be construed as a potential conflict of interest.

Publisher's note

frontiers | Frontiers in Microbiology

ORIGINAL RESEARCH
published: 12 May 2022
doi: 10.3389/fmicb.2022.911694

Molecular Typing and Rapid Identification of Human Adenoviruses Associated With Respiratory Diseases Using Universal PCR and Sequencing Primers for the Three Major Capsid Genes: Penton Base, Hexon, and Fiber

Xiaowei Wu[1†], Jing Zhang[1†], Wendong Lan[1†], Lulu Quan[1], Junxian Ou[1], Wei Zhao[1], Jianguo Wu[2,3], Patrick C. Y. Woo[4], Donald Seto[5] and Qiwei Zhang[1,2,3]**

[1]BSL-3 Laboratory, Guangdong Provincial Key Laboratory of Tropical Disease Research, School of Public Health, Southern Medical University, Guangzhou, China, [2]Guangdong Provincial Key Laboratory of Virology, Institute of Medical Microbiology, Jinan University, Guangzhou, China, [3]Foshan Institute of Medical Microbiology, Foshan, China, [4]Department of Microbiology, The University of Hong Kong, Hong Kong, Hong Kong SAR, China, [5]Bioinformatics and Computational Biology Program, School of Systems Biology, George Mason University, Manassas, VA, United States

Human adenoviruses (HAdVs) within species B, C, and E are responsible for highly contagious and potentially severe respiratory disease infections. The traditional method to type these pathogens was based on virus neutralization and hemagglutination assays, which are both time-consuming and difficult, particularly due to the nonavailability of reagents. Subsequent molecular typing based on the partial characterization of the hexon gene and/or the restriction enzyme analysis (REA) of the genomes is inadequate, particularly in identifying recombinants. Here, a rapid, simple, and cost-effective method for molecular typing HAdV respiratory pathogens is presented. This incorporates three pairs of universal PCR primers that target the variable regions of the three major capsid genes, i.e., hexon, penton base, and fiber genes, that span the genome. The protocol enables typing and characterization of genotypes within species B, C, and E, as well as of some genotypes within species D and F. To validate this method, we surveyed 100 children with HAdV-associated acute respiratory infections identified by direct immunofluorescence (Hong Kong; July through October, 2014). Throat swab specimens were collected and analyzed by PCR amplification and sequencing; these sequences were characterized by BLAST. HAdVs were detected in 98 out of 100 (98%) samples, distributing as follows: 74 HAdV-B3 (74%); 10 HAdV-E4 (10%); 7 HAdV-C2 (7%); 2 HAdV-C6 (2%); 1 HAdV-B7 (1%); 1 HAdV-C1 (1%); 2 co-infection (2%); and 1 novel recombinant (1%). This study is the first detailed molecular epidemiological survey of HAdVs in Hong Kong. The developed

OPEN ACCESS

Edited by:
Lingbao Kong,
Jiangxi Agricultural University, China

Reviewed by:
Xingui Tian,
First Affiliated Hospital of Guangzhou Medical University, China
Quanyi Wang,
Beijing Center for Disease Prevention and Control, China

***Correspondence:**
Qiwei Zhang
zhangqw@jnu.edu.cn
Donald Seto
dseto@gmu.edu

[†]These authors have contributed equally to this work

Specialty section:
This article was submitted to Virology, a section of the journal Frontiers in Microbiology

Received: *03 April 2022*
Accepted: *20 April 2022*
Published: *12 May 2022*

Citation:
Wu X, Zhang J, Lan W, Quan L, Ou J, Zhao W, Wu J, Woo PCY, Seto D and Zhang Q (2022) Molecular Typing and Rapid Identification of Human Adenoviruses Associated With Respiratory Diseases Using Universal PCR and Sequencing Primers for the Three Major Capsid Genes: Penton Base, Hexon, and Fiber. Front. Microbiol. 13:911694. doi: 10.3389/fmicb.2022.911694

method allows for the rapid identification of HAdV respiratory pathogens, including recombinants, and bypasses the need for whole genome sequencing for real-time surveillance of circulating adenovirus strains in outbreaks and populations by clinical virologists, public health officials, and epidemiologists.

Keywords: adenovirus, universal primers, epidemiology, molecular typing, recombination, co-infection, Hong Kong

INTRODUCTION

Human adenoviruses (HAdVs) belong to the *Adenoviridae* family, which are nonenveloped double-stranded DNA viruses (Lion, 2014). As human pathogens, HAdVs are responsible for a wide spectrum of diseases in the respiratory, ocular, gastrointestinal, and renal tracts, commonly (Lion, 2014). A measure of its importance as a respiratory pathogen, for example, and its pathogenicity attributes includes being attributed to approximately 5%–7% of the respiratory illnesses diagnosed in young children in four cities of Argentina during 1993–1994 (Carballal et al., 2001). These respiratory pathogens are highly contagious and can spread rapidly in crowded places such as hospitals, schools, the military, and newborn nurseries (Lynch and Kajon, 2016). Although respiratory tract infections (RTIs) caused by HAdVs are generally self-limiting and may even be mild, a number of severe and fatal infections have been reported in both children and adults (Carballal et al., 2001; Rebelo-de-Andrade et al., 2010; Carr et al., 2011; Cui et al., 2015; Yu et al., 2016; Zhang S. et al., 2016).

To date, 113 HAdV genotypes have been identified, characterized, and reported using whole genome analysis, including the original 51 serotypes[1]; these are parsed into species A–G, partially based on biological and pathogenicity attributes (Lion, 2014). Among these seven species, species B types (HAdV-B3, -B7, -B14, -B16, -B21, and -B55) and one species E type (HAdV-E4) are commonly associated with acute respiratory disease (ARD), which accounts for a high proportion of respiratory diseases in both children and adults (Madisch et al., 2006; Zhang et al., 2006, 2012b; Kajon et al., 2007; Rebelo-de-Andrade et al., 2010; Girouard et al., 2011; Zhao et al., 2014; Chen et al., 2016; Zeng et al., 2016; Cheng et al., 2018; Jing et al., 2019). The types in species C (HAdV-C1, -C2, -C5, -C6, and -C57) are generally associated with mild respiratory diseases and latent infections, but are important in immunocompromised patients (Lion, 2014). HAdVs comprising species D cause ocular and gastrointestinal diseases. Species A, F, and G types are associated with gastroenteritis (Lu et al., 2014). The predominant types are different among different countries or regions and change over time (Erdman et al., 2002; Chang et al., 2008; Lee et al., 2010). HAdV types C1 to B7 account for more than 80% of the HAdV infections in infants and children (Piedra et al., 1998). Globally, HAdV-B3 is among the most common types implicated in HAdV respiratory infections in children and adults (Schmitz et al., 1983; Gray et al., 2007; Chang et al., 2008; Yan et al., 2021). In South America, HAdV-B7 has been a predominant strain associated with RTIs requiring hospitalization in many countries (Li et al., 1996; Carballal et al., 2001). In Asia, HAdV-B3 and -B7 have been the predominant types associated with RTIs in children (Li et al., 1996; Lin et al., 2004; Chang et al., 2008; Tsou et al., 2012; Han et al., 2013; Zhao et al., 2014; Chen et al., 2016; Wang et al., 2016; Yu et al., 2016; Yan et al., 2021), while HAdV-B7 are associated with higher severity of illness and fatality rate (Zhao et al., 2014; Chen et al., 2016; Yu et al., 2016). In Europe, HAdV-B3 and HAdV-B7 are highly virulent and potentially deadly types, especially for children (Lion, 2014). Historically, types HAdV-B7 and -E4 predominate as a cause of ARD among military personnel in the United States (Sanchez et al., 2001; Erdman et al., 2002; Kolavic-Gray et al., 2002; Kajon et al., 2007).

In immunocompromised patients, particularly in the organ transplant setting, the most commonly reported adenovirus types include HAdV-C1, -C2, -C5, -A12, -A31, -B3, -B11, -B16, -B34, and -B35 (Barrero et al., 2012). These types may be associated with higher and more severe morbidity and mortality outcomes (Lion, 2014).

As a result, it is important to type HAdVs accurately and rapidly for clinical diagnoses and epidemiological investigations in order to provide information on the pathogen, including the distribution of infections by individual and specific types, as well as to detect and characterize emergent strains in the context of outbreaks (Xie et al., 2013; Li et al., 2014; Dongliu et al., 2016; Tan et al., 2016; Yi et al., 2017). As recombination is recognized as a significant evolutionary pathway for the emergence of novel HAdV pathogens, rapid characterization is important (Walsh et al., 2009, 2010; Zhou et al., 2012; Dehghan et al., 2013a, 2019; Robinson et al., 2013a,b).

HAdVs were traditionally typed according to serum neutralization and hemagglutination-inhibition tests, which are time-consuming and reagent-limited (Wigand, 1987; Seto et al., 2013).

Molecular typing based on either partial sequence characterization of HAdV hexon gene or restriction enzyme analysis (REA) of the genomics DNA are improvements but still not effective, for example, in their difficulty to identify recombinants (Seto et al., 2013). HAdV isolates with identical serum-neutralizing attribution but with unexpected biological or pathogenic characteristics have been reported (Walsh et al., 2010; Kaneko et al., 2011; Matsushima et al., 2011; Zhou et al., 2012), challenging the traditional view of "hexon-centric" identification. With the recent development in whole genome sequencing and bioinformatics analysis, a wider range of HAdV genomes from clinical isolates have been sequenced and analyzed (Seto et al., 2010). An important finding is that recombination, scored by characterizing the three major

[1]http://hadvwg.gmu.edu/

capsid genes, i.e., penton base, hexon, and fiber genes, contributes substantially to the genesis of novel and emergent pathogenic HAdVs. Among the 61 recent novel pathogenic genotypes identified and recognized since HAdV-52, nearly all are recombinants (Ishiko et al., 2008; Ishiko and Aoki, 2009; Walsh et al., 2009, 2010, 2011; Liu et al., 2011, 2012; Matsushima et al., 2011; Robinson et al., 2011; Zhang et al., 2012a; Hage et al., 2015; Cheng et al., 2018). A striking example is HAdV-B55. This is a "Trojan horse," as it is a highly contagious human respiratory pathogen that is a recombinant of HAdV-B11 and HAdV-B14 parentals (Yang et al., 2009; Zhang et al., 2012a; Dongliu et al., 2016; Cheng et al., 2018). It has a HAdV-14 genome chassis, including the HAdV-14 penton base gene and fiber gene, which encodes cell tropism (Pan et al., 2018), but a partial HAdV-11 hexon gene, which encodes the antigenic epitopes of the virus denoting it as a renal pathogen. This virus possesses the biological and pathogenic attributes of HAdV-14 and also avoids the neutralizing antibody against HAdV-14 in a population. It was noted to be previously mistyped as HAdV-11a by partial hexon sequencing and REA due to incomplete gene analysis and incorrect application of the REA method (Walsh et al., 2010; Seto et al., 2013; Zhang Q. et al., 2016).

Whole genome sequencing is very useful for epidemiological surveys and understanding archived intriguing pathogens (Ismail et al., 2018; Dehghan et al., 2019; Coleman et al., 2020) but may still be unfeasible for the routine large-scale molecular epidemiological monitoring of nonpandemic outbreaks, as well as for the rapid identification of viral pathogens during outbreaks (Zhu et al., 2009; Xie et al., 2013). Therefore, to circumvent the limitations of using only the hexon for sampling adenoviral pathogens and also to ascertain the high sequence diversity between different HAdV species, we developed a simple, rapid, cost-effective, practical, and universal typing method for the routine epidemiological surveillance of human respiratory adenoviruses.

At the same time, we characterized the molecular epidemiology of HAdVs circulating among inpatient and outpatient children during the ARD outbreaks in the late summer and early autumn of 2014 in Hong Kong, using our newly-developed HAdV molecular typing protocol. This is the first detailed molecular epidemiological survey of HAdVs circulating in Hong Kong.

MATERIALS AND METHODS

Viruses and Other Materials

Human adenovirus genotypes HAdV-B3, -B7, -B11, -B14, -B21, -B55, -C5, -D19, -E4, and -F41 have been isolated, identified, studied, and archived in our laboratory (Zhang et al., 2006, 2012a,b, 2017; Zhao et al., 2014; Yu et al., 2016). Molecular analysis have entailed the use of Taq PCR Master Mix kits (Takara Corp.; Japan), QIAamp DNA Mini kits (QIAgen Corp.; China), and PCR cleanup kits (Axygen Inc.; United States), applied according to the manufacturers' instructions. For characterization and reference, DL10000 and DL2000 DNA Markers were used, and are the products of Takara (Takara Corp.; Japan).

Clinical Specimens

This is a retrospective survey of an ARD outbreak in pediatric outpatients and inpatients with influenza-like symptoms in Queen Mary Hospital, Hong Kong from July 2014 through October 2014. For further details on the samples, please see Zhang et al. (2019). Briefly, nasopharyngeal swab specimens were collected and adenoviruses were detected using a Direct Immunofluorescence IMAGEN™ Adenovirus Detection Kit (Thermo Fisher; United States). Specific genotypes were identified and presented in this report.

The study protocol was approved by the Institutional Ethics Committee of Queen Mary Hospital in accordance with its guidelines for the protection of individual privacy, and adhering to the principles of the Declaration of Helsinki. Patient consent for using left-over specimens was waived.

Adenovirus Culturing and Isolation

The HAdV-positive nasopharyngeal swab specimens collected from 100 patients were inoculated onto A549 cells. These were cultured in a maintenance medium (Minimal Essential Medium containing 2% fetal bovine serum, 100 U/ml penicillin G, and 100 μg/ml streptomycin) at 37°C in an atmosphere containing 5% (v/v) carbon dioxide. Cytopathic effect (CPE) was monitored for 5–7 days, following which, if no CPE was observed, the cells would be frozen and thawed three times and then passaged in A549 cells again to check for CPE.

PCR Primers Design and PCR Amplification

The penton base, hexon, and fiber gene sequences from HAdV-A18, -B3, -B7, -B11, -B14, -B16, -B21, -B34, -B35, -B50, -B55, -B66, -B68, -C1, -C2, -C5, -C6, -D19, -D37, -E4, -F41, and -G52 were extracted from genome data archived in GenBank. These were aligned using ClustalW to find regions with high sequence similarities. Primers targeting the three major capsid genes were designed based on these bracketing conserved regions, and these were subsequently obtained from Invitrogen (Guangzhou, China).

PCR conditions were determined, and reactions were conducted in a total volume of 20 μl comprising 1× Taq Master Mix (10 μl), primer F (10 μmol/L, 0.5 μl), primer R (10 μmol/L, 0.5 μl), DNA template (1 μl), and water (8 μl). Primers Penton-F and Penton-R were designed for both the PCR amplification and the subsequent DNA sequencing of the amplified penton base gene product. PCR conditions are as follows: 94°C for 1 min; 34 cycles of 94°C for 30 s, 52°C for 30 s, and 72°C for 100 s; and a final extension of 72°C for 10 min. Similarly, Primers HVR-F and HVR-R were used for both the PCR amplification and subsequent DNA sequencing of the hexon gene product. Hexon PCR conditions are as follows: 94°C for 1 min; 34 cycles of 94°C for 30 s, 52°C for 30 s, and 72°C for 100 s; followed by a final extension of 72°C for 10 min. Finally,

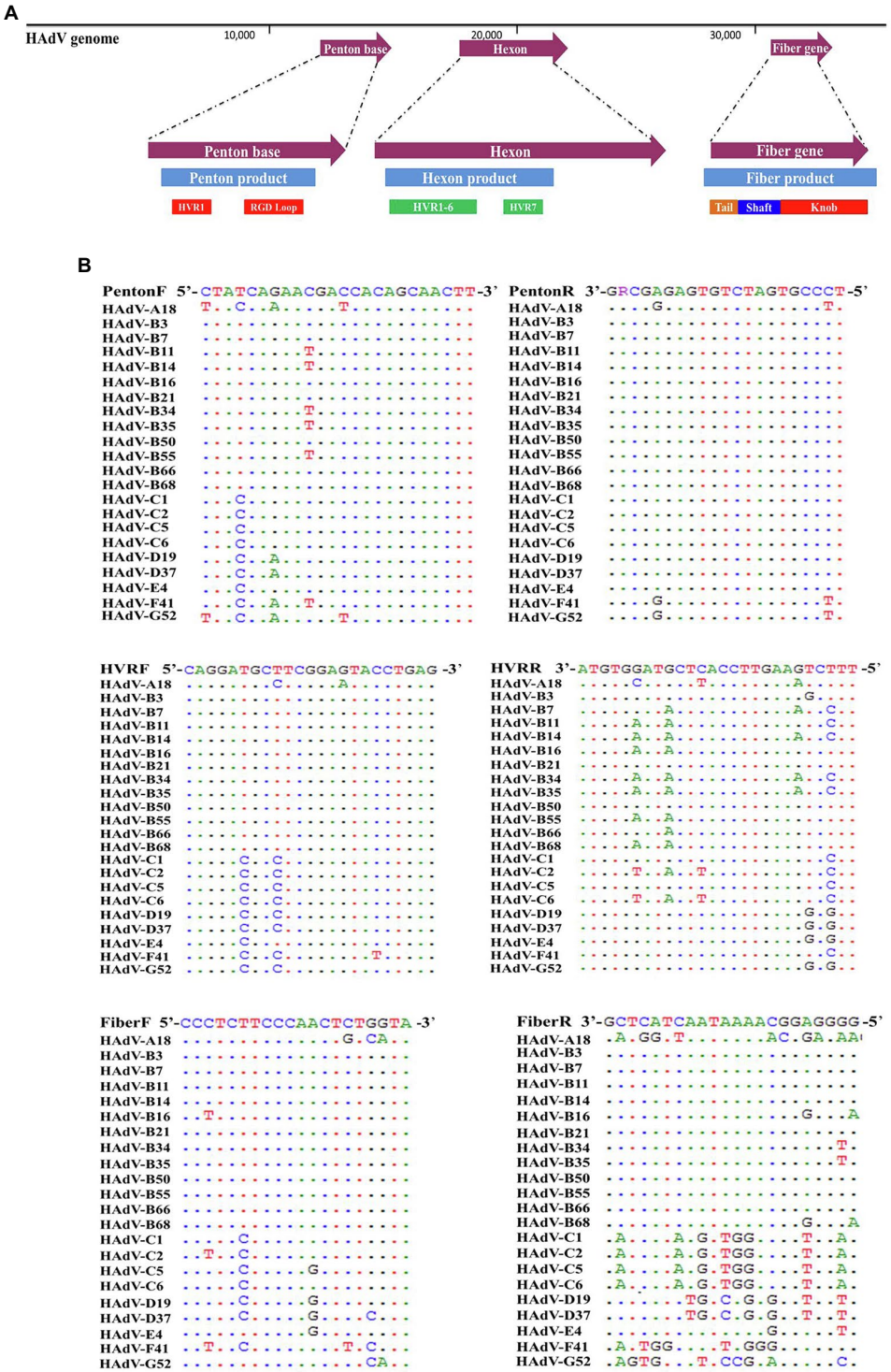

FIGURE 1 | (A) Schematic human adenoviruses (HAdV) genome, with the primer positions and the resultant PCR products noted for the three major capsid protein genes: penton base (left), hexon (middle), and fiber (right) genes. The relative locations of the capsid protein genes in the HAdV genome are also noted. These genes contain the genotyping and molecular characterization information for HAdVs. The purple arrows indicate the genes and their locations; the blue bars indicate the PCR products and their relative lengths; and other colored bars indicate important domains within each gene, including hypervariable regions (HVRs and RGD Loop), as well as the tail, shaft, and knob domains. **(B)** Alignment of HAdV universal primers for HAdV-A18, B3, -B7, B-11, -B14, -B16, -B21, -B34, -B35, -B50, -B55, -B66, -B68, -C1, -C2 -C5, -C6, -D9, -D19, -D37, -E4, -F41, and -G52. Divergence from the primer sequences is shown for the isolates tested. Each virus is identified with its genotype number as well as its species demarcation for reference. Dots represent identical bases, and base differences are noted. The bases are color-coded for visual comparisons.

Primers Fiber-F and Fiber-R were designed for both the PCR amplification and subsequent DNA sequencing of the fiber gene product. The PCR amplification conditions for this are as follows: 94°C for 1 min; 34 cycles of 94°C for 30 s, 52°C for 30 s, and 72°C for 72 s; followed by a final extension of 72°C for 10 min.

Sequencing and Molecular Typing of Clinical Adenovirus Specimens

All three major capsid genes of the HAdV isolates were PCR-amplified using the corresponding pairs of universal primers noted above, respectively. These PCR products were purified and then DNA-sequenced directly with both PCR primers. The assembled DNA sequences were characterized by a BLAST survey of the NCBI GenBank database. Genotype identity of each clinical specimen was determined based on the penton base, hexon, and fiber sequences to which they showed the highest sequence identities.

Genome Reference Sequences Used for Alignments and Primer Design

As noted, archived genome sequences from GenBank were used for the alignments and extraction of the penton base, hexon, and fiber gene sequences. Their accession numbers are as follows: HAdV-A12 (X73487), HAdV-B3 (DQ099432), HAdV-B3 (AY599834), HAdV-B7 (AY594255), HAdV-B7 (KC440171), HAdV-B11 (AY163756), HAdV-B14 (AY803294), HAdV-B16 (AY601636), HAdV-B21 (AY601633), HAdV-B34 (AY737797), HAdV-B35 (AY128640), HAdV-B50 (AY737798), HAdV-B55 (JX491639), HAdV-C1 (AC_000017), HAdV-C2 (J01917), HAdV-C5 (AC_000008), HAdV-C6 (KF268129), HAdV-D9 (AJ854486), HAdV-E4 (AY594253), HAdV-F40 (KU162869), and HAdV-G52 (DQ923122).

Phylogenetic Analysis

Molecular Evolutionary Genetics Analysis (MEGA) software, version 7.0,[2] a was used for the phylogenetic analyses of the penton base, hexon, and fiber genes as determined from the clinical specimens, along with additional sequences, for references, that were retrieved from GenBank. Phylogenetic trees were constructed using the maximum parsimony method with a bootstrap test of 1,000 replicates and the Tree-Bisection-Reconnection (TBR) model.

[2]https://www.megasoftware.net/

RESULTS

Three Pairs of Universal Primers Amplify the Three Major Capsid Genes: Penton Base, Hexon, and Fiber Genes

Three pairs of universal primers were designed for PCR amplification and DNA sequencing of the HAdV penton base, hexon, and fiber genes. Primers Penton-F and Penton-R were designed based on the conserved regions of the penton base sequences. Within the alignment of sequences, primer sequences selected for Penton-F and Penton-R are highly conserved in the majority of penton base genes, which ensures that all of the analyzed adenovirus types within species A to G could be PCR-identified (**Figure 1B**). The resultant PCR product is 1,253 bp (**Table 1**), located within penton base gene and encompasses the variable regions HVR1 and RGD loop (**Figure 1A**).

For the hexon, the universal amplification primers HVR-F and HVR-R were designed similarly. The primer sequences are conserved in HAdV genotypes across all of the species analyzed, yielding a PCR product of about 1,685 bp (**Table 1**). This amplicon contains the seven hypervariable regions (HVRs) comprising Loops 1 and 2 (**Figure 1A**), which are the epitope determinants used for serotyping.

Primers Fiber-F and Fiber-R were designed for fiber gene. Point mutations of primer Fiber-F exist only in one or two nucleotides located in the middle of the primers; this ensures an effective PCR amplification of the different HAdV genotypes (**Figure 1A**). These primers amplify HAdV genotypes from species B, D, and E, yielding a PCR product of about 1,153 bp for HAdV-B and -D, and 1,519 bp for HAdV-E4. However, due to higher sequence variation and the longer fiber gene

TABLE 1 | Universal primers for the detection, typing, and sequencing of HAdV.

Gene	Position	Length[a] (bp)	Primer	Primer sequence	Position[a]	PCR product	PCR condition
Penton base	13,904–15,538	1,635	Penton-F	5'-CTATCAGAACGACCACAGCAACTT-3'	14,152–14,175	1,253 bp	34 cycles of 94°C for 30 s; 52°C for 30 s; and 72°C for 100 s
			Penton-R	5'-TCCCGTGATCTGTGAGAGCRG-3'	15,384–15,404		
Hexon	18,422–21,256	2,835	HVR-F	5'-CAGGATGCTTCGGAGTACCTGAG-3'	18,473–18,495	1,685 bp	
			HVR-R	5'-TTTCTGAAGTTCCACTCGTAGGTGTA-3'	20,132–20,157		
Fiber	31,301–32,260	960 (1278[b])	Fiber-F	5'-CCCTCTTCCCAACTCTGGTA-3'	31,180–31,199	1,153 bp	
			Fiber-R	5'-GGGGAGGCAAAATAACTACTCG-3'	32,311–32,332	(1,519 bp[b])	
		1746[c]	Fiber-CR	5'-GAGGTGGCAGGTTGAATACTAG-3'	32,311–32,332	2027 bp[c]	

Sequences, genome locations, and the resultant predicted PCR product sizes are noted for each of the three major capsid protein genes. Fiber-CR is the species C-specific optimal primer due to their divergence from other HAdVs.

[a]*Positions are in the reference genome of HAdV-B3 (GenBank acc. no. DQ099432).*

[b]*The length of HAdV-4 fiber gene, for reference.*

[c]*The length of the PCR product of HAdV-C fiber gene, for reference.*

(about 1746 bp) of the species C HAdVs, Fiber-R matches poorly with these genotypes in HAdV-C. To compensate, another primer Fiber-CR was designed to match completely the sequences within species C (**Table 1**). This provides a product that is 2027 bp.

Universal Primers-Based PCR Amplification and Sequencing Provides Identification of Reference HAdV-B3, -B7, -B11, -B14, -B21, -B55, -C5, -D19, -E4, and -F41

Genomic DNA from reference samples of HAdV-B3, -B7, -B11, -B14, -B21, -B55, -C5, -D19, -E4, and -F41 was extracted and amplified by PCR amplification and identified by subsequent sequencing using these three pairs of universal primers (**Figure 2**). The PCR products were specific, yielding single distinct products, the expected predicted sizes: 1.2 kb (penton base), 1.6 kb (hexon), and 1.1 kb (fiber), respectively. However, there are two exceptions: one is the HAdV-E4 fiber gene (1,519 bp) and the other is the HAdV-C5 fiber gene (2027 bp). Both gene products are longer than their counterparts in the other HAdV genotypes. The species C fiber requires an alternative primer, Fiber-CR.

The Epidemiological Survey of HAdVs in Hong Kong From 100 Pediatric ARD Patients in 2014

A total of 100 HAdV-positive samples were analyzed using this protocol (**Table 2**). These indicated that the male and female rates were 50% and 49%, respectively (one was of unrecorded gender). Therefore, no significant gender difference was found. The median age with HAdV infection was 4 years, ranging from 0.5 to 14 years old, of which 60% were under 5 years. Of the 100 cases, 93 (93%) were hospitalized, with the median hospitalization duration of 3 days (1–36 days). Fourteen HAdV-positive cases were also co-infected with EV/RV; two co-infected with RSV, and one co-infected with influenza C.

The clinical diagnoses included one case of fatal pneumonia caused by HAdV-3; three cases of bronchitis; three cases of diarrhea; two cases of febrile seizure; two cases of rash; and 74 cases of upper respiratory tract infection (URTI; **Table 2**).

Molecular Typing of HAdV Clinical Samples

Hundred throat swabs specimens were successfully amplified by this PCR protocol using the three pairs of universal primers. These PCR products were sequenced using the same primers. BLAST analysis confirmed that 74 cases were HAdV-B3 (74%); 10 cases were HAdV-E4 (10%); seven cases were HAdV-C2 (7%); two cases were HAdV-C6 (2%); one case was HAdV-B7 (1%); one case was HAdV-C1 (1%); two cases were co-infected by different types of HAdVs (HAdV-B7 and HAdV-B55; HAdV-C1 and HAdV-B3) (2%); one case was putative recombinant (P1H2F2) (1%); the remaining two cases were PCR negative (**Figure 3A**). The two cases co-infected by different HAdV types were identified by double peaks emergent in the sequencing maps, i.e., either set of stripped peaks were identical with HAdV-B7 and HAdV-B55, respectively, or identical with HAdV-C1 and HAdV-B3. One case identified as putative recombinant showed clear and single-peaked for each base.

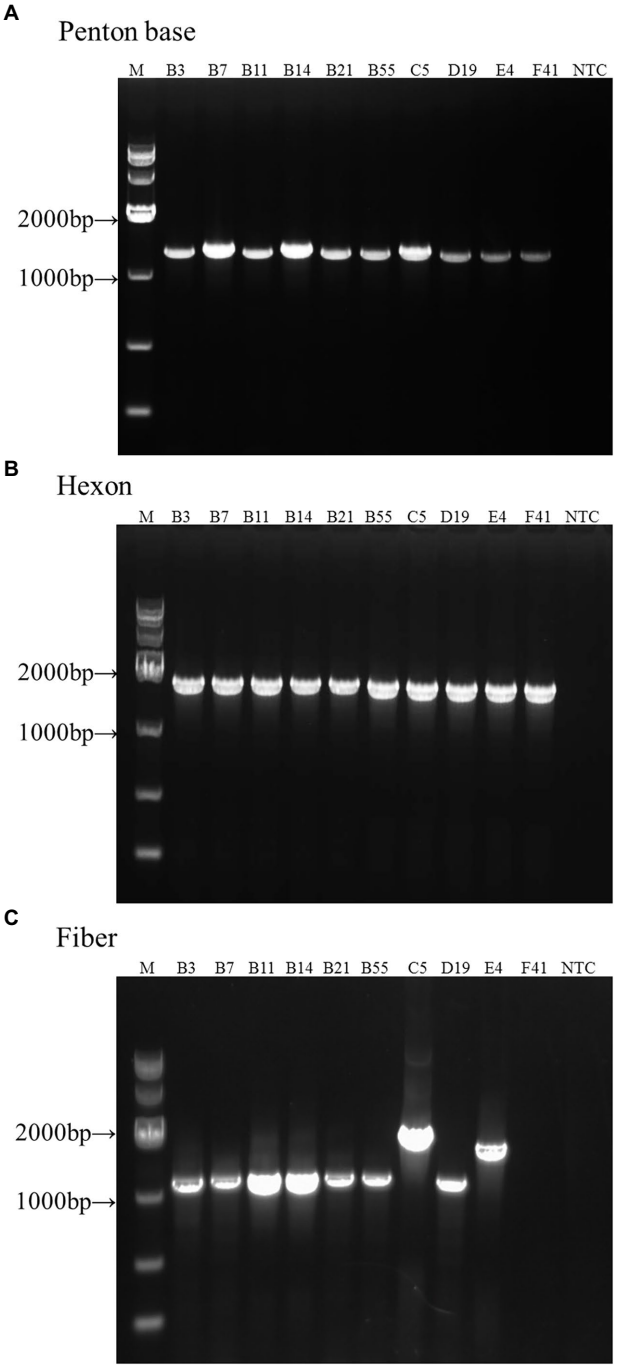

FIGURE 2 | One percent Agarose gel electrophoresis profiles of PCR products from HAdV-B3, -B7, -B11, -B14, -B21, -B55, -C5, -D19, -E4, and -F41 using universal primers for penton base, hexon, and fiber genes. **(A)** Penton base gene PCR amplification using primers Penton-F and Penton-R. **(B)** Hexon gene PCR amplification using primers HVR-F and HVR-R. **(C)** Fiber gene PCR amplification using primers Fiber-F and Fiber-R (Fiber-CR for HAdV-C5). Molecular weight sizing markers are in lane M. NTC, "no template" PCR control.

TABLE 2 | Comparison of demographic and clinical characteristics of 100 children with ARD according to HAdV type in Hong Kong, summer 2014.

HAdV species		All	HAdV-B3	HAdV-C1	HAdV-C2	HAdV-E4	HAdV-C6	HAdV-B7	Recombination or co-infection	Undetectable
Numbers		100	74	1	7	10	2	1	3	2
Gender (M/F)		50/49	38/35	0/1	5/2	3/7	1/1	1/0	2/1	0/2
Age (range)		4 (0.5–14)	2.5 (1–14)	4 (4)	3 (0.5–7)	5 (1–11)	3.5 (3–4)	7 (7)	2 (1–9)	3.5 (3–4)
Nationality	Chinese	86	63	1	5	9	2	1	3	2
	Occidental	2	2	-	-	-	-	-	-	-
	Korean	1	1	-	-	-	-	-	-	-
	Indian	1	1	-	-	-	-	-	-	-
	Nepalese	3	1	-	2	-	-	-	-	-
Hospitalized numbers		93	68	1	7	9	2	1	3	2
Hospitalized day (range)		3 (1–36)	3 (1–36)	3 (3)	3 (2–4)	2 (1–15)	2.5 (2–3)	4 (4)	2 (2–3)	3 (3)
Co-infection	EV/RV	14	10	-	1	2	-	-	-	1
	RSV	2	1	-	-	1	-	-	-	-
	Flu C	1	1	-	-	-	-	-	-	-
Clinical diagnosis										
URTI		74	55		6	8	1		2	1
Diarrhea		5	3	1					1	
Bronchiolitis		3	2							1
Febrile seizure		3	3							
Pneumonia*		1	1*							
Rash		2	2							
Adenoviremia transplant recipient		1	-			1				
Conjunctivitis/Febrile seizure		1	1							
Fever/GE		1	-		1			1		
Intussusception		1	-				1			
N/A		8	7			1				

**Death.*

Phylogenetic Analysis of HAdV Clinical Samples

Phylogenetic analysis of the hexon, penton base, and fiber gene of the Hong Kong clinical samples is shown in **Figure 3**. The phylogenetic analysis results are consistent with the BLAST results. Panels (B), (C), and (D) display the phylogenetic relationships of the penton base, hexon, and fiber genes, respectively. Of these 100 clinical HAdV isolates, HAdV-B3 ($n = 74$) was the most prevalent type. The three capsid genes formed a subclade with another China HAdV-3 isolate Guangzhou01 circulating in 2004 (Zhang et al., 2006). HAdV-E4 was the second most prevalent strain ($n = 10$). This is unexpected as HAdV-E4 was formerly and apparently constrained to military populations (van der Veen et al., 1969; Kolavic-Gray et al., 2002). However, this may not be surprising as a recombination of a viral replication motif, NF-I, that may have resulted in host adaption and allowed HAdV-E4 to infect a wider population was reported (Dehghan et al., 2013b; Zhang et al., 2019; Coleman et al., 2020).

GenBank Accession Numbers of the Capsid Protein Genes Sequenced From the Clinical Isolates

PCR products derived from the penton base, hexon, and fiber genes of the throat swab specimens were sequenced. Of these, sequences from each representative type were submitted to GenBank, and their GenBank accession numbers are summarized in **Table 3**.

DISCUSSION

PCR and DNA sequencing analysis of microbial DNA has been used for quick identification and better characterization of the pathogens (Tang et al., 1997). In the past, the identification of HAdV genotypes was traditionally performed by hexon protein analysis, e.g., virus neutralization, which depended on the interaction between serotype-specific antisera and serotype-specific antigenic epitopes in HVRs of the hexon protein (Dudding et al., 1972), or, later, by limited hexon gene sequencing (Lu and Erdman, 2006). The time-consuming and labor-intensive epitope detection method is seldom used today; the limited partial hexon sequencing provides partial and incomplete identification, as any recombinant HAdV will be missed. As a gold standard, whole genome sequencing and analysis is the most accurate method to identify, characterize, and type HAdVs properly. This is borne out by recent recognition of new genotypes that include recombinant HAdVs identified by this whole genome analysis method, including important pathogenic and emergent HAdVs. As an example, HAdV-D53 was recognized as a new genotype because genome recombination was detected amongst the three major capsid genes that span the genome. The penton base, hexon, and fiber genes originated from genotypes HAdV-D37, HAdV-D22, and HAdV-D8, respectively (Walsh et al., 2009). While HAdV-D22 is nonpathogenic, HAdV-D53 is a potent and highly contagious epidemic keratoconjunctivitis ocular pathogen (Walsh et al., 2009). Another example is the emergent genotype HAdV-B55 (Zhu et al., 2009;

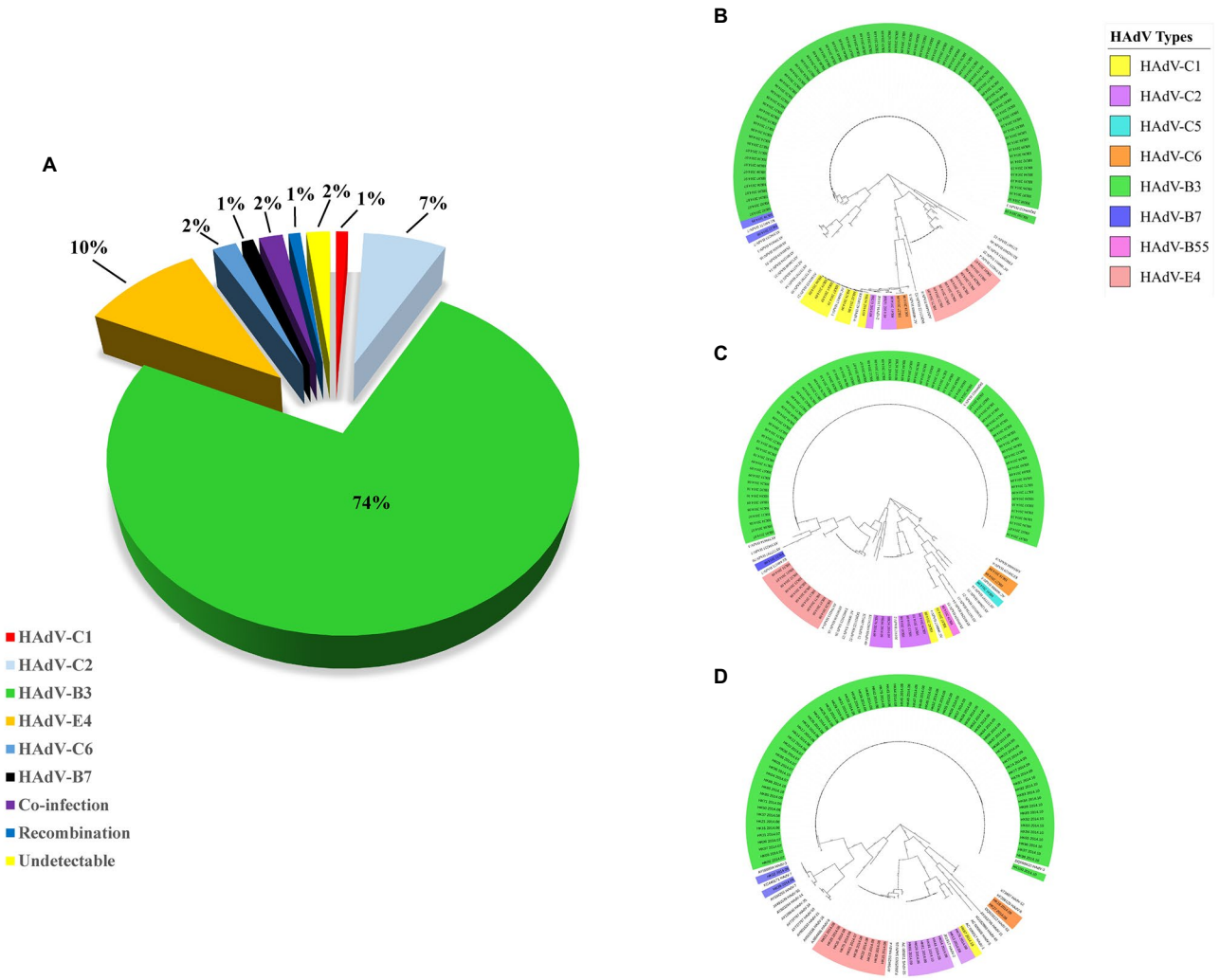

FIGURE 3 | (A) HAdV genotype distribution in hospitalized pediatric patients with ARIs from July through October, 2014. Panels **(B–D)** display the phylogenetic relationships of the penton base, hexon, and fiber genes, respectively, of the 98 identified HAdV clinical isolates. Additional reference sequences were retrieved from GenBank to provide context and reference. The phylogenetic trees were generated based on the Tree-Bisection-Reconnection (TBR) model by MEGA 7.0 (www.megasoftware.net/) using the maximum parsimony method with 1,000 boot-strap replicates and default parameters. The percentage of trees in which the associated taxa clustered together is shown next to the branches. The scale bar is in units of nucleotide substitutions per site.

Walsh et al., 2010). This is a highly contagious respiratory pathogen that is a recombinant containing the hexon epitope from a urinary tract pathogen HAdV-B11 along with the penton base and fiber genes from a respiratory tract pathogen HAdV-B14.

Given that whole genome sequencing is still relatively cost-prohibitive, particularly for large numbers of samples comprising outbreak and population sampling projects, and that genome recombination may only be indicated by assaying marker genes across the genome, such as the penton base, hexon, and fiber genes, a simple, rapid, cost-effective, practical, and universal detection and typing method for characterizing HAdVs is presented in this study. This protocol calls for using three pairs of universal PCR primers to target variable regions of the three capsid genes to provide products for characterizing the adenoviral isolates. The subsequent amplicon sequencing and BLAST analysis provides information as to the genotype identity and also whether there is any recombination across the genome. This method was validated by typing 98 clinical specimens successfully. In practice, all three pairs of universal primers that were chosen and optimized have worked for the genotyping of HAdV-B3, -B7, -B11, -B14, -B21, -B55, -C5, -D19, and -E4. However, because the HAdV-C fiber gene sequences are phylogenetically distinct from the other species, to compensate, a specific primer Fiber-CR was designed. This worked well for the HAdV-C fiber amplification. The universal primers for penton base and hexon genes successfully amplified the genotypes from across species B to F, even though the genomic sequences between different species are diverse. Isolates from the set of genotypes representing species HAdV-B, -C, -D, and -E can be detected and type-identified by this protocol using these universal primers. These include putative recombinants, for example, the HAdV-B55 isolate.

TABLE 3 | Genotyping and GenBank accession numbers of the clinical isolates.

Strain no.	Gene	Adenovirus Genotype	GenBank accession no.
HK18	Penton base	E6	OM988092
	Hexon		OM988093
	Fiber		OM988091
HK22	Penton base	B7	OM988085
	Hexon		OM988086
	Fiber		OM988084
HK35	Penton base	E4	QVS02965.1
	Hexon		QVS02970.1
	Fiber		QVS02985.1
HK39	Penton base	B7	OM988087
	Hexon	B55(double peaks)	OM988088
	Fiber	B7	OM988083
HK42	Penton base	C1	OM988098
	Hexon	C1	OM988097
	Fiber	B3 and C1(double peaks)	OM988094, ON098955
HK61		P1H2F2	ON054624
HK76	Penton	C2	OM988100
	Hexon		OM988096
	Fiber		OM988095
HK87	Penton	C1	OM988099
	Hexon		OM988090
	Fiber		OM988089
HK91	Penton	C2	AVZ45764.1
	Hexon		AVZ45769.1
	Fiber		AVZ45784.1

In contrast to a commonly used HAdV typing protocol published by Lu and Erdman (2006) and others which were based solely on the PCR amplification and/or sequencing of the HAdV hexon gene (Pring-Akerblom et al., 1999; Takeuchi et al., 1999; Sarantis et al., 2004; Zhu et al., 2009), the method presented in this report is more informative. Additionally, the Lu and Erdman (2006) protocol targets only the HVR1-6 rather than the entire epitope. Although HVR1-6 do contain type-specific epitopes, the adjacent HVR-7 region does as well (Sarantis et al., 2004; Yuan et al., 2009). As noted, these hexon-centric methods do not identify recombination across the genome, which appears to be an important molecular evolution mechanism in the genesis of novel and emergent HAdVs, as noted by the recent characterization and recognition of several emergent human adenoviral pathogens (Ishiko et al., 2008; Ishiko and Aoki, 2009; Walsh et al., 2009, 2010, 2011; Liu et al., 2011, 2012; Matsushima et al., 2011; Robinson et al., 2011; Zhang et al., 2012a; Hage et al., 2015). McCarthy, et al. proposed a clinical algorithm for detecting HAdV coinfections and strains by PCR amplification and sequencing of subregions of the hexon and fiber genes (McCarthy et al., 2009). However, the strains with recombination including the penton base gene, and the 5'-end of the genome, would be missed. For example, HAdV-D53 was a recombinant strain with a penton base of HAdV-37, hexon of HAdV-22, and fiber gene of HAdV-8 (Walsh et al., 2009). Another example is HAdV-D86, which contained hexon and fiber genes of HAdV-25 but penton base gene of HAdV-9 (P9H25F25; GenBank accession number KX868297; Kajan et al., 2018). On the contrary, our PCR amplification and DNA sequencing method not only targets three genes that essentially span the genome, but also includes the seven HVRs, which will identify any recombination within the hexon epitopes as well. The three PCR reactions can be performed concurrently and rapidly, optimizing detection time. This method will economically provide the identification and characterization of HAdVs, particularly recombinants, in the real-time surveillance, sampling, and screening of circulating large numbers of HAdV isolates during outbreaks and in populations for clinical microbiologists, public health officers, and epidemiologists.

DATA AVAILABILITY STATEMENT

The datasets presented in this study can be found in online repositories. The names of the repository/repositories and accession number(s) can be found in the article/supplementary material.

ETHICS STATEMENT

The studies involving human participants were reviewed and approved by Institutional Ethics Committee of Queen Mary Hospital. Written informed consent for participation was not required for this study in accordance with the national legislation and the institutional requirements.

AUTHOR CONTRIBUTIONS

DS and QZ contributed to the study design and manuscript writing. XW, JZ, WL, LQ, JO, PW, and QZ contributed to data analysis and data visualization. WZ, JW, DS, and QZ contributed to manuscript revision. All authors contributed to the article and approved the submitted version.

FUNDING

This work was supported by grants from the National Key Research and Development Program of China (2018YFE0204503), the National Natural Science Foundation of China (32170139 and 81730061), the Natural Science Foundation of Guangdong Province (2018B030312010, 2021A1515010788, and 2022A1515011190), and the Fundamental Research Funds for the Central Universities (21622101).

REFERENCES

Barrero, P. R., Valinotto, L. E., Tittarelli, E., and Mistchenko, A. S. (2012). Molecular typing of adenoviruses in pediatric respiratory infections in Buenos Aires, Argentina (1999-2010). *J. Clin. Virol.* 53, 145–150. doi: 10.1016/j.jcv.2011.11.001

Carballal, G., Videla, C. M., Espinosa, M. A., Savy, V., Uez, O., Sequeira, M. D., et al. (2001). Multicentered study of viral acute lower respiratory infections

in children from four cities of Argentina, 1993-1994. *J. Med. Virol.* 64, 167–174. doi: 10.1002/jmv.1032

Carr, M. J., Kajon, A. E., Lu, X., Dunford, L., O'Reilly, P., Holder, P., et al. (2011). Deaths associated with human adenovirus-14p1 infections, Europe, 2009–2010. *Emerg. Infect. Dis.* 17, 1402–1408. doi: 10.3201/1708.101760

Chang, S. Y., Lee, C. N., Lin, P. H., Huang, H. H., Chang, L. Y., Ko, W., et al. (2008). A community-derived outbreak of adenovirus type 3 in children in Taiwan between 2004 and 2005. *J. Med. Virol.* 80, 102–112. doi: 10.1002/jmv.21045

Chen, Y., Liu, F., Wang, C., Zhao, M., Deng, L., Zhong, J., et al. (2016). Molecular identification and epidemiological features of human adenoviruses associated with acute respiratory infections in hospitalized children in southern China, 2012-2013. *PLoS One* 11:e0155412. doi: 10.1371/journal.pone.0155412

Cheng, Z., Yan, Y., Jing, S., Li, W.-G., Chen, W.-W., Zhang, J., et al. (2018). Comparative genomic analysis of re-emergent human adenovirus type 55 pathogens associated With adult severe community-acquired pneumonia reveals conserved genomes and capsid proteins. *Front. Microbiol.* 9:1180. doi: 10.3389/fmicb.2018.01180

Coleman, K. K., Wong, C. C., Jayakumar, J., Nguyen, T. T., Wong, A. W. L., Yadana, S., et al. (2020). Adenoviral infections in Singapore: should new antiviral therapies and vaccines be adopted? *J. Infect. Dis.* 221, 566–577. doi: 10.1093/infdis/jiz489

Cui, X., Wen, L., Wu, Z., Liu, N., Yang, C., Liu, W., et al. (2015). Human adenovirus type 7 infection associated with severe and fatal acute lower respiratory illness and nosocomial transmission. *J. Clin. Microbiol.* 53, 746–749. doi: 10.1128/JCM.02517-14

Dehghan, S., Seto, J., Jones, M. S., Dyer, D. W., Chodosh, J., and Seto, D. (2013a). Simian adenovirus type 35 has a recombinant genome comprising human and simian adenovirus sequences, which predicts its potential emergence as a human respiratory pathogen. *Virology* 447, 265–273. doi: 10.1016/j.virol.2013.09.009

Dehghan, S., Seto, J., Liu, E. B., Ismail, A. M., Madupu, R., Heim, A., et al. (2019). A zoonotic adenoviral human pathogen emerged through genomic recombination among human and nonhuman simian hosts. *J. Virol.* 93:e00564-19. doi: 10.1128/jvi.00564-19

Dehghan, S., Seto, J., Liu, E. B., Walsh, M. P., Dyer, D. W., Chodosh, J., et al. (2013b). Computational analysis of four human adenovirus type 4 genomes reveals molecular evolution through two interspecies recombination events. *Virology* 443, 197–207. doi: 10.1016/j.virol.2013.05.014

Dongliu, Y., Guoliang, Y., Haocheng, X., Shuaijia, Q., Li, B., and Yanglei, J. (2016). Outbreak of acute febrile respiratory illness caused by human adenovirus B P14H11F14 in a military training camp in Shandong China. *Arch. Virol.* 161, 2481–2489. doi: 10.1007/s00705-016-2949-x

Dudding, B. A., Wagner, S. C., Zeller, J. A., Gmelich, J. T., French, G. R., and Top, F. H. Jr. (1972). Fatal pneumonia associated with adenovirus type 7 in three military trainees. *N. Engl. J. Med.* 286, 1289–1292. doi: 10.1056/nejm197206152862403

Erdman, D. D., Xu, W., Gerber, S. I., Gray, G. C., Schnurr, D., Kajon, A. E., et al. (2002). Molecular epidemiology of adenovirus type 7 in the United States, 1966-2000. *Emerg. Infect. Dis.* 8, 269–277. doi: 10.3201/eid0803.010190

Girouard, G., Garceau, R., Thibault, L., Bourque, C., Bastien, N., and Li, Y. (2011). Province-wide adenovirus type 3 outbreak with severe cases in New Brunswick. *Can. J. Infect. Dis. Med. Microbiol.* 22, e4–e6. doi: 10.1155/2011/575476

Gray, G. C., McCarthy, T., Lebeck, M. G., Schnurr, D. P., Russell, K. L., Kajon, A. E., et al. (2007). Genotype prevalence and risk factors for severe clinical adenovirus infection, United States 2004-2006. *Clin. Infect. Dis.* 45, 1120–1131. doi: 10.1086/522188

Hage, E., Gerd Liebert, U., Bergs, S., Ganzenmueller, T., and Heim, A. (2015). Human mastadenovirus type 70: a novel, multiple recombinant species D mastadenovirus isolated from diarrhoeal faeces of a haematopoietic stem cell transplantation recipient. *J. Gen. Virol.* 96, 2734–2742. doi: 10.1099/vir.0.000196

Han, G., Niu, H., Zhao, S., Zhu, B., Wang, C., Liu, Y., et al. (2013). Identification and typing of respiratory adenoviruses in Guangzhou, southern China using a rapid and simple method. *Virol. Sin.* 28, 103–108. doi: 10.1007/s12250-013-3308-7

Ishiko, H., and Aoki, K. (2009). Spread of epidemic keratoconjunctivitis due to a novel serotype of human adenovirus in Japan. *J. Clin. Microbiol.* 47, 2678–2679. doi: 10.1128/JCM.r00313-09

Ishiko, H., Shimada, Y., Konno, T., Hayashi, A., Ohguchi, T., Tagawa, Y., et al. (2008). Novel human adenovirus causing nosocomial epidemic keratoconjunctivitis. *J. Clin. Microbiol.* 46, 2002–2008. doi: 10.1128/jcm.01835-07

Ismail, A. M., Cui, T., Dommaraju, K., Singh, G., Dehghan, S., Seto, J., et al. (2018). Genomic analysis of a large set of currently-and historically-important human adenovirus pathogens. *Emerg. Microbes Infect.* 7:10. doi: 10.1038/s41426-017-0004-y

Jing, S., Zhang, J., Cao, M., Liu, M., Yan, Y., Zhao, S., et al. (2019). Household transmission of human adenovirus type 55 in case of fatal acute respiratory disease. *Emerg. Infect. Dis.* 25, 1756–1758. doi: 10.3201/eid2509.181937

Kajan, G. L., Lipiec, A., Bartha, D., Allard, A., and Arnberg, N. (2018). A multigene typing system for human adenoviruses reveals a new genotype in a collection of Swedish clinical isolates. *PLoS One* 13:e0209038. doi: 10.1371/journal.pone.0209038

Kajon, A. E., Moseley, J. M., Metzgar, D., Huong, H. S., Wadleigh, A., Ryan, M. A., et al. (2007). Molecular epidemiology of adenovirus type 4 infections in US military recruits in the postvaccination era (1997-2003). *J. Infect. Dis.* 196, 67–75. doi: 10.1086/518442

Kaneko, H., Aoki, K., Ishida, S., Ohno, S., Kitaichi, N., Ishiko, H., et al. (2011). Recombination analysis of intermediate human adenovirus type 53 in Japan by complete genome sequence. *J. Gen. Virol.* 92, 1251–1259. doi: 10.1099/vir.0.030361-0

Kolavic-Gray, S. A., Binn, L. N., Sanchez, J. L., Cersovsky, S. B., Polyak, C. S., Mitchell-Raymundo, F., et al. (2002). Large epidemic of adenovirus type 4 infection among military trainees: epidemiological, clinical, and laboratory studies. *Clin. Infect. Dis.* 35, 808–818. doi: 10.1086/342573

Lee, J., Choi, E. H., and Lee, H. J. (2010). Comprehensive serotyping and epidemiology of human adenovirus isolated from the respiratory tract of Korean children over 17 consecutive years (1991-2007). *J. Med. Virol.* 82, 624–631. doi: 10.1002/jmv.21701

Li, X., Kong, M., Su, X., Zou, M., Guo, L., Dong, X., et al. (2014). An outbreak of acute respiratory disease in China caused by human adenovirus type B55 in a physical training facility. *Int. J. Infect. Dis.* 28, 117–122. doi: 10.1016/j.ijid.2014.06.019

Li, Q. G., Zheng, Q. J., Liu, Y. H., and Wadell, G. (1996). Molecular epidemiology of adenovirus types 3 and 7 isolated from children with pneumonia in Beijing. *J. Med. Virol.* 49, 170–177. doi: 10.1002/(SICI)1096-9071(199607)49:3<170::AID-JMV3>3.0.CO;2-1

Lin, K. H., Lin, Y. C., Chen, H. L., Ke, G. M., Chiang, C. J., Hwang, K. P., et al. (2004). A two decade survey of respiratory adenovirus in Taiwan: the reemergence of adenovirus types 7 and 4. *J. Med. Virol.* 73, 274–279. doi: 10.1002/jmv.20087

Lion, T. (2014). Adenovirus infections in immunocompetent and immunocompromised patients. *Clin. Microbiol. Rev.* 27, 441–462. doi: 10.1128/cmr.00116-13

Liu, E. B., Ferreyra, L., Fischer, S. L., Pavan, J. V., Nates, S. V., Hudson, N. R., et al. (2011). Genetic analysis of a novel human adenovirus with a serologically unique hexon and a recombinant fiber gene. *PLoS One* 6:e24491. doi: 10.1371/journal.pone.0024491

Liu, E. B., Wadford, D. A., Seto, J., Vu, M., Hudson, N. R., Thrasher, L., et al. (2012). Computational and serologic analysis of novel and known viruses in species human adenovirus D in which serology and genomics do not correlate. *PLoS One* 7:e33212. doi: 10.1371/journal.pone.0033212

Lu, X., and Erdman, D. D. (2006). Molecular typing of human adenoviruses by PCR and sequencing of a partial region of the hexon gene. *Arch. Virol.* 151, 1587–1602. doi: 10.1007/s00705-005-0722-7

Lu, X., Joshi, A., and Flomenberg, P. (2014). "Adenoviruses," in *Viral Infections of Humans. Vol. 23*. eds. R. Kaslow, L. Stanberry and J. Le Duc (Boston, MA: Springer).

Lynch, J. P., and Kajon, A. E. (2016). Adenovirus: epidemiology, global spread of novel serotypes, and advances in treatment and prevention. *Semin. Respir. Crit. Care Med.* 37, 586–602. doi: 10.1055/s-0036-1584923

Madisch, I., Wolfel, R., Harste, G., Pommer, H., and Heim, A. (2006). Molecular identification of adenovirus sequences: a rapid scheme for early typing of human adenoviruses in diagnostic samples of immunocompetent and

immunodeficient patients. *J. Med. Virol.* 78, 1210–1217. doi: 10.1002/jmv.20683

Matsushima, Y., Shimizu, H., Phan, T. G., and Ushijima, H. (2011). Genomic characterization of a novel human adenovirus type 31 recombinant in the hexon gene. *J. Gen. Virol.* 92, 2770–2775. doi: 10.1099/vir.0.034744-0

McCarthy, T., Lebeck, M. G., Capuano, A. W., Schnurr, D. P., and Gray, G. C. (2009). Molecular typing of clinical adenovirus specimens by an algorithm which permits detection of adenovirus coinfections and intermediate adenovirus strains. *J. Clin. Virol.* 46, 80–84. doi: 10.1016/j.jcv.2009.06.008

Pan, H., Yan, Y., Zhang, J., Zhao, S., Feng, L., Ou, J., et al. (2018). Rapid construction of a replication-competent infectious clone of human adenovirus type 14 by Gibson assembly. *Viruses* 10:568. doi: 10.3390/v10100568

Piedra, P. A., Poveda, G. A., Ramsey, B., McCoy, K., and Hiatt, P. W. (1998). Incidence and prevalence of neutralizing antibodies to the common adenoviruses in children with cystic fibrosis: implication for gene therapy with adenovirus vectors. *Pediatrics* 101, 1013–1019. doi: 10.1542/peds.101.6.1013

Pring-Akerblom, P., Trijssenaar, F. E., Adrian, T., and Hoyer, H. (1999). Multiplex polymerase chain reaction for subgenus-specific detection of human adenoviruses in clinical samples. *J. Med. Virol.* 58, 87–92. doi: 10.1002/(SICI)1096-9071(199905)58:1<87::AID-JMV14>3.0.CO;2-R

Rebelo-de-Andrade, H., Pereira, C., Giria, M., Prudencio, E., Brito, M. J., Cale, E., et al. (2010). Outbreak of acute respiratory infection among infants in Lisbon, Portugal, caused by human adenovirus serotype 3 and a new 7/3 recombinant strain. *J. Clin. Microbiol.* 48, 1391–1396. doi: 10.1128/JCM.02019-09

Robinson, C. M., Singh, G., Henquell, C., Walsh, M. P., Peigue-Lafeuille, H., Seto, D., et al. (2011). Computational analysis and identification of an emergent human adenovirus pathogen implicated in a respiratory fatality. *Virology* 409, 141–147. doi: 10.1016/j.virol.2010.10.020

Robinson, C. M., Singh, G., Lee, J. Y., Dehghan, S., Rajaiya, J., Liu, E. B., et al. (2013a). Molecular evolution of human adenoviruses. *Sci. Rep.* 3:1812. doi: 10.1038/srep01812

Robinson, C. M., Zhou, X., Rajaiya, J., Yousuf, M. A., Singh, G., DeSerres, J. J., et al. (2013b). Predicting the next eye pathogen: analysis of a novel adenovirus. *MBio* 4, e00595–e00612. doi: 10.1128/mBio.00595-12

Sanchez, J. L., Binn, L. N., Innis, B. L., Reynolds, R. D., Lee, T., Mitchell-Raymundo, F., et al. (2001). Epidemic of adenovirus-induced respiratory illness among US military recruits: epidemiologic and immunologic risk factors in healthy, young adults. *J. Med. Virol.* 65, 710–718. doi: 10.1002/jmv.2095

Sarantis, H., Johnson, G., Brown, M., Petric, M., and Tellier, R. (2004). Comprehensive detection and serotyping of human adenoviruses by PCR and sequencing. *J. Clin. Microbiol.* 42, 3963–3969. doi: 10.1128/JCM.42.9.3963-3969.2004

Schmitz, H., Wigand, R., and Heinrich, W. (1983). Worldwide epidemiology of human adenovirus infections. *Am. J. Epidemiol.* 117, 455–466. doi: 10.1093/oxfordjournals.aje.a113563

Seto, D., Jones, M. S., Dyer, D. W., and Chodosh, J. (2013). Characterizing, typing, and naming human adenovirus type 55 in the era of whole genome data. *J. Clin. Virol.* 58, 741–742. doi: 10.1016/j.jcv.2013.09.025

Seto, J., Walsh, M. P., Mahadevan, P., Zhang, Q., and Seto, D. (2010). Applying genomic and bioinformatic resources to human adenovirus genomes for use in vaccine development and for applications in vector development for gene delivery. *Viruses* 2, 1–26. doi: 10.3390/v2010001

Takeuchi, S., Itoh, N., Uchio, E., Aoki, K., and Ohno, S. (1999). Serotyping of adenoviruses on conjunctival scrapings by PCR and sequence analysis. *J. Clin. Microbiol.* 37, 1839–1845. doi: 10.1128/JCM.37.6.1839-1845.1999

Tan, D., Zhu, H., Fu, Y., Tong, F., Yao, D., Walline, J., et al. (2016). Severe community-acquired pneumonia caused by human adenovirus in immunocompetent adults: a multicenter case series. *PLoS One* 11:e0151199. doi: 10.1371/journal.pone.0151199

Tang, Y. W., Procop, G. W., and Persing, D. H. (1997). Molecular diagnostics of infectious diseases. *Clin. Chem.* 43, 2021–2038. doi: 10.1093/clinchem/43.11.2021

Tsou, T. P., Tan, B. F., Chang, H. Y., Chen, W. C., Huang, Y. P., Lai, C. Y., et al. (2012). Community outbreak of adenovirus, Taiwan, 2011. *Emerg. Infect. Dis.* 18, 1825–1832. doi: 10.3201/eid1811.120629

van der Veen, J., Oei, K. G., and Abarbanel, M. F. (1969). Patterns of infections with adenovirus types 4, 7 and 21 in military recruits during a 9-year survey. *J. Hyg.* 67, 255–268. doi: 10.1017/s0022172400041668

Walsh, M. P., Chintakuntlawar, A., Robinson, C. M., Madisch, I., Harrach, B., Hudson, N. R., et al. (2009). Evidence of molecular evolution driven by recombination events influencing tropism in a novel human adenovirus that causes epidemic keratoconjunctivitis. *PLoS One* 4:e5635. doi: 10.1371/journal.pone.0005635

Walsh, M. P., Seto, J., Jones, M. S., Chodosh, J., Xu, W., and Seto, D. (2010). Computational analysis identifies human adenovirus type 55 as a re-emergent acute respiratory disease pathogen. *J. Clin. Microbiol.* 48, 991–993. doi: 10.1128/JCM.01694-09

Walsh, M. P., Seto, J., Liu, E. B., Dehghan, S., Hudson, N. R., Lukashev, A. N., et al. (2011). Computational analysis of two species C human adenoviruses provides evidence of a novel virus. *J. Clin. Microbiol.* 49, 3482–3490. doi: 10.1128/jcm.00156-11

Wang, Y. F., Shen, F. C., Wang, S. L., Kuo, P. H., Tsai, H. P., Liu, C. C., et al. (2016). Molecular epidemiology and clinical manifestations of adenovirus respiratory infections in Taiwanese children. *Medicine* 95:e3577. doi: 10.1097/MD.0000000000003577

Wigand, R. (1987). Pitfalls in the identification of adenoviruses. *J. Virol. Methods* 16, 161–169. doi: 10.1016/0166-0934(87)90001-2

Xie, Y.-X., Tu, B., Chen, W.-W., Zhou, Z.-P., Nie, W.-M., Wang, C.-L., et al. (2013). Clinical characteristics of 80 hospitalized cases of human adenovirus type 55 infection. *Infect. Dis.* 26, 45–47.

Yan, Y., Jing, S., Feng, L., Zhang, J., Zeng, Z., Li, M., et al. (2021). Construction and characterization of a novel recombinant attenuated and replication-deficient candidate human adenovirus type 3 vaccine: "adenovirus vaccine Within an adenovirus vector". *Virol. Sin.* 36, 354–364. doi: 10.1007/s12250-020-00234-1

Yang, Z., Zhu, Z., Tang, L., Wang, L., Tan, X., Yu, P., et al. (2009). Genomic analyses of recombinant adenovirus type 11a in China. *J. Clin. Microbiol.* 47, 3082–3090. doi: 10.1128/JCM.00282-09

Yi, L., Zou, L., Lu, J., Kang, M., Song, Y., Su, J., et al. (2017). A cluster of adenovirus type B55 infection in a neurosurgical inpatient department of a general hospital in Guangdong, China. *Influenza Other Respir. Viruses* 11, 328–336. doi: 10.1111/irv.12457

Yu, Z., Zeng, Z., Zhang, J., Pan, Y., Chen, M., Guo, Y., et al. (2016). Fatal community-acquired pneumonia in children caused by re-emergent human adenovirus 7d associated with higher severity of illness and fatality rate. *Sci. Rep.* 6:37216. doi: 10.1038/srep37216

Yuan, X., Qu, Z., Wu, X., Wang, Y., Liu, L., Wei, F., et al. (2009). Molecular modeling and epitopes mapping of human adenovirus type 3 hexon protein. *Vaccine* 27, 5103–5110. doi: 10.1016/j.vaccine.2009.06.041

Zeng, Z., Zhang, J., Jing, S., Cheng, Z., Bofill-Mas, S., Maluquer de Motes, C., et al. (2016). Genome sequence of a Cynomolgus macaque adenovirus (CynAdV-1) isolate from a primate Colony in the United Kingdom. *Genome Announc.* 4:e01193-16. doi: 10.1128/genomeA.01193-16

Zhang, Q., Dehghan, S., and Seto, D. (2016). Pitfalls of restriction enzyme analysis in identifying, characterizing, typing, and naming viral pathogens in the era of whole genome data, as illustrated by HAdV type 55. *Virol. Sin.* 31, 448–453. doi: 10.1007/s12250-016-3862-x

Zhang, Q., Jing, S., Cheng, Z., Yu, Z., Dehghan, S., Shamsaddini, A., et al. (2017). Comparative genomic analysis of two emergent human adenovirus type 14 respiratory pathogen isolates in China reveals similar yet divergent genomes. *Emerg. Microbes Infect.* 6:e92. doi: 10.1038/emi.2017.78

Zhang, J., Kang, J., Dehghan, S., Sridhar, S., Lau, S. K. P., Ou, J., et al. (2019). A survey of recent adenoviral respiratory pathogens in Hong Kong reveals emergent and recombinant human adenovirus type 4 (HAdV-E4) circulating in civilian populations. *Viruses* 11:129. doi: 10.3390/v11020129

Zhang, S. Y., Luo, Y. P., Huang, D. D., Fan, H., Lu, Q. B., Wo, Y., et al. (2016). Fatal pneumonia cases caused by human adenovirus 55 in immunocompetent adults. *Infect. Dis. Ther.* 48, 40–47. doi: 10.3109/23744235.2015.1055585

Zhang, Q., Seto, D., Cao, B., Zhao, S., and Wan, C. (2012a). Genome sequence of human adenovirus type 55, a re-emergent acute respiratory disease pathogen in China. *J. Virol.* 86, 12441–12442. doi: 10.1128/jvi.02225-12

Zhang, Q., Seto, D., Zhao, S., Zhu, L., Zhao, W., and Wan, C. (2012b). Genome sequence of the first human adenovirus type 14 isolated in China. *J. Virol.* 86, 7019–7020. doi: 10.1128/jvi.00814-12

Zhang, Q., Su, X., Gong, S., Zeng, Q., Zhu, B., Wu, Z., et al. (2006). Comparative genomic analysis of two strains of human adenovirus type 3 isolated from children with acute respiratory infection in southern China. *J. Gen. Virol.* 87, 1531–1541. doi: 10.1099/vir.0.81515-0

Zhao, S., Wan, C., Ke, C., Seto, J., Dehghan, S., Zou, L., et al. (2014). Re-emergent human adenovirus genome type 7d caused an acute respiratory disease outbreak in southern China after a twenty-one year absence. *Sci. Rep.* 4:7365. doi: 10.1038/srep07365

Zhou, X., Robinson, C. M., Rajaiya, J., Dehghan, S., Seto, D., Jones, M. S., et al. (2012). Analysis of human adenovirus type 19 associated with epidemic keratoconjunctivitis and its reclassification as adenovirus type 64. *Invest. Ophthalmol. Vis. Sci.* 53, 2804–2811. doi: 10.1167/iovs.12-9656

Zhu, Z., Zhang, Y., Xu, S., Yu, P., Tian, X., Wang, L., et al. (2009). Outbreak of acute respiratory disease in China caused by B2 species of adenovirus type 11. *J. Clin. Microbiol.* 47, 697–703. doi: 10.1128/JCM.01769-08

Conflict of Interest: The authors declare that the research was conducted in the absence of any commercial or financial relationships that could be construed as a potential conflict of interest.

frontiers | Frontiers in Microbiology

OPINION
published: 24 June 2022
doi: 10.3389/fmicb.2022.907406

Animal Models for COVID-19 Therapeutic Development: Where We Are and Where We Need to Go

Sihai Zhao[1,2], *Jianglin Fan*[3] *and Enqi Liu*[1]*

[1] Laboratory Animal Center, Health Science Center of Xi'an Jiaotong University, Xi'an, China, [2] Institute of Molecular Virology, Health Science Center of Xi'an Jiaotong University, Xi'an, China, [3] Department of Molecular Pathology, Faculty of Medicine, Graduate School of Medical Sciences, University of Yamanashi, Chuo, Japan

Keywords: animal models, COVID-19, therapeutics, vaccines, humanized mouse model

INTRODUCTION

Severe acute respiratory syndrome coronavirus 2 (SARS-CoV-2) causes coronavirus disease 2019 (COVID-19), which has spread worldwide and reached a pandemic level within several months (Bedford et al., 2020; Li et al., 2020; Hu et al., 2021). Globally, scientists are trying to understand and defeat COVID-19 using animal studies to explore potential therapeutics. Vaccination remains the best choice to protect susceptible populations; therefore, many institutions and companies have developed vaccines against SARS-CoV-2 infection and many therapeutics are under clinical investigations. For these undertakings, it is essential to use suitable COVID-19 animal models (Caldera-Crespo et al., 2021; Munoz-Fontela et al., 2022).

ESSENTIALS FOR ANIMAL MODELS OF COVID-19

Animal models are usually used in medical experimentation as an alternative to avoid potential hazards in humans (Liu and Fan, 2017). Appropriate COVID-19 animal models should be a very powerful tool in the study of the onset, development and culmination of this disease and provide helpful knowledge for its management. Making and choosing good models for COVID-19 requires taking full consideration of the following: (1) the animals should be susceptible to SARS-CoV-2, especially easily infected by the virus *via* the respiratory route; (2) the characteristics of the induced phenotypes or manifestations are similar to those of human COVID-19 patients, such as fever, coughing and myalgia or fatigue, pneumonia detected by computed tomography (CT) examination, along with sex- or age-related differences in severity (Huang et al., 2020); (3) immune responses should be similar to those in human coronavirus infections; and (4) the animals should have an appropriate cost. When testing vaccine protection effects, recovered infected animals should gain immunity to resist reinfection. These principles should be used for creating new models or evaluating candidate models for the development of COVID-19 therapeutics.

Due to the similarity of SARS-CoV-2 to other two beta coronaviruses, SARS-CoV-1 and Middle Eastern respiratory syndrome coronavirus (MERS-CoV), lessons from SARS-CoV-1 vaccine development can be helpful for accelerating SARS-CoV-2 vaccine development (Amanat and Krammer, 2020). Scientists have designed several SARS-CoV-2 vaccines to prevent COVID-19. Although the SARS-CoV-2 vaccine did not catch up with the first wave of the pandemic, the application of the vaccine has reduced the severe incidence of COVID-19 patients. Several faithful animal models for studying the pathogenesis of SARS-CoV-2 and its vaccine development have recently been created by scientists and have shed light on COVID-19 research. Here, we provide a brief review of these models, summarize what we have learned, and discuss their usefulness for testing the immunological response of vaccine injection and post-challenge safety.

OPEN ACCESS

Edited by:
Anna Kramvis,
University of the Witwatersrand, South Africa

Reviewed by:
Junki Maruyama,
University of Texas Medical Branch at Galveston, United States
Khan Sharun,
Indian Veterinary Research Institute (IVRI), India

***Correspondence:**
Enqi Liu
liuenqi@xjtu.edu.cn

Specialty section:
This article was submitted to Virology, a section of the journal Frontiers in Microbiology

Received: *29 March 2022*
Accepted: *30 May 2022*
Published: *24 June 2022*

Citation:
Zhao S, Fan J and Liu E (2022) Animal Models for COVID-19 Therapeutic Development: Where We Are and Where We Need to Go. Front. Microbiol. 13:907406. doi: 10.3389/fmicb.2022.907406

NON-HUMAN PRIMATE MODELS OF COVID-19

Non-human primates (the rhesus macaque *or Macaca mulatta*, cynomolgus monkey, or *Macaca fascicularis,* common marmoset or *Callithrix jacchus* and African green monkeys or *Chlorocebus aethiops*) have been used to explore the pathogenesis and test the potential therapies of SARS-CoV-2 (Hartman et al., 2020; Lu et al., 2020; Rockx et al., 2020; Yu et al., 2020; Woolsey et al., 2021). All the above mentioned primates can be infected by experimental inoculation with SARS-CoV-2. The rhesus macaque is the most susceptible to SARS-CoV2 infection, followed by the cynomolgus monkey and the common marmoset (Lu et al., 2020). The viral replication state of nasopharyngeal swabs, anal swabs and lungs in old rhesus macaques was more active than that in young monkeys for 14 days after SARS-CoV-2 challenge (Yu et al., 2020). In SARS-CoV-2-infected macaques, viruses were discharged from the nose and throat in the absence of clinical symptoms and could be detected in both type I and II pneumocytes in the foci of diffuse alveolar damage and ciliated epithelial cells of the nasal, bronchial, and bronchiolar mucosae (Rockx et al., 2020). SARS-CoV-2 also causes pulmonary infiltrates in these monkeys, a hallmark of human disease shown in CT scans, which can be detected by chest radiographs in all infected rhesus macaques (Munster et al., 2020). Another important finding is that monkeys that have recovered from SARS-CoV-2 infection cannot be infected again in the near future (Yu et al., 2020). This finding also provided an important clue for antibody-mediated protection, suggesting that COVID-19 can be prevented through either natural infection or vaccination. Autopsy examinations revealed that the lungs, throat, bronchi, and spleen were infected in both rhesus monkeys and cynomolgus monkeys (Lu et al., 2020; Yu et al., 2020). These observations suggested that the rhesus monkey and cynomolgus monkey models can be used to evaluate vaccines and drugs to treat or prevent COVID-19. Gao et al. developed a purified inactivated SARS-CoV-2 virus vaccine candidate (PiCoVacc) and then conducted a challenge experiment in rhesus monkeys. They reported that vaccine immunization significantly reduced the pathological changes in the lungs of rhesus monkeys and the viral titers were also significantly decreased whereas no antibody-dependent enhancement was observed (Gao et al., 2020).

A recent report showed that African green monkey (AGM), another non-human primate, had robust SARS-CoV-2 replication and developed pronounced respiratory disease (Hartman et al., 2020; Woolsey et al., 2021). Shedding of SARS-CoV-2 from both respiratory and gastrointestinal tracts was also documented in AGMs, which may mimic human COVID-19 cases (Hartman et al., 2020). Therefore, AGM may provide another option for COVID-19 therapeutics and vaccine evaluation. These data suggest that monkey models are useful to evaluate vaccines and therapeutics for treating or preventing COVID-19. The advantages and disadvantages of non-human primates compared with those of other animal models are summarized in **Table 1**. However, high costs and ethical issues may strictly limit the widespread use of non-human primate models in most institutions.

RODENT MODELS OF COVID-19

The genetically manipulated mouse model is relatively cheap and easy to use (Korner et al., 2020). It has been reported that SARS-CoV-2 infection can occur through the angiotensin converting enzyme II receptor (ACE2R) for cellular entry (Zhou et al., 2020). Since 11 of the 29 amino acids in the critical region of the human ACE2R receptor are different from those of the mouse, SARS-CoV-2 is unable to naturally infect mice. Therefore, human ACE2R transgenic mice were developed and analyzed for potential application in the study of COVID-19 (Netland et al., 2008; Bao et al., 2020). Although hACE2R transgenic mice showed signs of weight loss and interstitial pneumonia after infection, the symptoms were mild and much different from those of humans (Bao et al., 2020). The hACE2R transgenic mice developed by Netland et al. also exhibited brain infection of SARS-CoV-2, which is rare in humans (Netland et al., 2008). These drawbacks may puzzle or mislead researchers for interpretation of their studies. The development of lung cell-specific expression of the hACE2R gene in transgenic or knock-in models without endogenous mouse ACE2R gene may help to broaden the use of mouse models in COVID-19 studies in the future. Except for modifying the mouse ACE2R for SARS-CoV-2 infecting host cells, another reverse genetics strategy was to design a recombinant mouse-adapted SARS-CoV-2, designated as SARS-CoV-2 MA, which can use mouse ACE2R for entry into cells (Dinnon et al., 2020; Leist et al., 2020). SARS-CoV-2 MA was reported to successfully infect and replicate in the upper and lower airways in both adult and aged BALB/c mice (Dinnon et al., 2020). SARS-CoV-2 MA caused more severe disease in aged mice, which resembles the human features of COVID-19, and exhibited more clinically relevant phenotypes than those seen in Hfh4-ACE2R transgenic mice (Dinnon et al., 2020). This model provided a powerful tool for the study of SARS-CoV-2 pathogenesis and has been used to evaluate vaccine and antiviral therapeutics performance (Leist et al., 2020).

As rats are unsusceptible to SARS-CoV-2, they are not used to study of COVID-19. However, Syrian hamster ACE2R proteins are reported to be highly similar to human ACE2R with 3–4 mutations at the interface (Chan et al., 2020). After being infected with SARS-CoV-2, hamsters showed weight loss, drowsiness, hairiness, hunched back, and shortness of breath. Olfactory and taste dysfunctions are common in mildly symptomatic COVID-19 patients. The food-searching behavioral test showed that anosmia may happen in SARS-CoV-2-infected hamsters, and the level of anosmia was associated with olfactory epithelium damage (Reyna et al., 2022). In addition, high titers of SARS-CoV-2 were found in the hamster lungs and intestines. The phenotypes of human upper and lower respiratory tract infections are very similar to those of hamsters, so this model benefits scientists who like to use small animals to perform COVID-19 research or therapeutic screening (Sia et al., 2020).

OTHER ANIMAL MODELS OF COVID-19

Ferrets, another small animal, have special value in the research of virus-related diseases. After being infected with respiratory

TABLE 1 | Comparison of animal models and human COVID-19 features.

	Human	Primates	Mouse (hACE2 Tg)	Ferret	Hamster
ACE2R similarity with human	Same	High	Low (wide-type)	High	High
Susceptibility	+	+	+	+	+
Respiratory transmission	+	+	+	+	+
Pneumonia	+	+	Mild	+	+
Severity differences (sex-related)	+	NR	NR	NR	NR
Severity differences (age-related)	+	+	NR	NR	NR
Resistant to reinfection	±	+	NR	NR	NR
Cost		Extremely high	Low	Middle	Low
Animal size		Big	Small	Middle	Small
Animal sources		Limited	Easy	Limited	Easy
Widely used		±	+	–	–
Reproductive cycle		Long	short	Long	short

NR, not reported.

viruses, ferrets can show symptoms similar to those of humans. For example, ferrets infected with influenza virus can even sneeze like humans, and can easily transmit the virus to other ferrets (Herfst et al., 2012). SARS-CoV-2 can infect ferrets through the respiratory tract and can replicate in infected cells (Shi et al., 2020). The temperature of the infected ferrets rises slightly and infection does not cause serious illness or death. Although fatalities were not observed, SARS-CoV-2-infected ferrets shed the virus in nasal washes, saliva, urine, and feces up to 8 days post-infection (Kim et al., 2020). Ferrets give birth once per year, with 6–8 l, so they do not breed as rapidly as mice. To a certain extent, the slow reproduction speed may limit the wide application of ferrets. Similar to ferrets, farmed minks are also susceptible to coronaviruses. On farms, minks are infected with SARS-CoV-2 and can transmit it to humans (Enserink, 2020; Oreshkova et al., 2020; Sharun et al., 2021). Laboratory evidence also showed SARS-CoV-2 can be transmitted among minks and resulted severe respiratory syndrome (Shuai et al., 2021). Among middle- or large-sized animals, it was reported that SARS-CoV-2 can replicate efficiently in cats, with younger cats being more permissive and perhaps more importantly, the virus can transmit between cats *via* the airborne route (Shi et al., 2020). Dogs exhibit low susceptibility, whereas livestock, including pigs, chickens, and ducks, are not susceptible to SARS-CoV-2 (Shi et al., 2020). Previous reviews also have discussed the potentials of these animal species in COVID-19 studies (Munoz-Fontela et al., 2020; Sharun et al., 2020; Shou et al., 2021).

DISCUSSION AND PERSPECTIVES

The currently reported COVID-19 animal models were summarized in **Table 1**. The advantages and disadvantages of the COVID-19 animal models that are currently available was discussed in this and previous study (Shou et al., 2021). To date, it seems that no animal model is perfect when evaluating potential drugs and vaccines (Munoz-Fontela et al., 2022). The most useful animal model is the rhesus macaque, but because of the substantial cost and specific facility requirements, the monkey model is unlikely to be widely used in common laboratories. The ferret model has special applicability in the study of respiratory viruses, but the low breeding rate and the lack of suitable facilities make it difficult for wide use in COVID-19 studies. The limitations of COVID-19 animal models are also apparent (Sharun et al., 2020). First, no model can fully mimic human COVID-19, and the findings of each model are needed to confirm with other animal models and to increase its credibility. Second, although the non-human primate model can better represent human COVID-19, it faces stricter ethical review and is not easy to be widely used. Mice are cheap and there are many genetically modified models available, but their immune system responses differ from those of humans. Humanized mouse models may become a feasible study tool for COVID-19 research in the future. At present, various genetically engineered mouse models are currently on the way, and hopefully, these new models will provide a unique research tool to fight against COVID-19 in the future.

AUTHOR CONTRIBUTIONS

JF and EL designed this project. SZ wrote the paper. All authors contributed to the article and approved the submitted version.

FUNDING

This study was supported by grants from the Natural Science Foundation of Shaanxi Province (Grant Nos. 2020PT-004 and 2020PT-001).

REFERENCES

Amanat, F., and Krammer, F. (2020). SARS-CoV-2 vaccines: status report. *Immunity* 52, 583–589. doi: 10.1016/j.immuni.2020.03.007

Bao, L., Deng, W., Huang, B., Gao, H., Liu, J., Ren, L., et al. (2020). The pathogenicity of SARS-CoV-2 in hACE2 transgenic mice. *Nature* 583, 830–833. doi: 10.1038/s41586-020-2312-y

Bedford, J., Enria, D., Giesecke, J., Heymann, D. L., Ihekweazu, C., Kobinger, G., et al. (2020). COVID-19: towards controlling of a pandemic. *Lancet* 395, 1015–1018. doi: 10.1016/S0140-6736(20)30673-5

Caldera-Crespo, L. A., Paidas, M. J., Roy, S., Schulman, C. I., Kenyon, N. S., Daunert, S., et al. (2021). Experimental models of COVID-19. *Front. Cell. Infect. Microbiol.* 11, 792584. doi: 10.3389/fcimb.2021.792584

Chan, J. F., Zhang, A. J., Yuan, S., Poon, V. K., Chan, C. C., Lee, A. C., et al. (2020). Simulation of the clinical and pathological manifestations of Coronavirus disease 2019 (COVID-19) in a golden syrian hamster model: implications for disease pathogenesis and transmissibility. *Clin. Infect. Dis.* 71, 2428–2446. doi: 10.1093/cid/ciaa644

Dinnon, K. H. III., Leist, S. R., Schafer, A., Edwards, C. E., Martinez, D. R., Montgomery, S. A., et al. (2020). A mouse-adapted model of SARS-CoV-2 to test COVID-19 countermeasures. *Nature* 586, 560–566. doi: 10.1038/s41586-020-2708-8

Enserink, M. (2020). Coronavirus rips through Dutch mink farms, triggering culls. *Science* 368, 1169. doi: 10.1126/science.368.6496.1169

Gao, Q., Bao, L., Mao, H., Wang, L., Xu, K., Yang, M., et al. (2020). Development of an inactivated vaccine candidate for SARS-CoV-2. *Science* 369, 77–81. doi: 10.1126/science.abc1932

Hartman, A. L., Nambulli, S., McMillen, C. M., White, A. G., Tilston-Lunel, N. L., Albe, J. R., et al. (2020). SARS-CoV-2 infection of African green monkeys results in mild respiratory disease discernible by PET/CT imaging and shedding of infectious virus from both respiratory and gastrointestinal tracts. *PLoS Pathog.* 16, e1008903. doi: 10.1371/journal.ppat.1008903

Herfst, S., Schrauwen, E. J., Linster, M., Chutinimitkul, S., de Wit, E., Munster, V. J., et al. (2012). Airborne transmission of influenza A/H5N1 virus between ferrets. *Science* 336, 1534–1541. doi: 10.1126/science.1213362

Hu, B., Guo, H., Zhou, P., and Shi, Z. L. (2021). Characteristics of SARS-CoV-2 and COVID-19. *Nat. Rev. Microbiol.* 19, 141–154. doi: 10.1038/s41579-020-00459-7

Huang, C., Wang, Y., Li, X., Ren, L., Zhao, J., Hu, Y., et al. (2020). Clinical features of patients infected with 2019 novel coronavirus in Wuhan, China. *Lancet* 395, 497–506. doi: 10.1016/S0140-6736(20)30183-5

Kim, Y. I., Kim, S. G., Kim, S. M., Kim, E. H., Park, S. J., Yu, K. M., et al. (2020). Infection and rapid transmission of SARS-CoV-2 in ferrets. *Cell Host Microbe* 27, 704–709.e2. doi: 10.1016/j.chom.2020.03.023

Korner, R. W., Majjouti, M., Alcazar, M. A. A., and Mahabir, E. (2020). Of mice and men: the Coronavirus MHV and mouse models as a translational approach to understand SARS-CoV-2. *Viruses* 12, 880. doi: 10.3390/v12080880

Leist, S. R., Dinnon, K. H. III., Schafer, A., Tse, L. V., Okuda, K., Hou, Y. J., et al. (2020). A mouse-adapted SARS-CoV-2 induces acute lung injury and mortality in standard laboratory mice. *Cell* 183, 1070–1085.e12. doi: 10.1016/j.cell.2020.09.050

Li, Q., Guan, X., Wu, P., Wang, X., Zhou, L., Tong, Y., et al. (2020). Early transmission dynamics in Wuhan, China, of novel coronavirus-infected pneumonia. *N. Engl. J. Med.* 382, 1199–1207. doi: 10.1056/NEJMoa2001316

Liu, E., and Fan, J. (2017). *Fundamentals of Laboratory Animal Science, 1st Edn*. New York, NY: CRC Press. doi: 10.1201/9781315368993

Lu, S., Zhao, Y., Yu, W., Yang, Y., Gao, J., Wang, J., et al. (2020). Comparison of nonhuman primates identified the suitable model for COVID-19. *Signal Transduct. Target Ther.* 5, 157. doi: 10.1038/s41392-020-00269-6

Munoz-Fontela, C., Dowling, W. E., Funnell, S. G. P., Gsell, P. S., Riveros-Balta, A. X., Albrecht, R. A., et al. (2020). Animal models for COVID-19. *Nature* 586, 509–515. doi: 10.1038/s41586-020-2787-6

Munoz-Fontela, C., Widerspick, L., Albrecht, R. A., Beer, M., Carroll, M. W., de Wit, E., et al. (2022). Advances and gaps in SARS-CoV-2 infection models. *PLoS Pathog.* 18, e1010161. doi: 10.1371/journal.ppat.1010161

Munster, V. J., Feldmann, F., Williamson, B. N., van Doremalen, N., Perez-Perez, L., Schulz, J., et al. (2020). Respiratory disease in rhesus macaques inoculated with SARS-CoV-2. *Nature* 585, 268–272. doi: 10.1038/s41586-020-2324-7

Netland, J., Meyerholz, D. K., Moore, S., Cassell, M., and Perlman, S. (2008). Severe acute respiratory syndrome coronavirus infection causes neuronal death in the absence of encephalitis in mice transgenic for human ACE2. *J. Virol.* 82, 7264–7275. doi: 10.1128/JVI.00737-08

Oreshkova, N., Molenaar, R. J., Vreman, S., Harders, F., Oude Munnink, B. B., Hakze-van der Honing, R. W., et al. (2020). SARS-CoV-2 infection in farmed minks, the Netherlands, April and May 2020. *Euro Surveill.* 25, 2001005. doi: 10.2807/1560-7917.ES.2020.25.23.2001005

Reyna, R. A., Kishimoto-Urata, M., Urata, S., Makishima, T., Paessler, S., and Maruyama, J. (2022). Recovery of anosmia in hamsters infected with SARS-CoV-2 is correlated with repair of the olfactory epithelium. *Sci. Rep.* 12, 628. doi: 10.1038/s41598-021-04622-9

Rockx, B., Kuiken, T., Herfst, S., Bestebroer, T., Lamers, M. M., Oude Munnink, B. B., et al. (2020). Comparative pathogenesis of COVID-19, MERS, and SARS in a nonhuman primate model. *Science* 368, 1012–1015. doi: 10.1126/science.abb7314

Sharun, K., Tiwari, R., Natesan, S., and Dhama, K. (2021). SARS-CoV-2 infection in farmed minks, associated zoonotic concerns, and importance of the one health approach during the ongoing COVID-19 pandemic. *Vet. Q.* 41, 50–60. doi: 10.1080/01652176.2020.1867776

Sharun, K., Tiwari, R., Patel, S. K., Karthik, K., Iqbal Yatoo, M., Malik, Y. S., et al. (2020). Coronavirus disease 2019 (COVID-19) in domestic animals and wildlife: advances and prospects in the development of animal models for vaccine and therapeutic research. *Hum. Vaccin. Immunother.* 16, 3043–3054. doi: 10.1080/21645515.2020.1807802

Shi, J., Wen, Z., Zhong, G., Yang, H., Wang, C., Huang, B., et al. (2020). Susceptibility of ferrets, cats, dogs, and other domesticated animals to SARS-coronavirus 2. *Science* 368, 1016–1020. doi: 10.1126/science.abb7015

Shou, S., Liu, M., Yang, Y., Kang, N., Song, Y., Tan, D., et al. (2021). Animal models for COVID-19: hamsters, mouse, ferret, mink, tree shrew, non-human primates. *Front. Microbiol.* 12, 626553. doi: 10.3389/fmicb.2021.626553

Shuai, L., Zhong, G., Yuan, Q., Wen, Z., Wang, C., He, X., et al. (2021). Replication, pathogenicity, and transmission of SARS-CoV-2 in minks. *Natl. Sci. Rev.* 8, nwaa291. doi: 10.1093/nsr/nwaa291

Sia, S. F., Yan, L. M., Chin, A. W. H., Fung, K., Choy, K. T., Wong, A. Y. L., et al. (2020). Pathogenesis and transmission of SARS-CoV-2 in golden hamsters. *Nature* 583, 834–838. doi: 10.1038/s41586-020-2342-5

Woolsey, C., Borisevich, V., Prasad, A. N., Agans, K. N., Deer, D. J., Dobias, N. S., et al. (2021). Establishment of an African green monkey model for COVID-19 and protection against re-infection. *Nat. Immunol.* 22, 86–98. doi: 10.1038/s41590-020-00835-8

Yu, P., Qi, F., Xu, Y., Li, F., Liu, P., Liu, J., et al. (2020). Age-related rhesus macaque models of COVID-19. *Anim. Model Exp. Med.* 3, 93–97. doi: 10.1002/ame2.12108

Zhou, P., Yang, X. L., Wang, X. G., Hu, B., Zhang, L., Zhang, W., et al. (2020). A pneumonia outbreak associated with a new coronavirus of probable bat origin. *Nature* 579, 270–273. doi: 10.1038/s41586-020-2012-7

Conflict of Interest: The authors declare that the research was conducted in the absence of any commercial or financial relationships that could be construed as a potential conflict of interest.

frontiers | Frontiers in Microbiology

ORIGINAL RESEARCH
published: 24 June 2022
doi: 10.3389/fmicb.2022.917324

Phylogenomics and Spatiotemporal Dynamics of Bovine Leukemia Virus Focusing on Asian Native Cattle: Insights Into the Early Origin and Global Dissemination

*Kohei Nishikaku[1], Takahiro Yonezawa[2], Masahide Nishibori[3], Masashi Harada[4], Fuki Kawaguchi[5], Shinji Sasazaki[5], Yasushi Torii[1], Kazuhiko Imakawa[6], Kuniko Kawai[7], Jianquan Liu[8], Hideyuki Mannen[5] and Tomoko Kobayashi[1]**

[1] Laboratory of Animal Health, Department of Animal Science, Faculty of Agriculture, Tokyo University of Agriculture, Atsugi, Japan, [2] Laboratory of Animal Genetics, Department of Animal Science, Faculty of Agriculture, Tokyo University of Agriculture, Atsugi, Japan, [3] Laboratory of Animal Genetics, Graduate School of Integrated Sciences for Life, Hiroshima University, Higashi-Hiroshima, Japan, [4] Laboratory Animal Center, Osaka City University Graduate School of Medicine, Osaka, Japan, [5] Laboratory of Animal Breeding and Genetics, Graduate School of Agricultural Science, Kobe University, Kobe, Japan, [6] Laboratory of Molecular Reproduction, Research Institute of Agriculture, Tokai University, Kumamoto, Japan, [7] Department of Biology, School of Biological Science, Tokai University, Sapporo, Japan, [8] Key Laboratory for Bio-Resource and Eco-Environment of Ministry and Education, College of Life Sciences, Sichuan University, Chengdu, China

Bovine leukemia virus (BLV), the causative agent of enzootic bovine leukosis, is currently one of the most important pathogens affecting the cattle industry worldwide. Determining where and in which host it originated, and how it dispersed across continents will provide valuable insights into its historical emergence as the cattle pathogen. Various species in the *Bos* genus were domesticated in Asia, where they also diversified. As native cattle (taurine cattle, zebu cattle, yak, and water buffalo) are indigenous and adapted to local environments, we hypothesized that Asian native cattle could have harbored BLV and, therefore, that they were important for virus emergence, maintenance, and spread. In this study, phylogeographic and ancestral trait analyses—including sequences obtained from Asian native cattle—were used to reconstruct the evolutionary history of BLV. It was shown that, since its probable emergence in Asia, the virus spread to South America and Europe via international trade of live cattle. It was inferred that zebu cattle were the hosts for the early origin of BLV, while taurine cattle played the significant role in the transmission worldwide. In addition, the results of positive selection analysis indicate that yak had a substantially minor role in the transmission of this virus. In this study, endogenous deltaretrovirus sequences in bats, collected in Asian countries, were also analyzed on whether these sequences were present in the bat genome. Endogenous deltaretrovirus sequences were detected from bat species endemic to specific regions and geographically isolated for a long

OPEN ACCESS

Edited by:
Douglas Paul Gladue, Plum Island Animal Disease Center, Agricultural Research Service, United States Department of Agriculture, United States

Reviewed by:
Roberto Nardini, Istituto Zooprofilattico Sperimentale del Lazio e della Toscana "M. Aleandri," Italy
Julian Ruiz-Saenz, Cooperative University of Colombia, Colombia

***Correspondence:**
Tomoko Kobayashi
tk205370@nodai.ac.jp

Specialty section:
This article was submitted to Virology, a section of the journal Frontiers in Microbiology

Received: *13 April 2022*
Accepted: *30 May 2022*
Published: *24 June 2022*

Citation:
Nishikaku K, Yonezawa T, Nishibori M, Harada M, Kawaguchi F, Sasazaki S, Torii Y, Imakawa K, Kawai K, Liu J, Mannen H and Kobayashi T (2022) Phylogenomics and Spatiotemporal Dynamics of Bovine Leukemia Virus Focusing on Asian Native Cattle: Insights Into the Early Origin and Global Dissemination. Front. Microbiol. 13:917324. doi: 10.3389/fmicb.2022.917324

time. Endogenous deltaretrovirus sequences from these geographically isolated species represent ancient exogenous deltaretroviruses distributions. The phylogenetic analysis revealed that these newly obtained endogenous deltaretrovirus sequences were closely related to those of BLV from Asian native cattle, indicating that BLV-related ancient deltaretroviruses circulated in Asia long before the emergence of BLV. Together, our analyses provide evidence for origin and spatiotemporal dynamics of BLV.

Keywords: bovine leukemia virus (BLV), deltaretrovirus, endogenous retrovirus (ERV), virus evolution, retrovirus, Phylodynamics

INTRODUCTION

The rapid growth of the global cattle industry has been associated with changes in the spatial dynamics and types of pathogens in cattle population. Over the years, the domestication of wild cattle and/or the cross-breeding of indigenous animals with domesticated ones, which affect disease dynamics, resulting in emergence of pathogens. Moreover, the increasing global trade of live animals and selective breeding also elevate the risk of dissemination of pathogenic viruses (Perry et al., 2013).

Bovine leukemia virus (BLV) is one of the emerging pathogens in cattle population, and it belongs to the *deltaretrovirus* genus, *Retroviridae* family (Aida et al., 2013). BLV causes enzootic bovine leukosis (EBL), which is the most common neoplastic disease with B-cell lymphosarcoma in cattle. Although only a small fraction (3∼5%) of BLV-infected cattle develop lymphosarcoma, EBL is responsible for significant economic losses in dairy and beef cattle farms worldwide. EBL is listed as a disease of importance to international trade by OIE (the World Organization for Animal Health) (Ott et al., 2003; Benitez et al., 2020).

EBL in cattle was first reported in Germany in 1878 (Boeke and Stoye, 1997). The disease gradually spread from the initial endemic area of Memel in East Prussia (now Klaipeda, in Lithuania) along the coasts of the Baltic Sea by approximately 1920 (Sihvonen, 2015). During the two world wars, massive international trades of cattle probably contributed to the spread of BLV across Europe and other countries (Bendixen, 1963). In the mid-twentieth century, EBL had been reported in most cattle raising countries. BLV infections in Western Europe have been eradicated and remain free of infection to this day through continuous surveillance and eradication programs (OIE, 2021). However, BLV is still common in Canada, the United States, and many countries in eastern Europe, South America, and Asia (Polat et al., 2017). Previous detailed phylogenetic studies have indicated that BLV can be divided into at least 10 genotypes associated with different geographic distributions (Polat et al., 2017). For example, genotype 1 is found all over the world, genotype 4 is mainly found in Europe and Russia, and genotypes 6 and 10 are mainly found in Asia (Polat et al., 2017). As cell-free viruses are unstable, close physical contact and exchange of infected lymphocytes, or body fluids, are required for BLV transmission (Constable et al., 2017). Therefore, the worldwide distribution of BLV genotypes between distant geographic locations has been probably driven by the virus spreading through the transport of live infected animals.

Given the wide geographic distribution of BLV, little is known about the place or region where BLV originated. Europe is considered as the historical origin of EBL, however, while taurine cattle (*Bos taurus*) was introduced to Europe during the Neolithic period (8,000 years ago), the earliest record of the symptoms associated with BLV dates back to only 140 years ago (Scheu et al., 2015). This historical context raises the possibility that the emergence and rapid spread of BLV in taurine cattle populations occurred recently. BLV predominantly infects taurine cattle, but a number of studies reported that it also infects Asian native cattle, such as zebu (*B. indicus*), yak (*B. grunniens*) and, sporadically, water buffalo (*Bubalus bubalis*) (Ma et al., 2016; Wang et al., 2018). However, BLV dissemination routes relative to roles each host species played remain unknown.

Most agree with the thoughts that bats are reservoirs of emerging viruses. It was shown that bats could harbor exogenous retroviruses (Hayward et al., 2020). In fact, bats have been reservoirs for emerging viral diseases, including Hendra virus, Nipah virus, Marburg virus and Ebola virus, severe acute respiratory syndrome (SARS) virus as well as the current pandemic SARS-CoV-2 (Irving et al., 2021). Therefore, bats could be considered as the comparative phylogeography of widespread, co-distributed species, providing unique insights into regional biodiversity and diversification patterns (Roberts, 2006). Previous studies have reported that endogenous deltaretrovirus sequences are present in the bat genome (Farkasova et al., 2017; Hron et al., 2019). Although bat species are distributed worldwide, some species are endemic to specific regions and geographically isolated for a long time (Millien-Parra and Jaeger, 1999). Endogenous deltaretrovirus sequences from these geographically isolated species represent ancient exogenous deltaretroviruses distributions.

The aim of this study was to gain the information on the area, original host, and dispersal route of BLV, focusing in particular on Asian native cattle. In the present study, BLV infections were epidemiologically analyzed, and BLV proviral sequences were obtained from extensively collected samples of Asian native cattle. Bayesian phylogeographic techniques were used to infer the origin and dispersal routes of BLV. We then combined geographic distribution of bat species and phylogenetic relationships of bat endogenous

deltaretrovirus sequences with BLV to further validate Asian origin of BLV. The data generated through this study provide evidence that BLV was transmitted from Asian zebu cattle to taurine cattle and was then disseminated throughout the world.

RESULTS

Detection of Proviral Genome and Analysis of the Bovine Leukemia Virus Genetic Lineage in Native Cattle

To analyze the epidemiological distribution and obtain the BLV sequences from Asian native cattle, archived field samples from 256 zebu cattle (*B. indicus*), 16 native taurine cattle (*B. taurus*), 268 yaks (*B. grunniens*), and eight water buffaloes (*Bubalus bubalis*) collected in 11 Asian countries were used. In addition, samples from 37 zebu cattle in Madagascar were also analyzed. Among these samples, the BLV proviral DNA was detected in zebu cattle samples obtained from seven countries (Bhutan, Cambodia, Laos, Myanmar, Philippine, Vietnam, and Madagascar), native taurine cattle samples from Republic of Kazakhstan, and yak samples from three countries (China, Nepal, and Pakistan), while the proviral DNA was not detected in water buffalo samples (**Table 1**). These results indicate that BLV is widely distributed in Asian native cattle population (within the *Bos* genus).

Among these BLV-positive samples, sequences of the BLV *envelope glycoprotein gp51* gene (*BLVgp51*) were obtained from zebu cattle from Laos ($n = 2$), Myanmar ($n = 3$), Vietnam, Bhutan ($n = 1$), Madagascar ($n = 1$), and native taurine cattle from Kazakhstan ($n = 5$). The maximum likelihood (ML) phylogenetic analysis revealed that all sequences were classified into genotypes that have been previously reported (genotypes 1, 4, and 10) (**Figure 1** and **Table 1**).

Phylodynamic Analysis of Bovine Leukemia Virus From Asian Native Cattle

To gain insights into the temporal and spatial dissemination of BLV in Asian native cattle, the full length *BLVgp51* sequences were analyzed using a Bayesian Markov Chain Monte Carlo (MCMC) phylogeographic approach (**Figure 2** and **Table 2**). The maximum clade credibility (MCC) tree revealed that BLV sequences were segregated into two reciprocally monophyletic clusters, lineage I and lineage II, in 1791 (95% HPD: 1640–1889) and 1817 (95% HPD: 1680–1912), respectively (posterior probability = 1). BLV sequences from most zebu cattle and all yak samples obtained in Asian countries fell into lineage II, while sequences from taurine cattle samples from all over the world fell into lineage I.

To estimate where and which host BLV originated, ancestral traits at all internal tree nodes were reconstructed by a parsimony-based algorithm. The results of the analysis using sampling locations as terminal taxa showed that BLV sequences obtained from Asia reconstructed at the BLV root in 100% (node ID: A in **Figure 3B**), suggesting that BLV originated in Asia. Similarly, the results of the analysis using host species as terminal taxa showed that zebu cattle reconstructed at the BLV root in 100% (node ID: A in **Figure 3A**), suggesting that the ancestral host of BLV is zebu cattle. Overall, these results indicate that BLV was likely to have originated in Asian zebu cattle.

Positive Selection Analysis of Bovine Leukemia Virus Sequences in Each Lineage

To investigate whether lineages I and II appeared because of viral adaptation, BLV sequences from each lineage were separately analyzed for positive selection by using the CODEML site test in the Phylogenetic Analysis by Maximum Likelihood (PAML) program package. The non-synonymous (dN) and synonymous (dS) substitution rates of BLV envelope sequences were calculated. The Bayes empirical Bayes calculation of posterior probabilities in PAML identified five amino acids (121, 281, 290, 291, and 301) as being under positive selection with posterior probability >0.50 in the BLV sequences of lineage II (**Figure 4A**). The selected sites likely correspond to predicted BLV receptor binding sites (**Figure 4A**). Among the sequences classified in linage II, variants in three positively selected sites were only detected in BLV sequences from yaks (**Figure 4B**). No evidence of selection was detected for lineage I (data not shown).

Identification of Major Bovine Leukemia Virus Migratory Routes

To analyze BLV migration pathways in detail, the sampling locations were divided into 11 geographic areas (**Figure 5A**). In the results of the root state posterior probabilities (RSPP) of the tree location files obtained from BEAST analysis, Southeast Asia showed the highest RSPP value, indicating that the BLV progenitor is likely to have emerged in Asia (PSPP = 0.277, **Figure 5B**). Using the discrete phylogeographic model, the BLV dataset analysis identified a total of 46 well-supported transmission routes through the Bayes factor (BF) test using a cutoff value of three (**Table 3**). Based on the results of the ancestral trait reconstruction (**Figure 3B**), following the initial emergence of BLV in Asia, the progenitor of BLV lineage I reached Europe in 1824 (95% HDP, 1697–1912, node ID: C), and it subsequently reached South America in 1850 (95% HDP, 1744–1923, node ID: D). Then, the spread of BLV from South America to the United States and Mexico began in 1942 (95% HDP, 1913–1972; node ID: D) (**Figure 3** and **Table 2**). Potential transcontinental BLV spreads were also detected from North America to Japan, from Europe to Russia, and from Southeast Asia to China in 1950 (**Table 3** and **Figure 3**, summarized in **Figure 5C**). The Bayesian skyline plot analysis indicated that the effective population size significantly increased during the mid-1900s, followed by a slight decline after the 2000s (**Figure 5D**).

Endogenous Deltaretrovirus Sequences From Asian Bats

To obtain information about the long-term evolution of BLV in Asia, archived bat samples, which were collected in Asian countries were analyzed for the presence of endogenous deltaretrovirus sequences in their genome. Specifically, the

TABLE 1 | Detection of bovine leukemia virus (BLV) proviral genome in Asian native cattle.

Species	Countries	Collection year	Samples tested	*n*[a]	*env* PCR positive	*LTR* PCR positive	Positive (%)	(/All)	Obtained sequences	Genotype		
										1	4	10
Zebu cattle (*Bos indicus*) (*n* = 293)												
	Bhutan	2010	Blood	47	3	NT[b]	6.4	(3/47)	1	1	–[c]	–
	Cambodia	2001–2003	Blood	20	1	NT	5	(1/20)	0	–	–	–
	Laos	2011	Blood	47	10	NT	21.3	(10/47)	2	–	–	2
	Myanmar	2001, 2002	Blood	65	8	NT	12.3	(8/65)	3	–	–	3
	Philippines	2019	Blood	29	1	NT	3.4	(1/29)	0	–	–	–
	Vietnam	1996, 1997	Blood	48	3	NT	6.3	(3/48)	1	1	–	–
	Madagascar	2016, 2017	Blood	37	3	NT	8.1	(3/37)	1	–	–	1
Taurine cattle (*Bos taurus*) (*n* = 16)												
	Republic of Kazakhstan	2015	Blood	16	7	NT	43.7	(7/16)	5	-	5	-
Yak (*Bos grunniens*) (*n* = 268)												
	China	2011, 2013, 2015, 2017, 2018	Skin	97	NT	20	20.6	(20/97)	0	–	–	–
	Kyrgyzstan	2019	Blood	12	0	0	0	(0/12)	0	–	–	–
	Nepal	2018	Blood	72	NT	13	18	(13/72)	0	–	–	–
	Pakistan	2018	Skin	87	NT	16	18.3	(16/87)	0	–	–	–
Water Buffalo (*Bubalus bubalis*) (*n* = 8)												
	China	2018	Skin	8	NT	0	0	(0/8)	0	–	–	–
Total				585	36	49	14.5	(85/585)	13	2	5	6

[a]*Number of samples tested for BLVgp51 or LTR proviral DNA.*
[b]*Not tested.*
[c]*Not detected.*

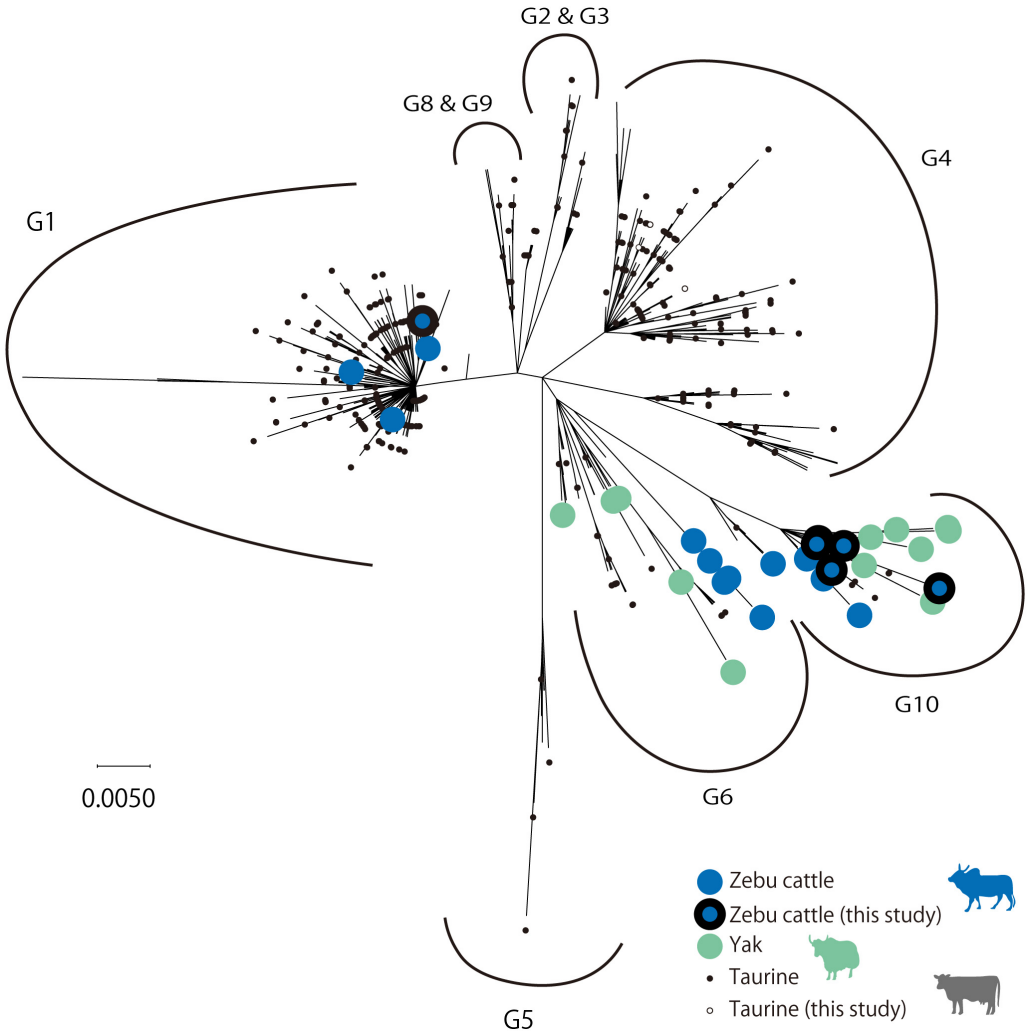

FIGURE 1 | Maximum likelihood (ML) phylogenetic tree of *BLVgp51* partial sequences. ML phylogenetic tree of the *BLVgp51* partial sequences (444 bp) derived from 699 bovine leukemia virus (BLV) sequences. The tree was constructed using the *BLVgp51* sequences from 13 native cattle in this study and 686 sequences from known BLV. The year and the location of sequence data collected were obtained from the GenBank database. Genotypes 1 through 10 are indicated by the letter "G." Native cattle are indicated by large circles, with zebu cattle and yak being identified by blue and gray colors, respectively; the sequences obtained in this study are surrounded by a black border. Taurine cattle are indicated by a small circle, and the sequences obtained in this study are represented by a white circle.

TABLE 2 | Time to most recent common ancestor (tMRCA) inferred from Bayesian analysis of BLVgp51 sequences.

Coalescent event	Node ID	Median	(95% HPD[a])
BLV root	A	1761	(1588–1871)
Lineage 1	B	1791	(1640–1889)
Genotype 4 and 7 root	C	1824	(1697–1912)
Genotype 1, 2, 3, 8, and 9 root	D	1850	(1744–1923)
Genotype 1 (United States/Mexico) root	E	1942	(1913–1972)
Genotype 4 root	F	1904	(1837–1954)
Lineage 2	G	1817	(1680–1912)
Genotype 6 root	H	1844	(1830–1961)
Genotype 10 root	I	1904	(1722–1930)

[a]*95% highest probability densities estimates.*

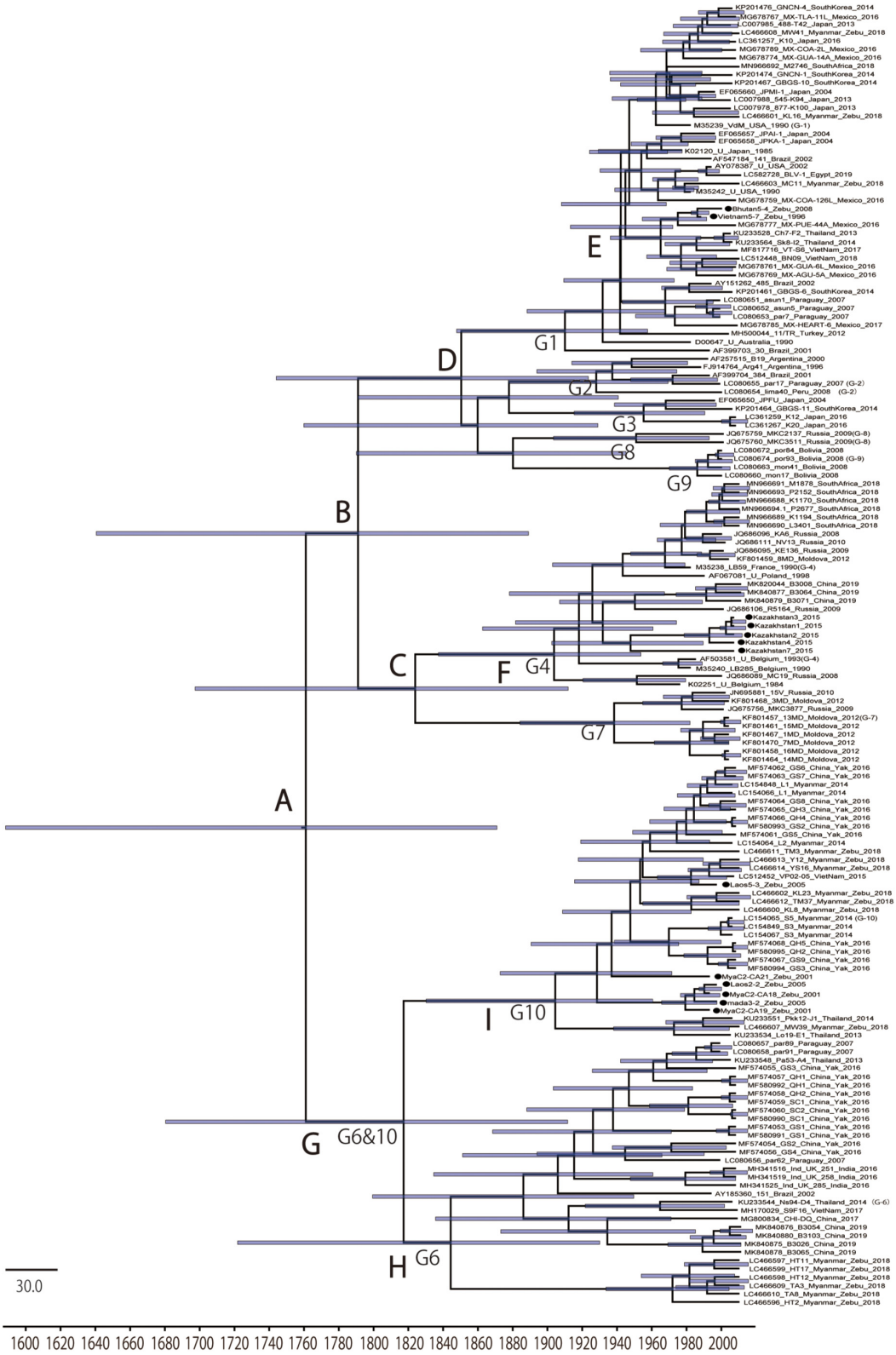

FIGURE 2 | Maximum clade credibility (MCC) tree of *BLVgp51*. Time-scaled maximum clade credibility (MCC) tree inferred from *BLVgp51* sequences (502–903 bp) of native cattle (n = 13, indicated by the black circle) and worldwide bovine leukemia virus (BLV) sequences (n = 143). Bars at nodes indicate a 95% HPD of tMRCA. The node abbreviations "G1–G10" and "A–I" indicate the BLV genotypes and the node ID, respectively, based on the coalescent event (node ID; **Table 2**). The sequences obtained in this study are marked by a black circle.

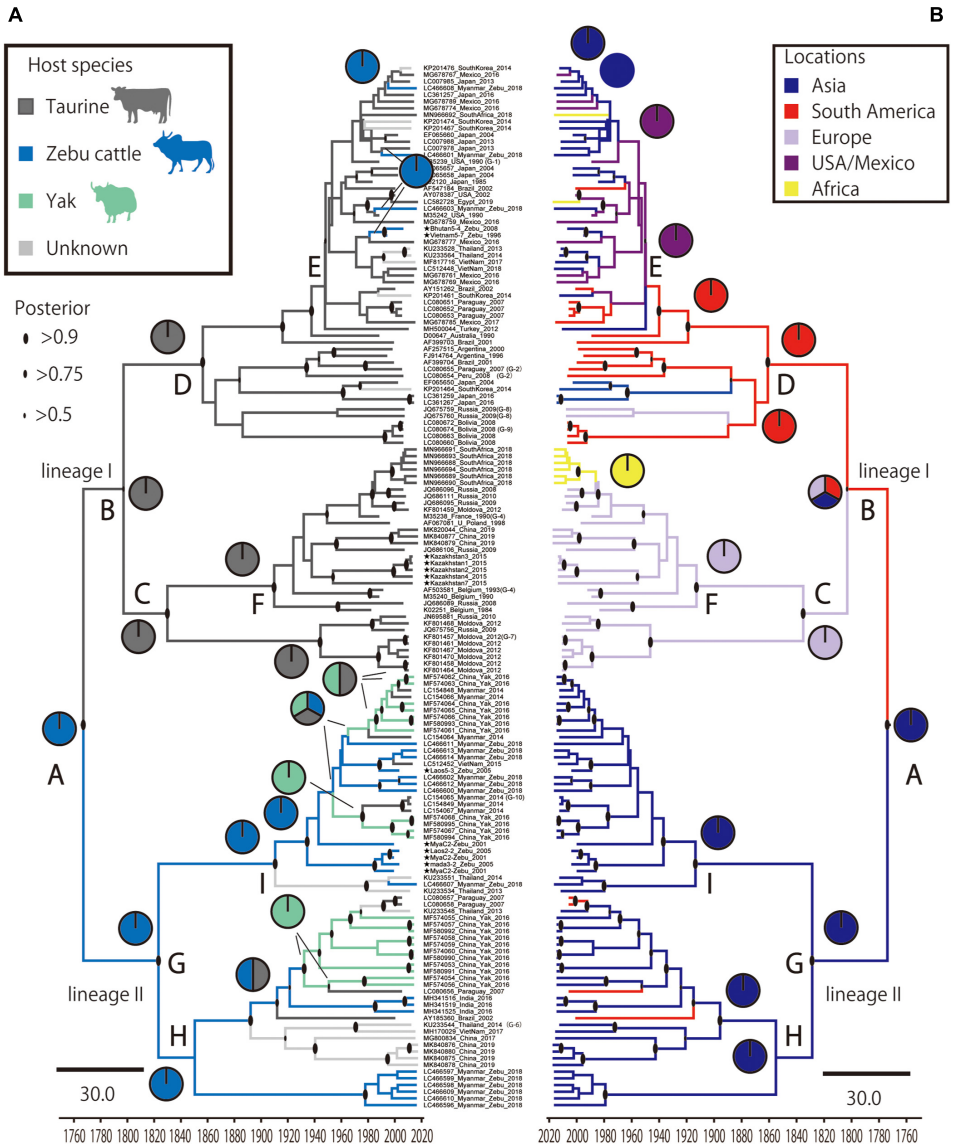

FIGURE 3 | Time scale phylogenetic tree and ancestral state reconstruction. Ancestral states of hosts **(A)** and locations **(B)** in bovine leukemia virus (BLV) were estimated using the maximum parsimony method in Mesquite using the MCC tree. On the left, the node pie-charts and branch colors for the host species indicate taurine cattle, zebu cattle, and yak, respectively; on the right, the node pie-charts and branch colors for the locations show Asia, South America, Europe, United States/Mexico, and Africa, respectively. The posterior probability of the MCC tree is indicated by the size of the black circle at each node. The node abbreviations **(A–I)** indicate the node ID based on the coalescent event (node ID; **Table 2**).

DNA samples of 41 bat species from eight bat families found in 10 Asian countries were examined (**Table 4**). The endogenous deltaretrovirus *long terminal repeats* (*LTR*) were detected in 19 bat species. Among these bat species, 17 are indigenous and mainly distributed in Asia. Moreover, three species (*Rhinolophus pumilus*, *R. perditus*, and *Hipposideros turpis*) were endemic to the Ryukyu Islands, which located at the southern part of the Japanese archipelago. Since the Ryukyu Islands are surrounded by deeper marine straits and were not connected to the mainland during the whole Quaternary, these results indicated that endogenous deltaretrovirus sequences have circulated in Asia around the end of Neogene Period (Millien-Parra and Jaeger, 1999). Moreover, the ML phylogenetic analysis using partial *LTR* sequences obtained from the analyzed samples revealed that endogenous deltaretrovirus sequences obtained from bats endemic to Asia were closely related to the BLV *LTR* of lineage II (**Figure 6**). As some endogenous deltaretrovirus positive bat species were diverged and distributed in Asia during the late Miocene to Pliocene, these results indicate that BLV-related ancient deltaretroviruses circulated in Asia long before the emergence of BLV (**Figure 6**).

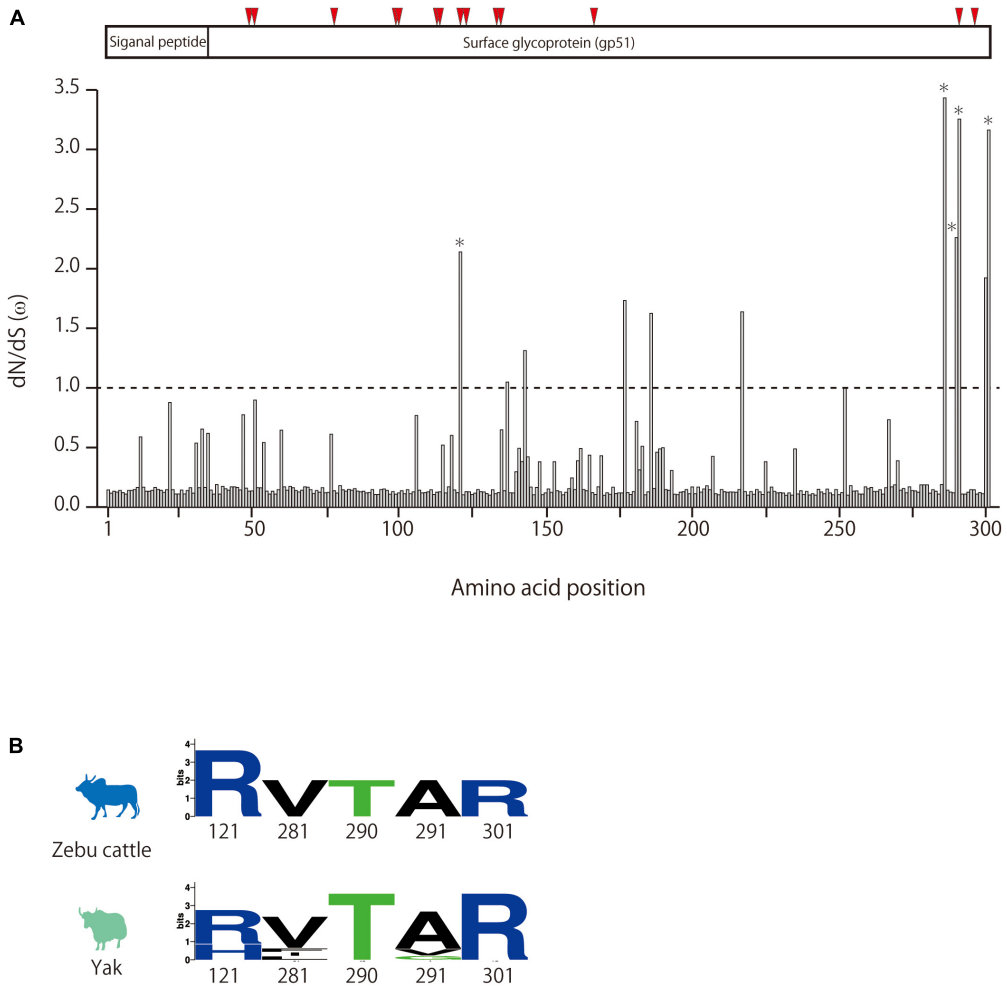

FIGURE 4 | Detection of positive selection pressure of BLVgp51 in bovine leukemia virus (BLV) lineage II using the PAML package site model. **(A)** dN/dS (ω) of BLVgp51 in BLV lineage II analyzed by site model. The Bayes empirical Bayes (BEB) method in the site model were used to infer the amino acid sites under positive selection. Weak evidence of positive selection was observed at five amino acid sites (indicate by *) in BLV lineage II. The proteins coded by BLVgp51 is displayed at the top of the figure. The binding sites for boAP3D1—one of the receptors for BLV—are indicated by red triangles (positions: 48, 50, 77, 98, 99, 112, 120, 135, 136, 187, 292, and 298). **(B)** The amino acid composition of the positive selection of zebu cattle and yak in BLV lineage II is visualized in Weblogo.

DISCUSSION

Bovine leukemia virus is highly prevalent in cattle worldwide, however, little is known about its emergence and evolutionary history. This in part reflects the fact that our current understanding of BLV diversity comes almost exclusively from domesticated, phenotypically and genetically selected taurine cattle. Native cattle are highly adapted to local environments and resources and are not so often exported to other countries compared to the major commercial cattle breeds (Ajmone-Marsan et al., 2010). Therefore, it was hypothesized that Asian native cattle could have harbored BLV, causing them to be important for virus emergence, maintenance, and spread (Chen et al., 2010; Qiu et al., 2012; Decker et al., 2014). This study represents the first analysis of genetic diversity of BLV in a wide range of native cattle population in Asia, and the first application of Bayesian phylogeographic analysis to gain new insights into the epidemiological and spatiotemporal dynamics of BLV. Together with the results from endogenous deltaretrovirus sequences obtained from the genome of indigenous Asian bats, these data provide evidence for origin and evolutionary dynamics of BLV.

The results of the phylodynamic and ancestral trait reconstruction analyses reveal that progenitor of BLV originally circulated in Asia (**Figure 3B**). This conclusion was also supported by the high RSPP value for Southeast Asia obtained from the BEAST analysis (RSPP = 0.227 for Southeast Asia; **Figure 5B**). Although our results are not consistent with the report of the first EBL cattle in Germany, Asia is still a potential geographic region where the emergence and maintenance of BLV could have occurred (Bendixen, 1963). BLV exhibits a relatively narrow host range and predominantly infects the *Bos* genus. Not only taurine cattle, but also diverse *Bos* species such as zebu, banteng, and gaur originated and were domesticated in Asia (Fuller, 2006; Melletti and Burton, 2014;

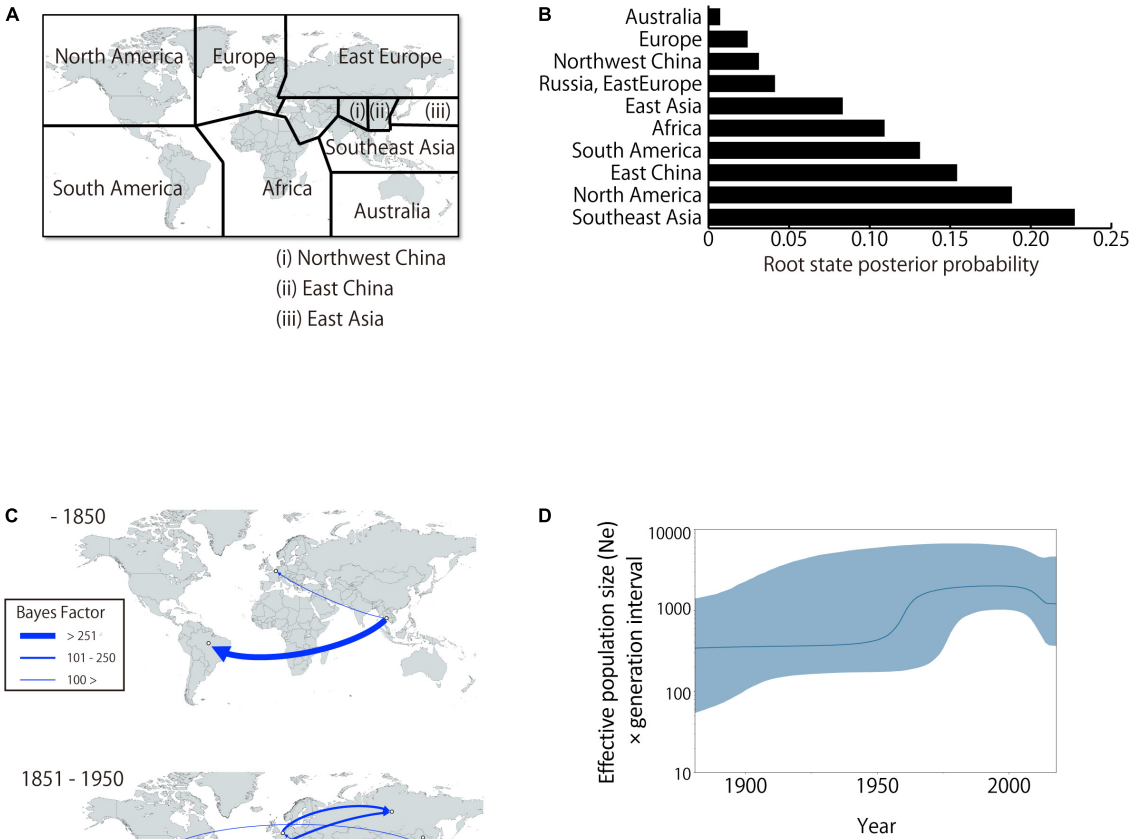

FIGURE 5 | Global dissemination routes and effective population size of bovine leukemia virus (BLV). **(A)** Area delimitation in biogeographic analysis. **(B)** The posterior probabilities for the root state locations. **(C)** Bayesian stochastic search variable selection was used to infer dispersal routes with the Bayes factor. Dispersal routes that presented a significant support (Bayes factor ≥ 3) are plotted. **(D)** Plot depicting changes in the Effective population size (Ne) × generation interval. The dark line shows the effective population size estimated through time. The blue shaded areas correspond to the 95% HPD.

Perez-Pardal et al., 2018). These species have been extensively cross-bred with other species of the *Bos* genus through the process of adaptation. This historical background may explain why the phylodynamic model inferred that Southeast Asia was the ancestral location of BLV origin. Further studies, including surveillance of diverse *Bos* species using a wide range of samples, will be needed to determine the more detailed geographic origin of BLV.

The results of ancestral trait reconstruction analysis reveal that zebu cattle were the source of BLV introduction into the taurine cattle population (**Figure 3**). This is also supported by the identification of a monophyletic clade, mainly constituted by zebu cattle and yak BLV (lineage II), sharing a MRCA with taurine BLV (lineage I). Lineage II also includes yak sequences, indicating that this animal should also be a source of cross-species transmission to taurine cattle. However, from the results of the Bayesian phylodynamic analysis and ancestral trait reconstruction analysis of lineage II, zebu cattle were reconstructed at the MRCA of the lineage II root in 100% (node ID: H and I in **Figure 3A**), suggesting that BLV in the yak

TABLE 3 | Connections between significant location pairs and their corresponding Bayes factor (BF).

Route No.	BF*	Locations**	
1	1327.3	Northwest China	North America
2	824.1	Northwest China	East China
3	775.7	East Asia	Russia, East Europe
4	635.2	Central Asia	Europe
5	505.8	Central Asia	Northwest China
6	374.2	Northwest China	Southeast Asia
7	373.7	Africa	North America
8	365.0	Northwest China	Russia, East Europe
9	327.4	East Asia	East China
10	309.8	East Asia	Australia
11	306.2	South America	Southeast Asia
12	298.7	Central Asia	East China
13	296.1	Central Asia	South America
14	273.7	South America	North America
15	226.0	East Asia	Northwest China
16	224.1	Northwest China	Europe
17	204.2	Russia, East Europe	North America
18	183.7	Central Asia	Africa
19	181.7	East China	South America
20	181.5	Northwest China	Australia
21	163.8	East China	Southeast Asia
22	160.9	North America	Australia
23	157.5	Central Asia	North America
24	147.2	East China	Africa
25	127.5	Russia, East Europe	South America
26	123.6	Europe	North America
27	120.5	South America	Australia
28	117.3	Northwest China	South America
29	109.7	Central Asia	Australia
30	105.1	Africa	Southeast Asia
31	93.2	Europe	Southeast Asia
32	87.6	Russia, East Europe	Africa
33	75.3	Africa	Australia
34	66.9	Europe	Australia
35	66.7	Russia, East Europe	Europe
36	61.4	East China	Europe
37	58.8	East Asia	Africa
38	46.1	Europe	Africa
39	44.2	East Asia	North America
40	40.6	East China	North America
41	33.3	Central Asia	Russia, East Europe
42	32.4	East China	Russia, East Europe
43	31.8	Northwest China	Africa
44	26.6	East China	Australia
45	26.2	Central Asia	Southeast Asia
46	11.3	Southeast Asia	North America

**Only transitions with BF > 3 are presented.*

***Countries or provinces included in each region: East China, Heilongjiang province; Northwest China, Gansu province; East Asia, Japan and South Korea; Southeast Asia, Myanmar, Bhutan, Thailand, Laos, and Vietnam; Europe, Belgium, Poland, Germany, and France; East Europe, Moldova, Africa include South Africa, and Egypt; North America, United States and Mexico; South America, Brazil, Paraguay, Argentina, Bolivia, and Peru (**Figure 5C**).*

population is the result of recent cross-species transmission from zebu cattle. These results are further supported by the positive selection analysis, which showed that the *BLVgp51* sequences from yak displayed a higher diversity and positive selection sites near predicted receptor binding sites (**Figure 4**). As the habitat of yak is limited to high altitude areas, it is concluded that the role of this animal played for the transmission cycle may be limited (Qiu et al., 2012).

TABLE 4 | List of the bat species analyzed.

Family	Scientific name	Sampling location		Sample IDs	LTR PCR positive samples /number of samples tested	Primer name in Supplementary Table 1 used for LTR amplification
		Country	Region			
Rhinolophidae (*n* = 10)						
	*Rhinolophus nippon***	Japan	Honshu	OCUM7420	1/1	B
		South Korea	-	OCUM5272	0/1	
	*Rhinolophus pumilus***	Japan	Ryukyu islands	OCUM6988	1/1	B
	*Rhinolophus perditus***	Japan	Ryukyu islands	OCUM6038	1/1	B
	*Rhinolophus monoceros***	Taiwan	-	OCUM6830	1/1	B
	*Rhinolophus cornutus***	Japan	Honshu	OCUM6163	1/1	B
		China	Guangzhou	OCUM8059	1/1	B
	*Rhinolophus macrotis***	China	Guangzhou	OCUM8079	1/1	B
	*Rhinolophus formasae***	Taiwan	-	OCUM7972	1/1	B
	*Rhinolophus rouxi***	China	Sichuan	OCUM7047	0/1	
Hipposideridae (*n* = 9)						
	*Hipposideros turpis***	Japan	Ryukyu islands	OCUM6031, OCUM6036	2/2	A
	*Hipposideros terasensis***	Taiwan	-	OCUM6847	0/1	
	*Hipposideros bicolor***	China	Guangzhou	OCUM7790, OCUM7800	2/2	A
	*Hipposideros armiger***	China	Guangzhou	OCUM7785	0/1	
	*Hipposideros armiger***	Nepal	-	OCUM6256	0/1	
	*Hipposideros larvatus***	Cambodia	-	OCUM8352	1/1	A
	*Coelops frithi***	Taiwan	-	OCUM6834	1/1	A
Pteropodidae (*n* = 2)						
	*Cynopterus sphinx***	Thailand	-	OCUM7872	0/1	
	*Pteropus dasymallus***	Japan			1/1	B
Miniopteridae (*n* = 2)						
	*Miniopterus fuliginosus***	Japan	Honshu	OCUM4814	1/1	A
	*Miniopterus fuscus***	Japan	Ryukyu islands	OCUM7583	1/1	A
Megadermatidae (*n* = 1)						
	*Megaderma lyra***	Thailand	-	OCUM7689	1/1	A
Emballonuridae (*n* = 2)						
	Emballonura nivalis	Borneo	-	OCUM889	0/1	
	*Taphozous melanopogon***	Cambodia	-	OCUM8356	0/1	
Vespertilionidae (*n* = 18)						
	*Tylonicteris pachypus***	China	Guangzhou	OCUM8100	0/1	
	Scotophilus heathsii	Tiwan	-	OCUM8101	0/1	
	*Ia io***	China	Sichuan	OCUM7071	1/1	C
	*Nyctalus aviator***	Japan	-	OCUM7225	0/1	
	*Nyctalus furvus***	Japan	Hokkaido	RTMM309	0/1	
	*Plecotus sacrimontis***	Japan	-	OCUM5366	0/1	
	*Barbastella pacifica***	Japan	Hokkaido	HK01629[a]	0/1	
	*Myotis gracilis**	Japan	Hokkaido	EZ1200[a]	0/1	
	*Myotis petax**	Japan	Hokkaido	KK0021[a]	0/1	
	*Myotis longicaudatus**	Japan	Hokkaido	KK0010[a]	1/1	C
	*Myotis bombinus***	Japan	-	OCUM5545	0/1	
	*Myotis pruinosus***	Japan	-	OCUM7495	1/1	C
	*Myotis ikonnikovi**	Japan	Hokkaido	KK0062[a]	0/1	
	*Murina ussuriensis**	Japan	Hokkaido	KK0063[a]	0/1	
	*Murina hilgendorfi**	Japan	-	OCUM7413	0/1	
	*Pipistrellus abramus**	Japan	Miyagi	KKT	0/1	
	*Pipistrellus endoi**	Japan	Miyagi	KKT	0/1	

(Continued)

TABLE 4 | (Continued)

Family	Scientific name	Sampling location		Sample IDs	LTR PCR positive samples /number of samples tested	Primer name in Supplementary Table 1 used for LTR amplification
		Country	Region			
	*Vespertilio sinensis**	Japan	Hokkaido	KK0203[a]	0/1	
Molossidae (*n* = 1)						
	*Tadarida insignis**	Japan	Mie	KKT	0/1	

**Indigenous to Asia and Russia.*
***Indigenous to Asia.*
-unspecified.
OCUM: Sample collection of the Osaka City University Graduate School of Medicine (collected by Dr. Masashi Harada). RTMM309: Sample belongs to the Rishiri Town Museum (provided by Dr. Kuniko Kawai). KKT: Samples provided by Dr. Kuniko Kawai.
[a]*Samples belong to the Tokai University (collected by Dr. Kuniko Kawai).*

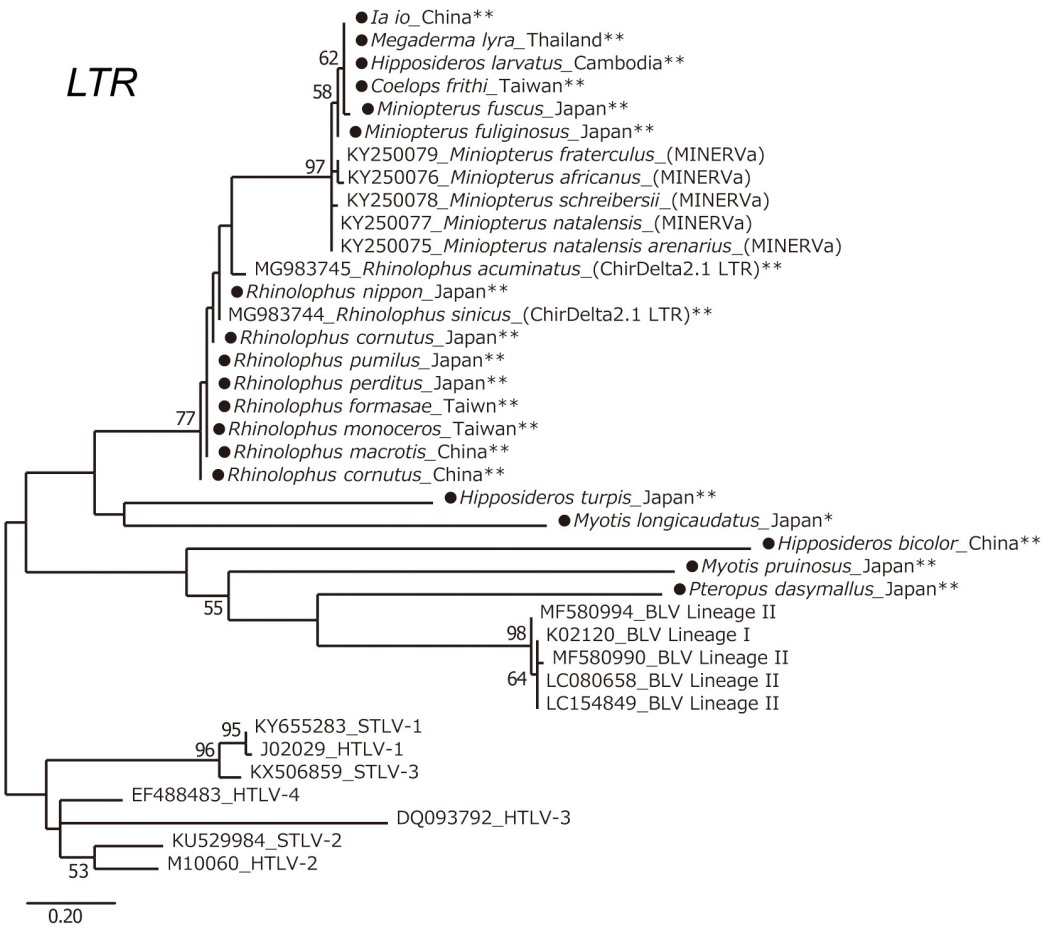

FIGURE 6 | Long terminal repeats (LTR) phylogenetic tree. Maximum likelihood (ML) phylogenetic tree based on deltaretrovirus LTR sequences. A ML phylogenetic tree was constructed from deltaretrovirus LTR sequences derived from 19 bat-specific endogenous deltaretroviruses in this study, and 19 sequences from known exogenous and endogenous deltaretroviruses obtained from GenBank. Sequences were aligned using ClustalW, and the phylogenetic tree was inferred by ML analysis in MEGA7. The robustness of the tree topology was evaluated with 1,000 bootstrap replicates. Bootstrap percentages greater than 50% are shown above branches. *Indigenous to Asia and Russia. **Indigenous to Asia. The sequences obtained in this study are marked by a black circle.

The results of the Bayesian phylodynamic analysis and ancestral trait reconstruction analysis of lineage I indicated that the ancestral BLV sequence of Asian zebu cattle was introduced to taurine cattle not only in South America, but also in Europe (**Figures 3B**, **5**, and route No. 31 of **Table 3**). Indeed, in the eighteenth century, zebu cattle were extensively exported from

Asia to South America, mainly to Brazil, and were cross-bred with local taurine cattle for genetic improvement (Felius et al., 2014). Our results indicate that this process may have contributed to the spread of BLV in the taurine population. On the other hand, it remains unclear how the BLV ancestor reached European countries, because zebu cattle were not introduced in large numbers to European countries. A possible explanation of the BLV spread in Europe could be that in the eighteenth century, western European countries were directly involved in trade with Asian countries as well as with South America via the Atlantic Ocean. Their major transit ports were used during transit on the route from Asia to South America. As a result, large numbers of live cattle from diverse countries in Asia, South America, and Europe may have temporarily been held in the same port, or in quarantine facilities, causing the risk of increased virus transmission in Europe (Acemoglu et al., 2005). It is known that zebu cattle that were en route to Brazil from India introduced the rinderpest to Belgium via the port of Antwerp (Mammerickx, 2003). After the spread of BLV in Europe, genotype 4 spread to Russia, diversified to genotype 7, and was thus maintained, while it was eradicated in Europe (Polat et al., 2017).

The present analysis, however, identifies taurine cattle as the host responsible for the later dissemination of BLV worldwide over time. This probably began after World War II, and it coincided with a drastic increase of live cattle trade between continents (Ajmone-Marsan et al., 2010). The phylogenetic analysis suggests that the BLV genotype 1 is predominantly distributed worldwide as a pandemic genotype, and its source location is South America (**Figure 3**, MRCA: D) (Polat et al., 2017). The global dispersal of genotype 1 appears to have occurred in two steps, starting with the widespread export of the virus from South America via the United States to the rest of the world around 1950, followed by local diffusion within the countries where it was introduced (**Figure 3**). The initial step coincided with the worldwide distribution of the established commercial breeds to many other countries, and the second step coincided with the cross breeding with local populations (Polat et al., 2017). The phylogenetic analysis also demonstrates that the significant increase in genetic diversity observed during the late-1900s, coincided with the increase of international animal trade activities (**Figure 5D**; Ajmone-Marsan et al., 2010; Felius et al., 2014). This increase in genetic diversity, which occurred worldwide, may be explained by the adaptation of BLV to the local cattle that presented diverse genetic backgrounds (**Figure 3**). The increase was then followed by a notable decline, which was associated with the successful eradication programs adopted in European countries (Polat et al., 2017).

In this study, endogenous deltaretrovirus sequences, which were closely related to BLV lineage II, were detected in the bat genome of several indigenous Asian species (**Table 4**). Previous studies suggest that bat species were infected with the ancestors of endogenous deltaretroviruses around the end of the Paleogene and beginning of the Neogene (Hron et al., 2019). The inferred date corresponds closely with the adaptive radiation of several bat clades and species including endogenous deltaretrovirus positive bat species; for example, the tMRCA of the *Myotis* and the *Hipposideros* Asian clade is estimated to be 8.8 MYA and 19.9 MYA, and the time of migration and genetic isolation of the Japanese population of *Rhinolophus nippon* is estimated to be 0.5 MYA (**Table 4**; Ruedi et al., 2013; Amador et al., 2018; Ikeda and Motokawa, 2021). On the other hand, molecular dating estimates in previous studies have suggested that the tribe Bovini rapidly diversified into the three subtribes—Bovina, Bubalina, and Pseudorygina—during the late Middle Miocene (around 13 MYA) (Melletti and Burton, 2014). As these ancestors of bats and Bovini subtribes are currently more diversified in Asia, it can be assumed that ancient exogenous deltaretroviruses would circulate, endogenized to bat genome and would be maintained as they evolve at the host mutation rate of evolution. The *LTR* sequences of endogenous deltaretrovirus were also detected from bat endemic to Ryukyu islands. Ryukyu islands became isolated from mainland during the whole Quaternary (Millien-Parra and Jaeger, 1999; Yamada, 2017). It is possible that transmission of ancient deltaretrovirus occurred directly between animals of the tribe Bovini and bat species or between hosts via an intermediate host, or were transmitted to both hosts from unknown host. Regardless of the route of transmission, having the result of our study as a presumption that ancient exogenous deltaretrovirus were circulated in Asia before the isolation of Ryukyu islands, we can assume that BLV-related ancient deltaretroviruses in the past would circulate in Asia long before the emergence of this virus. Interestingly, while human T-lymphotropic virus (HTLV) was inferred to have emerged as a result of cross-species transmission of simian T-lymphotropic virus (STLV) from animal reservoirs in Africa, and several previous studies pointed out that STLV originated in Asia. Therefore, these observations suggest that this region is likely to be the center of origin of deltaretroviruses (Slattery et al., 1999; Reid et al., 2016; Afonso et al., 2019). Further analysis is needed to detect other natural hosts of BLV, because the infection rate in zebu cattle is relatively low for the maintenance of deltaretrovirus as a reservoir (Mwenda et al., 1999; Takemura et al., 2002; Traina-Dorge et al., 2005; Jegado et al., 2019).

This study has several limitations, as the phylodynamic models were constructed using *BLVgp51* sequences, and the evolutionary history of other gene sequences was not included. Moreover, the host species of most of the analyzed sequences collected before 2000 were represented by taurine cattle. Although the topologies of ML phylogenetic tree of four BLV open reading frames were mostly compatible with each other, and it was shown to be appropriate for the trait analyses conducted in our previous study, the analysis of full length genomes from various species collected on different years could also provide basic information to deepen the long history of viral evolution (Ohnuki et al., 2021).

In summary, by analyzing BLV sequences from Asian native cattle and endogenous deltaretrovirus sequences from indigenous Asian bat species, it was inferred that ancient BLV emerged and circulated in Asia long before it was detected in Europe in the late 1800s. The potential cross-species transmission of BLV to taurine cattle, possibly through Asian zebu cattle, is likely to have occurred around the late 1800s in South America and Europe. These results can not only elucidate the mechanisms of BLV dissemination worldwide, but also provide new insights into the evolution of deltaretroviruses.

MATERIALS AND METHODS

Bovine Sample Collection

Blood samples were collected from 256 zebu cattle in six Asian countries. Each sample was unrelated and taken from one head per farm. The detailed sampling method has been described in our previous work (Lwin et al., 2018b). In addition, samples from 37 zebu cattle in Madagascar were also collected, because this population is closely related to Asian zebu populations (**Table 1**; Kaufman, 2008). Blood samples were also collected from 16 taurine cattle (*Bos taurus*) in the Republic of Kazakhstan. Blood samples and skin tissue samples from 268 yaks (*Bos grunniens*) and 16 water buffaloes (*Bubalus bubalis*) were collected in four countries (Kyrgyzstan, China, Pakistan, and Nepal) (Guo et al., 2006; Qiu et al., 2012). The DNA extraction procedure and the information on samples have been included in our previous study (Yonesaka et al., 2016; Lwin et al., 2018a,b).

Detection of Bovine Leukemia Virus Proviral DNA and Sequencing Analysis

A 1304 bp fragment of the complete *BLVgp51* gene was amplified by PCR using KOD FX Neo (TOYOBO, Osaka, Japan) with following primers (Forward Primer 5′-AGA TGG GAG CTA CAC CAT TCA-3′, Reverse Primer 5′-CAC AGA GGC CAC ATT AAG A-3′) to detect BLV proviral sequences in the genome of zebu cattle, taurine cattle and water buffaloes. The following cycling conditions were used: 94°C for 2 min, followed by 40 cycles of denaturation at 98°C for 10 s, and extension at 68°C for 60 s. The amplified PCR fragments were purified by QIAquick gel extraction kit (QIAGEN, Hiden, Germany), and were then sequenced (FASMAC, Atsugi, Japan). The sequences included a 903 bp sequence coding the complete BLV envelope GP51 region, corresponding to nucleotide positions 4826–5738 on the pBLV903 genome (GenBank accession number EF600696). The obtained sequences were analyzed in Sequencher^{TM}5.2.4 (GeneCodes, Michigan, United States).

A 198 bp fragment of the LTR of the BLV proviral genome in yak was amplified by nested PCR using PrimeSTAR GXL DNA polymerase (Takara, Shiga, Japan) with the following primers: BLTR256F (5′-GAG CTC TCT TGC CCG AGA C-3′) and BLTR453R (5′-GAA ACA AAC GCG GGT GCA AGC CAG-3′) for first PCR, and BLTR306F (5′-GTA AGG CAA ACC ACG GTT T-3′) and BLTR408R (5′-AGG AGG CAA AGG AGA GAG T-3′) for second PCR, as previously described (Polat et al., 2015). The following cycling conditions were used: 45 cycles of denaturation at 98°C for 10 s, annealing at 60°C for 15 s, extension at 68°C for 30 s.

The Maximum Likelihood Phylogenetic Tree

A total of 699 *BLVgp51* partial sequences (444 bp) as well as collection date and location data were retrieved from GenBank. These sequences were aligned with 13 sequences obtained in this study using MEGA7 software (Kumar et al., 2016). The best-fitting nucleotide substitution model was selected using the Akaike information criterion corrected (AICc). A ML phylogenetic tree of the *BLVgp51* sequences was inferred by applying the Kimura 2-parameter model plus gamma distribution (K2+G) model. The reliability of the phylogenetic relationships was evaluated by non-parametric bootstrap analysis with 1,000 replicates.

Phylogenetic Reconstruction and Phylodynamic Analysis of Bovine Leukemia Virus

To analyze the evolutionary history of BLV, the time to the most recent common ancestor (tMRCA) and the effective population size were estimated by employing the Bayesian MCMC approach in BEAST v 2.4.8 (Bouckaert et al., 2014). Coalescent theory has been applied to phylogenetic methods to reconstructing the epidemic history of viruses, providing estimates of origins, dating of common ancestors, and population dynamics. The best nucleotide substitution model for the Bayesian MCMC-derived phylogenetic tree was selected based on the Bayesian information criterion (BIC) values in MEGA7 (Kumar et al., 2016). The Hasegawa-Kishino-Yano (HKY) model that showed the lowest BIC value was used for this analysis. The temporal scale of the evolutionary process was inferred from the sampling dates of the sequences using relaxed clock models (exponential and lognormal relaxed clocks) and four demographic models (two parametric priors, coalescent constant population and coalescent exponential population; two non-parametric priors, coalescent extended skyline and coalescent Bayesian skyline). Therefore, the best fitting demographic models were selected based on the BF test and Akaike's information criterion for MCMC (AICM) values using Tracer v1.5 (Rambaut and Drummond, 2007). The BF and AICM analyses also showed that the exponential relaxed clock was better than the lognormal one in fitting the data. Also, under the exponential relaxed clock, the BF and AICM analyses showed that the coalescent exponential population fitted the data better than other demographic models did. For the Bayesian MCMC analysis, HKY+exponential relaxed clock+coalescent exponential population were selected. A total of 156 *BLVgp51* sequences (sequence length, 502–903 bp) were used for the analysis in BEAST. First, the sequences with collection date, country, and host information were obtained from the database. A 75% random sampling was performed for countries with more than 10 sequences registered, because the BLV database was biased toward many closely related sequences in the same country. Then, Bayesian MCMC simulations for 400 million cycles, sampling every 10,000 states, and 10% burn-in were applied to infer the BLV evolutionary phylogenetic tree under the best fitting model. The convergence was assessed by estimating the effective sample size (ESS) (>200) of a parameter sampled from the Bayesian MCMC using Tracer v 1.5 (Rambaut and Drummond, 2007). The maximum clade credibility (MCC) tree was constructed using TreeAnnotator v1.8.0 (Rambaut and Drummond, 2016), and finally, the MCC tree was generated in FigTree v 1.4.4 (Rambaut, 2019).

Ancestral State Reconstruction

To study the evolutionary history of BLV, ancestral state reconstruction analyses were performed using Mesquite v 3.61 (Maddison, 2016). The *BLVgp51* MCC tree previously estimated

in this study (**Figure 2**) was used for the input data. The ancestral states of each BLV in relation to its host and geography were reconstructed using a parsimony approach. The minimum number of trait changes along the tree that are necessary to explain the present host state and sampling location associations at the tree tips were calculated to estimate the evolutionary process.

Positive Selection Analysis

Of the 156 *BLVgp51* sequences (903 bp) used in this study, 63 were classified as lineage II, and were used to test the positive selection. The phylogenetic trees were reconstructed by employing the Bayesian MCMC method in BEAST v 2.4.8, and the resulting trees were then used for detecting positive selection. For the detection of positive selection pressure, the analysis was performed with the PAML 4.8 site model. Amino acid sites under positive selection pressure were identified by posterior probabilities through the Bayes empirical Bayes (BEB) method (Yang, 2007). The selected sites were compared to those obtained from the previous study of predicted BLV receptor binding sites (Corredor et al., 2018).

Spatial Phylogenetic Reconstruction of Evolutionary Dynamics

The global geographic origins of BLV and its significant dispersal routes between infected countries were inferred using discrete-state ancestral reconstruction methods in BEAST v 2.4.8. Each BLV isolate was assigned an individual location state, based on the country/region of the sample location data. Diffusions among the location states were modeled using an asymmetric model, with Bayesian stochastic search variable selection. The same settings as those described for the Bayesian phylogenetic dating analyses above were used. The resulting diffusion rates were then used to calculate BF in SPREAD (Bielejec et al., 2011). The migration pathways were interpreted as "supported" when the BF was $\geq$ 3. To minimize the impact of sampling bias, countries with a sample size of 10 or more were kept below 20% of the sample.

Detection of Bat Endogenous Deltaretrovirus and Its Relationship to Bovine Leukemia Virus

To assess the presence of endogenous deltaretrovirus sequences, DNA or tissue samples obtained from 46 bats originated in Asia—comprising 41 species and eight families were analyzed. The DNA was extracted by phenol chloroform method. The *LTR* and *gag* regions of endogenous deltaretroviruses were amplified by PCR using PrimeSTAR GXL DNA polymerase (Takara, Shiga, Japan) (information on the specific primers used is included in **Supplementary Table 1**). The following cycling conditions were used: 40 cycles of denaturation at 94°C for 10 s, annealing at 60°C for 15 s, and extension at 68°C for 45 s. The amplified fragments were purified by QIAquick gel extraction kit (QIAGEN, Hiden, Germany), and were then sequenced (FASMAC, Atsugi, Japan). All amplicons were sequenced directly, and sequences with ambiguous positions excluded from further analysis. To determine the evolutionary relationships of the obtained sequences among endogenous and exogenous deltaretroviruses, the *LTR* sequences were aligned using ClustalW in MEGA7, and a phylogenetic tree was estimated using the ML method with the K2+G model of nucleotide substitution. To evaluate the robustness of each node, bootstrap resampling analysis was performed with 1,000 replicates.

DATA AVAILABILITY STATEMENT

The datasets presented in this study can be found in online repositories. The names of the repository/repositories and accession number(s) can be found in the article/ **Supplementary Material**.

ETHICS STATEMENT

The animal study was reviewed and approved by Kobe University Animal Experimentation Regulations and the Animal Research Committee at Tokyo University of Agriculture, and we confirm that all experiments were performed in accordance with the committee's guidelines and regulations. Written informed consent was obtained from the owners for the participation of their animals in this study.

AUTHOR CONTRIBUTIONS

TK and KN conceived and designed the experiments and wrote the manuscript. KN performed the wet lab experiments. KN, TY, and TK performed the phylogenetic data analyses. KN, TY, MN, FK, SS, KK, HM, MH, and JL contributed to the yak, water buffalo, bats, and native cattle samples. TY, MN, YT, KK, JL, HM, and TK coordinated the project. TY, MN, KI, KK, JL, and HM provided guidance and expertised on the history of native cattle, yak, bat, and endogenous retroviruses. All authors read and approved the final manuscript.

FUNDING

This study was supported in part by JSPS KAKENHI Grants-in-Aid for Scientific Research C 21K05943 and Livestock Promotional Funds of Japan Racing Association.

SUPPLEMENTARY MATERIAL

The Supplementary Material for this article can be found online at: https://www.frontiersin.org/articles/10.3389/fmicb.2022.917324/full#supplementary-material

REFERENCES

Acemoglu, D., Johnson, S., and Robinson, J. (2005). The rise of Europe: atlantic trade, institutional change, and economic growth. *Am. Econ. Rev.* 95, 546–579.

Afonso, P. V., Cassar, O., and Gessain, A. (2019). Molecular epidemiology, genetic variability and evolution of HTLV-1 with special emphasis on African genotypes. *Retrovirology* 16, 1–15. doi: 10.1186/s12977-019-0504-z

Aida, Y., Murakami, H., Takahashi, M., and Takeshima, S. N. (2013). Mechanisms of pathogenesis induced by bovine leukemia virus as a model for human T-cell leukemia virus. *Front. Microbiol.* 4:328.

Ajmone-Marsan, P., Garcia, J. F., and Lenstra, J. A. (2010). On the origin of cattle: how aurochs became cattle and colonized the world. *Evol. Anthropol.* 19, 148–157.

Amador, L. I., Arévalo, R. L. M., Almeida, F. C., Catalano, S. A., and Giannini, N. P. (2018). Bat systematics in the light of unconstrained analyses of a comprehensive molecular supermatrix. *J. Mammal. Evol.* 25, 37–70.

Bendixen, H. J. (1963). Preventive Measures in Cattle Leukemia: leukosis Enzootica Bovis. *Ann. N. Y. Acad. Sci.* 108, 1241–1267. doi: 10.1111/j.1749-6632.1963.tb13448.x

Benitez, O. J., Norby, B., Bartlett, P. C., Maeroff, J. E., and Grooms, D. L. (2020). Impact of bovine leukemia virus infection on beef cow longevity. *Prev. Vet. Med.* 181:105055. doi: 10.1016/j.prevetmed.2020.105055

Bielejec, F., Rambaut, A., Suchard, M. A., and Lemey, P. (2011). SPREAD: spatial phylogenetic reconstruction of evolutionary dynamics. *Bioinformatics*. 15, 2910–2912. doi: 10.1093/bioinformatics/btr481

Boeke, J. D., and Stoye, J. P. (1997). "Retrotransposons, Endogenous Retroviruses, and the Evolution of Retroelements," in *Retroviruses*, eds J. M. Coffin, S. H. Hughes, and H. E. Varmus (New York, NY: Cold Spring Harbor).

Bouckaert, R., Heled, J., Kuhnert, D., Vaughan, T., Wu, C. H., Xie, D., et al. (2014). BEAST 2: a software platform for Bayesian evolutionary analysis. *PLoS Comput. Biol.* 10:e1003537.

Chen, S., Lin, B. Z., Baig, M., Mitra, B., Lopes, R. J., Santos, A. M., et al. (2010). Zebu cattle are an exclusive legacy of the South Asia neolithic. *Mol. Biol. Evol.* 27, 1–6. doi: 10.1093/molbev/msp213

Constable, P. D., Hinchcliff, K. W., Done, S. H., Gruenberg, W., and Radostits, O. M. (2017). *Veterinary medicine : a textbook of the diseases of cattle, horses, sheep, pigs and goats*. Amsterdam: Elsevier.

Corredor, A. P., González, J., Baquero, L. A., Curtidor, H., Olaya-Galán, N. N., Patarroyo, M. A., et al. (2018). In silico and in vitro analysis of boAP3d1 protein interaction with bovine leukaemia virus gp51. *PLoS One* 13:e0199397. doi: 10.1371/journal.pone.0199397

Decker, J. E., Mckay, S. D., Rolf, M. M., Kim, J., Molina Alcala, A., Sonstegard, T. S., et al. (2014). Worldwide patterns of ancestry, divergence, and admixture in domesticated cattle. *PLoS Genet.* 10:e1004254. doi: 10.1371/journal.pgen.1004254

Farkasova, H., Hron, T., Paces, J., Hulva, P., Benda, P., Gifford, R. J., et al. (2017). Discovery of an endogenous Deltaretrovirus in the genome of long-fingered bats (Chiroptera: Miniopteridae). *Proc. Natl. Acad. Sci. U S A* 114, 3145–3150. doi: 10.1073/pnas.1621224114

Felius, M., Beerling, M.-L., Buchanan, D. S., Theunissen, B., Koolmees, P. A., and Lenstra, J. A. (2014). On the History of Cattle Genetic Resources. *Diversity* 6, 705–750.

Fuller, D. Q. (2006). Agricultural origins and frontiers in South Asia: a working synthesis. *J. World Prehist.* 20, 1–86.

Guo, S., Savolainen, P., Su, J., Zhang, Q., Qi, D., Zhou, J., et al. (2006). Origin of mitochondrial DNA diversity of domestic yaks. *BMC Evol. Biol.* 6:73. doi: 10.1186/1471-2148-6-73

Hayward, J. A., Tachedjian, M., Kohl, C., Johnson, A., Dearnley, M., Jesaveluk, B., et al. (2020). Infectious KoRV-related retroviruses circulating in Australian bats. *Proc. Natl. Acad. Sci. U S A* 117, 9529–9536. doi: 10.1073/pnas.1915400117

Hron, T., Elleder, D., and Gifford, R. J. (2019). Deltaretroviruses have circulated since at least the Paleogene and infected a broad range of mammalian species. *Retrovirology* 16:33. doi: 10.1186/s12977-019-0495-9

Ikeda, Y., and Motokawa, M. (2021). Phylogeography of the Japanese greater horseshoe bat Rhinolophus nippon (Mammalia: Chiroptera) in Northeast Asia: new insight into the monophyly of the Japanese populations. *Ecol. Evol.* 11, 18181–18195. doi: 10.1002/ece3.8414

Irving, A. T., Ahn, M., Goh, G., Anderson, D. E., and Wang, L. F. (2021). Lessons from the host defences of bats, a unique viral reservoir. *Nature* 589, 363–370. doi: 10.1038/s41586-020-03128-0

Jegado, B., Kashanchi, F., Dutartre, H., and Mahieux, R. (2019). STLV-1 as a model for studying HTLV-1 infection. *Retrovirology* 16:41. doi: 10.1186/s12977-019-0503-0

Kaufman, J. C. (2008). *Greening the great red island : Madagascar in nature and culture. Africa Institute Occasional Paper*. Pretoria: Africa Institute of South Africa.

Kumar, S., Stecher, G., and Tamura, K. (2016). MEGA7: molecular Evolutionary Genetics Analysis Version 7.0 for Bigger Datasets. *Mol. Biol. Evol.* 33, 1870–1874. doi: 10.1093/molbev/msw054

Lwin, M., Mon, S. L. Y., Yamanaka, H., Nagano, Y., Mannen, H., Faruque, M. O., et al. (2018b). Genetic diversities and population structures of four popular Myanmar local cattle breeds. *Anim. Sci. J.* 89, 1648–1655. doi: 10.1111/asj.13112

Lwin, M., Mon, S. L. Y., Nagano, Y., Kawabe, K., Mannen, H., Okamoto, S., et al. (2018a). Genetic diversity of Myanmar cattle breeds using complete mitochondrial D-loop sequence. *J. Anim. Genet.* 46, 57–67.

Ma, J. G., Zheng, W. B., Zhou, D. H., Qin, S. Y., Yin, M. Y., Zhu, X. Q., et al. (2016). First Report of Bovine Leukemia Virus Infection in Yaks (*Bos mutus*) in China. *Biomed. Res. Int.* 2016:9170167. doi: 10.1155/2016/9170167

Maddison, W. P. A. D. R. M. (2016). *Measquite: a modular system for evolutionary analysis. Version 3.61*.

Mammerickx, M. (2003). La peste bovine, Jules Bordet et le centre Sérumigène de Cureghem. *Ann. Med. Vét.* 147, 197–205.

Melletti, M., and Burton, J. (2014). *Ecology, Evolution and Behaviour of Wild Cattle: Implications for Conservation*. Cambridge, MA: Cambridge University Press.

Millien-Parra, V., and Jaeger, J. J. (1999). Island biogeography of the Japanese terrestrial mammal assemblages: an example of a relict fauna. *J. Biogeogr.* 26, 959–972.

Mwenda, J. M., Sichangi, M. W., Isahakia, M., Van Rensburg, E. J., and Langat, D. K. (1999). The prevalence of antibodies to simian T-cell leukaemia/lymphotropic virus (STLV-I) in non-human primate colonies in Kenya. *Ann. Trop. Med. Parasitol.* 93, 289–297. doi: 10.1080/00034989958555

Ohnuki, N., Kobayashi, T., Matsuo, M., Nishikaku, K., Kusama, K., Torii, Y., et al. (2021). A target enrichment high throughput sequencing system for characterization of BLV whole genome sequence, integration sites, clonality and host SNP. *Sci. Rep.* 11:4521. doi: 10.1038/s41598-021-83909-3

OIE (2021). *Manual of Diagnostic Tests and Vaccines for Terrestrial Animals*. Paris: OIE.

Ott, S. L., Johnson, R., and Wells, S. J. (2003). Association between bovine-leukosis virus seroprevalence and herd-level productivity on US dairy farms. *Prev. Vet. Med.* 61, 249–262. doi: 10.1016/j.prevetmed.2003.08.003

Perez-Pardal, L., Sanchez-Gracia, A., Alvarez, I., Traore, A., Ferraz, J. B. S., Fernandez, I., et al. (2018). Legacies of domestication, trade and herder mobility shape extant male zebu cattle diversity in South Asia and Africa. *Sci. Rep.* 8:18027. doi: 10.1038/s41598-018-36444-7

Perry, B. D., Grace, D., and Sones, K. (2013). Current drivers and future directions of global livestock disease dynamics. *Proc. Natl. Acad. Sci. U S A* 110, 20871–20877. doi: 10.1073/pnas.1012953108

Polat, M., Ohno, A., Takeshima, S. N., Kim, J., Kikuya, M., Matsumoto, Y., et al. (2015). Detection and molecular characterization of bovine leukemia virus in Philippine cattle. *Arch. Virol.* 160, 285–296. doi: 10.1007/s00705-014-2280-3

Polat, M., Takeshima, S. N., and Aida, Y. (2017). Epidemiology and genetic diversity of bovine leukemia virus. *Virol. J.* 14:209. doi: 10.1186/s12985-017-0876-4

Qiu, Q., Zhang, G., Ma, T., Qian, W., Wang, J., Ye, Z., et al. (2012). The yak genome and adaptation to life at high altitude. *Nat. Genet.* 44, 946–949. doi: 10.1038/ng.2343

Rambaut, A. (2019). *Figtree v 1.4.4*.

Rambaut, A., and Drummond, A. (2007). *Tracer v1.5. beast. bio. ed. ac. uk/Tracer*.

Rambaut, A., and Drummond, A. (2016). *TreeAnnotator version 1.8.0*.

Reid, M. J., Switzer, W. M., Schillaci, M. A., Ragonnet-Cronin, M., Joanisse, I., Caminiti, K., et al. (2016). Detailed phylogenetic analysis of primate T-lymphotropic virus type 1 (PTLV-1) sequences from orangutans (Pongo pygmaeus) reveals new insights into the evolutionary history of PTLV-1 in Asia. *Infect Genet. Evol.* 43, 434–450. doi: 10.1016/j.meegid.2016.05.036

Roberts, T. E. (2006). History, ocean channels, and distance determine phylogeographic patterns in three widespread Philippine fruit bats (Pteropodidae). *Mol. Ecol.* 15, 2183–2199. doi: 10.1111/j.1365-294X.2006.02928.x

Ruedi, M., Stadelmann, B., Gager, Y., Douzery, E. J., Francis, C. M., Lin, L. K., et al. (2013). Molecular phylogenetic reconstructions identify East Asia as the cradle for the evolution of the cosmopolitan genus Myotis (Mammalia, Chiroptera). *Mol. Phylogenet. Evol.* 69, 437–449. doi: 10.1016/j.ympev.2013.08.011

Scheu, A., Powell, A., Bollongino, R., Vigne, J. D., Tresset, A., Cakirlar, C., et al. (2015). The genetic prehistory of domesticated cattle from their origin to the spread across Europe. *BMC Genet.* 16:54. doi: 10.1186/s12863-015-0203-2

Sihvonen, L. (2015). Enzootic bovine leukosis. *EFSA J.* 13:63.

Slattery, J. P., Franchini, G., and Gessain, A. (1999). Genomic evolution, patterns of global dissemination, and interspecies transmission of human and simian T-cell leukemia/lymphotropic viruses. *Genome Res.* 9, 525–540.

Takemura, T., Yamashita, M., Shimada, M. K., Ohkura, S., Shotake, T., Ikeda, M., et al. (2002). High prevalence of simian T-lymphotropic virus type L in wild ethiopian baboons. *J. Virol.* 76, 1642–1648. doi: 10.1128/jvi.76.4.1642-1648.2002

Traina-Dorge, V. L., Lorino, R., Gormus, B. J., Metzger, M., Telfer, P., Richardson, D., et al. (2005). Molecular epidemiology of simian T-cell lymphotropic virus type 1 in wild and captive sooty mangabeys. *J. Virol.* 79, 2541–2548. doi: 10.1128/JVI.79.4.2541-2548.2005

Wang, M., Wang, Y., Baloch, A. R., Pan, Y., Xu, F., Tian, L., et al. (2018). Molecular epidemiology and characterization of bovine leukemia virus in domestic yaks (Bos grunniens) on tshe Qinghai-Tibet Plateau, China. *Arch. Virol.* 163, 659–670. doi: 10.1007/s00705-017-3658-9

Yamada, F. (2017). The birth of two new national parks on the Central Ryukyus in the Ryukyu Chain and the task of a World Natural Heritage Site. *Mammal. Sci.* 57, 183–194.

Yang, Z. (2007). PAML 4: phylogenetic analysis by maximum likelihood. *Mol. Biol. Evol.* 24, 1586–1591.

Yonesaka, R., Sasazaki, S., Yasue, H., Niwata, S., Inayoshi, Y., Mukai, F., et al. (2016). Genetic structure and relationships of 16 Asian and European cattle populations using DigiTag2 assay. *Anim. Sci. J.* 87, 190–196. doi: 10.1111/asj.12416

Conflict of Interest: The authors declare that the research was conducted in the absence of any commercial or financial relationships that could be construed as a potential conflict of interest.

Publisher's Note: All claims expressed in this article are solely those of the authors and do not necessarily represent those of their affiliated organizations, or those of the publisher, the editors and the reviewers. Any product that may be evaluated in this article, or claim that may be made by its manufacturer, is not guaranteed or endorsed by the publisher.

frontiers | Frontiers in Microbiology

ORIGINAL RESEARCH
published: 08 July 2022
doi: 10.3389/fmicb.2022.904189

Enhancement of Rubella Virus Infection in Immortalized Human First-Trimester Trophoblasts Under Low-Glucose Stress Conditions

Quang Duy Trinh[1], Kazuhide Takada[1], Ngan Thi Kim Pham[1], Chika Takano[1], Takahiro Namiki[2], Ryo Ikuta[3], Shingo Hayashida[2], Shoko Okitsu[1], Hiroshi Ushijima[1], Shihoko Komine-Aizawa[1] and Satoshi Hayakawa[1]**

[1]Division of Microbiology, Department of Pathology and Microbiology, Nihon University School of Medicine, Tokyo, Japan, [2]Nihon University School of Medicine, Tokyo, Japan, [3]Department of Pediatric Surgery, Nihon University School of Medicine, Tokyo, Japan

OPEN ACCESS

Edited by:
Lingbao Kong, Jiangxi Agricultural University, China

Reviewed by:
Sujit Pujhari, University of South Carolina, United States
Nhu Nguyen, University of California, San Francisco, United States

***Correspondence:**
Shihoko Komine-Aizawa
aizawa.shihoko@nihon-u.ac.jp
Satoshi Hayakawa
hayakawa.satoshi@nihon-u.ac.jp

Specialty section:
This article was submitted to Virology, a section of the journal Frontiers in Microbiology

Received: *25 March 2022*
Accepted: *21 June 2022*
Published: *08 July 2022*

Citation:
Trinh QD, Takada K, Pham NTK, Takano C, Namiki T, Ikuta R, Hayashida S, Okitsu S, Ushijima H, Komine-Aizawa S and Hayakawa S (2022) Enhancement of Rubella Virus Infection in Immortalized Human First-Trimester Trophoblasts Under Low-Glucose Stress Conditions. Front. Microbiol. 13:904189. doi: 10.3389/fmicb.2022.904189

Rubella virus (RuV) infections in pregnant women, especially first-trimester infections, can lead to congenital rubella syndrome (CRS). However, the mechanisms of fetal RuV infection are not completely understood, and it is not observed in every pregnant woman infected with RuV. As gestational diabetes mellitus is a risk factor for congenital viral infections, we investigated the possible roles of hypoglycemia-related endoplasmic reticulum (ER) stress as a key factor for vertical RuV infection using immortalized human first-trimester trophoblasts. Low-glucose stress was induced prior to RuV infection by culturing HTR-8/SVneo and Swan.71 cells in low-glucose (LG) medium for 24 h or high-glucose medium for 6 h and then LG medium for an additional 18 h. Clinically isolated RuV was inoculated at a multiplicity of infection of 5 to 10. The intracellular localization of the RuV capsid protein was investigated 24 to 48 h post-infection (pi) with flow cytometry (FCM) analysis and fluorescence microscopy. Viral progeny production was monitored by FCM analysis. Increases in RuV infection in LG-induced ER-stressed trophoblasts were observed. No significant increase in apoptosis of RuV-infected cells was noted at days 2 and 5 pi, and substantial viral progeny production was observed until day 5 pi. An approximate fivefold increase in viral binding was noted for the LG-stressed cells. Although the detailed mechanisms underlying viral entry into LG-stressed cells are not known and require further investigation, these findings suggest that a certain degree of LG stress in early pregnancy may facilitate infection and cause CRS.

Keywords: rubella, trophoblasts, pregnancy, infection, low glucose, endoplasmic reticulum stress, congenital rubella syndrome

INTRODUCTION

Rubella virus (RuV) belongs to the family *Matonaviridae* and genus *Rubivirus* (Chen et al., 2018). RuV causes a mild, rash-producing, febrile illness in children, and it is well known for causing stillbirth, premature birth, or congenital defects called congenital rubella syndrome (CRS) in pregnant women, particularly during the first trimester. CRS occurs after the transplacental

transmission of RuV during the first 8 weeks of gestation in up to 90% of cases and during the second trimester in 25–35% (Hobman, 2013). Although most studies attribute fetal susceptibility to RuV-related teratogenesis in the first trimester of pregnancy to the critical periods of major organogenesis, the mechanisms involved in *in utero* transmission during these critical periods are not well established.

During the first trimester of pregnancy, the primary placental cells derived from the trophectoderm of the blastocyst, cytotrophoblasts (CTBs), differentiate into extravillous trophoblasts (EVTs), which invade uterine tissue and replace uterine spiral arterial walls (Silva and Serakides, 2016; Yoshida et al., 2021). This induction of trophoblast differentiation is promoted by low oxygen concentrations during placental formation in early pregnancy, which is also associated with enhanced endoplasmic reticulum (ER) stress (Chang et al., 2018).

The ER is a large cellular organelle that plays an essential role in protein synthesis and maturation. Excessive accumulation of unfolded or misfolded proteins in the lumen of the ER during conditions of hypoxemia, oxidative stress, impaired Ca^{2+} homeostasis, and glucose deprivation causes ER stress (Ni and Lee, 2007; Schwarz and Blower, 2016; Bastida-Ruiz et al., 2017; Burton et al., 2017; Guzel et al., 2017). Increased ER stress occurs naturally in the first trimester of pregnancy and in women with gestational diabetes mellitus (GDM), pregnancies are complicated with fetal growth restriction, preeclampsia, and during labor (Burton and Yung, 2011; Lian et al., 2011; Veerbeek et al., 2015; Yung et al., 2016). Of importance, patients with GDM are more suspicious for viral infections, including COVID-19 (Mamun and Khan, 2021).

We recently discovered that RuV has low infectivity to the first-trimester trophoblast cell lines HTR-8/SVneo and Swan.71 *in vitro*, suggesting that there might be other factors affecting the infectivity of RuV to these cells (Pham et al., 2022). Searching for such possible factors led us to hypothesize that ER stress may play a role in RuV infection in early pregnancy.

To partially answer the above question, the present study investigated the influence of low-glucose-induced ER stress on RuV infection in the immortalized human first-trimester trophoblast cells HTR-8/SVneo and Swan.71. By culturing these trophoblast cells in low-glucose (LG) medium for 24 h or high-glucose (HG) medium for 6 h and then LG medium for an additional 18 h to induce LG stress prior to RuV infection *in vitro*, we found that there was an enhancement of susceptibility to RuV in the treated trophoblast cells.

MATERIALS AND METHODS

Cell Culture and Virus

HTR-8/SVneo cells (originally obtained from human first-trimester placentas and immortalized *via* transfection with a cDNA construct encoding simian virus 40 large T antigen) and Swan.71 cells (Sw.71, derived from the telomerase-mediated transformation of a 7-week cytotrophoblast isolate described; Graham et al., 1993; Straszewski-Chavez et al., 2009) were kindly provided by Dr. Gil Mor (Wayne State University, Detroit, MI, United States) and were cultured in RPMI 1640 medium (Gibco-Invitrogen, Tokyo, Japan) supplemented with 10% fetal bovine serum (FBS), 10 mM HEPES (Invitrogen), 0.1 mM nonessential amino acids (Invitrogen), 1 mM sodium pyruvate (Invitrogen), and 100 units/ml penicillin–streptomycin (complete medium). Vero cells were purchased from the Japanese Collection of Research Bioresources Cell Bank and cultured in Dulbecco's modified Eagle's medium (DMEM; Gibco-Invitrogen, Tokyo, Japan) supplemented with 10% FBS and 100 units/ml penicillin–streptomycin. All cells were cultured in monolayers at 37°C in a humidified 5% CO_2 incubator.

The clinical RuV strain (3-B1-RK13) was transferred from Kitasato University School of Medicine (Tokyo, Japan). The viral stock solution was prepared by propagating the virus in Vero cells and concentrating the viral particles *via* ultracentrifugation at 52,000 × g for 90 min in a Himac CS100GX microultracentrifuge with an S50A rotor (Hitachi Koki Co., Ltd., Ibaraki, Japan). Viral titers were estimated with the TCID50 method or flow cytometry (FCM) analysis, as described previously (Grigorov et al., 2011; Pham et al., 2021).

Experimental Low-Glucose-Induced ER Stress Conditions in Trophoblast Cells

Trophoblast cells were seeded in 6-well plates (10^5 cells/well), 12-well plates (5×10^4 cells/well), 24-well plates (2.5×10^4 cells/well), or 96-well plates (5×10^3 cells/well) in complete medium and cultured for 2 days prior to experimentation. For the low-glucose stress inductions, the cells were cultured in serum-free RPMI containing 0.1% bovine serum albumin (BSA) and LG (0.5 mM glucose) for 24 h or HG (25 mM glucose) for 6 h followed by LG for 18 h (HG-LG, 24 h in total) to mimic the placental conditions in gestational diabetes with hypoglycemia (Khunti et al., 2016; Sarina Li et al., 2019). The cells cultured in serum-free normal RPMI containing 11 mM glucose (SF medium) were used as a control for the LG stress treatment. For comparative references, the cells were also cultured in the complete RPMI medium (FBS for abbreviation) or SF medium containing the ER stress activator thapsigargin (Tg, 25 nM) for 24 h.

Cell Viability Assay

Trophoblast cells were cultured in a 96-well plate and subjected to LG treatments, as described above. Cell viability was measured using a Cell Counting Kit-8 (Dojindo Laboratories, Kumamoto, Japan) according to the manufacturer's instructions. The cell density in each well was measured at 450 nm using a microplate reader (iMark Microplate Absorbance Reader, Bio-Rad, Hercules, CA, United States).

Western Blotting

Cells grown in 6-well plates were subjected to the LG treatments, as described above. The supernatant was removed 24 h posttreatment, and the cells were washed and lysed in 70 µl of cell lysis buffer (Cell Signaling Technology, Danvers, MA, United States). The protein concentrations in the lysates were quantified using a DC Protein Assay (Bio–Rad Laboratories,

Inc., Hercules, CA, United States). Cell lysates were loaded onto a NuPAGE 4–12% Bis-Tris protein gel (Invitrogen) and separated by electrophoresis. The separated proteins were transferred to polyvinylidene fluoride membranes (Invitrogen), and nonspecific binding sites were blocked using 1% BSA in phosphate-buffered saline (PBS) containing 0.05% Tween 20. Membranes were incubated with a primary rabbit polyclonal anti-GRP78 antibody (Abcam, Cambridge, United Kingdom), a mouse monoclonal anti-CHOP antibody, or a rabbit α-tubulin antibody (Cell Signaling Technology) at 4°C overnight. Membranes were incubated with a horseradish peroxidase-conjugated secondary antibody (Cell Signaling Technology) for 30 min at room temperature (RT) and visualized with a luminescent image analyzer (Image Reader LAS-4000 Mini, Fujifilm, Tokyo, Japan). After visualization, antibodies attached to the membranes were removed using Restore PLUS Western Blot Stripping Buffer (Thermo Fisher Scientific, MA, United States), and the membranes were reused to investigate the expression of other proteins.

Viral Infection

Cells were cultured in 96-well plates (for FCM analysis) or 6-well plates with glass coverslips for immunofluorescence (IF) assays, washed with SF medium 24 h posttreatment, and incubated with the virus at multiplicities of infection (MOIs) of 5 to 10 for a total of 3 h in a 35°C, humidified 5% CO_2 incubator with gentle shaking every 10 ~ 15 min during the first hour. The supernatant was removed, the cells were washed, and the medium was replaced with a fresh medium containing 2% FBS. The percentage of cells infected with the virus was determined 24 to 48 h post-infection (hpi) by FCM analysis and IF assays at 48 hpi. Negative control cells (mock-infected, infected with heat-inactivated RuV, or not exposed to the primary antibody during the staining procedures), as well as positive controls using RuV-infected Vero (or A549) cells, were also performed in parallel for comparison. Supernatants from day 2 pi were collected daily and replaced with the fresh medium until day 7 pi to monitor viral progeny production by FCM analysis.

To determine the infectivity of the supernatants, a 30 µl volume of serial 3-fold dilutions of the supernatants was used to infect (in duplicate) freshly seeded Vero cells in a 96-well plate (4 × 104 cells/well). Medium containing 2% FBS and NH4Cl was added 6 hpi to prevent a second round of infection (final concentration of NH4Cl, 20 mM). The cells were collected 24 hpi and subjected to intracellular staining of RuV capsid protein. Viral titers [in infectious units (IUs)] were determined by FCM analysis. The viral titer in a sample was calculated as the average of 3 titers measured in 3 consecutive wells with a percentage of RuV-infected cells lower than 40% and higher than 0.3%, as described previously (Grigorov et al., 2011; Pham et al., 2021).

Viral Binding Assay

The cells were seeded onto 12-, 24-, or 96-well plates and then subjected to the LG treatments, as described above. The cells were washed once with ice-cold PBS, and viral binding buffer (1% BSA in PBS containing 0.1% sodium azide) was added for incubation on ice for 10 min. The cells were inoculated with RuV on ice for 1 h with gentle shaking every 10–15 min. The cells were gently washed three times with ice-cold PBS, collected *via* trypsinization (for 96-well plates), subjected to surface staining procedures for RuV, and then subjected to FCM analysis. In other experiments, the cells were subjected to RNA extraction (for 24-well plates) and then real-time PCR or lysate collection (for 12-well plates) for Western blot analysis.

Immunofluorescence Assay

Cells cultured on glass coverslips in six-well plates were subjected to LG treatments and then incubated with RuV, as described above. The supernatant was removed 48 hpi, and the cells were fixed with cold methanol for 5 min, washed with PBS, and incubated with the mouse monoclonal anti-RuV capsid antibody (ab34749, Abcam) for 1 h at RT. Separate negative controls subjected to mock treatment, heat-inactivated RuV inoculation, and staining with normal mouse serum were established. The cells were washed with PBS and incubated with a goat anti-rabbit IgG H&L (Alexa Fluor 488) secondary antibody solution (ab150081, Abcam) for 30 min at RT. The samples were counterstained with 4′,6-diamidino-2-phenylindole dihydrochloride (DAPI; Lonza, Walkersville, MD, United States) for nuclear staining. After washing, the coverslips were mounted with VECTASHIELD Mounting Medium (Vector Labs, Burlingame, CA, United States), and fluorescence images were acquired using a fluorescence microscope (FLoid Cell Imaging Station; Life Technologies, CA, United States).

FCM Analysis

For determination of the percentages of RuV-infected cells by FCM analysis, the cells were collected *via* trypsinization or detachment medium [RPMI containing 2.9 mM EDTA, 2% FBS, Live/Dead Staining Solution (Live/Dead Fixable Near-IR Dead Cell Stain Kit, Thermo Fisher Scientific, MA, United States)]. The cells were washed with staining buffer (STB, cold PBS containing 5% FBS and 2 mM EDTA) and fixed and permeabilized using a BD Cytofix/Cytoperm Fixation/Permeabilization Solution Kit (BD Biosciences, San Diego, United States). Intracellular staining was performed with a mouse monoclonal anti-RuV capsid antibody (ab34749, Abcam) for 30 min at RT. The cells were washed and incubated with a goat anti-mouse IgG H&L (Alexa Fluor® 647) secondary antibody (ab150115, Abcam) solution for 30 min at RT. The cells were subjected to FCM analysis after washing and fixation. For each sample, at least 5,000 gated events were collected and analyzed on a BD FACSVerse cytometer using BD FACSuite software (version 1.2; BD Biosciences). Separate negative control groups without viral inoculation or incubated with heat-inactivated RuV were also established. For FCM analysis after the viral binding assay, cell surface staining procedures for RuV were performed on ice after trypsinization and STB washing using the same primary and secondary antibodies described above, with 1 h for each incubation.

RNA Extraction and RT-PCR

HTR-8/SVneo and Swan.71 cells were cultured in 24-well plates and subjected to LG culture conditions without or with RuV infection (in a viral binding assay), as described above. Total mRNA was extracted using TRIzol reagent (Life Technologies, Tokyo, Japan), and contaminated genomic DNA was removed by treatment with DNAse I (TaKaRa Bio, Inc., Otsu, Japan). Real-time RT-PCR was performed using a One-Step TB Green Prime-Script PLUS RT-PCR Kit (Perfect Real Time; TaKaRa Bio) in a QuantStudio 3 Real-Time PCR System (Applied Biosystems, MA, United States). The following primer sequences were used: GRP78/BiP, sense, 5′-TGT TCA ACC AAT TAT CAG CAA ACT C-3′ and antisense, 5′-TTC TGC TGT ATC CTC TTC ACC AGT-3′; CHOP, sense, 5′-AGA ACC AGG AAA CGG AAA CAG A-3′ and antisense, 5′-TCT CCT TCA TGC GCT GCT TT-3′; RuV, sense, 5′-CCA CTG AGA CCG GCT GCG A-3′; antisense, 5′-GCC TCG GGG AGG AAG ATG AC-3′; and peptidylprolyl isomerase A (PPIA), sense, 5′-ATG CTG GAC CCA ACA CAA AT-3′ and antisense, 5′-TCT TTC ACT TTG CCA AAC ACC-3′. The results were analyzed using the delta–delta Ct method.

Apoptosis Assay

Tests were performed on the studied trophoblast cells grown in 96-well plates using an ApoStrand ELISA apoptosis detection kit (BIOMOL, Plymouth Meeting, PA, United States). This detection system uses monoclonal antibodies to single-stranded DNA (ssDNA), which is present in apoptotic, but not necrotic, cells or cells with DNA breaks in the absence of apoptosis. The cells were seeded at a density of 5×10^3 cells/well and cultured for 2 days prior to the LG treatments and RuV infection, as described above. ELISA was performed for apoptotic measurement at day 2 and day 5 pi. Briefly, the cells were fixed for 30 min with the kit fixative as indicated by the manufacturer and dried at 56°C for 20 min. Formamide was added to the cells, and the cells were heated at 56°C for 30 min to denature the DNA in apoptotic cells. After blocking, the cells were incubated with an antibody mixture for 30 min, washed, and incubated with 100 µl of peroxidase substrate for 45 min. The absorbance was read at 405 nm using an ELISA plate reader. Negative controls without viral inoculation and positive controls (provided in the kit) were also included.

Statistical Analysis

Analysis of variance was used to analyze the results. A value of $p < 0.05$ obtained using the Tukey–Kramer test and Statcel 4 software (OMS Publishing, Inc., Tokorozawa, Saitama, Japan) was considered significant. Data were presented as the mean ± SEM.

RESULTS

Upregulation of GRP78 and CHOP Under Low-Glucose Stress Conditions

In some experiments, the LG treatment showed slightly lower cell densities, approximately 85 ~ 87% of the control group (the cells cultured in SF RPMI medium, data not shown) as measured by a Cell Counting Kit-8 assay. Real-time PCR demonstrated increased induction of the ER-stress-response gene transcription factor C/EBP homologous protein (CHOP, also called DDIT3 or GADD153) for the cells subjected to the above experiments. Upregulation of GRP78/BiP mRNA was observed in the LG-, HG-LG-, and Tg-treated groups, and this observation was confirmed in the Western blotting results obtained 24 h posttreatment (**Figure 1**).

Enhancement of RuV Infection and Replication in First-Trimester Trophoblast Cells Under Low-Glucose Stress Conditions

Enhanced Intracellular Localization of RuV Capsid Protein in LG-Stressed Cells by Immunofluorescence Assay

The studied trophoblast cells were cultured under LG stress conditions prior to RuV infection. An immunofluorescence assay using an anti-capsid protein antibody showed an enhancement of the intracellular localization of RuV capsid protein in the LG-stressed cells compared with the control (**Figure 2**).

High Percentages of RuV-Positive Cells Under LG Stress Conditions as Shown by Flow Cytometric (FCM) Analysis

For the cells cultured in SF medium used as the control for LG stress experiments, an average of 5% (ranging from 3 to 7%) of the gated cells showed signals of infection. However, noticeably high percentages of RuV-positive cells were observed in the LG- and HGLG-treated groups, ranging from 15 to 33%, as noted in several repeated experiments (**Figure 3**). No significant difference was noted in the percentages of RuV-positive cells of the cells cultured in complete medium (FBS) compared with those cultured in the control, which is consistent with no difference in the expression of GRP78 and CHOP between these two groups (**Figures 1**, **3**).

Successful Viral Progeny Production in LG-Stressed Trophoblast Cells

Successful replication of RuV in LG-stressed cells was observed with Western blot analysis at 24 hpi (**Figure 4A**). Viral titer monitoring using FCM analysis showed substantial viral progeny production from day 2 to day 5 pi. The highest viral titers of the supernatants of the cells precultured in LG or HGLG media were observed on day 3 pi (**Figure 4B**).

No Difference in Apoptosis Between Uninfected and RuV-Infected LG-Stressed Cells

Apoptosis assays were performed on trophoblast cells grown in 96-well plates on days 2 and 5 pi. The cells without RuV infection but simultaneously subjected to LG stress conditions were also subjected to the apoptosis assay. No significant difference in apoptosis was found between the LG-stressed and non-LG-stressed groups in the RuV-infected experimental

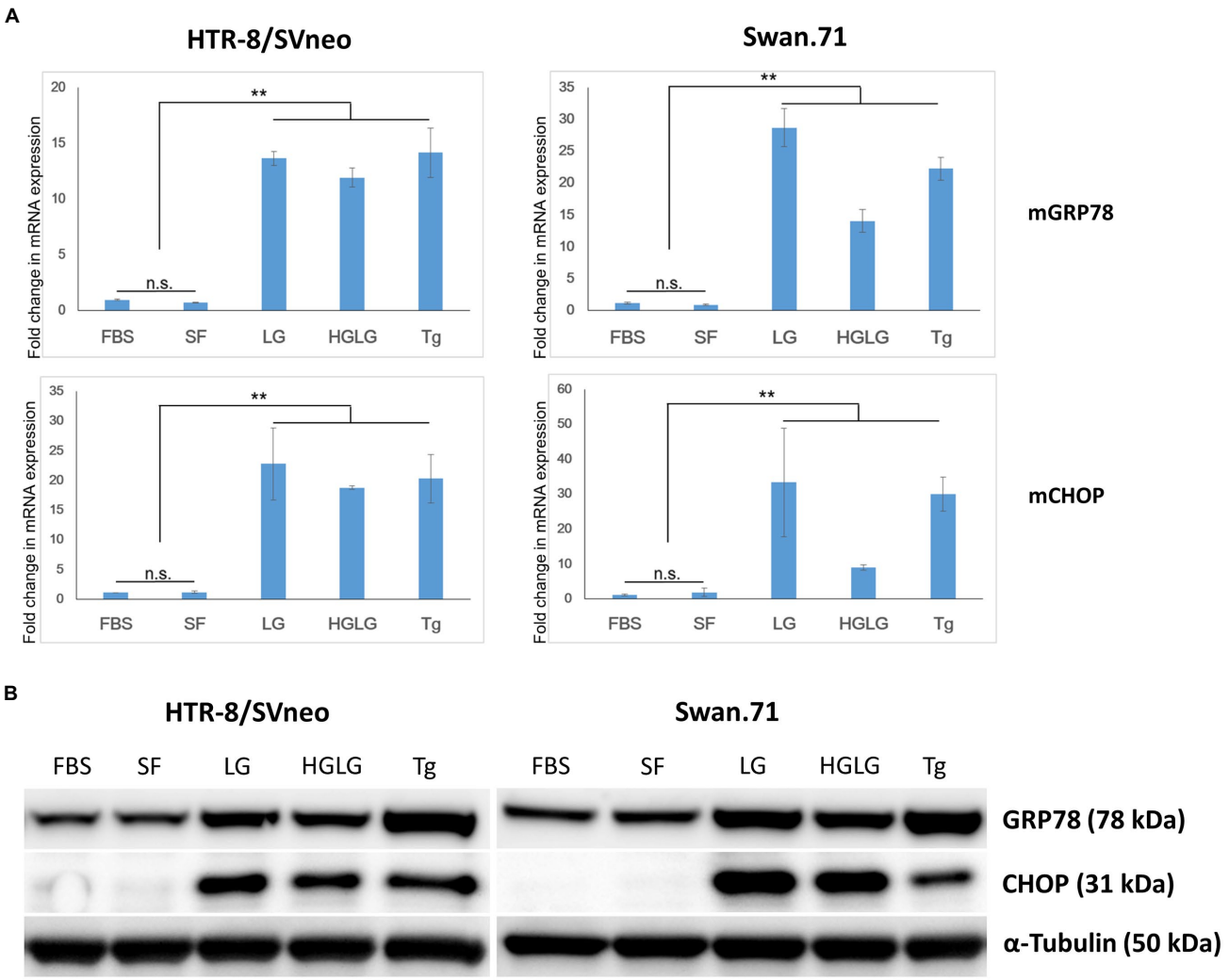

FIGURE 1 | Expression changes in ER stress-related markers in first-trimester trophoblast cells under low-glucose-induced ER stress conditions. Trophoblast cells were cultured in 6-well plates (for WB) or 24-well plates (for RNA extraction and PCR) in complete medium for 2 days before culture in LG (low glucose, 0.5 mM) medium for 24 h, HG (high glucose, 25 mM) medium for 6 h, and then LG medium for an additional 18 h. The cells cultured in SF medium (serum-free, RPMI/0.1% BSA) were used as a negative control. The cells cultured in complete medium (FBS) or in SF medium containing 25 nM thapsigargin (Tg) for 24 h were used as comparative references. **(A)** Enhancement of GRP78 and CHOP mRNA expression. The results are representative of three independent experiments. $^{**}p < 0.01$. **(B)** Increased expression of the ER stress-related markers GRP78 and CHOP by Western blotting.

groups. The absorbance values of LG-stressed cells infected with RuV were not different from those of the control cells or the stressed mock-infected cells (incubated with a culture medium or heat-inactivated virus). These results suggest that no significant apoptosis occurred in either of the RuV-infected groups (mock or LG-stressed) until day 5 pi (**Figure 4C**).

Enhancement of RuV Binding to LG-Stressed Trophoblast Cells by the Viral Binding Assay

After LG stress treatment, the cells were inoculated with RuV on ice for 1 h. The cells were washed and subjected to surface staining procedures for RuV. RNA was extracted for real-time PCR, and lysates were collected for Western blot analysis. The results obtained by FCM analysis showed that the percentages of RuV-positive cells increased significantly up to 5-fold in LG-stressed cells compared to the control cells (**Figure 5C**). These findings were confirmed by real-time PCR, which showed a corresponding increase in RuV RNA expression after normalization to the internal control, PPIA gene expression (**Figure 5B**). The enhancement of RuV binding to LG-stressed trophoblast cells was also observed with Western blot analysis (**Figure 5A**).

DISCUSSION

In this study, under the experimental LG stress conditions using LG or HGLG media, an enhancement of RuV infection of the human first-trimester trophoblast cell lines was noted.

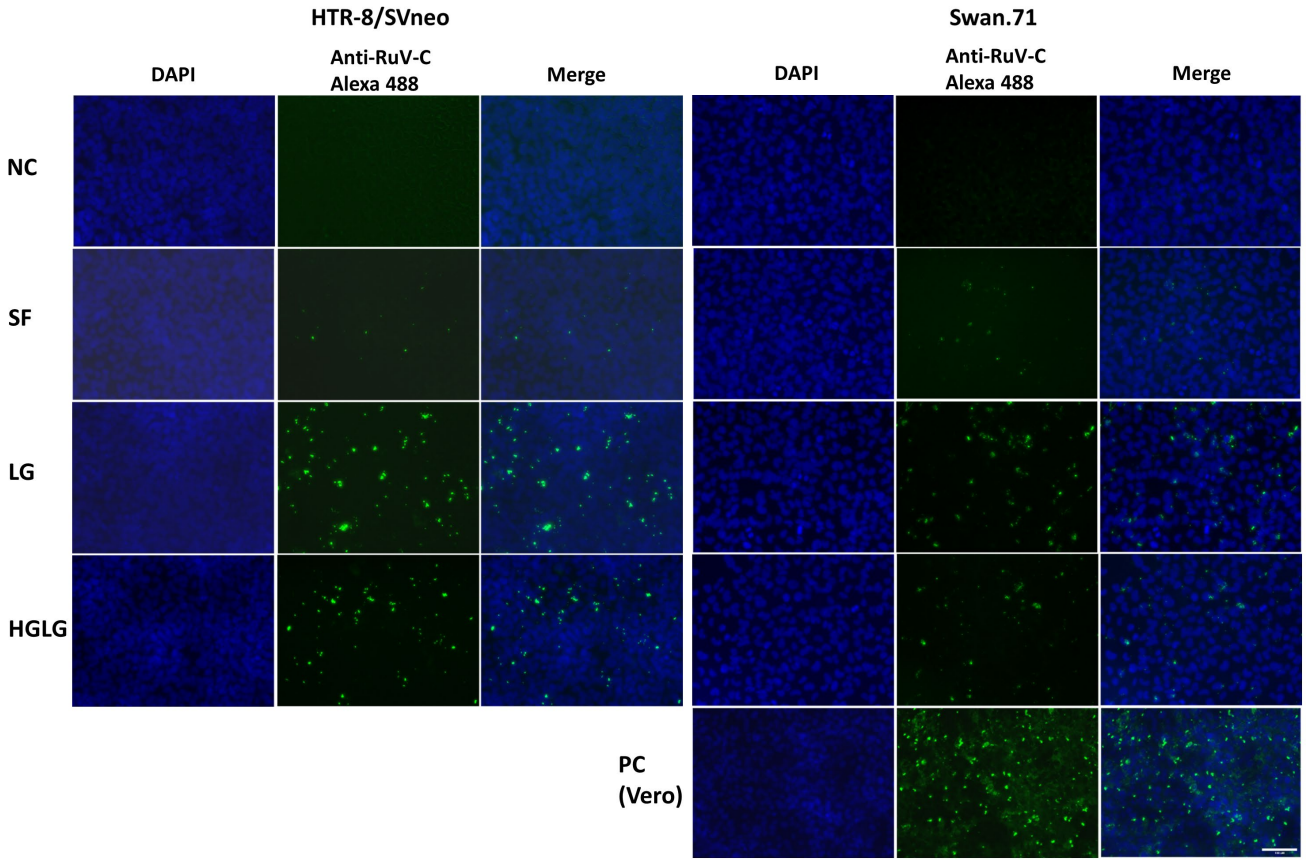

FIGURE 2 | Microscopy images of HTR-8/SVneo and Swan.71 cells infected with RuV under LG stress conditions. The cells were seeded onto 6-well plates containing glass coverslips and cultured for 1 to 2 days before LG stress treatments and viral infection. The cells were fixed 48 hpi and labeled with a mouse monoclonal anti-rubella viral capsid antibody (ab34749, Abcam), followed by an Alexa 488-conjugated goat anti-mouse IgG (H + L) secondary antibody (green). Nuclei were stained with DAPI (blue). RuV-infected Vero cells were used as positive controls. Trophoblast cells mock-infected, incubated with heat-inactivated RuV, or stained with mouse serum were used as negative controls. Images are representative of 3 independent experiments. RuV-C, rubella virus capsid. Scale bar: 100 μM.

Using an MOI of 5 to 10 to ensure that every single cell had the chance to theoretically come in contact with at least 1 infectious virus, the percentages of RuV-positive cells of the LG-stress groups reached over 30% on FCM analysis (**Figures 2, 3**). Increases in the percentages of RuV-infected cells observed along with enhanced expression of ER stress markers (GRP78 and CHOP) imply that LG-induced ER stress could enhance RuV infection in these trophoblast cells.

There is a gap in our understanding of the mechanisms of transplacental RuV infection in early pregnancy. Well-established studies of CRS found that this congenital abnormality often occurred in early pregnancy, with an incidence as high as 90% (Hobman, 2013). Current articles have reported that trophoblast cells are resistant to many viral infections, including RuV (Bayer et al., 2015; Trinh et al., 2018). Our latest experimental results showed that RuV has low infectivity to the first-trimester trophoblast cell lines HTR-8/SVneo and Swan.71 *in vitro* (Pham et al., 2022). Early studies suggested that transplacental RuV infection targets fetal endothelial cells and Hofbauer cells instead of trophoblasts (Perelygina et al., 2013, 2015). However, a very early study reported an *in vitro* RuV infection model employing choriocarcinoma cell lines and suggested some conditions permitting transplacental infection *via* trophoblasts (Sugiura, 1982). Thus, we investigated possible *in vivo* conditions that enable RuV infection into trophoblasts. Subsequently, with the finding of an increase in the susceptibility of these cells to RuV under low-glucose stress conditions, the present study provides a promising approach for understanding the mechanisms of RuV infection of first-trimester trophoblast cells.

Not only were significant increases in RuV infection in LG-induced ER-stressed trophoblast cells noted, but successful replication and a release of progeny virus into the supernatant were also observed (**Figures 4A,B**). Substantial viral progeny production was observed from day 2 to day 5 pi, with a peak at day 3 pi. These findings suggest that RuV can infect EVTs during pregnancy under some LG-induced ER stress conditions, replicate in these cells, and successfully produce progeny virus, which leads to RuV infection of other fetal cells and causes unfavorable outcomes for the fetus. To support the study findings, future studies utilizing other appropriate

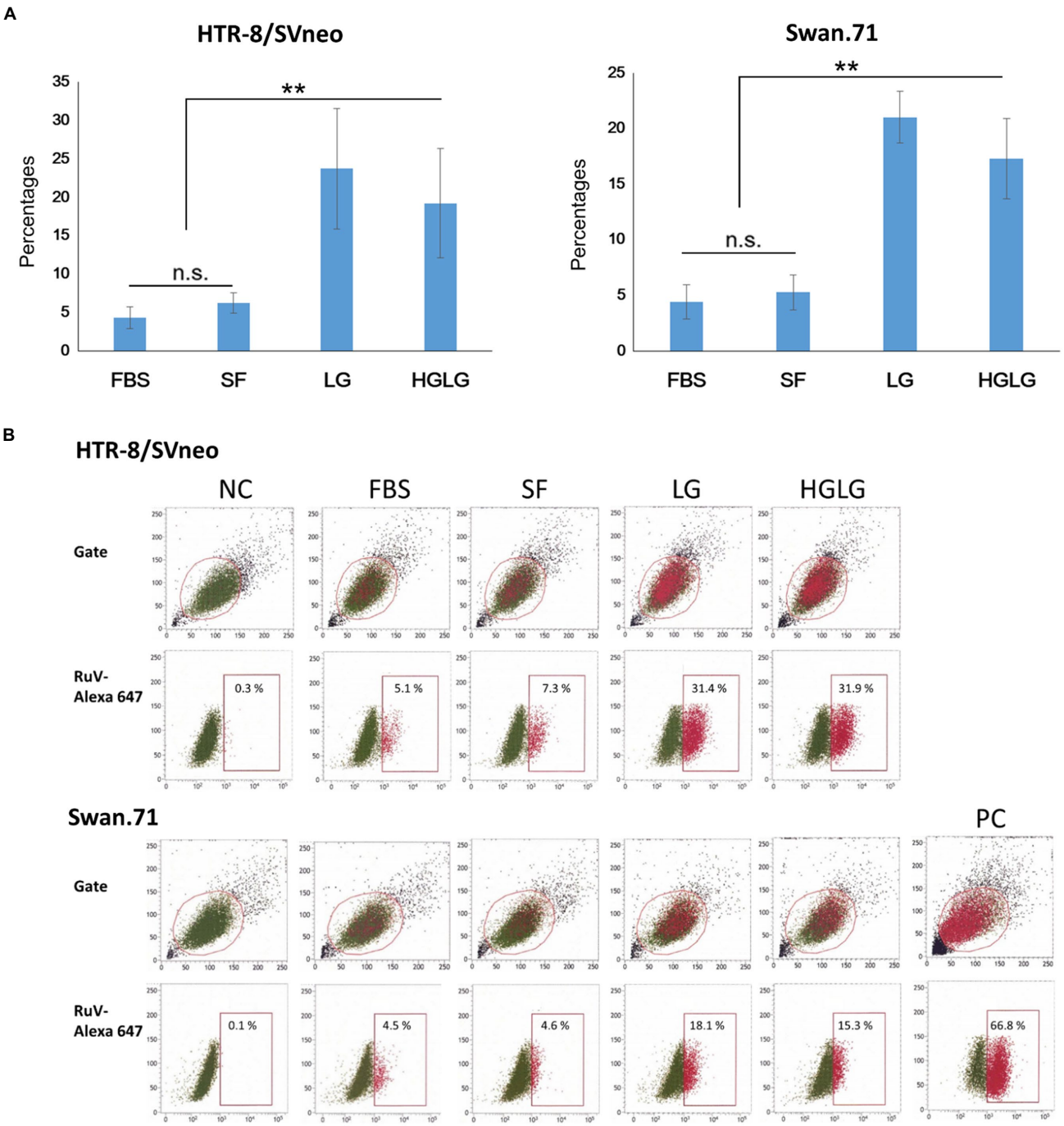

FIGURE 3 | (A) Percentages of the studied trophoblast, HTR-8/SVneo and Swan.71 cells positive for RuV as determined by FCM analysis at 24 hpi. Trophoblast cells were seeded at a density of 5×10^3 cells/well in a 96-well plate. After LG stress treatments and RuV infection at an MOI of 5–10, the cells were collected at 24 to 48 hpi and labeled with a Live/Dead Fixable Near-IR Dead Cell Stain Kit to exclude dead cells from analysis. Intracellular staining was performed with a mouse monoclonal anti-rubella viral capsid antibody followed by an Alexa-488 conjugated goat anti-mouse IgG (H+L) secondary antibody. Mock-infected cells using culture medium were used as negative controls (NCs). Vero cells infected with RuV performed in parallel were used as positive controls (PCs). The results are expressed as the mean of at least triplicate experiments in each group, and each graph is representative of three independent experiments. $^{**}p < 0.01$. **(B)** Representative images of flow cytometry analysis. Numbers displayed inside each panel correspond to the percentage of the cells positive for RuV capsid protein of the parent gated population.

cells, such as primary trophoblast cells and explant culture, as well as expanding to other trophoblast types, such as BeWo cells, are necessary.

RuV is well known for its ability to suppress apoptosis *via* its capsid protein (Willows et al., 2014). No significant amount of apoptosis occurred in RuV-infected, ER-stressed cells on days

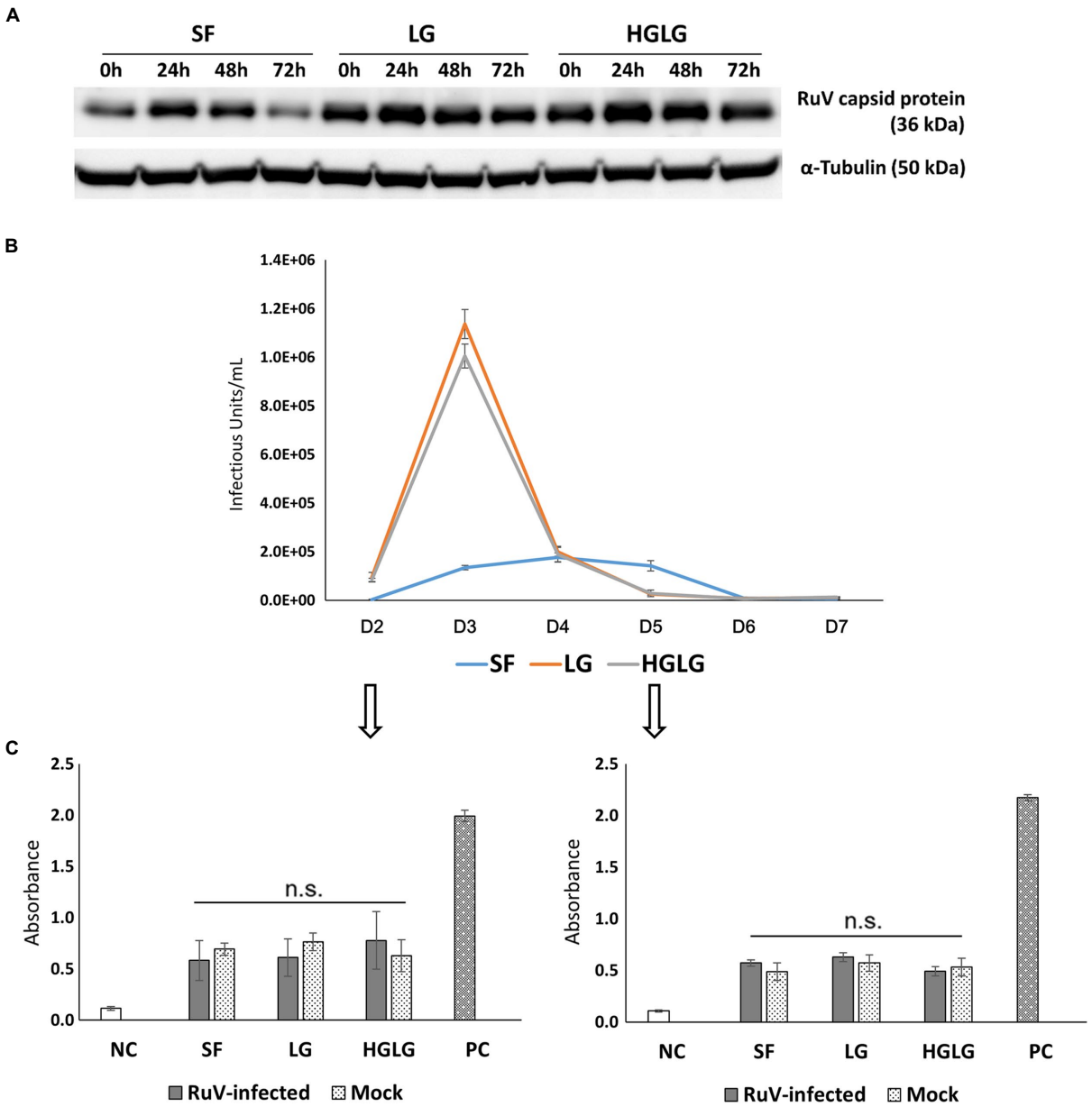

FIGURE 4 | Investigation of viral replication and apoptosis in LG-stressed RuV-infected HTR-8/SVneo cells. **(A)** Viral replication in LG-stressed RuV-infected cells shown by Western blotting. Trophoblast cells were cultured in 12-well plates, subjected to LG stress, and then inoculated with RuV. At 0, 24, 48, and 72 hpi, the lysate was collected for Western blot analyses. Cells cultured in SF medium were used as the controls for LG stress treatments. **(B)** Titers of viral progeny in the supernatants collected from day 2 to day 7 pi as determined by FCM analysis. Trophoblast cells were cultured in a 96-well plate and subjected to LG stress and RuV infection as described. From 48 hpi, the entire supernatant was collected daily and replaced with a new medium until day 7 pi. The collected supernatants were used to infect freshly prepared Vero cells and titered by FCM analysis as described elsewhere. The graph is representative of two independent experiments. The results are expressed as the mean of at least triplicate experiments in each group, and the graph is representative of two independent experiments. **(C)** No enhancement of apoptosis of LG stress-infected trophoblast cells. Trophoblast cells were seeded at a density of 5×10^3 cells/well onto a 96-well flat-bottom plate as specified by the manufacturer. After 2 d of culture and subsequent LG stress and RuV infection, ELISA detection of single-stranded DNA present in apoptotic cells was performed at days 2 and 5 pi. The cells subjected to LG stress and mock infection were treated in parallel and used for comparison. Single-stranded DNA provided in the ELISA kit was used as a positive control. The results are expressed as the mean of at least triplicate experiments in each group, and the graph is representative of two independent experiments. NC, negative control; mock, mock-infected with virus-free medium; PC, positive control; n.s., nonsignificant.

2 and 5 pi in the present study, which suggests that the viral progeny production pattern was not associated with apoptosis, but that an intracellular resource was necessary for viral production.

Recent findings have shown that RuV has two distinct binding mechanisms for viral entry: a Ca^{2+}-dependent mechanism observed in lymphoid cells and a Ca^{2+}-independent mechanism

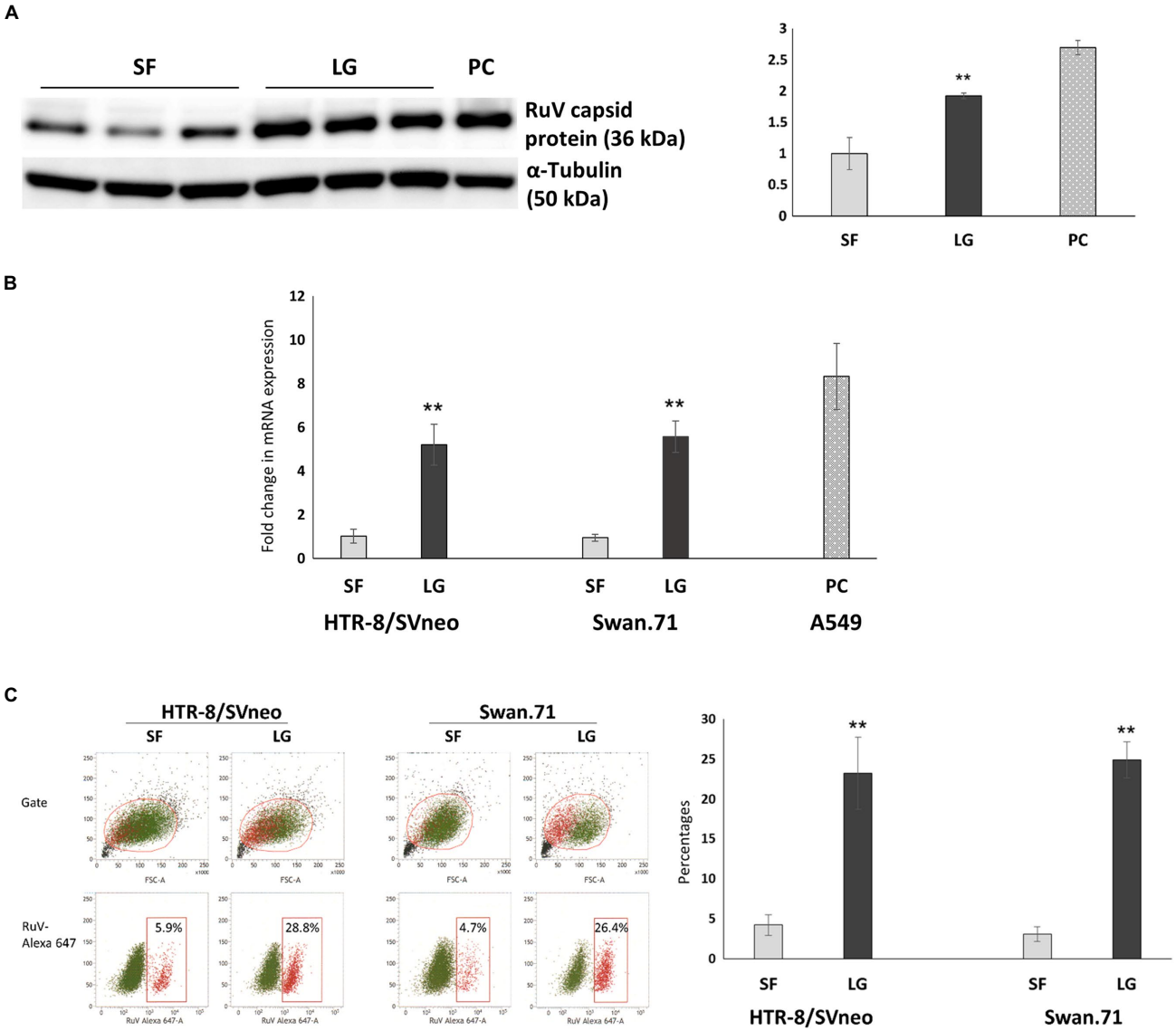

FIGURE 5 | Viral binding assays showed an enhancement of RuV binding to LG-stressed trophoblast cells. After LG stress treatment, the cells were inoculated with RuV at an MOI of 5 to 10 on ice for 1 h. After washing, the cells were lysed and subjected to Western blot analysis, RNA extraction, and real-time PCR, or surface staining procedures for RuV were performed, and the cells were analyzed by FCM. **(A)** Increased expression of the RuV capsid protein in HTR-8/SVneo cells under LG stress, as shown by Western blot analysis. The graph was constructed based on band intensities (arbitrary units) normalized to the value of the cells cultured in SF medium. Values shown are the mean of three independent experiments ± SEM. PC, A549 cells. **(B)** Increased viral RNA expression in HTR-8/SVneo and Swan.71 cells cultured in LG medium. Data shown are the means of fold-change of relative expression values (normalized to the internal control PPIA gene expression) ± SEM. **(C)** Increased percentages of RuV-positive HTR-8/SVneo and Swan.71 cells cultured in LG medium determined by FCM analysis. **(B,C)** The results are expressed as the mean (± SEM) of at least triplicate experiments in each group, and the graph is representative of two independent experiments. $^{**}p < 0.01$.

involving unidentified RuV receptor(s) (Otsuki et al., 2018). Myelin oligodendrocyte glycoprotein (MOG) is a receptor for RuV, but it is primarily expressed in the central nervous system (Cong et al., 2011) and not detected in trophoblasts (Trinh et al., 2018). We used the viral binding assay and observed successful RuV binding of the studied trophoblast cells under LG culture, which is representative of the experimental LG-induced ER stress treatment. Compared to the controls, the treatment increased viral binding to the studied cells up to 5-fold. The finding implies that alternative receptors expressed during the LG-induced ER stress process may be involved in viral entry. Recent studies suggest that microorganisms can utilize proteins or components of the cellular stress responses to facilitate their infection process. Viruses, including the SARS-CoV-2, can bind to the GRP78 protein involved in the unfolded protein responses in ER stress for their entry into target cells

(Rayner et al., 2020; Gonzalez-Gronow et al., 2021; Trinh, 2022). Therefore, to determine which proteins induce RuV infection enhancement in the treated trophoblast cells in this study, the GRP78 and other proteins such as GRP94 of the low-glucose ER stress response are highly potential candidates.

In conclusion, although the mechanisms underlying RuV entry into LG-induced ER-stressed cells and RuV replication in these cells are not known and require further investigation using appropriate approaches, these findings suggest that a certain degree of LG-induced ER stress in early pregnancy may facilitate infection and cause CRS.

DATA AVAILABILITY STATEMENT

The original contributions presented in the study are included in the article/supplementary material; further inquiries can be directed to the corresponding authors.

AUTHOR CONTRIBUTIONS

QT, SK-A, HU, and SH: conceptualization. QT, KT, NP, and SK-A: methodology and formal analysis. SK-A and SH: validation. QT, KT, NP, and TN: investigation. KT, CT, SO, HU, SK-A, and SH: resources. QT and NP: writing—original draft preparation. QT, KT, CT, TN, SO, SK-A, HU, and SH: writing—review and editing. QT and SH: funding acquisition. All authors contributed to the article and approved the submitted version.

FUNDING

This study was supported by Grants-in-Aid for Scientific Research under the Japan Society for the Promotion of Science (JSPS KAKENHI) grant numbers 17H04341 (to SH) and 20 K08829 (to QT).

REFERENCES

Bastida-Ruiz, D., Aguilar, E., Ditisheim, A., Yart, L., and Cohen, M. (2017). Endoplasmic reticulum stress responses in placentation - A true balancing act. *Placenta* 57, 163–169. doi: 10.1016/j.placenta.2017.07.004

Bayer, A., Delorme-Axford, E., Sleigher, C., Frey, T. K., Trobaugh, D. W., Klimstra, W. B., et al. (2015). Human trophoblasts confer resistance to viruses implicated in perinatal infection. *Am. J. Obstet. Gynecol.* 212:e78. doi: 10.1016/j.ajog.2014.07.060

Burton, G. J., and Yung, H. W. (2011). Endoplasmic reticulum stress in the pathogenesis of early-onset pre-eclampsia. *Pregnancy Hypertens* 1, 72–78. doi: 10.1016/j.preghy.2010.12.002

Burton, G. J., Yung, H. W., and Murray, A. J. (2017). Mitochondrial - endoplasmic reticulum interactions in the trophoblast: stress and senescence. *Placenta* 52, 146–155. doi: 10.1016/j.placenta.2016.04.001

Chang, C. W., Wakeland, A. K., and Parast, M. M. (2018). Trophoblast lineage specification, differentiation and their regulation by oxygen tension. *J. Endocrinol.* 236, R43–R56. doi: 10.1530/JOE-17-0402

Chen, R. M., Merits, A., Bolling, B., Nasar, F., Coffey, L., Powers, A., et al. (2018). Create a new family *Matonaviridae* to include the genus *Rubivirus*, removed from the family *Togaviridae*. Available at: https://talk.ictvonline.org/files/ictv_official_taxonomy_updates_since_the_8th_report/m/animal-ssrna-viruses/8087 (accessed on 8016 February 2022).

Cong, H., Jiang, Y., and Tien, P. (2011). Identification of the myelin oligodendrocyte glycoprotein as a cellular receptor for rubella virus. *J. Virol.* 85, 11038–11047. doi: 10.1128/JVI.05398-11

Gonzalez-Gronow, M., Gopal, U., Austin, R. C., and Pizzo, S. V. (2021). Glucose-regulated protein (GRP78) is an important cell surface receptor for viral invasion, cancers, and neurological disorders. *IUBMB Life* 73, 843–854. doi: 10.1002/iub.2502

Graham, C. H., Hawley, T. S., Hawley, R. G., MacDougall, J. R., Kerbel, R. S., Khoo, N., et al. (1993). Establishment and characterization of first trimester human trophoblast cells with extended lifespan. *Exp. Cell Res.* 206, 204–211. doi: 10.1006/excr.1993.1139

Grigorov, B., Rabilloud, J., Lawrence, P., and Gerlier, D. (2011). Rapid titration of measles and other viruses: optimization with determination of replication cycle length. *PLoS One* 6:e24135. doi: 10.1371/journal.pone.0024135

Guzel, E., Arlier, S., Guzeloglu-Kayisli, O., Tabak, M. S., Ekiz, T., Semerci, N., et al. (2017). Endoplasmic reticulum stress and homeostasis in reproductive physiology and pathology. *Int. J. Mol. Sci.* 18:0792. doi: 10.3390/ijms18040792

Hobman, T. C. (2013). "Rubella Virus," in *Fields Virology. Vol. 1. 6th Edn.* eds. D. M. Knipe and P. Howley (Philadelphia: Lippincott Williams & Wilkins), 687–711.

Khunti, K., Alsifri, S., Aronson, R., Cigrovski Berkovic, M., Enters-Weijnen, C., Forsen, T., et al. (2016). Rates and predictors of hypoglycaemia in 27 585 people from 24 countries with insulin-treated type 1 and type 2 diabetes: the global HAT study. *Diabetes Obes. Metab.* 18, 907–915. doi: 10.1111/dom.12689

Lian, I. A., Loset, M., Mundal, S. B., Fenstad, M. H., Johnson, M. P., Eide, I. P., et al. (2011). Increased endoplasmic reticulum stress in decidual tissue from pregnancies complicated by fetal growth restriction with and without pre-eclampsia. *Placenta* 32, 823–829. doi: 10.1016/j.placenta.2011.08.005

Mamun, M. M. A., and Khan, M. R. (2021). COVID-19 Delta variant-of-concern: A real concern for pregnant women With gestational diabetes mellitus. *Front Endocrinol (Lausanne)* 12:778911. doi: 10.3389/fendo.2021.778911

Ni, M., and Lee, A. S. (2007). ER chaperones in mammalian development and human diseases. *FEBS Lett.* 581, 3641–3651. doi: 10.1016/j.febslet.2007.04.045

Otsuki, N., Sakata, M., Saito, K., Okamoto, K., Mori, Y., Hanada, K., et al. (2018). Both Sphingomyelin and cholesterol in the host cell membrane are essential for rubella virus entry. *J. Virol.* 92:3017. doi: 10.1128/JVI.01130-17

Perelygina, L., Adebayo, A., Metcalfe, M., and Icenogle, J. (2015). Differences in establishment of persistence of vaccine and wild type rubella viruses in fetal endothelial cells. *PLoS One* 10:e0133267. doi: 10.1371/journal.pone.0133267

Perelygina, L., Zheng, Q., Metcalfe, M., and Icenogle, J. (2013). Persistent infection of human fetal endothelial cells with rubella virus. *PLoS One* 8:e73014. doi: 10.1371/journal.pone.0073014

Pham, N. T. K., Trinh, Q. D., Takada, K., Komine-Aizawa, S., and Hayakawa, S. (2022). Low susceptibility of rubella virus in first-trimester trophoblast cell lines. *Viruses* 14:1169. doi: 10.3390/v14061169

Pham, N. T. K., Trinh, Q. D., Takada, K., Takano, C., Sasano, M., Okitsu, S., et al. (2021). The epithelial-to-Mesenchymal transition-Like process induced by TGF-beta1 enhances rubella virus binding and infection in A549 cells via the Smad pathway. *Microorganisms* 9:0662. doi: 10.3390/microorganisms9030662

Rayner, J. O., Roberts, R. A., Kim, J., Poklepovic, A., Roberts, J. L., Booth, L., et al. (2020). AR12 (OSU-03012) suppresses GRP78 expression and inhibits SARS-CoV-2 replication. *Biochem. Pharmacol.* 182:114227. doi: 10.1016/j.bcp.2020.114227

Sarina Li, D. F., Feng, Z. Q., Du, J., Zhao, W. H., Huang, N., et al. (2019). Mechanism of placenta damage in gestational diabetes mellitus by investigating TXNIP of patient samples and gene functional research in cell line. *Diabetes Ther* 10, 2265–2288. doi: 10.1007/s13300-019-00713-z

Schwarz, D. S., and Blower, M. D. (2016). The endoplasmic reticulum: structure, function and response to cellular signaling. *Cell. Mol. Life Sci.* 73, 79–94. doi: 10.1007/s00018-015-2052-6

Silva, J. F., and Serakides, R. (2016). Intrauterine trophoblast migration: A comparative view of humans and rodents. *Cell Adhes. Migr.* 10, 88–110. doi: 10.1080/19336918.2015.1120397

Straszewski-Chavez, S. L., Abrahams, V. M., Alvero, A. B., Aldo, P. B., Ma, Y., Guller, S., et al. (2009). The isolation and characterization of a novel telomerase immortalized first trimester trophoblast cell line, swan 71. *Placenta* 30, 939–948. doi: 10.1016/j.placenta.2009.08.007

Sugiura, K. (1982). Studies on trans-placental infection of rubella virus. *J. Jûzen Medical Soc.* 91, 42–61.

Trinh, Q. D. (2022). Recent research in cell stress and microbial infection. *Microorganisms* 10:622. doi: 10.3390/microorganisms10030622

Trinh, Q. D., Pham, N. T. K., Takada, K., Komine-Aizawa, S., and Hayakawa, S. (2018). Myelin Oligodendrocyte glycoprotein-independent rubella infection of keratinocytes and resistance of first-trimester Trophoblast cells to rubella virus In vitro. *Viruses* 10:0023. doi: 10.3390/v10010023

Veerbeek, J. H., Tissot Van Patot, M. C., Burton, G. J., and Yung, H. W. (2015). Endoplasmic reticulum stress is induced in the human placenta during labour. *Placenta* 36, 88–92. doi: 10.1016/j.placenta.2014.11.005

Willows, S., Ilkow, C. S., and Hobman, T. C. (2014). Phosphorylation and membrane association of the rubella virus capsid protein is important for its anti-apoptotic function. *Cell. Microbiol.* 16, 1201–1210. doi: 10.1111/cmi.12272

Yoshida, T., Takada, K., Komine-Aizawa, S., Kamei, Y., Ishihara, O., and Hayakawa, S. (2021). *Lactobacillus crispatus* promotes invasion of the HTR-8/SVneo trophoblast cell line. *Placenta* 111, 76–81. doi: 10.1016/j.placenta.2021.06.006

Yung, H. W., Alnaes-Katjavivi, P., Jones, C. J., El-Bacha, T., Golic, M., Staff, A. C., et al. (2016). Placental endoplasmic reticulum stress in gestational diabetes: the potential for therapeutic intervention with chemical chaperones and antioxidants. *Diabetologia* 59, 2240–2250. doi: 10.1007/s00125-016-4040-2

Conflict of Interest: The authors declare that the research was conducted in the absence of any commercial or financial relationships that could be construed as a potential conflict of interest.

Publisher's Note: All claims expressed in this article are solely those of the authors and do not necessarily represent those of their affiliated organizations, or those of the publisher, the editors and the reviewers. Any product that may be evaluated in this article, or claim that may be made by its manufacturer, is not guaranteed or endorsed by the publisher.

frontiers | Frontiers in Microbiology

TYPE Original Research
PUBLISHED 10 August 2022
DOI 10.3389/fmicb.2022.932842

OPEN ACCESS

EDITED BY
Chao Shen,
Wuhan University, China

REVIEWED BY
Yan-Dong Tang,
Harbin Veterinary Research Institute (CAAS), China
Natalia Sampaio,
Hudson Institute of Medical Research, Australia

*CORRESPONDENCE
Ruofei Feng
fengruofei@xbmu.edu.cn

†These authors have contributed equally to this work

SPECIALTY SECTION
This article was submitted to Virology, a section of the journal Frontiers in Microbiology

RECEIVED 30 April 2022
ACCEPTED 27 June 2022
PUBLISHED 10 August 2022

CITATION
Xie J, Li X, Yang S, Yan Z, Chen L, Yang Y, Li D, Zhang X and Feng R (2022) DDX56 inhibits PRV replication through regulation of IFN-β signaling pathway by targeting cGAS. *Front. Microbiol.* 13:932842. doi: 10.3389/fmicb.2022.932842

DDX56 inhibits PRV replication through regulation of IFN-β signaling pathway by targeting cGAS

Jingying Xie[1,2†], Xiangrong Li[1†], Shunyu Yang[2], Zhenfang Yan[1], Lei Chen[1], Yanmei Yang[2], Dianyu Li[1], Xiangbo Zhang[1] and Ruofei Feng[1,3*]

[1]Key Laboratory of Biotechnology and Bioengineering of State Ethnic Affairs Commission, Biomedical Research Center, Northwest Minzu University, Lanzhou, China, [2]College of Life Science and Engineering, Northwest Minzu University, Lanzhou, China, [3]Gansu Tech Innovation Center of Animal Cell, Biomedical Research Center, Northwest Minzu University, Lanzhou, China

Pseudorabies virus (PRV) is an agent of Aujeszky's disease, and causes great economic losses to pig farming. Re-outburst of pseudorabies implies that new control measures are urgently needed. We show here that DDX56 possesses the ability to inhibit PRV replication *in vitro*, which may be an important factor for PRV infection. Overexpression of DDX56 inhibited PRV genomic DNA transcription and lower titers of PRV infection in PK15 cells, whereas down-regulation of the DDX56 expression had a promotion role on virus replication. Further study demonstrated that DDX56 exerted its proliferation-inhibitory effects of PRV through up-regulating cGAS-STING-induced IFN-β expression. Moreover, we found that DDX56 could promote cGAS expression and direct interaction also existed between DDX56 and cGAS. Based on this, DDX56-regulated IFN-β pathway may be targeted at cGAS. To verify this, down-regulated cGAS expression in DDX56 over-expression cells was performed. Results indicated that knockdown of cGAS expression could abrogate the inhibition role of DDX56 on PRV proliferation and weaken the effect of DDX56 on IFN-β expression. In addition, DDX56 played a promotion role in IRF3 phosphorylation and nucleus translocation. Altogether, our results highlight DDX56's antiviral role in PRV infection, and our findings contribute to a better understanding of host factors controlling PRV replication.

KEYWORDS

pseudorabies virus, DDX56 protein, innate immune response, IFN-β, cGAS

Introduction

Pseudorabies virus (PRV), a member of the alpha herpesvirinae subfamily, is responsible for Aujeszky's disease. With a genome of ∼140 kb, it encodes more than 70 proteins (Pomeranz et al., 2005). PRV can infect a diverse range of domesticated and wild hosts. It was reported recently that PRV could pose a risk to humans, as indicated by some cases with clinical signs. Pigs are the natural host and reservoir for PRV (Fonseca et al., 2012; Ai et al., 2018). Until now, PRV has been studied in regard to its pathogenesis, but

little is known about the host factors affecting viral replication. Therefore, researchers should investigate the host factors that regulate viral replication, and understanding host-virus interactions may lead to the development of more effective antiviral therapies.

The DEAD-box (Asp-Glu-Ala-Asp) proteins are ATP-dependent RNA helicases that contribute to RNA metabolism (Zirwes et al., 2000). These helicases also take part in host immune defense. For example, DDX1, DDX21, and DHX36 form a complex with adaptor protein TRIF in the cytosol to control IFN responses (Zhang et al., 2011a). Also, DDX60, DDX3, and DHX9 are also involved in type I IFN induction and RNA sensing (Oshiumi et al., 2010; Miyashita et al., 2011; Zhang et al., 2011b). There may be many other helicases that possess unidentified antiviral activity. Another RNA helicase from the DEAD-box family, DDX56, is an evolutionary conserved antiviral factor that controls alphavirus infection (Taschuk et al., 2020). By directly interacting with viral proteins or host proteins, the DDX56 protein can affect some viruses' replication. In this respect, it is one of several cellular factors that could affect the replication of certain viruses, for instance, the west Nile virus (WNV) (Xu and Hobman, 2012; Reid and Hobman, 2017), foot and mouth disease virus (FMDV) (Fu et al., 2019), influenza A virus (IAV) (Pirinçal and Turan, 2021), and encephalomyocarditis virus (EMCV) (Xu et al., 2022). Nevertheless, the mechanism by which porcine DDX56 controls PRV infection and its underlying mechanisms have yet to be fully elucidated.

Porcine DDX56 was studied here in relation to PRV infection and its underlying mechanisms. We observed that DDX56 exerts an inhibitory effect on PRV proliferation. To exert its antiviral effects, DDX56 increases cGAS-STING-induced IFN-β production. Deeper research found that DDX56 could promote cGAS expression and interact with cGAS under physiological conditions. Knockdown of cGAS expression could abrogate the inhibition role of DDX56 on PRV proliferation and weaken the effect of DDX56 on IFN-β expression. In addition, DDX56 plays a promotion role in IRF3 phosphorylation and nucleus translocation. Altogether, we gain a better understanding of host control of PRV proliferation with these findings and shed light on understanding the interaction between the host and PRV infection.

Materials and methods

Cells and viruses

Porcine kidney (PK15) and baby hamster kidney (BHK-21) cells were used in this study. They were maintained in Dulbecco's modified Eagle's medium (DMEM) supplemented with 10% newborn bovine serum (NBS) and grown at a 37°C/5% CO_2 incubator. The PRV Bartha-K61 is an attenuated vaccine strain and stored in our laboratory. Bartha-K61 was propagated in BHK-21 cells, and the supernatants of infected cells were clarified and stored at −80°C.

Antibodies and chemicals

The commercial antibodies used in this study were purchased from the indicated manufacturers. An Anti-FLAG tag rabbit polyclonal antibody (D110005), an Anti-cGAS rabbit polyclonal antibody (D163570), HRP (horseradish peroxidase)-conjugated Goat Anti-Rabbit IgG (D110058), and HRP-conjugated Goat Anti-Mouse IgG (D110087) were used and bought from Sangon Biotech (Shanghai, China). Polyclonal antibody of MAVS (14341-1-AP), HA tag, and IRF3 (11312-1-AP) were purchased from Proteintech (Wuhan, China). Antibody of STING (13647S), TBK1 (3013S), Myc-Tag (2276S), and Phospho-IRF-3 (Ser386) (37829S) were bought from Cell Signaling Technology. Monoclonal Antibody of GAPDH (AF5009) and β-actin (AA128) were obtained from Beyotime Biotechnology (Shanghai, China). Anti-Histone H3 Polyclonal Antibody (K106623P) was purchased from Solarbio (Beijing, China).

Porcine DDX56, MAVS, and cGAS siRNAs were synthesized from RiboBio Co., Ltd (Guangzhou, China). Plasmids encoding DDX56 (Myc tag), and important adaptor proteins in the cGAS-STING pathway, including cGAS (HA tag), STING (HA tag), TBK1 (FLAG tag) and the active form of IRF3 (IRF3/5D) (FLAG tag) were constructed in-house. TransStart®Top Green qPCR SuperMix (+Dye II) was purchased from Transgen (Beijing, China). Premix Ex Taq™ (Probe qPCR) was bought from Takara Biomedical Technology (Beijing, China). Lipofectamine 3000 was purchased from Invitrogen. ISD (tlrl-isdc) and poly (dA:dT) (tlrl-patc) were purchased from InvivoGen.

Western blotting

Myc-DDX56 expression plasmids were generated by amplifying the DDX56 gene from PK15 cells and cloned into the pCMV-Myc vector. Subsequently, PK15 cells were transfected with the expression plasmid using Lipofectamine® 3000 reagent according to the manufacturer's instructions. Cells were collected and whole-cell extracts were prepared from cells with RIPA lysis buffer (Solarbio, Beijing, China). Cell extracts were subjected to SDS-PAGE and the separated proteins were transferred to the PVDF membranes (Millipore). Skimmed milk diluted in PBS/Tween® 20 was used to block the non-specific antibody binding sites, followed by the specific primary and HRP (horseradish peroxidase)-conjugated secondary antibodies. Detection of the proteins was carried out using an ECL reagent (BioRad, United States) and GAPDH or β-actin was used as loading controls.

Viral infection

PK15 cells transfection was performed using Lipofectamine 3000 (Invitrogen, United States) according to the manufacturer's instruction. Then, the cells were infected with PRV at 100 $TCID_{50}$. The viral inoculum was removed 2 h later, and the infected cells were cultured in DMEM containing 3% NBS. Cell-free culture supernatants and lysates were harvested at 24-h post-infection to evaluate the effect of DDX56 on PRV replication.

RNA extraction and RT-qPCR

The IFN-β mRNA transcription level was determined using relative qPCR. Total RNA was extracted and performed as previously described (Xie et al., 2020). All primers used in this study are available upon request.

Detection and quantitation of the PRV genome

The viral genomic copies of PRV were achieved by quantitative RT-PCR. Viral DNA was isolated using Viral Genomic DNA Extraction Kit (TIANGEN, Beijing, China) and performed as previously described (Xie et al., 2020).

RNAi assay

siRNA targeting DDX56 was transfected into PK15 cells to verify the effect of DDX56 knockdown. Lipofectamine® 3000 was used to transfect PK-15 cells with siNC or siDDX56 for 24 h, followed by inoculation with 100 $TCID_{50}$ PRV. Cell supernatants were tested for viral titers in BHK-21 cells using the $TCID_{50}$ assay.

Co-immunoprecipitation assay

Cells were collected with NP40 supplemented with a proteasome inhibitor and incubated with the indicated antibodies for 10 h at 4°C. Each lysate was then treated with 10 μl of Protein G agarose slurry (Beyotime, China). After incubation at 4°C for 4 h, the lysates were centrifuged at 2,500 rpm for 5 min. After collecting the beads, they were washed in ice-cold PBS five times. The precipitate was mixed with SDS buffer and boiled for 5 min at 95°C. After centrifuging at 6,000 rpm for 1 min, the supernatant was analyzed.

Virus titration

BHK-21 cells were used in these experiments. The related operations were as followed: five replicates of BHK-21 cells were infected with tenfold serial dilutions of PRV, and fresh DMEM was added after 2 h at 37°C. The PRV titers were determined after 48–72 h at 37°C using the Reed-Muench method.

Enzyme-linked immunosorbent assay

IFN-β secretion expression levels in the cell supernatants were detected using a swine IFN-β enzyme-linked immunosorbent assay (ELISA) kit (Jianglaibio, Shanghai, China) according to the manufacturer's instructions.

Nuclear and cytoplasmic extraction

PK15 cells were transfected with Myc tagged DDX56 plasmids for 24 h, then the cells were infected with PRV or mock uninfected for another 24 h. Cells were washed with PBS and lysed with 400 μl of extracting solution A with protease inhibitors and phosphatase inhibitors (BestBio, China). The homogenate was centrifuged at 4°C 1,000 g for 5 min. Next, the supernatant was saved as cytoplasm and placed on ice for 30 min. The pellet was re-suspended with 200 μL extracting solution B, which included protease inhibitor and phosphatase inhibitors. 5 μL solution C was also added. Placed on ice for 30 min, and then kept it as the nuclei. The precipitates were analyzed by western blotting using specific antibodies.

Statistical analysis

ANOVA was used to compare measurements. Student's *t*-test was used to determine statistical significance. Values were expressed in graph bars as the mean ± SD of at least three independent experiments unless otherwise noted. Asterisks denoted statistically significant differences (*** $p < 0.001$, ** $p < 0.01$ and * $p < 0.05$).

Results

Overexpression of DDX56 inhibits PRV replication in PK15 cells

To test whether DDX56 affects PRV replication in PK15 cells, the plasmid expression Myc-DDX56 was constructed first and transfected into PK15 cells for study. Myc-tagged DDX56 was successfully expressed in PK15 cells (Figure 1A). Cells overexpressing DDX56 were infected with PRV. As a result,

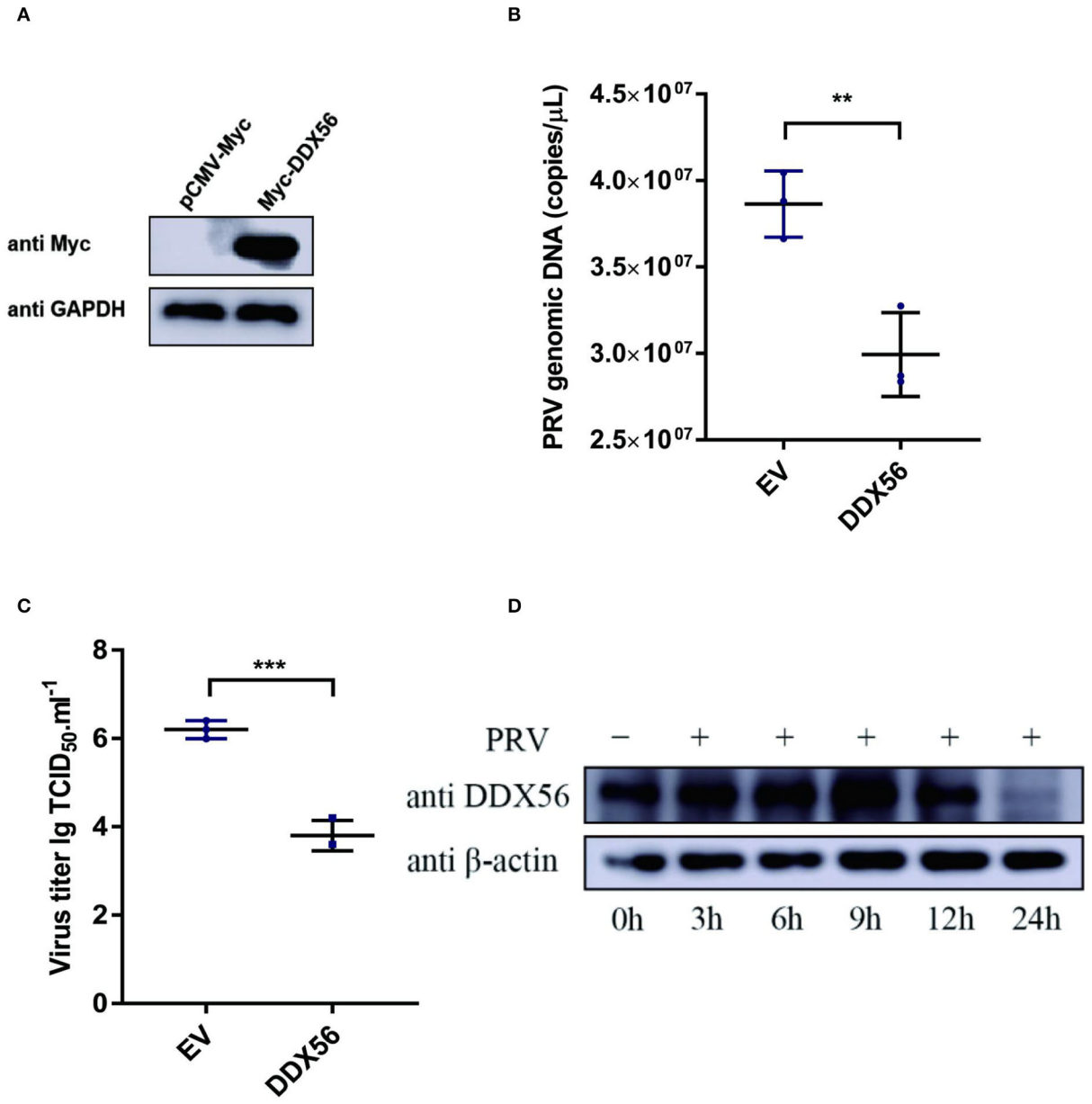

FIGURE 1
Overexpression of DDX56 inhibits PRV replication in PK15 cells. **(A)** Empty vector (EV, 1 μg) or the pCMV-Myc-DDX56 plasmid (1 μg) was transfected into PK15 cells for 24 h before measuring DDX56 (65 kDa) expression by immunoblotting. GAPDH (37 kDa) served as a loading control. **(B,C)** Empty vector (EV, 1 μg) or the pCMV-Myc-DDX56 plasmid (1 μg) was transfected into PK15 cells for 24 h and then infected with 100 $TCID_{50}$ PRV for 24 h before measuring PRV genomic DNA copy numbers and titers. Viral copy number was determined by Real-Time quantity PCR **(B)** and viral titer was detected by $TCID_{50}$ assay (Reed–Muench method) **(C)**. Data were listed as mean ± SD of three independent experiments and measured in technical duplicate. ***$p < 0.001$, **$p < 0.01$. **(D)** PK15 cells were mock-infected or infected with 100 $TCID_{50}$ PRV for 3 h, 6 h, 9 h, 12 h, and 24 h, respectively. Cells were collected at the indicated time points. Western blotting was performed for DDX56 (65 kDa) detection. β-actin (42 kDa) served as loading control.

PRV DNA copies were lower in DDX56 overexpression cells compared to the control group (Figure 1B). To confirm this result, viral titers were also detected. As Figure 1C shows, there was a notably decreased virus titer in the DDX56-overexpressed cells. Then we tested DDX56 protein expression upon PRV infection. As shown in Figure 1D, DDX56 expression was significantly induced in the PK15 cells at 9 h post-infection. The expression level of DDX56 decreased with the prolongation of infection time (within 9 h). As shown in Figures 1B,C, it had been proved that overexpression of DDX56 could inhibit

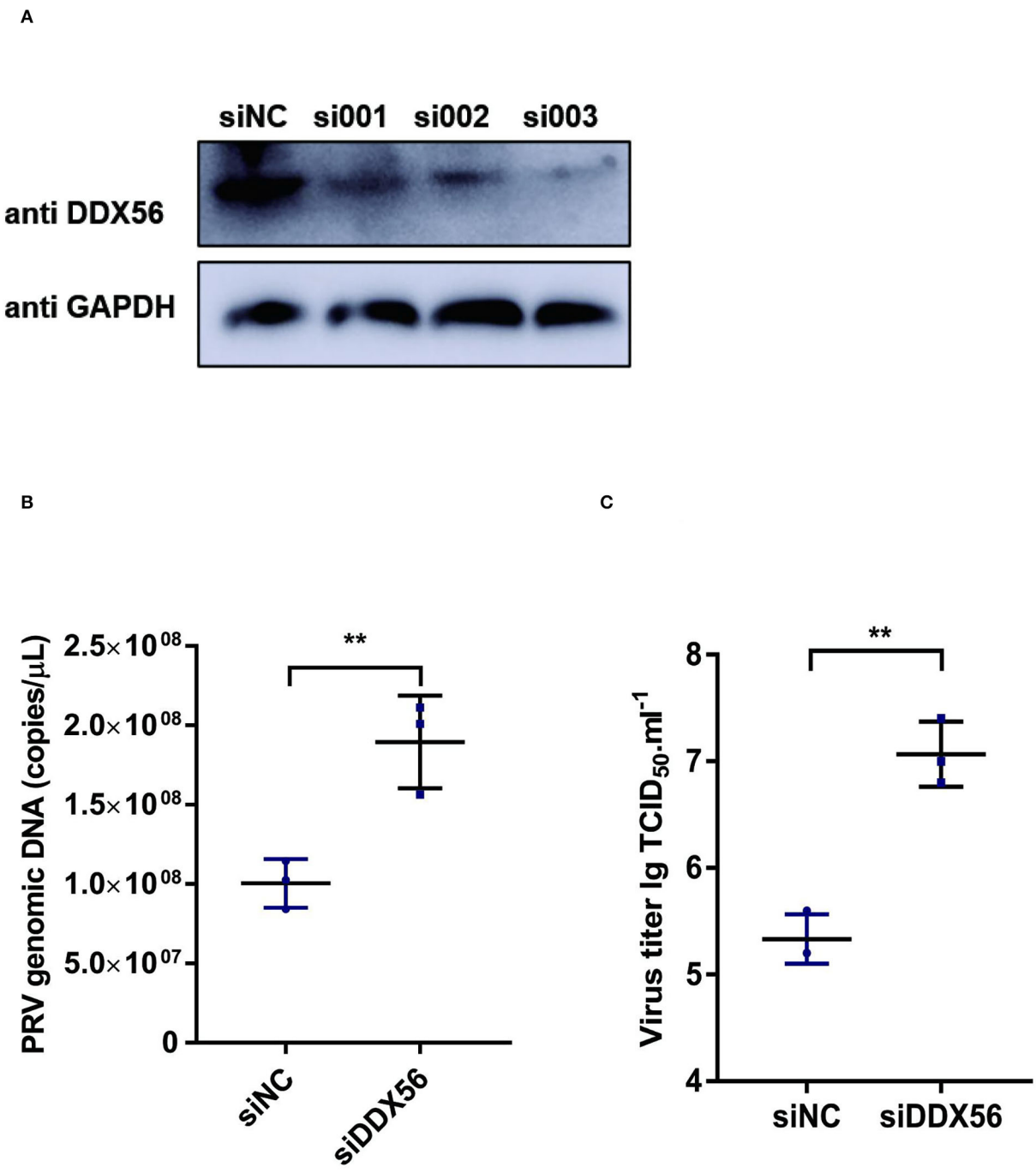

FIGURE 2
Knockdown of DDX56 promotes PRV proliferation in PK15 cells. **(A)** siRNA targeting DDX56 was transfected into PK15 cells for 24 h. Cells were lysed with RIPA and DDX56 (65 kDa) expression was determined by western blotting using an antibody specific for DDX56. GAPDH (37 kDa) served as loading control. **(B,C)** PK15 cells were transfected with siRNA targeting DDX56 (siRNA Mixture, siDDX56) for 24 h then 100 $TCID_{50}$ PRV was inoculated into these cells for another 24 h before measuring viral copy numbers and titers. Viral copy number was determined by Real-Time quantity PCR **(B)** and viral titer was detected by $TCID_{50}$ assay (Reed–Muench method) **(C)**. Data were presented as mean ± SD of three independent experiments and measured in technical duplicate. ** $p < 0.01$.

virus proliferation, but the expression level of DDX56 decreased significantly at 12 h, especially at 24 h after infection. These results suggest that PRV may have a mechanism to inhibit the expression of DDX56 to achieve its proliferation. Taken together,

these results indicate that PRV infection could promote DDX56 expression in the early stage and overexpression of DDX56 serves an inhibitory role in PRV multiplication.

Knockdown of DDX56 promotes PRV proliferation in PK15 cells

To further verify the effect of DDX56 on PRV replication, an RNAi assay was performed in PK15 cells. Results showed that DDX56 expression was decreased significantly in the siRNA transfection group as shown in Figure 2A. Then we analyzed the effect of DDX56 knockdown on PRV infection. As shown in Figure 2B, the viral genomic DNA copies were increased in the siDDX56 group compared to the control siNC group. Besides, the virus titers of the DDX56 knockdown PK15 cells were also higher than that of the siNC control cells (Figure 2C). Together, these data demonstrate that DDX56 knockdown facilitates PRV replication in PK15 cells.

DDX56 promotes IFN-β expression

The underlying mechanism by which DDX56 interferes with PRV proliferation was investigated by asking if DDX56 could enhance the cellular innate immune response to PRV infection as type I IFN is one of the most important molecules and serves as a potent antiviral effector on viral infection (Chen et al., 2018). Thus, we examined IFN-β expression in DDX56 overexpression PK15 cells during PRV infection as well as in control cells. We found that IFN-β mRNA transcription levels increased in DDX56 overexpression PK15 cells (Figure 3A).

Immunostimulatory DNA (ISD) is a double-stranded DNA 60-mer oligonucleotide derived from the HSV-1 genome and has a high capacity to induce IFN-β production (Unterholzner et al., 2010). ISD serves as an IFN-β activator in this study. We then investigated the effect of DDX56 on ISD-triggered IFN-β transcription. As shown in Figure 3B, DDX56 significantly increased the IFN-β expression when co-transfected with ISD.

Poly(dA:dT) is a poly(deoxyadenylic-deoxythymidylic) acid sodium salt. It is a repetitive synthetic double-stranded DNA sequence of poly(dA-dT):poly(dT-dA) and a synthetic analog of B-DNA. It can be sensed by cytosolic DNA sensors cGAS, and triggers the production of type I interferons (Unterholzner, 2013; Wu et al., 2013). Moreover, DDX56 also significantly increased IFN-β expression when co-transfected with poly (dA:dT) (Figure 3C), supporting the idea that DDX56 is responsible for up-regulating the IFN-β expression. Similar results were obtained by ELISA detection (Figure 3D). Together, these findings suggest that DDX56 helps increase the IFN-β production.

DDX56 promotes endogenous cGAS expression

PRV is a typical DNA virus and the cGAS-STING pathway is the major sensor for recognizing its viral DNA during virus infection. As shown in Figure 3A, DDX56 could promote PRV-triggered IFN-β activation. In this part, we wanted to know if DDX56 affected molecules associated with the cGAS-STING signaling pathway, including cGAS, STING, TBK1, and IRF3(5D). As exhibited in Figure 4A, the expression level of cGAS was apparently increased in DDX56 overexpression PK15 cells. There was almost no difference in the STING and IRF3 expression between pCMV-Myc and Myc-DDX56 transfection group. Since cGAS is an interferon-stimulated gene, and DDX56 overexpression may stimulate IFN production, we wondered if the upregulation of cGAS is an effect resulting from increased IFN expression. We first examined the effect of DDX56 overexpression alone on IFN-β mRNA transcription, and RT-qPCR detection found that DDX56 overexpression alone did not affect IFN-β expression (Figure 4B). For DNA virus, Toll-like receptor 9 (TLR9), cyclic GMP-AMP (cGAMP) synthase (cGAS), DAI (DLM-1/ZBP1), absent in melanoma 2 (AIM2), and IFN gamma-inducible protein 16 (IFI16) serve as the main PRRs that recognize viral DNA (Brennan and Bowie, 2010; Xia et al., 2016). PRRs then recruit a series of signal transduction molecules, such as myeloid differentiation primary response gene 88 (MyD88), mitochondrial antiviral-signaling protein (MAVS), and intracellular stimulator of IFN genes (STING). These proteins then transfer the different signals to the downstream molecules in different signaling pathways, which eventually lead to activation and translocation of several transcription factors, including NF-κB, interferon regulatory factor 3 (IRF3), and IRF7 into the nucleus to induce the expression of IFN-I and proinflammatory cytokines (Koyama et al., 2008; Hu and Shu, 2020; Wan et al., 2020). As MAVS is a key linker molecule of type I IFN signaling pathway, we performed DDX56 overexpression in the context of RNAi MAVS expression, and then examined the expression of cGAS at the same time. Interestingly, we found that there was still a significant increase in the expression of cGAS in the presence of knockdown MAVS expression (Figure 4C). Altogether, we can clearly conclude that DDX56 overexpression can promote the expression of cGAS and that this process is independent of the increased expression of IFN-β.

cGAS might be the potential target of DDX56 protein

To further formalize the effect of DDX56 on the expression of cGAS, we then co-transfected DDX56 and molecules belonging to the cGAS-STING signaling pathway. As shown

10.3389/fmicb.2022.932842

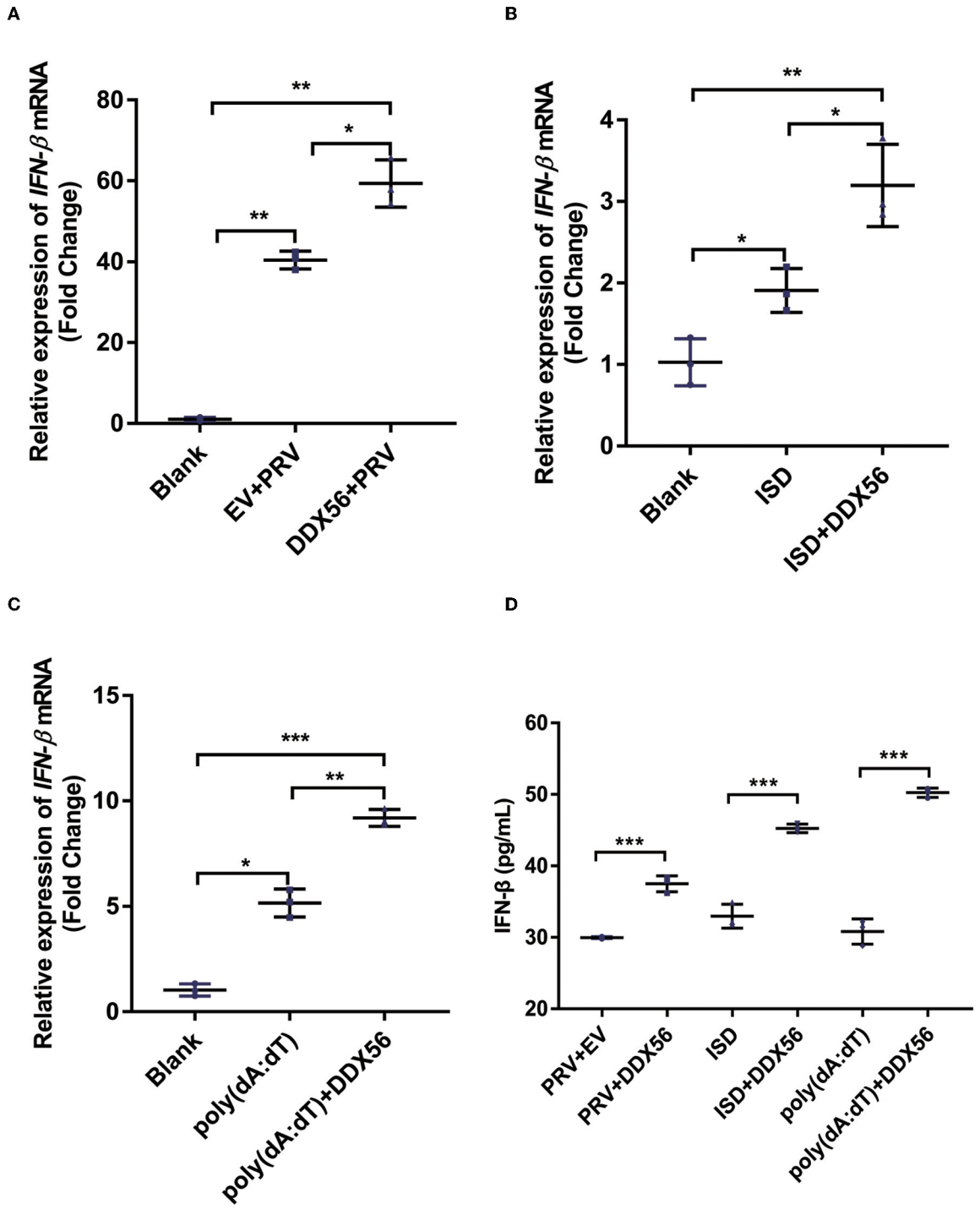

FIGURE 3
DDX56 promotes IFN-β expression. **(A)** Empty vector (EV, 1 μg) or pCMV-Myc-DDX56 (1 μg) plasmid was transfected into PK15 cells for 24 h, then followed by infection with 100 $TCID_{50}$ PRV for another 24 h. Cells were collected for RNA extraction. RT-qPCR was used for detecting IFN-β mRNA. Data were presented as means ± SD of three independent experiments, measured in technical duplicates. ** $p < 0.01$, * $p < 0.05$. **(B)** Empty vector (EV, 1 μg) or pCMV-Myc-DDX56[[Inline Image]] (1 μg) plasmid was transfected into PK15 cells for 24 h, then stimulated with 1 μg ISD for another 12 h. Cells were collected for RNA extraction. RT-qPCR was used for IFN-β mRNA detection. Data were presented as means ± SD of three independent experiments, measured in technical duplicates. ** $p < 0.01$, * $p < 0.05$. **(C)** Empty vector (EV, 1 μg) or pCMV-Myc-DDX56 (1 μg) plasmid was transfected for 24 h, then stimulated with 1 μg poly(dA:dT) for another 12 h. Cells were collected for RNA extraction. RT-qPCR was used for IFN-β mRNA detection. **(D)** IFN-β concentration in cell culture supernatant was detected by ELISA. Data were presented as mean ± SD of three independent experiments, measured in technical duplicates. *** $p < 0.001$; ** $p < 0.01$, * $p < 0.05$.

10.3389/fmicb.2022.932842

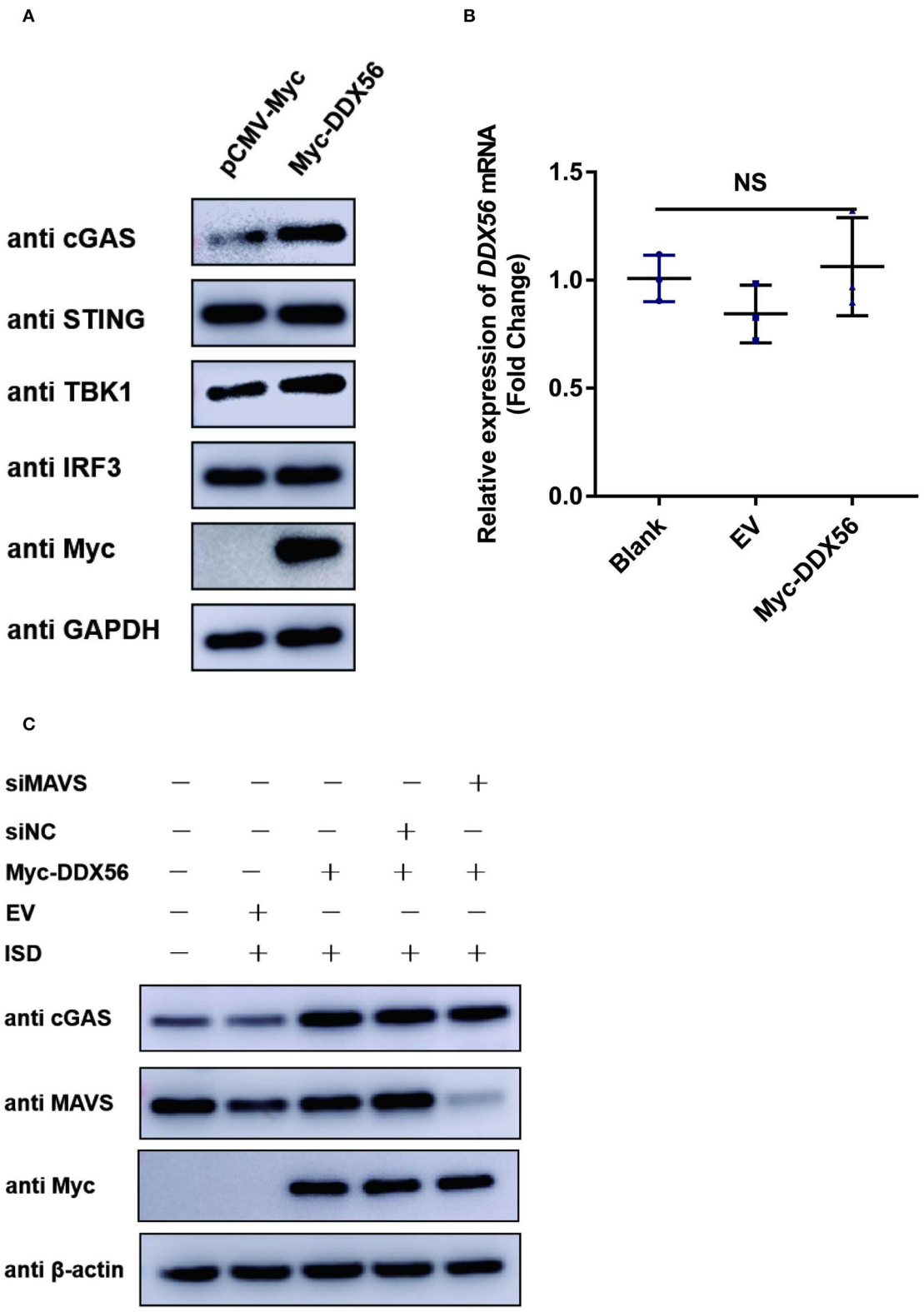

FIGURE 4
DDX56 promotes endogenous cGAS expression. **(A)** Empty vector (EV, 1 μg) or pCMV-Myc-DDX56 (1 μg) plasmid was transfected into PK15 cells for 24 h, and cells were collected for western blot analysis using specific antibodies to detect the expression of cGAS(58 kDa), STING(42 kDa),
(Continued)

FIGURE 4 (Continued)
TBK1(84 kDa) and IRF3(55 kDa). GAPDH (37 kDa) was used as a loading control. **(B)** PK15 cells were transfected with empty vector (EV, 1 μg) or pCMV-Myc-DDX56 (1 μg) plasmid for 24 h, then cells were collected for cellular RNA extraction. RT-qPCR was performed for IFN-β mRNA detection. Data were presented as mean ± SD of three independent experiments, measured in technical duplicates. NS stands for no significance. **(C)** PK15 cells were transfected with siRNA targeting MAVS (siRNA Mixture, siMAVS) for 24 h, then an empty vector (EV, 1 μg) or pCMV-Myc-DDX56 (1 μg) plasmid was transfected into above cells for another 24 h. Before being collected, cells were stimulated with 1 μg ISD for 12 h. Cellular proteins were extracted and subjected to western blotting for MAVS (56 kDa), cGAS (58 kDa), and Myc tagged DDX56 (65 kDa) detection. β-actin (42 kDa) served as loading control.

in Figure 5, DDX56 could promote cGAS expression compared to the control group (Figure 5A). There was no effect on the expression of exogenous STING, TBK1, and IRF3 (Figures 5B,D). These results were consistent with the detection of endogenous correlation factors (Figure 4). Taken together, these results indicate that DDX56 is responsible for the increase of cGAS expression.

Virus infection is blocked by the innate immune response system in which the IFN signaling pathway plays an essential role. To examine the function of DDX56 on cGAS-STING-triggered IFN-β transcription, an RT-qPCR assay was performed and the results are exhibited in Figure 5. DDX56 could promote cGAS and STING-triggered IFN-β activation (Figures 5A,B). However, DDX56 had no effect on IFN-β activation induced by TBK1 and IRF3 (5D) (Figures 5C,D). Combined with western blotting detection results, we speculate that cGAS might be a DDX56 function target to enhance the IFN-β signaling pathway.

DDX56 interacts directly with cGAS in PK15 cells

cGAS plays an extremely important role in type I IFN production in response to PRV infection (Wang et al., 2018). As DDX56 protein showed a significant promotion effect on cGAS expression and its triggered IFN-β activation (Figure 5A), suggesting that it could target cGAS to enhance the host innate immune response. An anti-Myc antibody was used for the co-immunoprecipitation (Co-IP) assay to determine if DDX56 binds to cGAS after co-transfection of HA-cGAS and Myc-DDX56 plasmids. As shown in Figure 6A, it was found that DDX56 co-precipitated with cGAS, suggesting a direct interaction between the two proteins. Co-IP was performed to confirm the interaction between DDX56 and endogenous cGAS by transfecting PK15 cells with Myc-vector or Myc-DDX56-expressing plasmids along with HA-cGAS. An anti-cGAS antibody was used to detect and visualize the cGAS expression. As shown in Figure 6B, DDX56 protein was immunoprecipitated with endogenous cGAS.

We then also proved if DDX56 interacted with TBK1 under physiological conditions. PK15 cells were transfected with Myc-DDX56 and FLAG-TBK1. Then Co-IP experiments were performed using Myc tag antibody or FLAG tag antibody. As shown in Figures 6C,D, there were no bands detected in FLAG tag antibody detection or Myc tag antibody after Co-IP. These results demonstrate that DDX56 interacts directly with cGAS and DDX56 targets cGAS to promote host immune response.

cGAS is essential for DDX56 to promote IFN-β pathway activation

As DDX56 could promote cGAS expression and there was also a direct interaction between DDX56 and cGAS, we wanted to know if cGAS was a key adaptor in DDX56-inhibited PRV infection. siRNAs targeting cGAS were designed and synthesized. Then siRNAs were transfected into PK15 cells to evaluate their role in knockdown cGAS expression. As shown in Figure 7A, siRNA targeting cGAS could effectively decrease cGAS protein expression. Then siRNAs mixture was used for the following experiments. DDX56-overexpressed PK15 cells were transfected with sicGAS and siNC served as the negative control. The expression of Myc tagged DDX56 and cGAS was proved by western blotting (Figure 7B). Then the cells were infected with PRV. IFN-β and viral genomic copies number were detected. Knockdown cGAS expression efficiently decreased DDX56-enhanced IFN-β mRNA transcription (Figure 7C). In Figure 7D, DDX56 overexpression could inhibit PRV replication. But when RNAi of cGAS expression was performed using sicGAS in the DDX56 overexpression group, we found PRV copies number was higher than that in the siNC transfection group. These data demonstrate that cGAS is the target molecule of DDX56 that promotes-β expression and inhibits PRV replication.

In our previous study of DDX56 on EMCV replication, we found that DDX56 had a different effect on EMCV proliferation (Xu et al., 2022). To make clear how the same protein exerts contradictory effects on different classes of viruses, we tested the effects of DDX56 on IRF3 phosphorylation during PRV infection. Results are shown as Figure 8A. DDX56 did not affect IRF3, but it promoted PRV-induced IRF3 phosphorylation. IRF3 nuclear translocation is a precondition for IFN production. Hence, we checked the effect of DDX56 expression on IRF3 nuclear translocation. PK15 cells were transfected with Myc-DDX56 for 24 h before treating with PRV for a further 24 h. As expected, DDX56 expression promoted IRF3 translocation into the nucleus (Figure 8B). Together, these findings demonstrate that DDX56 facilitates IFN-β production through interacting

10.3389/fmicb.2022.932842

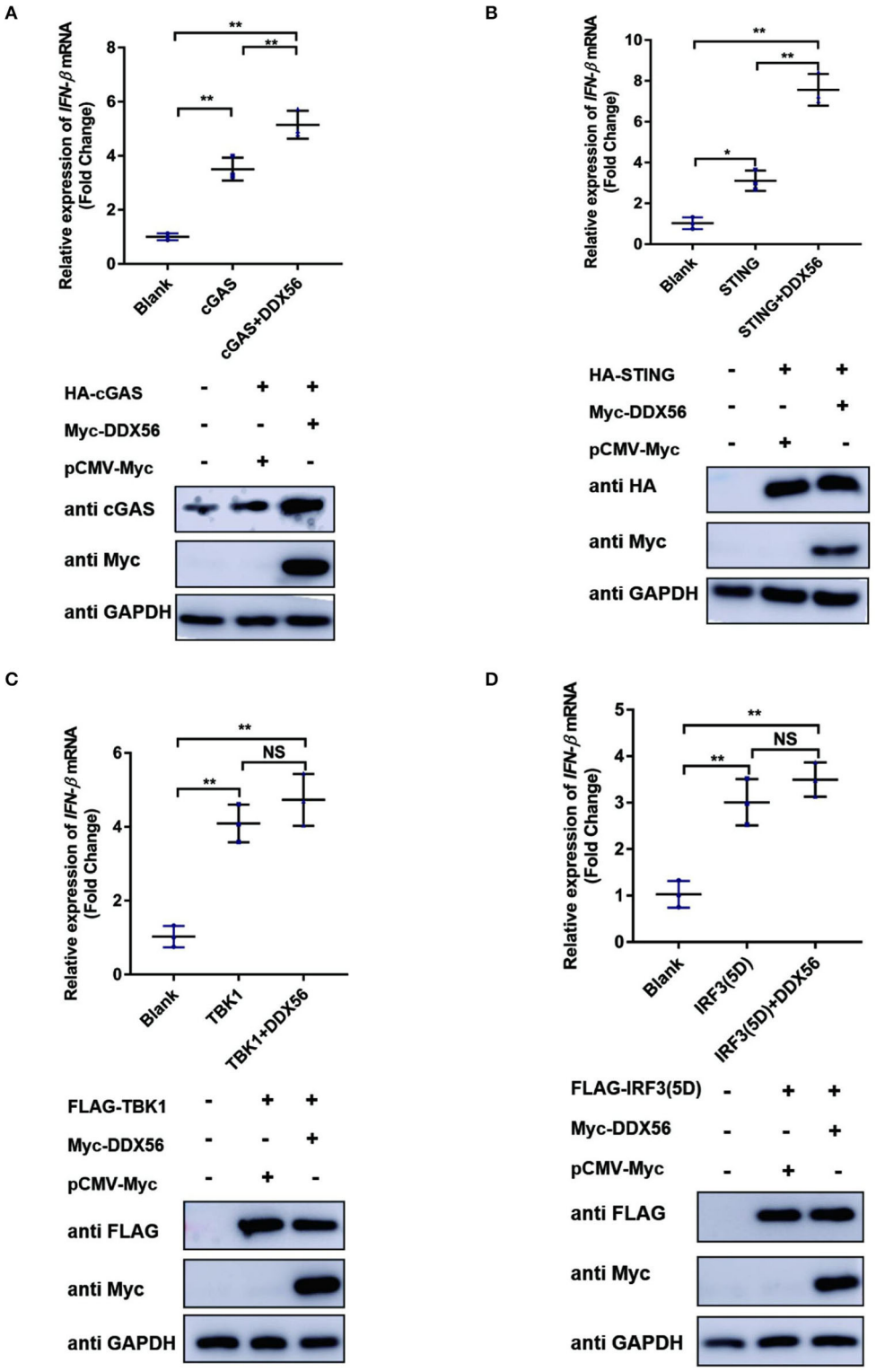

FIGURE 5
cGAS might be the potential target of DDX56 protein. In PK15 cells, the empty vector (EV, 1 μg) or pCMV-Myc-DDX56 plasmids (1 μg) was co-transfected with indicated plasmids encoding cGAS (250 ng) **(A)**, STING (250 ng) **(B)**, TBK1 (250 ng) **(C)** or IRF3 (5D) (250 ng) **(D)** for 30 h. Then the RNA was extracted and IFN-β levels were determined by RT-qPCR. Western blotting was used to assess the expression of several adaptor molecules as well as the DDX56 protein. GAPDH was used as a loading control. Data were presented as mean ± SD of three independent experiments, measured in technical duplicates. ** $p < 0.01$ and * $p < 0.05$.

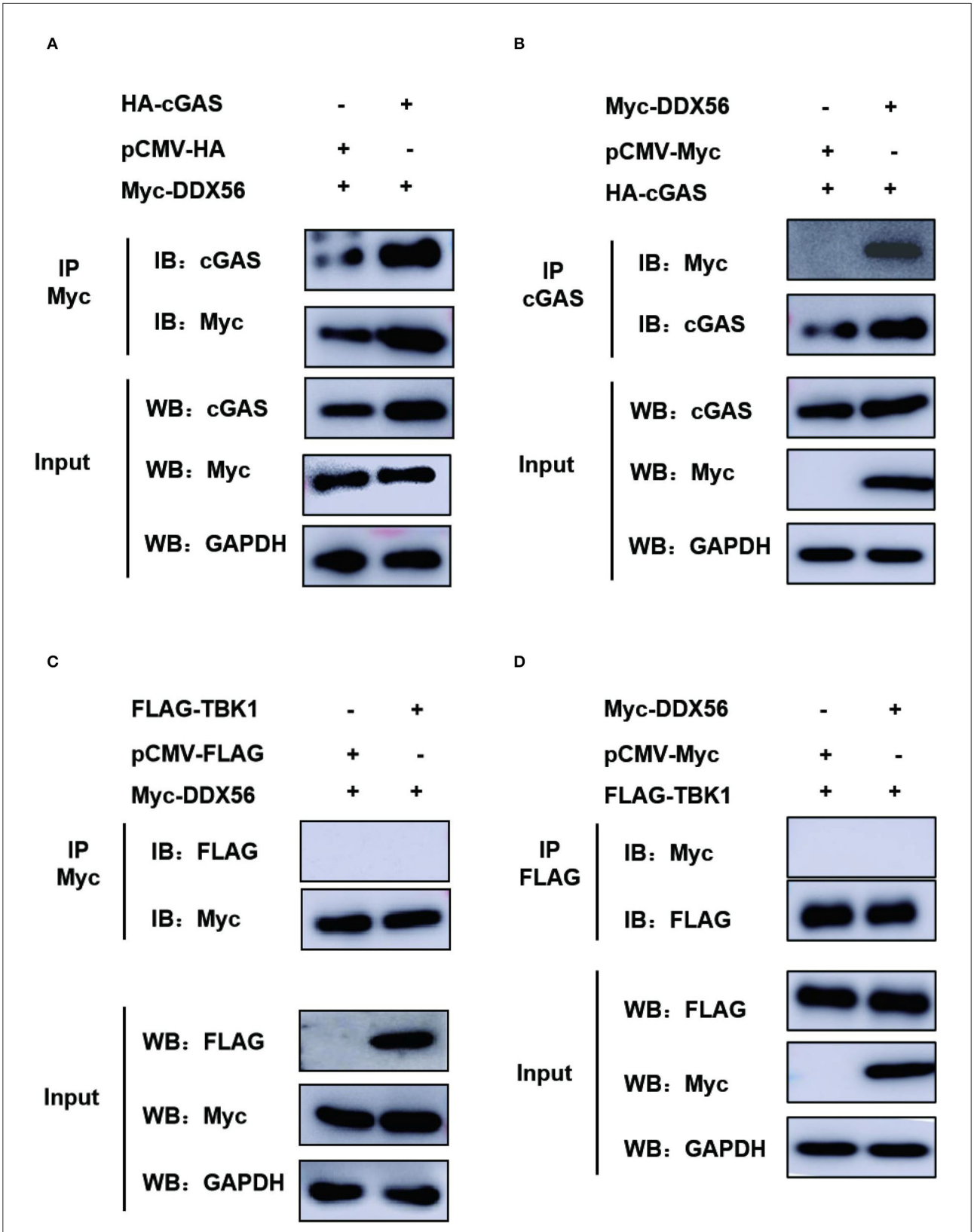

FIGURE 6
There is a direct interaction between DDX56 and cGAS. **(A,B)** The interaction between DDX56 and cGAS was confirmed by a co-immunoprecipitation assay. In PK15 cells, empty vector (EV, 1 μg) or pCMV-Myc-DDX56 (1 μg) plasmids and the indicated plasmids

(Continued)

FIGURE 6 (Continued)
expressing cGAS (250 ng) were co-transfected for 30 h. Using a lysis buffer supplemented with phosphatase inhibitor cocktail, cells were collected and protein G agarose was incubated with anti-Myc or anti-cGAS antibody. Whole-cell lysates (input) and immunoprecipitation (IP) complexes were analyzed using specific antibodies by western blotting. **(C,D)** The interaction between DDX56 and TBK1 was confirmed by a co-immunoprecipitation assay. In PK15 cells, empty vector (EV, 1 μg) or pCMV-Myc-DDX56 (1 μg) plasmids and the indicated plasmids expressing TBK1 (250 ng) were co-transfected for 30 h. Using a lysis buffer supplemented with phosphatase inhibitor cocktail, cells were collected and protein G agarose was incubated with anti-Myc or anti-FLAG antibody. Whole-cell lysates (input) and immunoprecipitation (IP) complexes were analyzed using specific antibodies by western blotting.

with cGAS and advances the phosphorylation and nuclear translocation of IRF3.

Discussion

In the swine industry, PRV is a destructive pathogen causing enormous losses. Understanding what factors control PRV proliferation is essential to better understanding host-virus interactions. The inhibitory role of DDX56 in PRV infection may provide potential targets for antiviral therapies. Here, we demonstrate that DDX56 overexpression significantly reduced the replication of PRV infection, whereas DDX56 knockdown increased viral growth. These findings suggest that DDX56 is a potentially useful target to effectively control PRV infection.

Pathogen-associated molecular patterns (PAMPs) are recognized by host cellular recognition receptors (PRRs) and trigger IFNs and pro-inflammatory cytokines during virus infection. All these responses are beneficial to viral replication inhibition, infected cells clearance, and the adaptive immune response orchestration, even to eliminate infected pathogens (Kawai and Akira, 2006; Carpenter et al., 2014; Beachboard and Horner, 2016; Chen et al., 2017). A cytosolic DNA sensor, Cyclic GMP-AMP (cGAMP) synthase (cGAS) activates the type I IFN response in response to pathogen DNA. cGAS catalyzes the synthesis of cGAMP from pathogen DNA, eliciting an IFN response, then activates the endoplasmic reticulum (ER)-anchored stimulator of interferon genes (STING). The STING translocates from the ER to the Golgi apparatus, where it recruits and phosphorylates TANK-binding kinase 1 (TBK1) and IκB kinase (IKK). These events activate IRF3 and NF-κB, which in turn activate type I IFN production (Fitzgerald et al., 2003; Sharma et al., 2003; Sun et al., 2013; Xia et al., 2016).

It has been shown that DDX56 can regulate the natural immune response signaling pathway, especially the IFN-β pathway (Fu et al., 2019; Xu et al., 2022). We first detected the role of DDX56 on PRV, ISD, and poly(dA:dT)-induced IFN-β activation. Results showed that DDX56 significantly promoted PRV, ISD, and poly(dA:dT)-triggered IFN-β transcription. Our study examined how DDX56 affected cGAS-STING-TBK1, since this axis is crucial for host defense against DNA viruses (Kato et al., 2017). Then we tested the effect of DDX56 on cGAS-STING signaling pathway-associated factors that triggered IFN-β expression. Results indicated that DDX56 indeed promoted IFN-β expression, especially cGAS and STING-induced IFN-β expression. Interestingly, DDX56 also increased cGAS expression and interacted with cGAS. In the ZCCHC3 protein study, scientists found that ZCCHC3 could interact with cGAS and promote the binding of cGAS to DNA (Lian et al., 2018). In this study, DDX56 presented an anti-PRV activity. Further studies are necessary to determine whether DDX56 binds to PRV DNA or promotes the activation of cGAS. Furthermore, if DDX56 deletion impairs innate response *in vivo* during PRV infection still needs to be further investigated in the future.

In our previous study of DDX56 on EMCV replication, we found that DDX56 could directly interact with viral protein to antagonize virus-triggered IFN-β production and promote EMCV proliferation (Xu et al., 2022). In this study, we found that DDX56 had an inhibitory role on PRV infection. Whether viral proteins are involved in this process or whether DDX56 interacts with viral proteins is unknown and needs further investigation at a later stage.

To validate if cGAS is the key factor for DDX56 regulating-IFN-β pathway, siRNAs targeting cGAS were designed and synthesized. Knockdown of cGAS expression by RNAi, followed by overexpression of DDX56 in these cells, showed that IFN-β transcription was decreased during PRV infection and viral copies number was increased compared to DDX56 overexpression group. These data revealed that DDX56 targets cGAS to exert its antiviral effect. We all know that cGAS is an important DNA sensor during PRV virus infection (Wang et al., 2018), and maybe DDX56 is a co-sensor of cGAS for PRV recognition.

To summarize, we showed that porcine DDX56 expression inhibited PRV proliferation in PK15 cells (Figure 9). Overexpression of DDX56 markablely inhibited PRV replication and the decreased DDX56 expression had a promotion role on PRV infection. Mechanistically, DDX56 upregulated IFN-β expression and then resulted in suppressing viral proliferation. Further mechanism exploration revealed that DDX56 could induce cGAS expression and there was a direct interaction between DDX56 and cGAS. These data demonstrated that cellular protein DDX56 targets cGAS to exert its antiviral effect. In addition, DDX56 also promoted IRF3 phosphorylation and its nuclear translocation. Further research is needed to determine if DDX56's ATPase or helicase activities are responsible for its inhibition of PRV replication. Together, these results illustrate the critical role of DDX56 during PRV infection

10.3389/fmicb.2022.932842

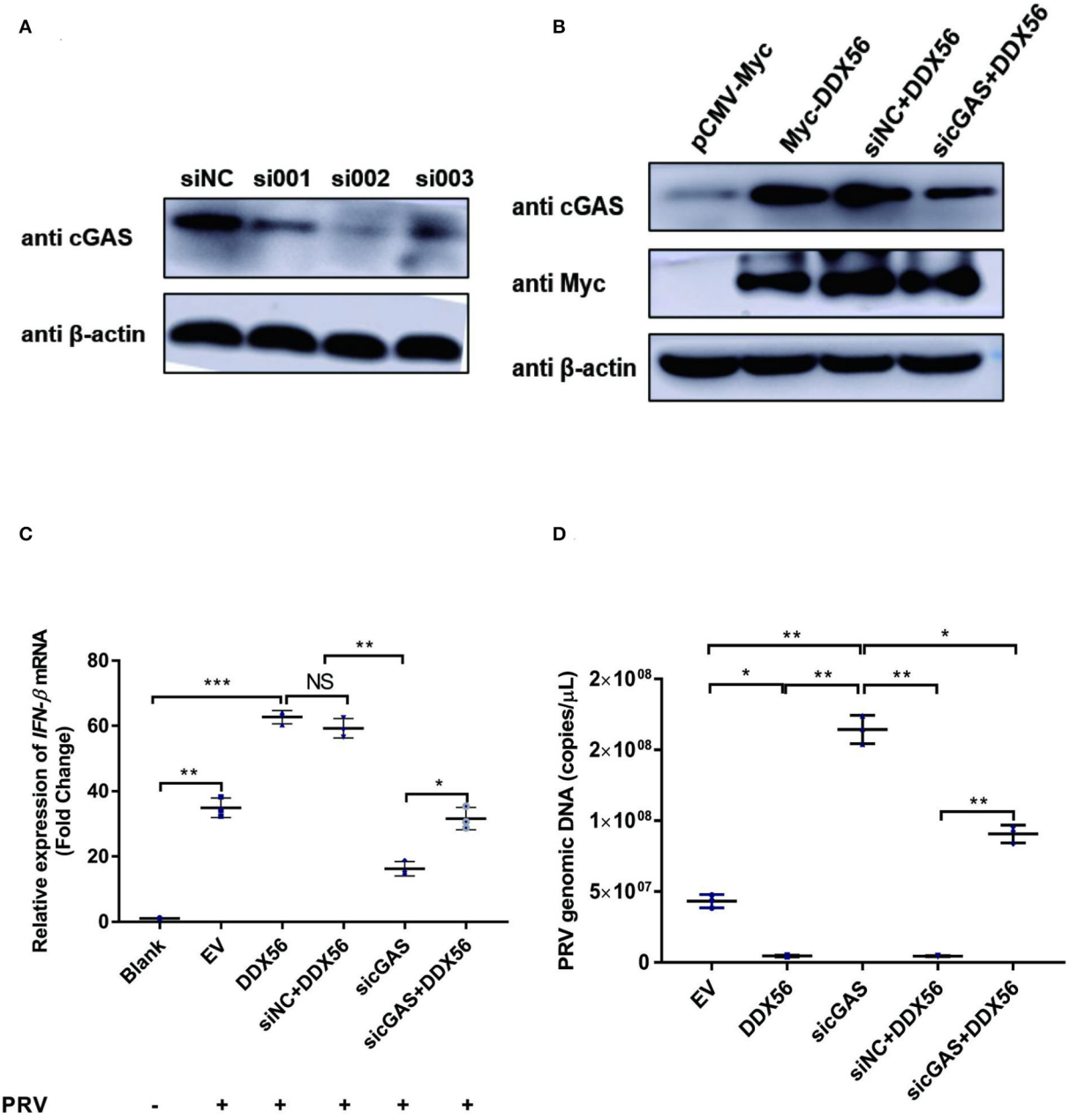

FIGURE 7
cGAS is essential for DDX56 to promote IFN-β pathway activation. **(A)** siRNA targeting cGAS was transfected into PK15 cells for 24 h. Then cells were lysed with RIPA and cGAS expression was determined by western blotting using an antibody specific for cGAS (58 kDa). β-actin (42 kDa) served as a loading control. **(B)** siRNA targeting cGAS was transfected into PK15 cells for 24 h. Then cells were transfected with empty vector (EV, 1 μg) or pCMV-Myc-DDX56 (1 μg) plasmids. 24 h later, cells were collected and lysated with RIPA. Endogenous cGAS (58 kDa) and Myc tagged DDX56 (65 kDa) protein expression were detected by western blotting. β-actin (42 kDa)served as a loading control. **(C)** siRNA targeting cGAS was transfected into PK15 cells for 24 h. Then cells were transfected with empty vector (EV, 1 μg) or pCMV-Myc-DDX56 (1 μg) plasmids for another 24 h. PRV infection was performed at 100 $TCID_{50}$. Cells were collected for RNA extraction 24 h post-infection. RT-qPCR was performed for IFN-β mRNA detection. Data were presented as mean ± SD of three independent experiments, measured in technical duplicates. *** $p < 0.001$, ** $p < 0.01$ and * $p < 0.05$. **(D)** siRNA targeting cGAS was transfected into PK15 cells for 24 h. Then cells were transfected with empty vector (EV, 1 μg) or pCMV-Myc-DDX56 (1 μg) plasmids for another 24 h. PRV infection was performed at 100 $TCID_{50}$. Cell culture supernatant was collected and viral genomic DNA was extracted. Real-Time quantity PCR was used to determine viral copy number. Data were presented as mean ± SD of three independent experiments, measured in technical duplicate. ** $p < 0.01$ and * $p < 0.05$.

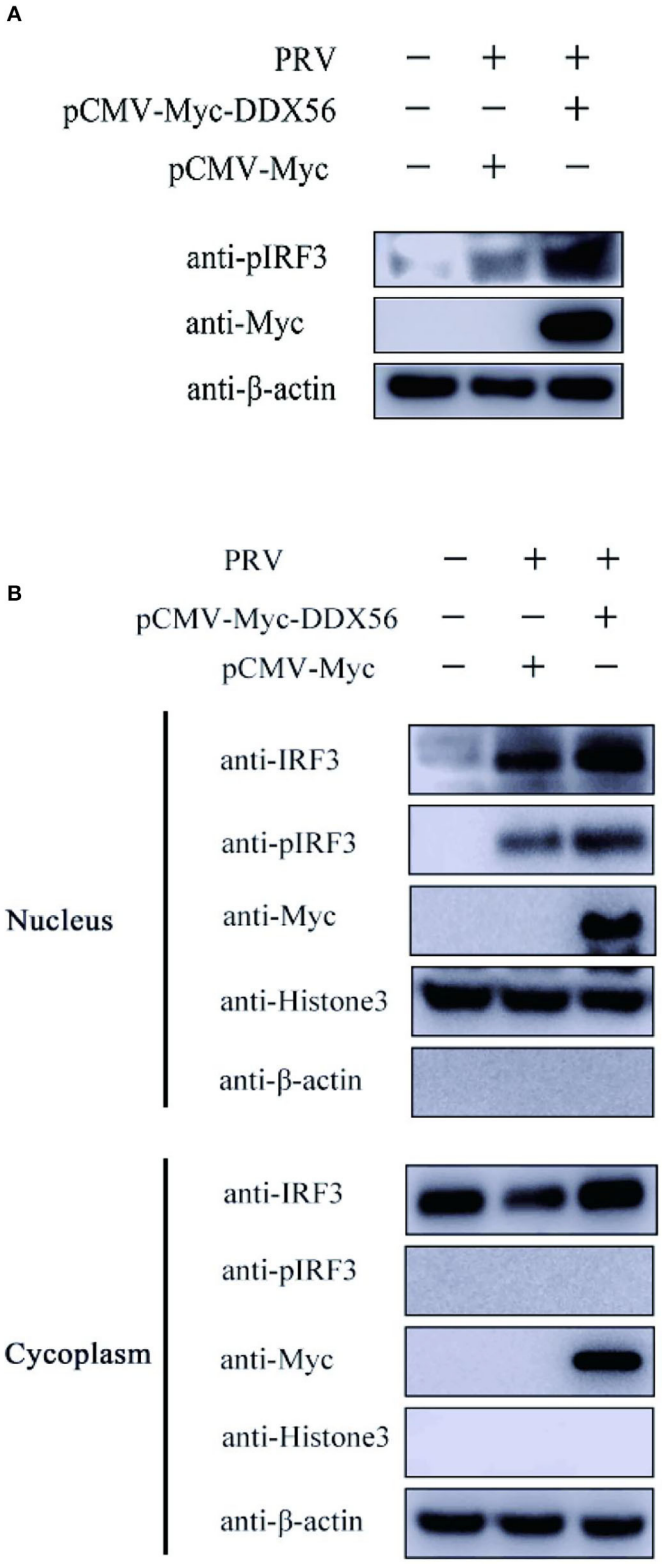

FIGURE 8
DDX56 promotes IRF3 phosphorylation and nuclear translocation induced by PRV. **(A)** PK15 cells were transfected with empty vector (EV, 1 μg) or pCMV-Myc-DDX56 (1 μg) plasmid for 24 h, then cells were infected with 100 $TCID_{50}$ PRV for 12 h. Cells were collected for IRF3

(Continued)

FIGURE 8 (Continued)
phosphorylation (55 kDa) detection. β-actin (42 kDa) served as a loading control. **(B)** PK15 cells were transfected with empty vector (EV, 1 μg) or pCMV-Myc-DDX56 (1 μg) plasmid for 24 h. Cells were then stimulated with 100 $TCID_{50}$ PRV for 12 h before collection. Nuclear and Cytoplasmic Extraction was used to separate DDX56 proteins, or IRF3 protein in the cytoplasm and nucleus, then DDX56 (65 kDa), IRF3 (55 kDa), and IRF3 phosphorylation level (55 kDa) were confirmed by immune blotting using specific antibodies. β-actin (42 kDa) was used as a loading control in cytoplasma and Histone 3 (17 kDa) was used as a loading control in the nucleus.

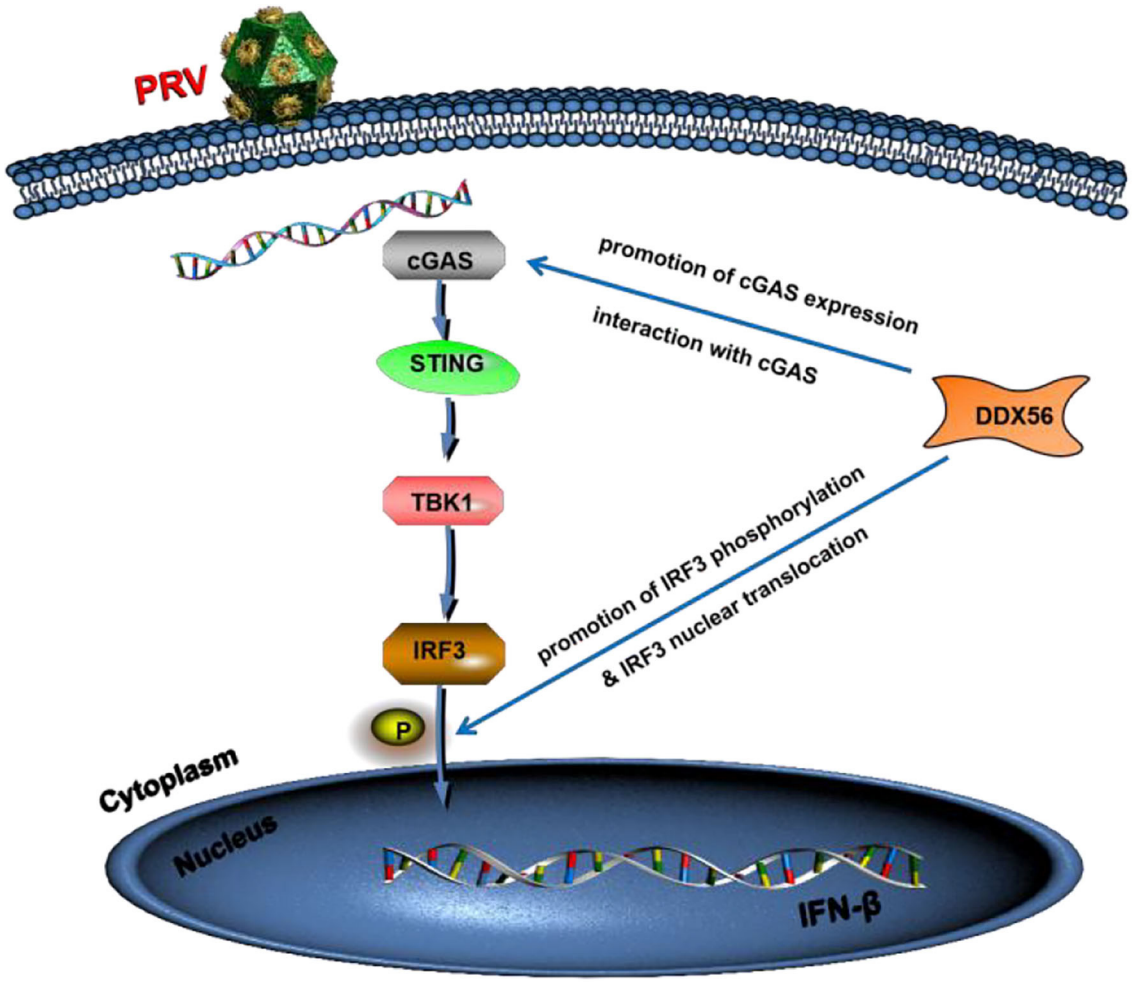

FIGURE 9
Model of DDX56 promotes IFN-β pathway activation to inhibit PRV infection. Cellular protein DDX56 promotes cGAS expression and interacts with cGAS. Further study shows DDX56 does not affect IRF3, but it promotes PRV-induced IRF3 phosphorylation. As expected, DDX56 expression promoted IRF3 translocation into the nucleus. Together, these findings demonstrate that DDX56 plays a positively regulation role in IFN-β production through interacting with cGAS and promoted the phosphorylation and nuclear translocation of IRF3.

and these results contribute to understanding the host-virus interaction that occurs during PRV infection.

Data availability statement

The original contributions presented in the study are included in the article/Supplementary Material, further inquiries can be directed to the corresponding author/s.

Author contributions

JX, XL, and RF contributed to the conception and design of the study. JX, XL, SY, and ZY did the experiments. LC, XZ, YY, and DL performed the statistical analysis. JX and XL wrote the first draft of the manuscript. SY, ZY, and LC wrote sections of the manuscript. All authors contributed to manuscript revision, read, and approved the submitted version.

Funding

This work was supported by Open Funds of the Biomedical Research Center from Northwest Minzu University (EB202101), the Fundamental Research Funds for the Central Universities (31920220068), and the Young Doctor Fund Project of Gansu Province Education Department (2021QB-064).

Conflict of interest

The authors declare that the research was conducted in the absence of any commercial or financial relationships that could be construed as a potential conflict of interest.

Publisher's note

Supplementary material

The Supplementary Material for this article can be found online at: https://www.frontiersin.org/articles/10.3389/fmicb.2022.932842/full#supplementary-material

References

Ai, J. W., Weng, S. S., Cheng, Q., Cui, P., Li, Y. J., Wu, H. L., et al. (2018). Human endophthalmitis caused by pseudorabies virus infection, China, 2017. *Emerg. Infect. Dis.* 24, 1087–1090. doi: 10.3201/eid2406.171612

Beachboard, D. C., and Horner, S. M. (2016). Innate immune evasion strategies of DNA and RNA viruses. *Curr. Opin. Microbiol.* 32, 113–119. doi: 10.1016/j.mib.2016.05.015

Brennan, K., and Bowie, A. (2010). Activation of host pattern recognition receptors by viruses. *Curr. Opin. Microbiol.* 13, 503–507. doi: 10.1016/j.mib.2010.05.007

Carpenter, S., Ricci, E. P., Mercier, B. C., Moore, M. J., and Fitzgerald, K. A. (2014). Post-transcriptional regulation of gene expression in innate immunity. *Nat. Rev. Immunol.* 14, 361–376. doi: 10.1038/nri3682

Chen, N., Xia, P., Li, S., Zhang, T., Wang, T. T., and Zhu, J. (2017). RNA sensors of the innate immune system and their detection of pathogens. *IUBMB Life* 69, 297–304. doi: 10.1002/iub.1625

Chen, X., Liu, S., Goraya, M. U., Maarouf, M., Huang, S., and Chen, J. L. (2018). Host immune response to influenza A virus infection. *Front. Immunol.* 9, 320. doi: 10.3389/fimmu.2018.00320

Fitzgerald, K. A., McWhirter, S. M., Faia, K. L., Rowe, D. C., Latz, E., Golenbock, D. T., et al. (2003). IKKepsilon and TBK1 are essential components of the IRF3 signaling pathway. *Nat. Immunol.* 4, 491–496. doi: 10.1038/ni921

Fonseca, A. A., Camargos, M. F., Sales, M. L., Heinemann, M. B., Leite, R. C., and Reis, J. K. P. (2012). Pseudorabies virus can be classified into five genotypes using partialsequences of UL44. *Brazil. J. Microbiol.* 43, 1632–1640. doi: 10.1590/S1517-83822012000400048

Fu, S., Yang, W., Ru, Y., Zhang, K., Wang, Y., Liu, X. T., et al. (2019). DDX56 cooperates with FMDV 3A to enhance FMDV replication by inhibiting the phosphorylation of IRF3. *Cell Signal.* 64, 109393. doi: 10.1016/j.cellsig.2019.109393

Hu, M., and Shu, H. (2020). Innate immune response to cytoplasmic DNA: mechanisms and diseases. *Annu. Rev. Immunol.* 38, 79–98. doi: 10.1146/annurev-immunol-070119-115052

Kato, K., Omura, H., Ishitani, R., and Nureki, O. (2017). Cyclic GMP-AMP as an endogenous second messenger in innate immune signaling by cytosolic DNA. *Annu. Rev. Biochem.* 86, 541–566. doi: 10.1146/annurev-biochem-061516-044813

Kawai, T., and Akira, S. (2006). Innate immune recognition of viral infection. *Nat. Immunol.* 7, 131–137. doi: 10.1038/ni1303

Koyama, S., Ishii, K., Coban, C., and Akira, S. (2008). Innate immune response to viral infection. *Cytokine* 43, 336–341. doi: 10.1016/j.cyto.2008.07.009

Lian, H., Wei, J., Zang, R., Ye, W., Yang, Q., Zhang, X. N., et al. (2018). ZCCHC3 is a co-sensor of cGAS for dsDNA recognition in innate immune response. *Nat. Commun.* 1, 3349. doi: 10.1038/s41467-018-05559-w

Miyashita, M., Oshiumi, H., Matsumoto, M., and Seya, T. (2011). DDX60, a DEXD/H box helicase, is a novel antiviral factor promoting RIG-I-like receptor-mediated signaling. *Mol. Cell Biol.* 31, 3802–3819. doi: 10.1128/MCB.01368-10

Oshiumi, H., Sakai, K., Matsumoto, M., and Seya, T. (2010). DEAD/H BOX 3 (DDX3) helicase binds the RIG-I adaptor IPS-1 to up-regulate IFN-beta-inducing potential. *Eur. J. Immunol.* 40, 940–948. doi: 10.1002/eji.200940203

Pirinçal, A., and Turan, K. (2021). Human DDX56 protein interacts with influenza A virus NS1 protein and stimulates the virus replication. *Genet. Mol. Biol.* 1, e20200158. doi: 10.1590/1678-4685-gmb-2020-0158

Pomeranz, L. E., Reynolds, A. E., and Hengartner, C. J. (2005). Impact on neurovirology and veterinary medicine. *Microbiol. Mol. Biol. Rev. Mol. Biol. Pseudorabies Virus.* 69, 462–500. doi: 10.1128/MMBR.69.3.462-500.2005

Reid, C. R., and Hobman, T. C. (2017). The nucleolar helicase DDX56 redistributes to West Nile virus assembly sites. *Virology* 500, 169–177. doi: 10.1016/j.virol.2016.10.025

Sharma, S., TenOever, B. R., Grandvaux, N., Zhou, G. P., Lin, R., Hiscott, J. (2003). Triggering the interferon antiviral response through an IKK-related pathway. *Science* 300, 1148–1151. doi: 10.1126/science.1081315

Sun, L., Wu, J., Du, F., Chen, X., and Chen, Z. J. (2013). Cyclic GMP-AMP synthase is a cytosolic DNA sensor that activates the type I interferon pathway. *Science* 339, 786–791. doi: 10.1126/science.1232458

Taschuk, F., Tapescu, I., Moy, R. H., and Cherry, S. (2020). DDX56 binds to Chikungunya virus RNA to control infection. *mBio* 11, e02623–e02620. doi: 10.1128/mBio.02623-20

Unterholzner, L. (2013). The interferon response to intracellular DNA: why so many receptors? *Immunobiology* 11:1312–1321. doi: 10.1016/j.imbio.2013.07.007

Unterholzner, L., Keating, S. E., Baran, M., Horan, K. A., Jensen, S. B., Sharma, S., et al. (2010). IFI16 is an innate immune sensor for intracellular DNA. *Nat. Immunol.* 11, 997–1004. doi: 10.1038/ni.1932

Wan, D., Jiang, W., and Hao, J. (2020). Research advances in how the cGAS-STING pathway controls the cellular inflammatory response. *Front. Immunol.* 11, 615. doi: 10.3389/fimmu.2020.00615

Wang, J., Lu, S. F., Wan, B., Ming, S. L., Li, G. L., Su, B. Q., et al. (2018). Maintenance of cyclic GMP-AMP homeostasis by ENPP1 is involved in pseudorabies virus infection. *Mol. Immunol.* 95, 56–63. doi: 10.1016/j.molimm.2018.01.008

Wu, J., Sun, L., Chen, X., Du, F., Shi, H., Chen, C., et al. (2013). Cyclic GMP-AMP is an endogenous second messenger in innate immune signaling by cytosolic DNA. *Science* 6121, 826–830. doi: 10.1126/science.1229963

Xia, P., Wang, S., Gao, P., Gao, G., and Fan, Z. (2016). DNA sensor cGAS-mediated immune recognition. *Protein Cell* 7, 777–791. doi: 10.1007/s13238-016-0320-3

Xie, J., Bi, Y., Xu, S., Han, Y., Idris, A., Zhang, H., et al. (2020). Host antiviral protein IFITM2 restricts pseudorabies virus replication. *Virus Res.* 287, 198105. doi: 10.1016/j.virusres.2020.198105

Xu, S., Xie, J., Zhang, X., Chen, L., Bi, Y., Li, X., et al. (2022). DDX56 antagonizes IFN-β production to enhance EMCV replication by inhibiting IRF3 nuclear translocation. *Vet. Microbiol.* 264, 109304. doi: 10.1016/j.vetmic.2021.109304

Xu, Z., and Hobman, T. C. (2012). The helicase activity of DDX56 is required for its role in assembly of infectious West Nile virus particles. *Virology* 433, 226–235. doi: 10.1016/j.virol.2012.08.011

Zhang, Z., Kim, T., Bao, M., Facchinetti, V., Jung, S. Y., Ghaffari, A. A., et al. (2011a). DDX1, DDX21, and DHX36 helicases form a complex with the adaptor molecule TRIF to sense dsRNA in dendritic cells. *Immunity* 34, 866–878. doi: 10.1016/j.immuni.2011.03.027

Zhang, Z., Yuan, B., Lu, N., Facchinetti, V., and Liu, Y. J. (2011b). DHX9 pairs with IPS-1 to sense double-stranded RNA in myeloid dendritic cells. *J. Immunol.* 187, 4501–4508. doi: 10.4049/jimmunol.1101307

Zirwes, R. F., Eilbracht, J., Kneissel, S., and Schmidt-Zachmann, M. S. (2000). A novel helicase-type protein in the nucleolus: protein NOH61. *Mol. Biol. Cell* 4, 1153–1167. doi: 10.1091/mbc.11.4.1153

frontiers | Frontiers in Microbiology

TYPE Original Research
PUBLISHED 05 October 2022
DOI 10.3389/fmicb.2022.1024899

OPEN ACCESS

EDITED BY
Lingbao Kong,
Jiangxi Agricultural University, China

REVIEWED BY
Zhiwei Wu,
Nanjing University, China
Yuan Zhang,
Wuhan Institute of Virology (CAS), China

*CORRESPONDENCE
Zhen Luo
zhluo18@jnu.edu.cn
Jianguo Wu
jwu898@jnu.edu.cn

†These authors have contributed equally to this work

SPECIALTY SECTION
This article was submitted to Virology, a section of the journal Frontiers in Microbiology

RECEIVED 22 August 2022
ACCEPTED 21 September 2022
PUBLISHED 05 October 2022

CITATION
Ruan Z, Liang Y, Chen Z, Yin J, Li C, Pan P, Zhang Q, Wu J and Luo Z (2022) Enterovirus 71 non-structural protein 3A hijacks vacuolar protein sorting 25 to boost exosome biogenesis to facilitate viral replication. *Front. Microbiol.* 13:1024899. doi: 10.3389/fmicb.2022.1024899

Enterovirus 71 non-structural protein 3A hijacks vacuolar protein sorting 25 to boost exosome biogenesis to facilitate viral replication

Zhihui Ruan[1†], Yicong Liang[1†], Zicong Chen[1], Jialing Yin[1], Chengcheng Li[1], Pan Pan[1,2], Qiwei Zhang[1,2], Jianguo Wu[1,2*] and Zhen Luo[1,2*]

[1]Guangdong Provincial Key Laboratory of Virology, Institute of Medical Microbiology, Jinan University, Guangzhou, China, [2]Foshan Institute of Medical Microbiology, Foshan, China

Human enterovirus 71 (EV71) is one of the major agents of the hand, foot, and mouth disease (HFMD), and occasionally causes severe neurological complications. There is clinical evidence that EV71 infection increases the exosomes in the serum of severe HFMD patients, suggesting a role of exosomes in EV71 pathogenesis. However, the relationship between exosomes and EV71 replication remains elusive. In this study, we initially found that EV71 infection elevated exosome biogenesis in the cultured cells. Among EV71 non-structural proteins, we identified EV71 3A, but not 3B, constitutively promoted exosome secretion. In detail, EV71 3A protein interacted with vacuolar protein sorting 25 (VPS25), while knock-down of VPS25 reduced EV71 3A protein- and EV71-induced exosome production. Further studies revealed VPS25 located on exosomes and its expression correlated to the exosome production. During EV71 infection, knock-down of VPS25 decreased exosome biogenesis to attenuate viral replication. Consistently, GW4869, an exosome inhibitor, exerted an obviously antiviral activity against EV71 replication companied with the decrease of exosome secretion or formation. These findings suggest the binding of EV71 3A and VPS25 benefited exosome biogenesis, thereby boosting viral replication. This study uncovers a novel mechanism underlying EV71-mediated exosomes in the regulation of viral replication, which provides potential anti-viral strategies against the EV71 infection and transmission in HFMD.

KEYWORDS

enterovirus 71 (EV71), EV71 3A protein, vacuolar protein sorting 25, exosome, viral replication, hand, foot and mouth disease (HFMD)

Introduction

Human enterovirus 71 (EV71) is one of the major pathogens responsible for hand, foot, and mouth disease (HFMD) with severe neurological complications (Solomon et al., 2010). EV71 belongs to the enterovirus genus in the *Picornaviridae* family, containing a single-stranded, positive-sense RNA of approximately 7.4 kb divided into a single large open reading frame (ORF), 5′- and 3′-untranslated regions (UTRs). After EV71 enters host cells, viral RNA is translated into a large polyprotein, which is segmented into four structural viral capsid proteins (VP4, VP2, VP3, and VP1) and seven non-structural proteins (2A, 2B, 2C, 3A, 3B, 3C, and 3D) (Wong et al., 2010). In the process of the viral life cycle, the endocytic pathway is important for enterovirus replication. Exactly, enterovirus non-structural proteins tether host lipid droplets and reorganize the secretory pathway to generate distinct organelles for RNA replication (Hsu et al., 2010; Laufman et al., 2019), which arranges cell membrane and associated proteins to generate extracellular vesicles.

The biogenesis pathway of extracellular vesicles has obvious overlapping processes with virus assembly and budding (Ju et al., 2021). Exosomes are a type of extracellular vesicles with a saucer-shape of 30–200 nm in diameter and released outside the cell in a form secreted after fusion of intracellular multivesicular bodies (MVBs) with the cell membrane (Thery et al., 2002; Kalluri and LeBleu, 2020). The microenvironment of cells may affect the content of exosomes and their biomarkers. Exosomes usually contain proteins from extracellular matrix and cell membrane, cytosol and nucleus, metabolites, and nucleic acids (Kalluri and LeBleu, 2020). The common proteins exist in almost all exosomes, for example, tetraspanins (such as CD9, CD63, and CD81), hepatocyte growth factor receptor tyrosine kinase substrate (HRS), and tumor susceptibility gene 101 (Tsg101) and thus are used as markers for exosome identification (Shao et al., 2018). In the immune system, exosomes are involved in immune cell interactions, including antigen presentation, immune-activating functions, immunosuppressive properties, and immune tolerance (Thery et al., 2009; Robbins and Morelli, 2014). The function of exosomes in viral infection and replication has been gradually uncovered. A dual role of exosomes is observed in the forms of both promotion and inhibition of viral infection (Alenquer and Amorim, 2015; Schorey et al., 2015). Nonetheless, accumulating evidence suggests that virus-modified exosomes contribute to viral infection and immune escape. The number of secreted exosomes and their content vary depending on their biogenesis, cellular origin, and cellular state. Clinically, the difference in exosomal microRNA content is highly relevant to the severity of HFMD caused by EV71 infection (Jia et al., 2014; Min et al., 2018). Current evidence suggests that exosomes can promote EV71 transmission in human neural (Mao et al., 2016; Too et al., 2016) and intestinal epithelial cells (Huang et al., 2020). It is also reported that exosomes promote EV71 infection by transferring miR-146a to suppress type I interferon responses (Fu et al., 2017), and cloak the virion to non-lytically transmit EV71 (Gu et al., 2020). However, the mechanism by which EV71 modulates exosome biogenesis remains unknown.

The role of the endosomal sorting complex required for transport (ESCRT) machinery in the multivesicular endosomes (MVEs) as intraluminal vesicles (ILVs) biosynthesis regulates exosome formation (van Niel et al., 2018). Through manipulating ESCRT components, several ESCRT subunits could act selectively on MVBs for exosome secretion (Vietri et al., 2020). ESCRT-II is required for the formation of MVBs and the sorting of endosomal cargo proteins into MVBs, and the ESCRT-II complex may be involved in the recruitment of the ESCRT-III complex (Vietri et al., 2020), which may be involved in promoting budding of certain RNA viruses (Pincetic et al., 2008). Vacuolar protein sorting 25 (VPS25) is a component of the ESCRT-II complex, and the protein subunits in the ESCRT-II complex are arranged in the form of the letter "Y" with VPS22 and VPS36 (Hierro et al., 2004; Wernimont and Weissenhorn, 2004). Thus, the potential function of VPS25 in the regulation of exosome biogenesis upon EV71 infection is of high interest.

In this study, we observed the difference in the cellular secretion of exosome upon EV71 infection, showing that EV71 infection and EV71 3A protein overexpression can promote the secretion of exosome. Through a protein-protein interaction screening, we found that EV71 3A protein physically binds to a component of ESCRT-II complex VPS25 protein, thereby promoting exosome secretion. Further studies demonstrated that the VPS25-mediated exosome biogenesis facilitates EV71 replication. Altogether, our findings highlighted a novel mechanism by which EV71 3A hijacks VPS25 to favor the biogenesis of exosome leading to the facilitation of viral replication.

Materials and methods

Cell culture

Human rhabdomyosarcoma cells (RD), embryonic 293T cells (HEK293T) were obtained from ATCC (Manassas, VA, USA). The cells were cultured in DMEM (Gibco, Carlsbad, CA, USA) containing 10% fetal bovine serum (FBS) (Gibco) or Exosome-depleted FBS (VivaCell Biosciences Inc., Shanghai, China), supplemented with 100 U/ml penicillin and 100 mg/ml streptomycin sulfate (Gibco) at 37°C in a 5% CO_2 incubator.

Virus infection

Human EV71 (Xiangyang-Hubei-09) was preserved in our laboratory (GenBank accession number JN230523.1). EV71 was propagated in RD cells. EV71 infected RD cells with different multiplicities of infection (MOIs) and the unbound virus was washed away after 2 h. Then, the infected cells were maintained with a fresh medium at 37°C. The determination of virus titer was performed by serial dilutions for the infectivity in RD cells detected by TCID50 (50% Tissue Culture Infective Dose) as previously described (Luo et al., 2014).

Plasmid construction

The full-length *VPS25* gene (GenBank accession no. NM_032353.4) was cloned into pcDNA3.1-3 × FLAG vector to generate plasmid encoding FLAG-VPS25, and cloned into pBiFc-VN173 vector (Addgene plasmid #22010) to express VPS25 fusion protein using ClonExpress MultiS One Step Cloning Kit (Vazyme Biotech, Nanjing, China) as previously described (Luo et al., 2017). The DNA fragment of EV71 3A gene was ligated into eGFP-C1 vector to generate plasmids expressing GFP-tagged 3A and cloned into pBiFC-VC155 vector (Addgene plasmid #22011) to express 3A fusion protein, respectively. The information on primers is listed in **Table 1**.

Reagents

The specific small interfering RNAs (siRNA) to the negative control (NC) and *VPS25* gene were synthesized by Guangzhou RiboBio Co., Ltd. (Guangzhou, China). The sequences of siRNA were as followed: si-VPS25-1#: 5′-GCA CAAGGCCGAGATCATC; si-VPS25-2#: 5′-GGGAAACTCA TCTATCAGT; si-NC: 5′-TTCTCCGAACGTGTCACGT. An exosome inhibitor GW4869 (Catalog number: HY-19363) and membrane dyes Dil (Catalog number: HY-D0083) were purchased from MedChemExpress (MCE) Corporation (Shanghai, China). The Cell Counting Kit 8 (CCK8) was purchased from Dojindo Laboratories (Kumamoto, Japan). 4′,6-Diamidine-2′-phenylindole dihydrochloride (DAPI) (Catalog number: 28718-90-3) was purchased from Sigma-Aldrich (St. Louis, MO, USA).

TABLE 1 List of primers used in this study.

Primer title	Orientation (5′−3′)
FLAG-VPS25 F	AGTCCAGTGTGGTGGAATTCCATGGCGATGAGTTT CGAGTGGCCGTG
FLAG-VPS25 R	GCCCTCTAGACTCGAGCGGCCGCCTAGAAGAACTT GACGCCTCGGCC
GFP-3A F	TCGAGCTCGGCCCACCCAAGTTCAGGC
GFP-3A R	TCGAAGCTTTTGAAACCCTGCAAAGAGCTTGT
VN173-VPS25 F	AAAGACGATGACGACAAGCTTATGGCGATGAGTTT CGAGTG
VN173-VPS25 R	GATGGATCTTCTAGAGTCGACGAAGAACTTGACGC CTCGGCC
VC155-3A F	TGGCCATGGAG GCCCGAATTCACGGCCCACCC AAGT
VC155-3A R	TTTGCACGCCGGACGGGTACCTTGAAACCCTGCAA AGAGCTTGT

F, forward; R, reverse.

Antibodies

CoraLite®488-conjugated CD9 monoclonal antibody (Catalog number: CL488-60232), HRP-conjugated GFP monoclonal antibody (Catalog number: HRP-66002), rabbit IgG control polyclonal antibody (Catalog number: 30000-0-AP), mouse antibody against β-actin (Catalog number: 66009-1-Ig), and rabbit antibodies against VPS25 (Catalog number: 15669-1-AP), GFP (Catalog number: 50430-2-AP), HRS (Catalog number: 10390-1-AP), and Tsg101 (Catalog number: 28283-1-AP) were purchased from ProteinTech Group (Wuhan, China). Mouse antibody against CD63 (Catalog number: sc-5275) was purchased from Santa Cruz Biotechnology (Santa Cruz, CA, USA). Rabbit antibodies against CD9 (Catalog number: 98327S) and calnexin (Catalog number: 2679) were purchased from Cell Signaling Technology (Beverly, MA, USA). Rabbit antibody against HA (Catalog number: H6908) and mouse antibody against FLAG (Catalog number: F3165) were purchased from Sigma-Aldrich (St. Louis, MO, USA). Rabbit antibody against EV71 VP1 (Catalog number: GTX132339) was purchased from GeneTex, Inc. (Irvine, CA, USA). Rabbit antibody against EV71 3C (Catalog number: A10003) was purchased from ABclonal Technology (Wuhan, China). Mouse antibody against EV71 3A was kindly provided by Dr. Yongbo Yang of Central China Normal University.

Exosome isolation and purification

Cells were cultured in a medium with Exosome-depleted FBS for 24 h. Exosome isolation and purification was subjected to the warranted performance as previously described (Thery et al., 2006; Lobb et al., 2015). Firstly, the cell supernatant was collected and centrifuged at 2,000 × *g* for 10 min and 10,000 × *g* for 30 min to remove dead cells and debris, respectively. Then, the exosomes were then isolated by using an ultra-centrifuge (Optima XE-100, Beckman Coulter, Indianapolis, IN, USA) at 100,000 × *g* at 4°C for 70 min. The harvested exosomes were washed in PBS and subjected to the repeated ultracentrifugation as above to remove contaminating proteins. Finally, the purified exosomes were resuspended in

PBS and stored in ultra-low adhesion microcentrifuge tubes at −80°C.

The quantification of exosome preparations is based on the same volume of cell supernatants from different groups. To compare the exosome production, the equal volume of exosomes in PBS of each sample with a total protein amount ranging from 0.5 to 2.0 μg was loaded in gels for Western blot analysis. After cell supernatants were collected, the cells in the plated were digested with trypsin and further washed with PBS. The suspended cell was subjected to centrifugation at 4,000 × *g* for 5 min. The sedimented cells were lysed in RIPA buffer to prepare cell lysis for Western blot analysis.

Transmission electron microscopy and immunoelectron microscopy

Briefly, exosome samples were adsorbed at activated formvar/carbon-coated grids, fixed in 2.5% glutaraldehyde for 30 min, pelleted by ultracentrifugation, and placed on grids, followed by negative staining using 1% uranyl acetate in water. Grids were examined using a JEM1400 120 kV Transmission Electron Microscope (JEOL Ltd., Peabody, MA, USA). Immunogold labeling was performed as previously described (Peters et al., 2021). For immunogold labeling, exosome samples were added and grids were plated with rabbit polyclonal antibody against VPS25 or isotype IgG at a ratio of 1:50 dilution in blocking buffer (0.5% BSA, 0.5% ovalbumin in PBS) for incubation for 1 h. Followed by triple washes for 5 min in PBST, the 10 nm gold-labeled goat anti-rabbit secondary antibody at 1:50 dilution was used to incubate samples for 1 h incubation. After three additional washes in PBST, samples were fixed in 8% glutaraldehyde for 30 s. Images were captured using the Transmission Electron Microscope.

Nanoparticle tracking analysis

The exosome samples were prepared in an optimal dilution. The size and count of exosomes were assessed by nanoparticle tracking analysis (NTA) (NTA 3.4 Build 3.4.003) on NanoSight NS300 (Malvern Panalytical, Malvern, UK).

Immunoprecipitation and immunoblot analysis

HEK293T cells were cultured in the 6-cm dish and harvested after transfection with plasmids for 48 h. The cells were lysed in 800 μl RIPA buffer and 80 μl lysate was reserved for direct immunoblot analysis. The rest of lysate was incubated with primary antibody overnight together with Protein G Agarose (GE Healthcare, Milwaukee, WI, USA) for another 2 h. After five rounds of washes, proteins were fractionated by SDS-PAGE and transferred to nitrocellulose membrane. Non-specific sites were blocked with 5% skim milk for 1 h at room temperature. After three times of PBST wash, the nitrocellulose membrane was incubated with primary and secondary antibodies. Blots were analyzed using a ChemiDoc imaging system (Bio-Rad Laboratories, Hercules, CA, USA).

Immunofluorescence microscopy

Rhabdomyosarcoma cells were seeded on 20-mm coverslips and infected with EV71. Then, the medium was removed and cells were washed with PBS, fixed with 4% formaldehyde for 30 min, and permeabilized with 0.2% Triton X-100 for 10 min at room temperature. After another PBS wash, cells were blocked in PBS containing 5% BSA for 1 h and incubated with mouse anti-EV71-3A antibody dilution (v/v = 1:200) and rabbit anti-VPS25 antibody dilution (v/v = 1:200) overnight at 4°C. Samples were incubated with FITC-conjugated goat anti-mouse and Cy3-conjugated goat anti-rabbit IgG dilution (v/v = 1:500) (ProteinTech Group, Wuhan, China) for 45 min at room temperature. For nuclei staining, 1 μg/ml DAPI in methanol was used and incubated with samples for 10 min at room temperature. After washing with PBS, the cells were observed by Leica TCS SP8 confocal laser scanning microscopy (Leica Microsystem, Wetzlar, Germany).

For the immunofluorescence staining of exosomes, exosomes were labeled with Dil membrane dye as previously described (Jiang Y. et al., 2020) and CoraLite® 488-conjugated CD9 antibody dilution (v/v = 1:200). Labeled exosomes were washed with PBS and ultracentrifuged at 100,000 × *g* for 70 min at 4°C for three times. The samples were dropped on a glass slide and observed under Leica TCS SP8 confocal laser scanning microscopy with Lightning mode.

Bimolecular fluorescence complementation assay

The bimolecular fluorescence complementation (BiFc) assay was performed to examine physical protein-protein interaction as previously described (Luo et al., 2017; Pan et al., 2021). The plasmids expressing VN173, VC155, or fusion protein VN173-VPS25, VC155-3A were co-transfected into HEK293T cells using Lipofectamine 2000 (Invitrogen, Carlsbad, CA, USA). At 24 h post-transfection, cells were pre-cultured at 4°C for 10 min. The fusion proteins in living cells were observed by Leica TCS SP8 confocal laser scanning microscopy.

Immunocapture-based enzyme-linked immunosorbent assay of exosome

The enzyme-linked immunosorbent assay (ELISA) measurement of protein on the surface of exosome was performed as previously reported (Chen et al., 2018). For the detection of VPS25 on exosome, ELISA plates (96-well) (Nunc Cell Culture) were coated with 0.1 μg/per well (100 μl) of mouse anti-CD63 antibody overnight at 4°C. Free binding sites were blocked with 200 μl of 5% BSA for 1 h at room temperature. Then, 100 μl of exosome samples purified from the equal volume of cell culture supernatants suspended in PBS, were added to each well. Rabbit anti-VPS25 antibody dilution (v/v = 1:200) was added to each well and incubated for 1 h at room temperature. HRP conjugated secondary antibody (Catalog number: SA00001-2) (ProteinTech Group, Wuhan, China) diluted in PBS containing 0.1% BSA was incubated for 1 h at room temperature. Plates were developed with TMB Substrate Solution (Catalog number: P0209-100 ml) (Beyotime Biotechnology, Jiangsu, China) and stopped with H_2SO_4. The OD values in plates were determined at 450 nm with a Varioskan LUX multimode microplate reader (Thermo Scientific, Waltham, MA, USA).

Statistics

Statistical analysis was performed by Student's *t*-test using Prism 7 software (GraphPad Software Inc., San Diego, CA, USA). A *P*-value < 0.05 was considered to indicate statistical significance.

Results

Enterovirus 71 infection promotes exosome biogenesis

To investigate the relationship between EV71 infection and exosome secretion, we preliminarily determined whether EV71 infection influenced the secretion of cellular exosomes. In both mock and EV71-infected cell supernatants, the extracted extracellular vesicles were observed with a typical exosome structure by transmission electron microscopy (TEM) assay (**Figure 1A**) and measured with a diameter of around 104 nm by NTA (**Figure 1B**). Subsequently, the particle and protein concentration of extracted exosomes in the samples was counted. It was displayed that both particle number and protein concentration of exosome secreted from EV71-infected cells was significantly increased than that of uninfected ones (**Figure 1C**). The content of exosomal markers, HRS, Tsg101, CD9, and CD63 proteins in the extracted exosomes (Fernandez-Llama et al., 2010; Jiang Z. et al., 2020) were further verified by Western blot assay. The purification of extracted exosome was confirmed by the absence of Calnexin protein (**Figure 1C**, upper panel). Meanwhile, the protein levels of HRS, Tsg101, CD9, and CD63 were elevated in the exosome secretion by EV71 infection (**Figure 1D**). To further confirm the identity of the vesicles recovered from the cultured cells supernatant, we performed immunostaining using membrane dye Dil and fluorophore-conjugated CD9 antibody on the exosome preparation. It was presented that the exosomes were specifically stained with Dil companied with colocalization with CD9 protein (**Figure 1E**). Altogether, these data indicated that EV71 infection promotes the secretion of exosome in host cells.

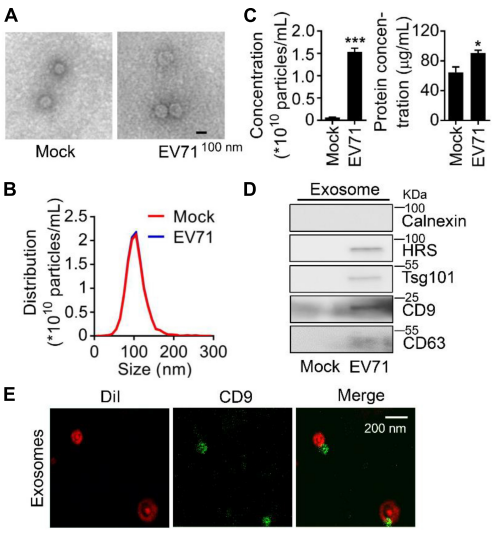

FIGURE 1
Enterovirus 71 (EV71) infection promotes exosome biogenesis. RD cells were mock-infected or infected with EV71 (MOI = 0.5). At 24 h post-infection, cell supernatants were harvested for exosome extraction. **(A–C)** The characteristics of exosomes were examined by transmission electron microscope (TEM) and nanoparticle tracking analysis (NTA) to observe the morphology **(A)**, size and distribution **(B)**, particles and protein concentration **(C)** of exosomes, respectively. The size is expressed by diameter. **(D)** The extracted exosomes were detected by Western blot analysis. HRS, Tsg101, CD9, and CD63 are used as exosome markers, and Calnexin is a marker of the cytosol to reflect cellular contamination. **(E)** The extracted EV71-induced exosomes were stained by Dil (red) and fluorophore-conjugated CD9 antibody (green), then examined by Leica TCS SP8 confocal laser scanning microscopy with Lightning mode. WCL, whole cell lysate. Graph shows as mean ± SD. *$P < 0.05$; ***$P < 0.001$.

Enterovirus 71 non-structural protein 3A participates in the increased exosome biogenesis

Considering that enterovirus non-structural proteins reorganize host lipid droplets and secretory pathways to arrange cell membrane and cargo proteins to generate extracellular

10.3389/fmicb.2022.1024899

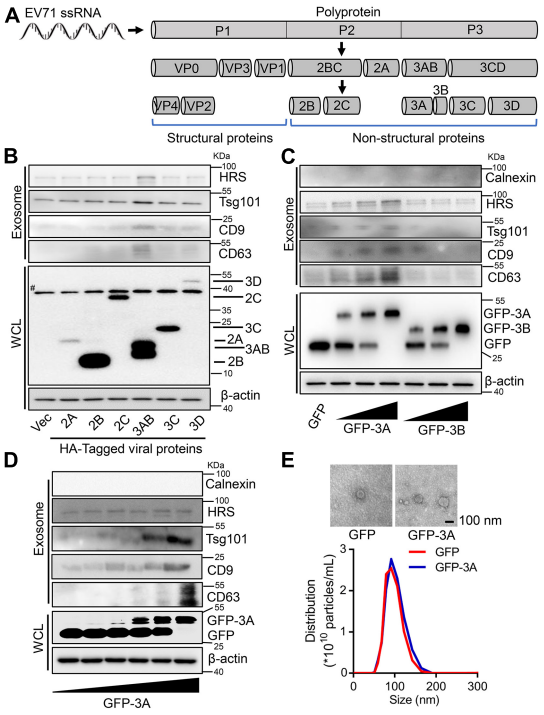

FIGURE 2

Enterovirus 71 (EV71) 3A protein increases exosome biogenesis. **(A)** Schematic diagram of EV71 structure and non-structural proteins. **(B–D)** RD cells were transfected with 2 μg plasmids expressing HA-tagged EV71 non-structural proteins **(B)**, or different doses (0, 0.5, 1, and 2 μg) of plasmids expressing GFP-tagged 3A or 3B protein **(C)**, or different doses (0, 0.2, 0.5, 1, 1.5, and 2 μg) of plasmids expressing GFP-tagged 3A protein **(D)**. At 24 h post-transfection, the extracted exosomes from cell supernatants and cell lysates were collected for Western blot analysis. HRS, Tsg101, CD9, and CD63 are used as exosome markers, while Calnexin is a marker of cytosol. β-actin is presented as an internal reference protein in cell lysates. WCL, whole cell lysate. #, the non-specific band. **(E)** RD cells were transfected with 2 μg plasmids expressing GFP or GFP-tagged 3A protein. At 24 h post-transfection, the extracted exosomes from cell supernatants were observed by TEM and measured by size and distribution, respectively.

vesicles (Hsu et al., 2010; Laufman et al., 2019), we further explore the regulation of EV71 non-structural proteins on secretion of exosomes. Initially, we constructed and expressed a series of EV71 non-structural proteins (Figure 2A). Among six non-structural proteins, EV71 3AB protein obviously increased HRS, Tsg101, CD9, and CD63 proteins levels in the collected exosomes (Figure 2B), suggesting EV71 3AB protein could stimulate the production of exosome. Then, the increased expression of 3A protein significantly promoted HRS, Tsg101, CD9, and CD63 protein levels in the exosomes (Figure 2C, left panel), whereas the increased expression of 3B protein failed to affect the levels of corresponding proteins in the exosomes (Figure 2C, right panel), indicating EV71 3A, but not 3B protein constructively enhanced exosome secretion. Consistently, overexpression of GFP-3A protein constitutively enhanced HRS, Tsg101, and CD9 protein levels in the exosomes in a dose-dependent manner (Figure 2D). Of note, the extracted exosomes from the supernatants of GFP and GFP-3A expressed cells were detected by TEM observation (Figure 2E, upper panel). Consistently, NTA data revealed that the diameter of purified exosomes was not affected by either overexpression of GFP or GFP-3A protein (Figure 2E, lower panel), while both particles and protein concentration of exosomes was increased by GFP-3A but not GFP protein, suggesting an increase of exosome secretion (Supplementary Figure 1). Therefore, these results concluded that EV71 3A protein specifically increases exosome biogenesis.

Enterovirus 71 3A protein interacts with vacuolar protein sorting 25

Since specialized ESCRT components could act on MVBs for exosome secretion (Vietri et al., 2020), the mechanism underlying EV71 3A protein promoting the secretion of exosome was further investigated. In the expressed GFP or GFP-3A protein cell lysates, we performed a co-immunoprecipitation (Co-IP) assay using anti-GFP antibody to separate the possible cellular proteins interacting with 3A protein by SDS-PAGE (Figure 3A), and the precipitated protein samples were subjected to mass spectrometry analysis (Table 2). As a typical component of the ESCRT-II complex (Wernimont and Weissenhorn, 2004), VPS25 potentially interacted with EV71 3A protein. Next, Co-IP assays revealed that VPS25 could immunoprecipitate 3A protein using anti-FLAG antibody

TABLE 2 List of potential proteins interacting with EV71 3A protein.

Protein name	Description or alias
Vimentin	HUMAN Vimentin
VPS25	HUMAN Vacuolar protein sorting 25
hnRNPA2B1	HUMAN Heterogeneous nuclear ribonucleoprotein A2/B1
hnRNPA3	HUMAN Heterogeneous nuclear ribonucleoprotein A3
hnRNPA1	HUMAN Heterogeneous nuclear ribonucleoprotein A1
Nucleolin	HUMAN Nucleolin
ACTG	HUMAN Actin, cytoplasmic 2
HSP90AB1	HUMAN Heat shock protein HSP 90-beta
hnRNPA/B	HUMAN Heterogeneous nuclear ribonucleoprotein A/B
GRP75/HSPA9	HUMAN Stress-70 protein, mitochondrial
HSP60	HUMAN 60 kDa heat shock protein, mitochondrial
hnRNPU	HUMAN Heterogeneous nuclear ribonucleoprotein U
HSP90B1	HUMAN Endoplasmin
HSPB1	HUMAN Heat shock protein beta-1
HSP72	HUMAN Heat shock-related 70 kDa protein 2
hnRNPC1/C2	HUMAN Heterogeneous nuclear ribonucleoproteins C1/C2

10.3389/fmicb.2022.1024899

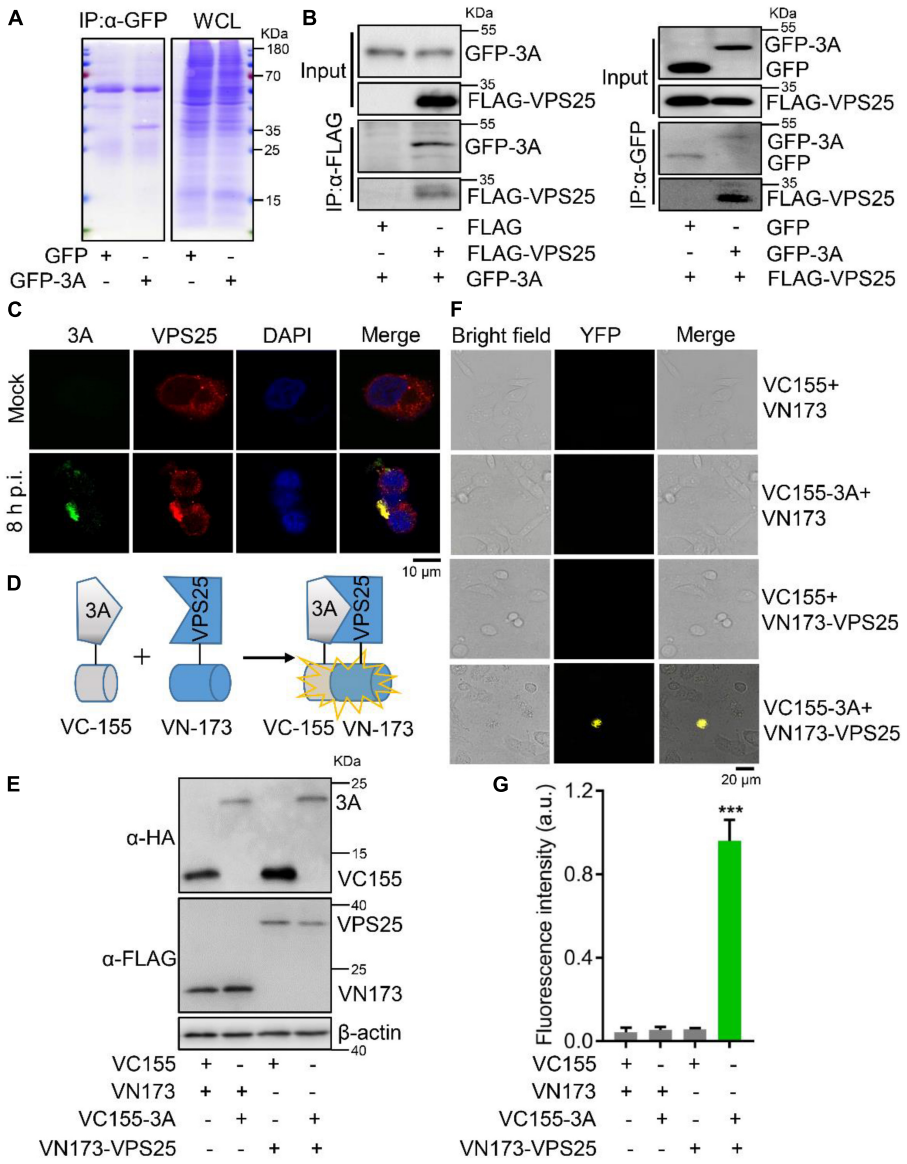

FIGURE 3

Enterovirus 71 (EV71) 3A protein interacts with VPS25. **(A)** RD cells were transfected with plasmids expressing GFP or GFP-tagged 3A. Cell lysates were immunoprecipitated with anti-GFP (α-GFP) antibody. The protein samples were separated by SDS-PAGE and visualized with Coomassie blue staining. **(B)** HEK293T cells were co-transfected with empty or indicated plasmids expressing FLAG-tagged VPS25 or GFP-tagged 3A, followed by the immunoprecipitated with anti-FLAG (α-FLAG) or anti-GFP (α-GFP) antibody, respectively. The corresponding proteins were detected by Western blot analysis. **(C)** RD cells were infected with EV71 (MOI = 0.5) for 8 h. Immunofluorescence assay was performed after labeling proteins of EV71 3A (green), VPS25 (red), and staining nuclei with DAPI (blue). **(D)** Schematic of bimolecular fluorescence complementation assay (BiFc). **(E–G)** RD cells were co-transfected with Venus BiFc plasmids expressing control protein (VC155 or VN173), 3A protein (VC155-3A), and VPS25 protein (VN173-VPS25), respectively. At 24 h post-transfection, the expression of corresponding proteins was detected by Western blot analysis **(E)** or visualized by confocal microscopy **(F)**. The fluorescence intensity was analyzed using ImageJ software **(G)**. YFP, yellow fluorescence protein; a.u., arbitrary unit. Graph shows as mean ± SD. ***$P < 0.001$.

(Figure 3B, left), or 3A protein immunoprecipitated VPS25 using anti-HA antibody (Figure 3B, right).

To confirm this interaction, RD cells were infected with EV71 at 8 h p.i. Notably, we observed that VPS25 protein colocalized with EV71 3A protein in the cytosol (Figure 3C), indicating the occurrence of robust interaction between 3A and VPS25 proteins during viral replication (Supplementary Figure 2). To further verify the physical interaction of EV71 3A and VPS25, the BiFc assay was employed in the living cells (Figure 3D). The indicated fusion protein with the complementary yellow fluorescence protein (YFP) fragment VC155-3A and VN173-VPS25 were expressed (Figure 3E). In

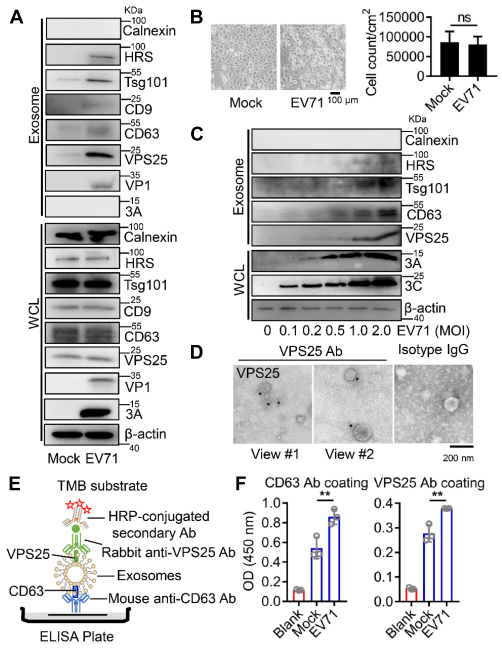

FIGURE 4
The location of VPS25 in EV71-induced exosome biogenesis. **(A–C)** RD cells were mock-infected or infected with EV71 (MOI = 0.5) for 24 h **(A,B)**. The cell images and count were captured **(B)**. RD cells were infected with EV71 at different MOIs **(C)**. At 24 h post-infection, extracted exosomes and cell lysates were analyzed by Western blot. **(D)** The extracted exosomes from panel **(A)** were detected by immunoelectron microscopy using anti-VPS25 antibody. **(E)** Schematic of immunocapture-based ELISA to detect protein on the surface of exosomes. **(F)** RD cells were mock-infected or infected with EV71 (MOI = 0.5). At 24 h post-infection, exosomes extracted from 10 mL of cell supernatant were detected by ELISA in the CD63 and VPS25 antibodies coating plates, respectively. Ab, antibody. Graph shows as mean ± SD. ns, not-significant. $^{**}P < 0.01$.

the absence of either VC155-3A or VN173-VPS25, the YFP in cells failed to be observed as expected (Figure 3F), while in the presence of VC155-3A and VN173-VPS25, the YFP in cells was observed (Figure 3F) and intensity of fluorescence was robustly detected (Figure 3G), suggesting a strong physical interaction between 3A and VPS25 proteins. Taken together, these results illustrated that EV71 3A physically interacts with VPS25.

Vacuolar protein sorting 25 locates on exosome during Enterovirus 71-induced exosome biogenesis

Because of the interaction between VPS25 and EV71 3A, we next examined the impact of VPS25 on EV71 3A-induced exosome secretion. We found the protein levels of HRS, Tsg101, CD9, and CD63 along with VPS25 were elevated in the exosome secretion upon EV71 infection (Figure 4A, upper panel), whereas the expression of the above proteins was not significantly increased in whole-cell lysates during EV71 infection (Figure 4A, lower panel). Interestingly, VP1 but not 3A protein could be observed in EV71-induced exosomes (Figure 4A, upper panel), suggesting the evidence of EV71 virion in exosome as previously reported (Gu et al., 2020). We also observed that the number of cells was not significantly changed after EV71 infection (Figure 4B). In addition, the protein levels of HRS, Tsg101, and CD63 along with VPS25 increased in a dose manner upon EV71 infection (Figure 4C), suggesting a positive correlation between VPS25 protein level and the generation of exosomes.

We suspected that VPS25 protein could locate on the exosomes. In an immunoelectron microscopy experiment, VPS25 protein was specifically labeled and visualized on exosomes compared to a control (Figure 4D). To further verify this specific location, an ELISA measurement of VPS25 protein on the surface of exosome was introduced as previously reported (Chen et al., 2018). In this assay, the purified exosomes from cell culture supernatants were initially captured by the anti-CD63 antibody coating in a plate, and then detected exosomal VPS25 protein with anti-VPS25 antibody (Figure 4E). Using the immunocapture-based ELISA, exosomal VPS25 protein was specifically detected and increased in EV71-induced exosome captured by the anti-CD63 antibody compared to mock control (Figure 4F, left panel). In turn, exosomal CD63 protein was also detected with a higher level in EV71-induced exosome captured by the anti-VPS25 antibody compared to mock control (Figure 4F, right panel). Thus, we discovered that VPS25 protein correlates to the production of exosomes and locates on exosomes.

Vacuolar protein sorting 25 is responsible for enterovirus 71-induced exosome biogenesis

To confirm the association between VPS25 protein and exosome generation, we utilized siRNA to silence endogenous VPS25 protein expression. The knock-down efficiency of VPS25 was accessed and the protein level of VPS25 was robustly decreased by siVPS25-1# relative to siVPS25-2# or siNC (Figure 5A). In addition, there was no significant cytotoxicity when cells were transfected with either siNC or siVPS25-1# at the concentration ranging from 50 to 150 nM (Figure 5B). Subsequently, we reduced the expression of VPS25 protein by using siRNA and then transfected plasmids expressing GFP or GFP-3A to cells. The knock-down of VPS25 did not affect the endogenous expression of Calnexin, HRS, Tsg101, CD9, and CD63 in cell lysates (Figure 5C, lower panel). The exosome secretion

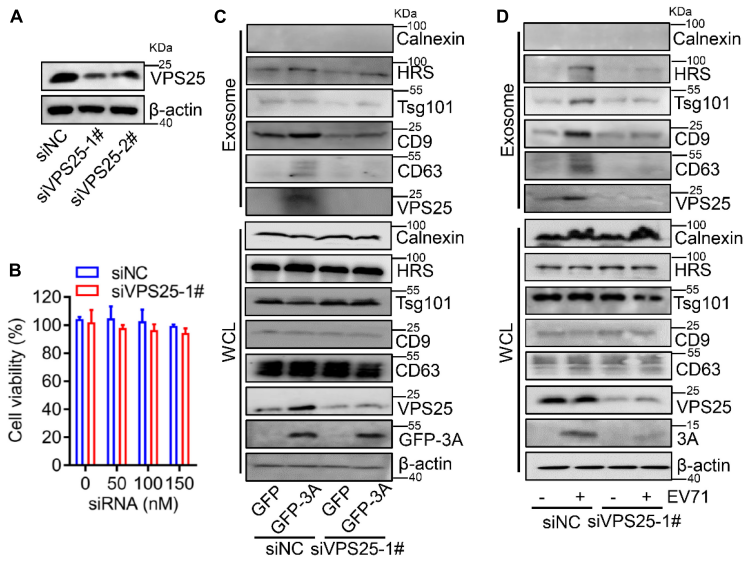

FIGURE 5
Vacuolar protein sorting 25 (VPS25) mediates EV71-induced exosome biogenesis. **(A,B)** RD cells were transfected with 100 nM siRNA negative control (siNC), or against VPS25 (siVPS25-1#, -2#), respectively. At 48 h post-transfection, the level of VPS25 protein was measured by Western blot **(A)**. Until 72 h post-transfection, the cell viability was measured using the CCK8 assay **(B)**. **(C,D)** RD cells were transfected with siNC or siVPS25-1# for 24 h and then transfected with plasmids expressing GFP or GFP-tagged 3A **(C)**, or infected with EV71 (MOI = 0.5) **(D)** for another 24 h. The extracted exosomes and cell lysates were analyzed by Western blot. The equal volume of exosomes in PBS of each sample with a total protein amount ranging from 0.5 to 2.0 μg was loaded. WCL, whole cell lysate.

was enhanced in the presence of 3A protein, whereas this induction was restored by siVPS25-1# (Figure 5C, upper panel), demonstrating that VPS25 mediates EV71 3A-induced exosome biogenesis.

Because of the role of VPS25 in 3A-promoted exosome secretion, we explored the relationship between VPS25 protein and exosome upon EV71 infection. The cells were transfected with siVPS25-1# or siNC and then infected with EV71. We observed that the knock-down of VPS25 did not affect the endogenous expression of Calnexin, HRS, Tsg101, CD9, and CD63 in cell lysates (Figure 5D, lower panel). The exosome secretion was induced by EV71 infection, whereas this induction was restored by siVPS25-1# (Figure 5D, upper panel), indicating VPS25 mediates EV71-induced exosome biogenesis. Notably, we found cellular EV71 3A expression was decreased in the presence of siVPS25-1# upon EV71 infection (Figure 5D, lower panel). Altogether, VPS25 is important for EV71-induced exosome biogenesis.

Vacuolar protein sorting 25 mediates enterovirus 71-induced exosome to facilitate viral replication

In the life cycle of enteroviruses, the first round of infection is deemed to be before 16 h post-infection (Su et al., 2020). In order to examine whether VPS25 affects EV71 intracellular replication, we designed kinetic time points within the first round of EV71 infection (Figure 6A). At both 8 and 12 h post-EV71 infection as an early stage, the viral protein VP1 and 3A expression was not affected in the cells transfected with siVPS25-1# relative to siNC (Figure 6B). Next, the function of VPS25-mediated exosome in EV71 replication was investigated. In the cells transfected with siVPS25-1# upon EV71 infection for 24 h, the viral expression of protein VP1 and 3A was significantly decreased (Figure 6C), suggesting inhibition of intracellular EV71 replication beyond the first round of infection. In a parallel experiment, the titer of progeny EV71 was significantly reduced by siVPS25-1# (Figure 6D). Moreover, the EV71-induced cytotoxicity was significantly reduced when cells were transfected with siVPS25-1# in a dose-dependent manner (Figure 6E). Altogether, the data demonstrated that VPS25 mediates EV71-induced exosome to benefit viral replication.

GW4869 inhibits viral replication by the repression of enterovirus 71-induced exosome biogenesis

Then, GW4869, an inhibitor of exosome biogenesis/release (Essandoh et al., 2015), which targets nSMase in an endocytic pathway to modulate exosome biogenesis (Figure 7A), was applied to test the effect of exosomes on EV71 replication. In cell lysates, GW4869 did not affect the endogenous

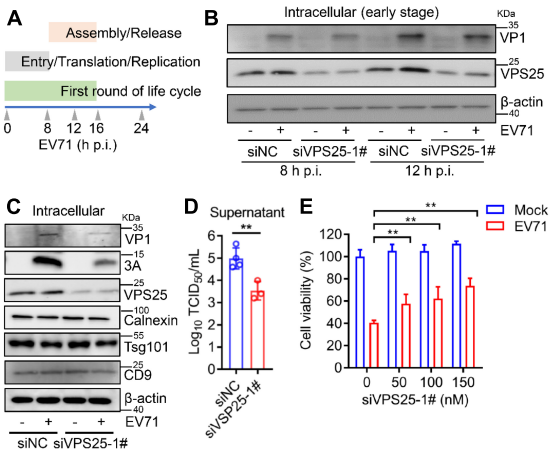

FIGURE 6
Vacuolar protein sorting 25 (VPS25) mediates EV71-induced exosome to facilitate viral replication. **(A)** Schematic of kinetic time points in the EV71 life cycle. **(B–D)** RD cells were transfected with 100 nM siNC or siVPS25-1# for 24 h and then infected with EV71 (MOI = 0.5). At 8 and 12 h p.i., the cell lysates were analyzed by Western blot **(B)**. At 24 h p.i., the cell lysates were analyzed by Western blot **(C)** and the progeny virus titer was measured by TCID50 assay **(D)**. **(E)** RD cells were transfected with different doses of siNC or siVPS25-1# (0, 50, 100, and 150 nM) for 24 h and then infected with EV71 (MOI = 0.5) for another 24 h. Cell viability was measured using the CCK8 assay. Graph shows as mean ± SD. $^{**}P < 0.01$.

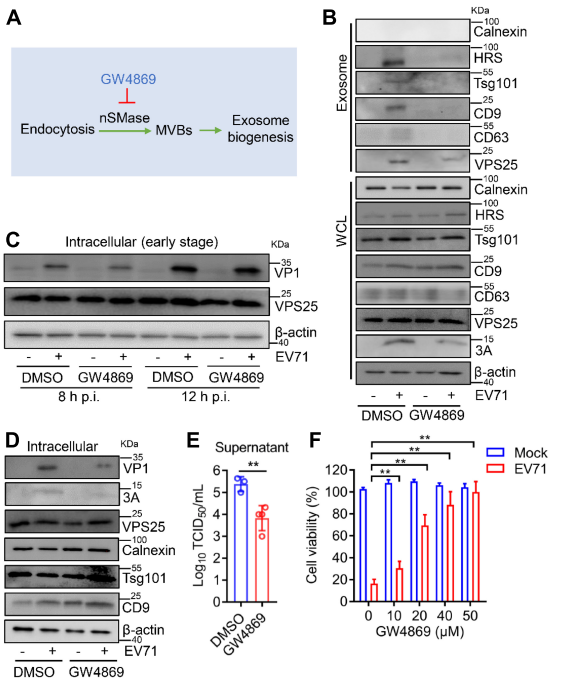

FIGURE 7
GW4869 inhibits viral replication via reducing exosome biogenesis. **(A)** GW4869 acts as an exosome inhibitor in the endocytic pathway. **(B–F)** RD cells were incubated with GW4869 (20 μM) for 2 h and then infected with EV71 (MOI = 0.5). At 24 h p.i., the extracted exosomes and cell lysates were analyzed by Western blot **(B)**. At 8 and 12 h p.i., the cell lysates were analyzed by Western blot **(C)**. At 24 h p.i., cell lysates were analyzed by Western blot **(D)** and progeny virus titer was measured by TCID50 assay **(E)**. WCL, whole cell lysate. **(F)** RD cells were incubated with different doses of DMSO or GW4869 (0, 10, 20, 40, and 50 μM) for 2 h and then infected with EV71 (MOI = 0.5) for another 24 h. Cell viability was measured using the CCK8 assay. Graph shows as mean ± SD. $^{**}P < 0.01$.

expression of Calnexin, HRS, Tsg101, CD9, CD63, and VPS25 (Figure 7B, lower panel). In exosomes, the protein level of VPS25 companied with HRS, Tsg101, CD9, and CD63 was increased by EV71, whereas this induction significantly reduced in the presence of GW4869 (Figure 7B, upper panel). We also noticed that the cellular EV71 3A expression were obviously decreased in the presence of GW4869 upon EV71 infection (Figure 7B, lower panel), suggesting EV71-induced exosome biogenesis plays a role in viral replication.

To further investigate the exosome in EV71 replication, the impact of GW4869 on EV71 intracellular replication was accessed. At both 8 and 12 h p.i., GW4869 did not affect the expression of EV71 VP1 protein (Figure 7C), implying that GW4869 had no obvious effect on EV71 intracellular replication at the early stage. At 24 h p.i., in the cells treated with GW4869 upon EV71 infection, the viral protein VP1 and 3A expression were significantly repressed (Figure 7D). Parallelly, the titer of progeny EV71 was obviously decreased by GW4869 (Figure 7E). Additionally, the EV71-induced cytotoxicity was significantly restored when cells were exposed to GW4869 in a dose-dependent manner (Figure 7F). These results revealed that EV71-induced exosome biogenesis plays a positive role in viral replication. Collectively, our study proposed a novel mechanism by which EV71 3A protein interacts with a component of the ESCRT-II complex, VPS25 to mediate exosome biogenesis and the release of progeny EV71, leading to facilitating viral infection and replication (Figure 8).

Discussion

Upon viral infection, the modulation of the biosynthesis of exosome is involved in viral infection and etiology. For example, exosomes exploit interferon-alpha-induced intercellular antiviral activity against hepatitis B virus (HBV) (Yao et al., 2018). Exosomes mediate Zika virus (ZIKV) to support cell-to-cell transmission in cortical neurons (Zhou et al., 2019). Regarding EV71 infection, exosomes benefit the spread of virus and facilitate viral replication (Mao et al., 2016; Fu et al., 2017; Huang et al., 2020). Clinically, the changes in exosomes are highly relevant to the severity of HFMD caused by EV71 infection (Jia

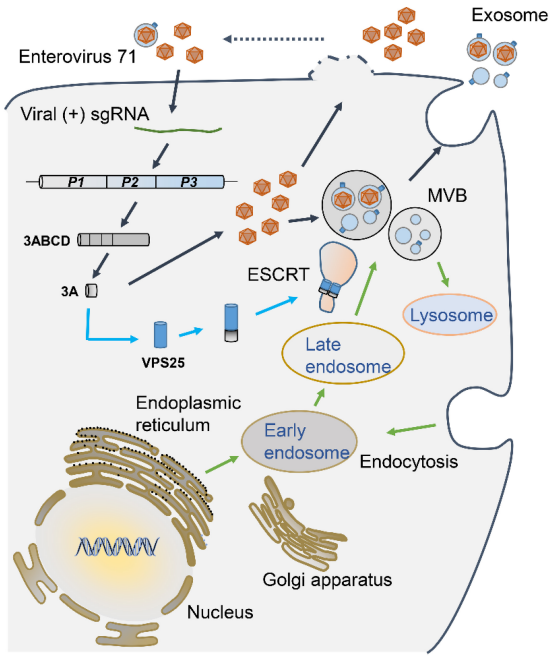

FIGURE 8
A proposed mechanism underlying VPS25 mediates EV71-induced exosome biogenesis to facilitate viral replication. Upon EV71 infection, viral single positive-sense RNA utilizes host translation machinery to translate a polyprotein, which is cleaved into structural and non-structural protein. Among viral non-structural proteins, EV71 3A protein physically interacts with VPS25, a component of the ESCRT-II complex, which participates in MVB generation and exosome biogenesis. The release of progeny EV71 could be in the forms of lytical and non-lytical manners. VPS25-mediated exosomes are engaged in the EV71 transmission and infection, thereby facilitating EV71 replication.

et al., 2014; Min et al., 2018). Here, we demonstrate that EV71 infection promotes the secretion of exosomes. However, the molecular mechanisms of the regulation on exosome generation during EV71 infection are not fully understood.

Based on the fact that enterovirus non-structural proteins reorganize host lipid droplets and secretory pathways to arrange cell membrane and cargo proteins to generate extracellular vesicles (Hsu et al., 2010; Laufman et al., 2019), we figured out that EV71 3A protein specifically induced exosome biogenesis. Further studies explored that EV71 3A physically interacted with VPS25, a component of the ESCRT-II complex, to mediate exosome biogenesis. The 3A protein of Picornavirus interacts directly or indirectly with many host cell proteins. It has been reported that the 3A proteins from multiple picornaviruses utilize the Golgi Adaptor Protein ACBD3 to recruit phosphatidylinositol 4-kinase class III beta (PI4KIIIβ) to promote virus replication (Greninger et al., 2012; Xiao et al., 2017). It also is reported that the 3A protein of enterovirus is a small hydrophobic protein and promotes viral replication by promoting the binding of capsule membrane to form replication complex (RC) and replication organelles (RO) (Arita et al., 2010; Ishikawa-Sasaki et al., 2014). In this study, we uncover a novel regulatory manner that EV71 3A constitutively promoted exosome secretion, which extends an exact function from 3A protein of EV71 on the regulation of exosome biogenesis.

Endosomal sorting complex required for transport complex is an ancient membrane remodeling and fragmentation system, mainly manipulating from MVBs to exosomes or extracellular vesicles biogenesis (Hurley, 2015; Guo et al., 2021). VPS25, belonging to the ESCRT-II complex members, plays an important role in the formation of exosomes (Juan and Furthauer, 2018). Our results provide direct evidence that VPS25 protein is present on exosomes and mediates both EV71- and EV71 3A-induced exosome biogenesis. It could be explained that the interaction of EV71 3A and VPS25 proteins participates in ESCRT pathway and acts on MVBs generation, thereby facilitating exosome biogenesis. However, the detailed events of the dynamic regulation of ESCRT complex on exosome biogenesis need further exploration.

Exosomes can be released from almost all of the cells infected with virus, which plays an important role in viral infection (van der Grein et al., 2018). Many viruses utilize the exosome generation pathway and interact with ESCRT complex proteins to enhance the viral replication process (Thery et al., 2002). HIV-1 (Human immunodeficiency virus I) utilizes exosomal machinery for HIV-1 RNA and protein trafficking (Madison and Okeoma, 2015). During Epstein-Barr virus (EBV) replication, the ESCRT machinery regulates the virus maturation (Lee et al., 2012). As previously mentioned, EV71 can resort to exosomes to spread between cells and suppress the innate immune response to enhance viral replication (Fu et al., 2017; Huang et al., 2020). Our current work also explored the role of VPS25-mediated exosome in EV71 replication. Employing siRNA silencing and inhibitor of exosome biogenesis, we found out that VPS25-mediated exosome promoted EV71 infection. Considering the fact that exosomes cloak the EV71 virion in a non-lytical manner to benefit viral transmission (Gu et al., 2020), we speculate the VPS25-mediated exosomes could also be engaged in the EV71 transmission and replication. Hence, it could be concluded that VPS25 regulates exosome biogenesis and possibly promotes the release of exosomal progeny EV71, and eventually facilitates EV71 infection and replication.

Besides exosomes, there are also certain roles of some extracellular vesicles' populations (especially size > 200 nm) in viral replication. For example, intercellular transfer of membrane proteins from microparticles may have implications for HIV-1 infection (Mack et al., 2000). Microvesicles

containing infectious virus were readily observed in cultures of differentiated progenitor cells infected with Coxsackievirus B3 (CVB3) (Robinson et al., 2014). There are interesting and compelling findings regarding the importance of exosomes and other extracellular vesicles during viral infection, which will allow for a better understanding of virulence mechanisms and immune responses, as well as the development of new diagnostics and vaccines (Schorey et al., 2015). Notably, the factors in exosomes and other extracellular vesicles involved in EV71 replication require clarification in future work.

In sum, we illuminated that EV71 promotes the secretion of exosomes through its non-structural protein 3A binding to VPS25, thereby facilitating viral replication, which provides insight into the regulatory mechanism of exosome biogenesis. We believe that the understanding of the relationship between EV71 and exosomes will be beneficial to the exploration of viral pathogenesis and the development of antiviral therapy in EV71-associated diseases.

Data availability statement

The original contributions presented in this study are included in the article/**Supplementary material**, further inquiries can be directed to the corresponding authors.

Author contributions

ZR, YL, JW, and ZL: conceptualization and design. ZR, YL, ZC, JY, and CL: data curation. ZC, JY, and CL: formal analysis. ZR, YL, PP, and QZ: methodology. ZC, JY, CL, PP, and QZ: investigation. PP, QZ, JW, and ZL: validation. JW and ZL: funding acquisition, supervision, and writing – review and editing. ZR, YL, and ZL: writing – original draft. All authors had finally approved the version of the manuscript to be published and agreed to be accountable for all aspects of the work.

Funding

This study was supported by the National Natural Science Foundation of China (32070148, 31800147, and 81730061), National Key Research and Development Program of China (BWS21J025), and Guangzhou Basic Research Program–Basic and Applied Basic Research Project (202102020260).

Acknowledgments

We would like to thank Yongbo Yang from Central China Normal University for providing a mouse anti-EV71 3A antibody.

Conflict of interest

The authors declare that the research was conducted in the absence of any commercial or financial relationships that could be construed as a potential conflict of interest.

Publisher's note

Supplementary material

The Supplementary Material for this article can be found online at: https://www.frontiersin.org/articles/10.3389/fmicb.2022.1024899/full#supplementary-material

References

Alenquer, M., and Amorim, M. J. (2015). Exosome biogenesis. regulation, and function in viral infection. *Viruses* 7, 5066–5083. doi: 10.3390/v7092862

Arita, M., Takebe, Y., Wakita, T., and Shimizu, H. (2010). A bifunctional anti-enterovirus compound that inhibits replication and the early stage of enterovirus 71 infection. *J. Gen. Virol.* 91, 2734–2744. doi: 10.1099/vir.0.023374-0

Chen, G., Huang, A. C., Zhang, W., Zhang, G., Wu, M., Xu, W., et al. (2018). L1 contributes to immunosuppression and is associated with anti-PD-1 response. *Nature* 560, 382–386. doi: 10.1038/s41586-018-0392-8

Essandoh, K., Yang, L., Wang, X., Huang, W., Qin, D., Hao, J., et al. (2015). Blockade of exosome generation with GW4869 dampens the sepsis-induced inflammation and cardiac dysfunction. *Biochim. Biophys. Acta* 1852, 2362–2371. doi: 10.1016/j.bbadis.2015.08.010

Fernandez-Llama, P., Khositseth, S., Gonzales, P. A., Star, R. A., Pisitkun, T., and Knepper, M. A. (2010). Tamm-Horsfall protein and urinary exosome isolation. *Kidney Int.* 77, 736–742. doi: 10.1038/ki.2009.550

Fu, Y., Zhang, L., Zhang, F., Tang, T., Zhou, Q., Feng, C., et al. (2017). Exosome-mediated miR-146a transfer suppresses type I interferon response and facilitates EV71 infection. *PLoS Pathog.* 13:e1006611. doi: 10.1371/journal.ppat.1006611

Greninger, A. L., Knudsen, G. M., Betegon, M., Burlingame, A. L., and Derisi, J. L. (2012). The 3A protein from multiple picornaviruses utilizes the golgi adaptor protein ACBD3 to recruit PI4KIIIbeta. *J. Virol.* 86, 3605–3616. doi: 10.1128/JVI.06778-11

Gu, J., Wu, J., Fang, D., Qiu, Y., Zou, X., Jia, X., et al. (2020). Exosomes cloak the virion to transmit Enterovirus 71 non-lytically. *Virulence* 11, 32–38. doi: 10.1080/21505594.2019.1705022

Guo, Y., Wang, H., Huang, L., Ou, L., Zhu, J., Liu, S., et al. (2021). Small extracellular vesicles-based cell-free strategies for therapy. *MedComm* 2, 17–26. doi: 10.1002/mco2.57

Hierro, A., Sun, J., Rusnak, A. S., Kim, J., Prag, G., Emr, S. D., et al. (2004). Structure of the ESCRT-II endosomal trafficking complex. *Nature* 431, 221–225. doi: 10.1038/nature02914

Hsu, N. Y., Ilnytska, O., Belov, G., Santiana, M., Chen, Y. H., Takvorian, P. M., et al. (2010). Viral reorganization of the secretory pathway generates distinct organelles for RNA replication. *Cell* 141, 799–811. doi: 10.1016/j.cell.2010.03.050

Huang, H. I., Lin, J. Y., Chiang, H. C., Huang, P. N., Lin, Q. D., and Shih, S. R. (2020). Exosomes facilitate transmission of enterovirus A71 from human intestinal epithelial cells. *J. Infect. Dis.* 222, 456–469. doi: 10.1093/infdis/jiaa174

Hurley, J. H. (2015). ESCRTs are everywhere. *EMBO J.* 34, 2398–2407. doi: 10.15252/embj.201592484

Ishikawa-Sasaki, K., Sasaki, J., and Taniguchi, K. (2014). A complex comprising phosphatidylinositol 4-kinase IIIbeta, ACBD3, and Aichi virus proteins enhances phosphatidylinositol 4-phosphate synthesis and is critical for formation of the viral replication complex. *J. Virol.* 88, 6586–6598. doi: 10.1128/JVI.00208-14

Jia, H. L., He, C. H., Wang, Z. Y., Xu, Y. F., Yin, G. Q., Mao, L. J., et al. (2014). MicroRNA expression profile in exosome discriminates extremely severe infections from mild infections for hand, foot and mouth disease. *BMC Infect. Dis.* 14:506. doi: 10.1186/1471-2334-14-506

Jiang, Y., Wang, L., Zhang, P., Liu, X., Di, H., Yang, J., et al. (2020). Chemoenzymatic labeling of extracellular vesicles for visualizing their cellular internalization in real time. *Anal. Chem.* 92, 2103–2111. doi: 10.1021/acs.analchem.9b04608

Jiang, Z., Liu, G., and Li, J. (2020). Recent progress on the isolation and detection methods of exosomes. *Chem. Asian J.* 15, 3973–3982. doi: 10.1002/asia.202000873

Ju, Y., Bai, H., Ren, L., and Zhang, L. (2021). The role of exosome and the ESCRT pathway on enveloped virus infection. *Int. J. Mol. Sci.* 22:9060. doi: 10.3390/ijms22169060

Juan, T., and Furthauer, M. (2018). Biogenesis and function of ESCRT-dependent extracellular vesicles. *Semin. Cell Dev. Biol.* 74, 66–77. doi: 10.1016/j.semcdb.2017.08.022

Kalluri, R., and LeBleu, V. S. (2020). The biology, function, and biomedical applications of exosomes. *Science* 367:eaau6977. doi: 10.1126/science.aau6977

Laufman, O., Perrino, J., and Andino, R. (2019). Viral generated inter-organelle contacts redirect lipid flux for genome replication. *Cell* 178, 275–289.e16. doi: 10.1016/j.cell.2019.05.030

Lee, C. P., Liu, P. T., Kung, H. N., Su, M. T., Chua, H. H., Chang, Y. H., et al. (2012). The ESCRT machinery is recruited by the viral BFRF1 protein to the nucleus-associated membrane for the maturation of Epstein-Barr Virus. *PLoS Pathog.* 8:e1002904. doi: 10.1371/journal.ppat.1002904

Lobb, R. J., Becker, M., Wen, S. W., Wong, C. S., Wiegmans, A. P., Leimgruber, A., et al. (2015). Optimized exosome isolation protocol for cell culture supernatant and human plasma. *J. Extracell. Vesicles* 4:27031. doi: 10.3402/jev.v4.27031

Luo, Z., Dong, X., Li, Y., Zhang, Q., Kim, C., Song, Y., et al. (2014). PolyC-binding protein 1 interacts with 5'-untranslated region of enterovirus 71 RNA in membrane-associated complex to facilitate viral replication. *PLoS One* 9:e87491. doi: 10.1371/journal.pone.0087491

Luo, Z., Ge, M., Chen, J., Geng, Q., Tian, M., Qiao, Z., et al. (2017). HRS plays an important role for TLR7 signaling to orchestrate inflammation and innate immunity upon EV71 infection. *PLoS Pathog.* 13:e1006585. doi: 10.1371/journal.ppat.1006585

Mack, M., Kleinschmidt, A., Bruhl, H., Klier, C., Nelson, P. J., Cihak, J., et al. (2000). Transfer of the chemokine receptor CCR5 between cells by membrane-derived microparticles: a mechanism for cellular human immunodeficiency virus 1 infection. *Nat. Med.* 6, 769–775. doi: 10.1038/77498

Madison, M. N., and Okeoma, C. M. (2015). Exosomes: implications in HIV-1 Pathogenesis. *Viruses* 7, 4093–4118. doi: 10.3390/v7072810

Mao, L., Wu, J., Shen, L., Yang, J., Chen, J., and Xu, H. (2016). Enterovirus 71 transmission by exosomes establishes a productive infection in human neuroblastoma cells. *Virus Genes* 52, 189–194. doi: 10.1007/s11262-016-1292-3

Min, N., Sakthi Vale, P. D., Wong, A. A., Tan, N. W. H., Chong, C. Y., Chen, C. J., et al. (2018). Circulating Salivary miRNA hsa-miR-221 as clinically validated diagnostic marker for hand, foot, and mouth disease in pediatric patients. *EBioMedicine* 31, 299–306. doi: 10.1016/j.ebiom.2018.05.006

Pan, P., Li, G., Shen, M., Yu, Z., Ge, W., Lao, Z., et al. (2021). DENV NS1 and MMP-9 cooperate to induce vascular leakage by altering endothelial cell adhesion and tight junction. *PLoS Pathog.* 17:e1008603. doi: 10.1371/journal.ppat.1008603

Peters, J. J., Leitz, J., Oses-Prieto, J. A., Burlingame, A. L., and Brunger, A. T. (2021). Molecular characterization of AMPA-receptor-containing vesicles. *Front. Mol. Neurosci.* 14:754631. doi: 10.3389/fnmol.2021.754631

Pincetic, A., Medina, G., Carter, C., and Leis, J. (2008). Avian sarcoma virus and human immunodeficiency virus, type 1 use different subsets of ESCRT proteins to facilitate the budding process. *J. Biol. Chem.* 283, 29822–29830. doi: 10.1074/jbc.M804157200

Robbins, P. D., and Morelli, A. E. (2014). Regulation of immune responses by extracellular vesicles. *Nat. Rev. Immunol.* 14, 195–208. doi: 10.1038/nri3622

Robinson, S. M., Tsueng, G., Sin, J., Mangale, V., Rahawi, S., McIntyre, L. L., et al. (2014). Coxsackievirus B exits the host cell in shed microvesicles displaying autophagosomal markers. *PLoS Pathog.* 10:e1004045. doi: 10.1371/journal.ppat.1004045

Schorey, J. S., Cheng, Y., Singh, P. P., and Smith, V. L. (2015). Exosomes and other extracellular vesicles in host-pathogen interactions. *EMBO Rep.* 16, 24–43. doi: 10.15252/embr.201439363

Shao, H., Im, H., Castro, C. M., Breakefield, X., Weissleder, R., and Lee, H. (2018). New technologies for analysis of extracellular vesicles. *Chem. Rev.* 118, 1917–1950. doi: 10.1021/acs.chemrev.7b00534

Solomon, T., Lewthwaite, P., Perera, D., Cardosa, M. J., McMinn, P., and Ooi, M. H. (2010). Virology, epidemiology, pathogenesis, and control of enterovirus 71. *Lancet Infect. Dis.* 10, 778–790. doi: 10.1016/S1473-3099(10)70194-8

Su, Y. S., Hsieh, P. Y., Li, J. S., Pao, Y. H., Chen, C. J., and Hwang, L. H. (2020). The heat shock protein 70 family of chaperones regulates all phases of the enterovirus A71 life cycle. *Front. Microbiol.* 11:1656. doi: 10.3389/fmicb.2020.01656

Thery, C., Amigorena, S., Raposo, G., and Clayton, A. (2006). Isolation and characterization of exosomes from cell culture supernatants and biological fluids. *Curr. Protoc. Cell Biol.* 3:22. doi: 10.1002/0471143030.cb0322s30

Thery, C., Ostrowski, M., and Segura, E. (2009). Membrane vesicles as conveyors of immune responses. *Nat. Rev. Immunol.* 9, 581–593. doi: 10.1038/nri2567

Thery, C., Zitvogel, L., and Amigorena, S. (2002). Exosomes: composition, biogenesis and function. *Nat. Rev. Immunol.* 2, 569–579. doi: 10.1038/nri855

Too, I. H., Yeo, H., Sessions, O. M., Yan, B., Libau, E. A., Howe, J. L., et al. (2016). Enterovirus 71 infection of motor neuron-like NSC-34 cells undergoes a non-lytic exit pathway. *Sci. Rep.* 6:36983. doi: 10.1038/srep36983

van der Grein, S. G., Defourny, K. A. Y., Slot, E. F. J., and Nolte-'t Hoen, E. N. M. (2018). Intricate relationships between naked viruses and extracellular vesicles in the crosstalk between pathogen and host. *Semin. Immunopathol.* 40, 491–504. doi: 10.1007/s00281-018-0678-9

van Niel, G., D'Angelo, G., and Raposo, G. (2018). Shedding light on the cell biology of extracellular vesicles. *Nat. Rev. Mol. Cell Biol.* 19, 213–228. doi: 10.1038/nrm.2017.125

Vietri, M., Radulovic, M., and Stenmark, H. (2020). The many functions of ESCRTs. *Nat. Rev. Mol. Cell Biol.* 21, 25–42. doi: 10.1038/s41580-019-0177-4

Wernimont, A. K., and Weissenhorn, W. (2004). Crystal structure of subunit VPS25 of the endosomal trafficking complex ESCRT-II. *BMC Struct. Biol.* 4:10. doi: 10.1186/1472-6807-4-10

Wong, S. S., Yip, C. C., Lau, S. K., and Yuen, K. Y. (2010). Human enterovirus 71 and hand, foot and mouth disease. *Epidemiol. Infect.* 138, 1071–1089. doi: 10.1017/S0950268809991555

Xiao, X., Lei, X., Zhang, Z., Ma, Y., Qi, J., Wu, C., et al. (2017). Enterovirus 3A facilitates viral replication by promoting phosphatidylinositol 4-Kinase IIIbeta-ACBD3 interaction. *J. Virol.* 91:e791-17. doi: 10.1128/JVI.00791-17

Yao, Z., Qiao, Y., Li, X., Chen, J., Ding, J., Bai, L., et al. (2018). Exosomes exploit the virus entry machinery and pathway to transmit alpha interferon-induced antiviral activity. *J. Virol.* 92:e1578-18. doi: 10.1128/JVI.01578-18

Zhou, W., Woodson, M., Sherman, M. B., Neelakanta, G., and Sultana, H. (2019). Exosomes mediate Zika virus transmission through SMPD3 neutral Sphingomyelinase in cortical neurons. *Emerg. Microb. Infect.* 8, 307–326. doi: 10.1080/22221751.2019.1578188

frontiers | Frontiers in Microbiology

TYPE Opinion
PUBLISHED 05 October 2022
DOI 10.3389/fmicb.2022.1011891

OPEN ACCESS

EDITED BY
Chengming Wang,
Auburn University, United States

REVIEWED BY
Gerald Misinzo,
SACIDS Foundation for One Health, Sokoine University of Agriculture, Tanzania
Yongming Sang,
Tennessee State University , United States

*CORRESPONDENCE
Julian Ruiz-Saenz
julianruizsaenz@gmail.com;
julian.ruizs@campusucc.edu.co

SPECIALTY SECTION
This article was submitted to Virology, a section of the journal Frontiers in Microbiology

RECEIVED 04 August 2022
ACCEPTED 16 September 2022
PUBLISHED 05 October 2022

CITATION
Ruiz-Saenz J, Diaz A, Bonilla-Aldana DK, Rodríguez-Morales AJ, Martinez-Gutierrez M and Aguilar PV (2022) African swine fever virus: A re-emerging threat to the swine industry and food security in the Americas.
Front. Microbiol. 13:1011891.
doi: 10.3389/fmicb.2022.1011891

African swine fever virus: A re-emerging threat to the swine industry and food security in the Americas

Julian Ruiz-Saenz [1]*, Andres Diaz[2], D. Katterine Bonilla-Aldana[3], Alfonso J. Rodríguez-Morales[3,4], Marlen Martinez-Gutierrez[5] and Patricia V. Aguilar[6,7]

[1]Grupo de Investigación en Ciencias Animales—GRICA, Universidad Cooperativa de Colombia, Bucaramanga, Colombia, [2]PIC—Pig Improvement Company, Querétaro, Mexico, [3]Grupo de Investigación Biomedicina, Faculty of Medicine, Fundación Universitaria Autónoma de las Américas, Pereira, Colombia, [4]Faculty of Health Sciences, Universidad Cientifica del Sur, Lima, Peru, [5]Grupo de Investigación en Microbiología Veterinaria, Escuela de Microbiología, Universidad de Antioquia, Medellín, Colombia, [6]Department of Pathology, University of Texas Medical Branch, Galveston, TX, United States, [7]Center for Tropical Diseases, Institute for Human Infection and Immunity, University of Texas Medical Branch, Galveston, TX, United States

KEYWORDS

African swine fever, reservoirs, Arbovirus, emerging disease, pigs

Introduction

African swine fever (ASF) is a devastating disease for the swine industry, characterized by hemorrhagic fever with up to 100% mortality rate, and with a tremendous socioeconomic impact worldwide (Dixon et al., 2020). The disease was first reported in East Africa in the early 1920s as an acute hemorrhagic fever that caused the death of almost all infected domestic pigs (Montgomery, 1921; Plowright et al., 1969). Since then, the African swine fever virus (ASFV) has remained endemic in Africa affecting up to 35 African countries and has emerged in Europe, Asia, and now in the Americas.

Reemergence of ASFV

Since the reemergence of ASFV in Europe through the Caucasus region in 2007, the virus has rapidly expanded and reached the Russian Federation, East Europe, and Asia (Dixon et al., 2020). In 2018, the detection of ASFV in China, killing at least half of the swine population of China (Zhou et al., 2018), and subsequent dissemination to Southeast Asia; threat one of the most significant swine industries of the world, which contains half the world's swine population (Dixon et al., 2020; Gaudreault et al., 2020). The high socioeconomic impact of ASFV infection results from direct death and culling of the animals and loss of business in the swine production chain, costs of disease control, and international trade blocks (Zhou et al., 2018). In addition, large epidemics can result

in dramatic reductions in the size of national pig herds and inflation of prices of pig and pork products (Dixon et al., 2020; Gaudreault et al., 2020).

It is well-known that the highly virulent ASFV genotype II that emerged in the Caucasus region in 2007 is responsible for the contemporary European/Asiatic epidemic (Sánchez-Vizcaíno et al., 2013; Ge et al., 2018; Cwynar et al., 2019). The virus has spread to domestic pigs and wild boards across Eastern Europe and Asia (Gavier-Widén et al., 2015; Li et al., 2019). Multiple efforts are in place to avoid the dissemination of the ASFV throughout the European Union. However, the disease was first identified in Lithuania, Poland, Latvia, and Estonia in 2014 (de la Torre et al., 2015), and by 2019, it was in Belgium, Bulgaria, Slovakia, Estonia, Hungary, Latvia, Lithuania, Poland, and Romania. By the end of 2020, Germany reported their first case of ASF in domestic pigs (Sauter-Louis et al., 2021b). The current epidemiology of ASF in wild boars in East Europe plays a vital role in the risk of ASFV transmission to the domestic population (Sauter-Louis et al., 2021a; de la Torre et al., 2022).

In the Americas, ASFV emerged in late 1970s in Brazil, Cuba, and the Caribbean Island with a full eradication at early 1980s (De Paula Lyra et al., 1986). Nevertheless, ASFV re-emerged in the Americas in 2021. On 28 July 2021, the United States Department of Agriculture (USDA, 2021) confirmed the presence of ASFV in the Dominican Republic and it turned on the alarms for the swine industry in the Americas. According to the Department of Agriculture of the Dominican Republic, the virus has been detected in at least 22 out of the 31 provinces in the country (Agricultura, 2021). As stated by the World Organization of Animal Health (WOAH), the genotype II was detected in all positive samples (WOAH, 2021a,c).

On 20 September 2021, the Chief Veterinary Officer from Haiti reported a new case of ASF to the WOAH, becoming the second Country with ASFV positive samples in the Americas. The sample was collected from a backyard farm in a province bordering the Dominican Republic and was tested by the USDA Laboratories through a cooperative testing program. The report filed with the WOAH indicates the outbreak in Haiti began in late August and killed several swine (WOAH, 2021d) and by the end of October 2021, a total of seven outbreaks of ASF have been identified, affecting multiple provinces all over the country (WOAH, 2021b).

With a case fatality rate close to 87% in the Dominican Republic (WOAH, 2021a), lack of approved vaccines, the current ASF outbreaks highlight the devastating consequences for the swine industries (Busch et al., 2021). ASFV is now confirmed in at least 60 countries worldwide (in which ∼80% of the swine population resides). Furthermore, global ASF outbreaks have increased 25% since 2018 (Gaudreault et al., 2020), changing the swine industry's global dynamics.

ASFV is a complex, enveloped virus that contains a large (170–190-kb) double-stranded DNA (dsDNA) genome (Tulman et al., 2009). ASFV is the only known member of the *Asfarviridae* family (Alonso et al., 2018) and it is currently grouped into 24 genotypes, all of them being associated with disease (Achenbach et al., 2017). Although most of the genotypes have been linked to ASF outbreaks in various parts of sub-Saharan Africa, genotype I dominates in Central and West Africa (Minoungou et al., 2021; Njau et al., 2021). The first description of AFSV outside Africa, was reported in 1958 and again in 1961 from Lisbon Portugal with subsequent spread to other regions of Europe and Latin America of the genotype I (Mur et al., 2016). During the 1970s and 1980s, ASF become endemic in the Iberian Peninsula and many other countries were affected by sporadic ASFV outbreaks due to the introduction and use of food waste from international planes or boats to feed pigs. Strong and long-lasting efforts were put in different places to achieve eradication in most of Europe, for a comprehensive review see Danzetta et al. (2020).

Virulence is not fully associated with the viral genotype, and infection can lead to a broad spectrum of disease severity, from highly lethal to subclinical or asymptomatic, depending on host characteristics and the specific viral strain (Boinas et al., 2004). While a highly virulent ASFV has been widely reported in Eurasia (90–100% mortality in domestic pigs and European wild boar), reduced virulence strains and attenuated strains of the ASFV genotype II were found in Estonia and Latvia (Zani et al., 2018; Gallardo et al., 2019; Vilem et al., 2020) suggesting a threat for control programs due to the risk of pigs with chronic and carriers behaviors besides of the difficulty of early detection of ASF epizootics due to a lack of clear specific clinical signs of infection, as well as the presence of non-viremic animals (Gallardo et al., 2018).

Based on genotyping, whole genome sequencing and phylogenetic analysis, the ASFV that spread through Europe (Georgia 2007/1) has been proved to originate in South East Africa, but the exact location of the origin of this genotype includes Mozambique, Malawi, Zambia, southern Tanzania, and Madagascar (Quembo et al., 2018; Njau et al., 2021). However, the recently confirmation of the ASFV genotype II in Lagos, Nigeria (West Africa), complicates the already constrained control measures against the disease in the region (Adedeji et al., 2021) and emphasize the risk of worldwide dissemination of this highly pathogenic genotype II.

Vectors and host/reservoirs

ASFV can also be transmitted by soft ticks of the genus *Ornithodoros* in the family *Argasidae*, which act as biological vectors of ASFV (Pereira De Oliveira et al., 2019). To date, eight *Ornithodoros* taxa have been demonstrated as competent vectors of ASFV, including *O. marocanus, O. puertoricensis, O. coriaceus, O. moubata porcinus, O. erraticus, O. moubata complex, O. turicata , and O. savignyi* (Groocock et al., 1980; Mellor and Wilkinson, 1985; Hess et al., 1987; Endris et al., 1991, 1992; Kleiboeker et al., 1998; Rennie et al., 2000; Ribeiro et al., 2015; Golnar et al., 2019). Although *O. erraticus* ticks has been proven competent to replicate the ASFV genotype

II, it failed to transmit the Eurasian ASFV strains to naive pigs (Diaz et al., 2012; Pereira De Oliveira et al., 2019) under experimental conditions, suggesting that other determinants beyond viral replication also influence ASFV vector competence (Pereira De Oliveira et al., 2020b). However, recent analysis had shown successful infection of domestic pigs by ingesting *O. erraticus* ticks that fed on ASFV-infected pigs suggesting that *O. erraticus* may act as a reservoir of ASFV and suggesting new transmission routes of ASFV (Pereira De Oliveira et al., 2020a).

In the Americas, multiple *Ornithodoros* species could be considered potential vectors of ASFV. At least three *Ornithodoros* species found in the US are considered high-risk competent vectors (*O. coriaceus, O. turicata*, and *O. puertoricensis*). However, it remains unknown if other soft ticks in the Americas can also transmit ASFV (Golnar et al., 2019). Critical role of certain *Ornithodoros* species in the Americas and the Caribbean need to be clarified since *O. puertoricensis* could be an efficient vector for ASFV (Butler and Gibbs, 1984; Butler et al., 1985). Nevertheless, the presence of these ticks in Haiti and the Dominican Republic did not appear to complicate the eradication of AFV from these countries in 1978 possibly due to a lack of contact between infected pigs and *O. puertoricensis* (Kleiboeker and Scoles, 2001) or perhaps due to a low stadial transmission of ASFV in the *O. puertoricensis*, which was found to decrease from nearly 100% to less than 35% from the nymphal to adult stage (Endris et al., 1991) that reduced the risk of transmission. This low transmission could be due to the presence of endogenous viral elements of the ASFV, which might have been integrated into soft tick genomes and serve as templates for siRNA and piRNA thereby possibly protecting the tick against viral infection as has been recently reported for *O. moubata* and *O. porcinus* field-collected ticks from Africa (Forth et al., 2020).

In regard to competent hosts, at least three susceptible species of swine are present in the Americas: domestic pigs (*Sus scrofa domesticus*), the invasive feral boars (*Sus scrofa*) in wildlife, and common warthogs (*Phacochoerus africanus*) in different zoos (Golnar et al., 2019). ASFV is easily transmitted from persistently infected host/reservoirs to uninfected animals (de Carvalho Ferreira et al., 2013; Gallardo et al., 2015). Therefore, the possibility that wild fauna in the Americas can become persistently infected and spread the virus to susceptible animals urge to be considered (Brown and Bevins, 2018). In fact, a recent analysis of the risk of ASFV establishment and spillover in the United States has been reported. Based on feral swine distribution, soft ticks, and the inventory of domestic swine in the US this report indicates that certain areas of California, Florida, and much of the southwestern United States are high risk zones for ASFV establishment and spillover (Wormington et al., 2019).

Boar hunting and human movements across borders with contaminated fomites or meat represent the major risk for naive populations. Hence, the presence of the ASFV genotype II in the Dominican Republic and Haiti highlights the urgent need for better transnational discussion regarding but not limited to (1) preventive measurements; (2) appropriate disposal of swine products potentially contaminated with ASFV; (3) early detection of the virus if introduced into a naive country; (4) prompt and coordinated response of producers, local authorities, and governments; (5) education; and (6) communication between countries. This discussion should include not only governments and decision-makers, but also large, medium, and small-sized pork producers.

Prevention, control, and preparedness

Despite prevention and control efforts, ASF has led to an unprecedented crisis in the global pig sector representing a global risk to animal health and welfare, national and international economies, rural development, social/political behavior, national food security, and national and international markets (Gf-TADs, 2020). The Global Framework for the Progressive Control of Transboundary Animal Diseases (GF-TADs), funded by WOAH, and FAO has established a plan for preparation and early detection of a possible arrival of ASFV to the Americas (Komal, 2020). Once the virus was reported in China, countries of the Americas came together to discuss prevention and to establish preparedness plans. However, this was not enough to avoid the arrival and dissemination of the ASFV in the Dominican Republic and the subsequent transborder transmission to Haiti. The economic impact of ASFV in the pork industry of the Americas could be devastating. Five out of 15 of the major pork exporters of the world are in the Americas and the presence of ASF in a country will limit its trade capabilities of pork.

Given the current global situation and the detection of the virus in the Dominican Republic and Haiti, the swine industry recognizes a high risk of introducing ASFV into the continental part of the Americas (Figure 1). Hence, multiple preparedness efforts are being established in each country to avoid introducing and disseminating the disease. Responsible importation of supplies potentially contaminated with ASFV and appropriate downtime for hard-to-clean and disinfecting supplies is encouraged. Strict biosecurity practices and compliance at all swine production and management levels should be mandatory if producers want to keep the disease out of their system.

Since ASF is not a public health risk, people can regularly eat pork or pork-derived products. However, no pork or pork products should be transported from a country with ASF to another country. Additionally, no pork or pork products should be allowed into swine production facilities, given the risk of introduction through contaminated pork. ASFV DNA has been

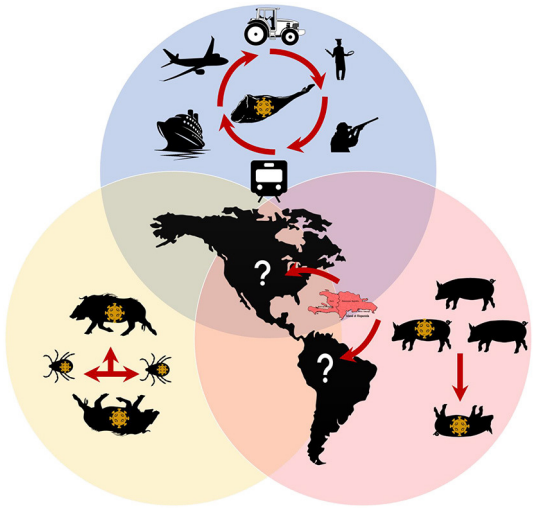

FIGURE 1
ASFV transmission known and gaps in the Americas. Red arrows represent potential routes for ASFV transmission. **Blue shape**: Human movement with contaminated fomites or contaminated pork represent the major risk for naive populations. **Yellow shape**: The potential role of wild Boars and *Ornithodoros* tick vectors still to be determined in the Americas. **Orange shape**: Virus transmission in pig farms has been confirmed in the Dominican Republic and Haiti. See text for references.

found in multiple pork products brought into South Korea and Taiwan by travelers (Kim et al., 2019; Wang et al., 2019), although no live virus has been isolated from such products. Furthermore, pigs should not be fed with food waste from restaurants or any kitchen. Clean and dirty areas must be clearly defined at feed mills, swine farms, and truck wash facilities (Li and Tian, 2018). There should be biosecurity protocols in place to avoid the contamination of feed or supplies for feed manufacturing. All supplies must be cleaned and disinfected before crossing into the clean area of swine facilities. Moreover, every swine production facility must have a response plan including management and disposal of mortality in case of an ASF outbreak.

Backyard production may possess different risks or perceptions regarding the disease than industrialized swine production. Hence, communication between authorities, producers, and local governments is key to reduce the risk of dissemination if the virus hits a given country. Active surveillance at different levels is required for early detection. Early detection of the virus is a crucial component minimize the impact of ASF introduction into a country. Unfortunately, in the Americas, PCR diagnosis can only be attempted until a suspect case is reported. Hence, if the clinical manifestation of the disease happens 2–3 weeks after the introduction into a farm, it might be too late to detect the virus (2–3 weeks after introduction into a commercial swine farm) and avoid dissemination within a region given the continuous flow and movement of pigs in the modern swine industry. Several European Union countries allow producers to monitor ASF status in the farms without needing to wait for clinical signs. It is also important to denote that recently based on expert perceived opinion, passive surveillance of wild boar and syndromic surveillance of pig mortality has been considered to be the most effective for controlling ASFV spread, whereas culling of all infected herds and movement bans for neighboring herds were considered as the most effective intervention strategies (Guinat et al., 2017).

As important measures, the USDA has recommended to the WOAH to establish the first foreign animal disease protection zone in United States, Puerto Rico, and the US Virgin Islands. Also, the Animal and Plant Health Inspection Service (APHIS) has suspended movement of live swine, swine germplasm, swine products, and swine byproducts from Puerto Rico and the US Virgin Island in an effort to keep ASF out of the US mainland. The establishment of an WOAH officially recognized protection zone would allow the US to maintain its ASF disease-free status, continue exporting pork and live swine, even if ASF is discovered within the protection zone (APHIS-USDA, 2021).

A new eradication of ASFV from the Haiti and the Dominican Republic can be achieved in spite we are facing a different epidemiological context. Previous eradication in the Americas showed that classical surveillance strategies, both at farm and slaughterhouse levels, conventional biosecurity and sanitary measures and well-structured collaboration among institutions in affected countries hand-in-hand to the international organizations (FAO and WOAH) is keystone for ASFV eradication (Danzetta et al., 2020). Countries should strengthen their surveillance systems based on previously known capabilities developed through the current "Continental Plan for the eradication of Classical Swine Fever (CSF) from the Americas," that has achieved a CSF free status in most of the American continent in a step-by-step process of management, control, and elimination of the disease in infected countries (Ganges et al., 2020; WOAH, 2021e). The continuous support from USDA and other high-income countries will be crucial for the ASFV contention and eradication in the Hispaniola Island, which could be more economically profitable than assuming the losses of a possible arrival of the ASFV to continental soil.

The current economic crisis in Latin American countries like Venezuela (Suárez et al., 2018) highlights a possible risk of ASF introduction into South America, given the high probability of pork importation products to Venezuela from ASFV-positive countries. In addition, the current COVID-19 pandemic seems to be negative for the control of the ASFV. Low-income countries in Africa have reported increasing ASF incidence in association with the coronavirus emerging disease, mainly due to the redistribution of resources and attention toward mitigating the COVID-19 pandemic (Uwishema et al., 2021). It is essential to consider the socio-political conditions

of the many nations of the Caribbean. The introduction of ASFV into Haiti and its dissemination throughout the country may increase the strong socio/economic disparities, and long-standing governance problems as well as ecological disturbance due to Natural disasters and uncontrolled COVID-19 infections (Oxford-Analytica, 2020; Hoffman, 2021). The same could apply for Cuba and other Caribbean nations in geographic proximity (Gorry, 2021); the close relationship, international trading and people movement between positive and naive nations could favor ASFV transmission.

The urgent need for a vaccine

Finally, no effective ASFV vaccine exists commercially. However, multiple vaccine developments are in progress due to the current situation of ASF worldwide (Bosch-Camós et al., 2020), Vaccine efficacy and vaccination strategies is a subject that needs to be taken into consideration to prevent a possible dissemination of ASFV in the Americas (Rivera-Benítez et al., 2021). Multiple vaccine development strategies have been employed, with varying levels of success (Gaudreault et al., 2020). The most promissory vaccine candidate has been achieved by deletion of the ASFV I177L gene (ASFV-G-ΔI177L) resulting in sterile immunity against the epidemic ASFV Genotype II (Borca et al., 2020). Besides, this attenuated ASFV strain has proven being effective to protect pig breeds against genotype II ASFV challenge (Tran et al., 2021) and completely protected against virulent ASFV challenge when it was administered by the oronasal route, even at large-scale experiments (Borca et al., 2021b; Tran et al., 2022). The stable adaptation of this live attenuated vaccine strain to cell culture (Borca et al., 2021a) and its oronasal distribution will allow to produce an ASF vaccine on a commercial scale and it possible use for wildlife. Moreover, an accompanying genetic test to discriminate between infected and vaccinated animals (DIVA) has been developed, and are a promising option to support the control and eradication of the ASFV genotype II during a potential vaccination program (Velazquez-Salinas et al., 2021).

Concluding remarks

Despite the multiple multilateral efforts to avoid ASFV emergence into the Americas, the virus has arrived and spread rapidly from one country to another. This situation highlights the need to establish local, regional, and transnational measures to avoid the spread of ASFV to other countries in the region (Kading et al., 2019). It is imperative to establish and follow national and international guidelines on preventive surveillance and diagnosis including enhancing communication among countries, strengthen vector surveillance, and increase public awareness of ASFV. Finally, we encourage to establish regional networks of cooperation, as has been implanted in the European Union (EFSA et al., 2021), that help to research/understand major gaps in knowledge in the Americas as much as to harmonize diagnostic techniques, share real-time surveillance data and help to avoid the possible dissemination of ASFV in the Region.

Author contributions

All authors listed have made a substantial, direct, and intellectual contribution to the work and approved it for publication.

Funding

This work was financially supported CONADI-UCC Grant to JR-S and by the Fogarty International Center and the National Institute of Allergy and Infectious Diseases, of the National Institutes of Health under Award Number D43 TW010331 to PA. The content is solely the responsibility of the authors and does not necessarily represent the official views of the National Institutes of Health.

Conflict of interest

Author AD is employed by Pig Improvement Company.

The remaining authors declare that the research was conducted in the absence of any commercial or financial relationships that could be construed as a potential conflict of interest.

Publisher's note

References

Achenbach, J., Gallardo, C., Nieto-Pelegrín, E., Rivera-Arroyo, B., Degefa-Negi, T., Arias, M., et al. (2017). Identification of a new genotype of African swine fever virus in domestic pigs from Ethiopia. *Transbound. Emerg. Dis.* 64, 1393–1404. doi: 10.1111/tbed.12511

Adedeji, A. J., Luka, P. D., Atai, R. B., Olubade, T. A., Hambolu, D. A., Ogunleye, M. A., et al. (2021). First-time presence of African swine fever virus genotype II in Nigeria. *Microbiol. Resour. Announc.* 10, e00350–e00321. doi: 10.1128/MRA.00350-21

Agricultura, M. D. (2021). "Boletin 2. ¡Juntos podemos vencer a la PPA!," in *Comisión Oficial Para El Control Y Erradicación De Brotes De La Peste Porcina Africana*, ed M.D.A. (República Dominicana: Ministerio de Agricultura).

Alonso, C., Borca, M., Dixon, L., Revilla, Y., Rodriguez, F., Escribano, J. M., et al. (2018). ICTV virus taxonomy profile: Asfarviridae. *J. Gen. Virol.* 99, 613–614. doi: 10.1099/jgv.0.001049

APHIS-USDA (2021). *USDA Submits Dossier to the World Organisation for Animal Health to Finalize African Swine Fever Protection Zone.* Program Updates, USDA, USA.

Boinas, F., Hutchings, G., Dixon, L., and Wilkinson, P. (2004). Characterization of pathogenic and non-pathogenic African swine fever virus isolates from *Ornithodoros erraticus* inhabiting pig premises in Portugal. *J. Gen. Virol.* 85, 2177–2187. doi: 10.1099/vir.0.80058-0

Borca, M. V., Rai, A., Ramirez-Medina, E., Silva, E., Velazquez-Salinas, L., Vuono, E., et al. (2021a). A cell culture-adapted vaccine virus against the current African swine fever virus pandemic strain. *J. Virol.* 95, e00123–e00121. doi: 10.1128/JVI.00123-21

Borca, M. V., Ramirez-Medina, E., Silva, E., Vuono, E., Rai, A., Pruitt, S., et al. (2020). Development of a highly effective African swine fever virus vaccine by deletion of the I177L gene results in sterile immunity against the current epidemic Eurasia strain. *J. Virol.* 94, e02017–e02019. doi: 10.1128/JVI.02017-19

Borca, M. V., Ramirez-Medina, E., Silva, E., Vuono, E., Rai, A., Pruitt, S., et al. (2021b). ASFV-G-ΔI177L as an effective oral nasal vaccine against the Eurasia strain of Africa swine fever. *Viruses* 13:765. doi: 10.3390/v13050765

Bosch-Camós, L., López, E., and Rodriguez, F. (2020). African swine fever vaccines: a promising work still in progress. *Porcine Health Manage.* 6, 1–14. doi: 10.1186/s40813-020-00154-2

Brown, V. R., and Bevins, S. N. (2018). A review of African swine fever and the potential for introduction into the United States and the possibility of subsequent establishment in feral swine and native ticks. *Front. Vet. Sci.* 5:11. doi: 10.3389/fvets.2018.00011

Busch, F., Haumont, C., Penrith, M.-L., Laddomada, A., Dietze, K., Globig, A., et al. (2021). Evidence-based African swine fever policies: do we address virus and host adequately? *Front. Vet. Sci.* 8:637487. doi: 10.3389/fvets.2021.637487

Butler, J., and Gibbs, E. (1984). Distribution of potential soft tick vectors of African swine fever in the Caribbean region (Acari: Argasidae). *Prev. Vet. Med.* 2, 63–70. doi: 10.1016/0167-5877(84)90049-7

Butler, J., Wilson, D., Garris, G., Koch, H., Crum, J., and Castellanos, V. (1985). Survey for potential soft tick (Acari: Argasidae) vectors of African swine fever on the island of Hispaniola. *Exp. Appl. Acarol.* 1, 63–72. doi: 10.1007/BF01262200

Cwynar, P., Stojkov, J., and Wlazlak, K. (2019). African swine fever status in Europe. *Viruses* 11:310. doi: 10.3390/v11040310

Danzetta, M. L., Marenzoni, M. L., Iannetti, S., Tizzani, P., Calistri, P., and Feliziani, F. (2020). African swine fever: lessons to learn from past eradication experiences. A systematic review. *Front. Vet. Sci.* 7:296. doi: 10.3389/fvets.2020.00296

de Carvalho Ferreira, H., Weesendorp, E., Quak, S., Stegeman, J., and Loeffen, W. (2013). Quantification of airborne African swine fever virus after experimental infection. *Vet. Microbiol.* 165, 243–251. doi: 10.1016/j.vetmic.2013.03.007

de la Torre, A., Bosch, J., Iglesias, I., Muñoz, M. J., Mur, L., Martínez-López, B., et al. (2015). Assessing the risk of African swine fever introduction into the European Union by wild boar. *Transbound. Emerg. Dis.* 62, 272–279. doi: 10.1111/tbed.12129

de la Torre, A., Bosch, J., Sánchez-Vizcaíno, J. M., Ito, S., Muñoz, C., Iglesias, I., et al. (2022). African swine fever survey in a European context. *Pathogens* 11:137. doi: 10.3390/pathogens11020137

De Paula Lyra, T., Saraiva, V., Hermida Lage, G., and Samarcos, M. (1986). Eradication of African swine fever from Brazil. *Rev. Sci. Tech. l'OIE (France)* 5, 771–787. doi: 10.20506/rst.5.3.261

Diaz, A. V., Netherton, C. L., Dixon, L. K., and Wilson, A. J. (2012). African swine fever virus strain Georgia 2007/1 in *Ornithodoros erraticus* ticks. *Emerg. Infect. Dis.* 18, 1026–1028. doi: 10.3201/eid1806.111728

Dixon, L. K., Stahl, K., Jori, F., Vial, L., and Pfeiffer, D. U. (2020). African swine fever epidemiology and control. *Annu. Rev. Anim. Biosci.* 8, 221–246. doi: 10.1146/annurev-animal-021419-083741

EFSA, European Food Safety Authority, Nielsen, S. S., Alvarez, J., Bicout, D. J., Calistri, P., Depner, K., et al. (2021). Research priorities to fill knowledge gaps in the control of African swine fever: possible transmission of African swine fever virus by vectors. *EFSA J.* 19:e06676. doi: 10.2903/j.efsa.2021.6676

Endris, R., Haslett, T., and Hess, W. (1991). Experimental transmission of African swine fever virus by the tick *Ornithodoros* (Alectorobius) *puertoricensis* (Acari: Argasidae). *J. Med. Entomol.* 28, 854–858. doi: 10.1093/jmedent/28.6.854

Endris, R., Hess, W., and Caiado, J. (1992). African swine fever virus infection in the Iberian soft tick, *Ornithodoros* (Pavlovskyella) *marocanus* (Acari: Argasidae). *J. Med. Entomol.* 29, 874–878. doi: 10.1093/jmedent/29.5.874

Forth, J. H., Forth, L. F., Lycett, S., Bell-Sakyi, L., Keil, G. M., Blome, S., et al. (2020). Identification of African swine fever virus-like elements in the soft tick genome provides insights into the virus' evolution. *BMC Biol.* 18:136. doi: 10.1186/s12915-020-00865-6

Gallardo, C., Nurmoja, I., Soler, A., Delicado, V., Simón, A., Martin, E., et al. (2018). Evolution in Europe of African swine fever genotype II viruses from highly to moderately virulent. *Vet. Microbiol.* 219, 70–79. doi: 10.1016/j.vetmic.2018.04.001

Gallardo, C., Soler, A., Nieto, R., Sánchez, M., Martins, C., Pelayo, V., et al. (2015). Experimental transmission of African swine fever (ASF) low virulent isolate NH/P68 by surviving pigs. *Transbound. Emerg. Dis.* 62, 612–622. doi: 10.1111/tbed.12431

Gallardo, C., Soler, A., Rodze, I., Nieto, R., Cano-Gómez, C., Fernandez-Pinero, J., et al. (2019). Attenuated and non-haemadsorbing (non-HAD) genotype II African swine fever virus (ASFV) isolated in Europe, Latvia 2017. *Transbound. Emerg. Dis.* 66, 1399–1404. doi: 10.1111/tbed.13132

Ganges, L., Crooke, H. R., Bohórquez, J. A., Postel, A., Sakoda, Y., Becher, P., et al. (2020). Classical swine fever virus: the past, present and future. *Virus Res.* 289:198151. doi: 10.1016/j.virusres.2020.198151

Gaudreault, N. N., Madden, D. W., Wilson, W. C., Trujillo, J. D., and Richt, J. A. (2020). African swine fever virus: an emerging DNA Arbovirus. *Front. Vet. Sci.* 7:215. doi: 10.3389/fvets.2020.00215

Gavier-Widén, D., Gortázar, C., Stahl, K., Neimanis, A. S., Rossi, S., Hard Av Segerstad, C., et al. (2015). African swine fever in wild boar in Europe: a notable challenge. *Vet. Rec.* 176, 199–200. doi: 10.1136/vr.h699

Ge, S., Li, J., Fan, X., Liu, F., Li, L., Wang, Q., et al. (2018). Molecular characterization of African swine fever virus, China, 2018. *Emerg. Infect. Dis.* 24, 2131–2133. doi: 10.3201/eid2411.181274

Gf-TADs (2020). *African Swine Fever: An Unprecedented Global Threat—A Challenge to Livelihoods, Food Security and Biodiversity. Call for Action*. Available online at: http://www.gf-tads.org/events/events-detail/fr/c/1152886/ (accessed 26 October, 2020).

Golnar, A. J., Martin, E., Wormington, J. D., Kading, R. C., Teel, P. D., Hamer, S. A., et al. (2019). Reviewing the potential vectors and hosts of African swine fever virus transmission in the United States. *Vector Borne Zoonotic Dis.* 19, 512–524. doi: 10.1089/vbz.2018.2387

Gorry, C. (2021). In Haiti, Cubans among first responders, again: Luis Orlando Oliveros-Serrano MD Coordinator, Cuban Medical Team in Haiti. *MEDICC Rev.* 24, 19–20. doi: 10.37757/MR2022.V24.N1.1

Groocock, C., Hess, W., and Gladney, W. (1980). Experimental transmission of African swine fever virus by *Ornithodoros coriaceus*, an argasid tick indigenous to the United States. *Am. J. Vet. Res.* 41, 591–594.

Guinat, C., Vergne, T., Jurado-Diaz, C., Sánchez-Vizcaíno, J. M., Dixon, L., and Pfeiffer, D. U. (2017). Effectiveness and practicality of control strategies for African swine fever: what do we really know? *Vet. Rec.* 180:97. doi: 10.1136/vr.103992

Hess, W. R., Endris, R. G., Haslett, T. M., Monahan, M. J., and Mccoy, J. P. (1987). Potential arthropod vectors of African swine fever virus in North America and the Caribbean basin. *Vet. Parasitol.* 26, 145–155. doi: 10.1016/0304-4017(87)90084-7

Hoffman, D. M. (2021). The Haitian orphanage crisis: exporting neoliberal family ideals in the debate on vulnerable childhoods in Haiti. *Child. Soc.* 35, 577–592. doi: 10.1111/chso.12442

Kading, R. C., Abworo, E. O., and Hamer, G. L. (2019). Rift valley fever virus, Japanese encephalitis virus, and African swine fever virus: three transboundary, vector-borne, veterinary biothreats with diverse surveillance, and response capacity needs. *Front. Vet. Sci.* 6:458. doi: 10.3389/fvets.2019.00458

Kim, H.-J., Lee, M.-J., Lee, S.-K., Kim, D.-Y., Seo, S.-J., Kang, H.-E., et al. (2019). African swine fever virus in pork brought into South Korea by travelers from China, August 2018. *Emerg. Infect. Dis.* 25, 1231–1233. doi: 10.3201/eid2506.181684

Kleiboeker, S. B., Burrage, T. G., Scoles, G. A., Fish, D., and Rock, D. L. (1998). African swine fever virus infection in the argasid host, *Ornithodoros porcinus* porcinus. *J. Virol.* 72, 1711–1724. doi: 10.1128/JVI.72.3.1711-1724.1998

Kleiboeker, S. B., and Scoles, G. A. (2001). Pathogenesis of African swine fever virus in *Ornithodoros* ticks. *Anim. Health Res. Rev.* 2, 121–128. doi: 10.1079/AHRR200133

Komal, J. (2020). Regional efforts in the Americas to prevent ASF introduction. African *Swine Fever Unprecedented Global Threat: A Global Challenge* to *Livelihoods*, *Food Security, and Biodiversity*. The Global Framework for the Progressive Control of Transboundary Animal Diseases (GF-TADs).

Li, L., Ren, Z., Wang, Q., Ge, S., Liu, Y., Liu, C., et al. (2019). Infection of African swine fever in wild boar, China, 2018. *Transbound. Emerg. Dis.* 66, 1395–1398. doi: 10.1111/tbed.13114

Li, X., and Tian, K. (2018). African swine fever in China. *Vet. Rec.* 183, 300–301. doi: 10.1136/vr.k3774

Mellor, P., and Wilkinson, P. (1985). Experimental transmission of African swine fever virus by *Ornithodoros savignyi* (Audouin). *Res. Vet. Sci.* 39, 353–361. doi: 10.1016/S0034-5288(18)31726-0

Minoungou, G. L., Diop, M., Dakouo, M., Ouattara, A. K., Settypalli, T. B. K., Lo, M. M., et al. (2021). Molecular characterization of African Swine fever viruses in Burkina Faso, Mali, and Senegal 1989–2016. *Transbound. Emerg. Dis.* 68, 2842–2852. doi: 10.1111/tbed.14240

Montgomery, R. E. (1921). On a form of swine fever occurring in British East Africa (Kenya Colony). *J. Comp. Pathol. Ther.* 34, 159–191. doi: 10.1016/S0368-1742(21)80031-4

Mur, L., Atzeni, M., Martínez-López, B., Feliziani, F., Rolesu, S., and Sanchez-Vizcaino, J. M. (2016). Thirty-five-year presence of African swine fever in Sardinia: history, evolution and risk factors for disease maintenance. *Transbound. Emerg. Dis.* 63, e165–e177. doi: 10.1111/tbed.12264

Njau, E. P., Domelevo Entfellner, J.-B., Machuka, E. M., Bochere, E. N., Cleaveland, S., Shirima, G. M., et al. (2021). The first genotype II African swine fever virus isolated in Africa provides insight into the current Eurasian pandemic. *Sci. Rep.* 11:13081. doi: 10.1038/s41598-021-92593-2

Oxford-Analytica (2020). *Pandemic to Worsen Recession and Instability in Haiti*. Haiti: Emerald Expert Briefings.

Pereira De Oliveira, R., Hutet, E., Duhayon, M., Guionnet, J.-M., Paboeuf, F., Vial, L., et al. (2020a). Successful infection of domestic pigs by ingestion of the European soft tick *O. Erraticus* that fed on African swine fever virus infected pig. *Viruses* 12:300. doi: 10.3390/v12030300

Pereira De Oliveira, R., Hutet, E., Lancelot, R., Paboeuf, F., Duhayon, M., Boinas, F., et al. (2020b). Differential vector competence of *Ornithodoros* soft ticks for African swine fever virus: what if it involves more than just crossing organic barriers in ticks? *Parasit. Vect.* 13:618. doi: 10.1186/s13071-020-04497-1

Pereira De Oliveira, R., Hutet, E., Paboeuf, F., Duhayon, M., Boinas, F., Perez De Leon, A., et al. (2019). Comparative vector competence of the Afrotropical soft tick *Ornithodoros moubata* and Palearctic species, *O. erraticus* and *O. verrucosus*, for African swine fever virus strains circulating in Eurasia. *PLoS ONE* 14:e0225657. doi: 10.1371/journal.pone.0225657

Plowright, W., Parker, J., and Peirce, M. (1969). African swine fever virus in ticks (*Ornithodoros moubata*, Murray) collected from animal burrows in Tanzania. *Nature* 221, 1071–1073. doi: 10.1038/2211071a0

Quembo, C. J., Jori, F., Vosloo, W., and Heath, L. (2018). Genetic characterization of African swine fever virus isolates from soft ticks at the wildlife/domestic interface in Mozambique and identification of a novel genotype. *Transbound. Emerg. Dis.* 65, 420–431. doi: 10.1111/tbed.12700

Rennie, L., Wilkinson, P., and Mellor, P. (2000). Effects of infection of the tick *Ornithodoros moubata* with African swine fever virus. *Med. Vet. Entomol.* 14, 355–360. doi: 10.1046/j.1365-2915.2000.00251.x

Ribeiro, R., Otte, J., Madeira, S., Hutchings, G. H., and Boinas, F. (2015). Experimental infection of *Ornithodoros erraticus* sensu stricto with two portuguese African swine fever virus strains. Study of factors involved in the dynamics of infection in ticks. *PLoS ONE* 10:e0137718. doi: 10.1371/journal.pone.0137718

Rivera-Benítez, J. F., De La Luz-Armendáriz, J., Gómez-Núñez, L., Vargas, F. D., Escatell, G. S., Ramírez-Medina, E., et al. (2021). Swine health: history, challenges and prospects. *Rev. Mex. Cienc. Pecu.* 12, 149–185. doi: 10.22319/rmcp.v12s3.5879

Sánchez-Vizcaíno, J. M., Mur, L., and Martínez-López, B. (2013). African swine fever (ASF): five years around Europe. *Vet. Microbiol.* 165, 45–50. doi: 10.1016/j.vetmic.2012.11.030

Sauter-Louis, C., Conraths, F. J., Probst, C., Blohm, U., Schulz, K., Sehl, J., et al. (2021a). African swine fever in wild boar in Europe—a review. *Viruses* 13:1717. doi: 10.3390/v13091717

Sauter-Louis, C., Forth, J. H., Probst, C., Staubach, C., Hlinak, A., Rudovsky, A., et al. (2021b). Joining the club: first detection of African swine fever in wild boar in Germany. *Transbound. Emerg. Dis.* 68, 1744–1752. doi: 10.22541/au.160253806.62312023/v1

Suárez, J., Carreño, L., Paniz-Mondolfi, A., and Canosa, F. J. M. (2018). Infectious diseases, social, economic and political crises, anthropogenic disasters and beyond: Venezuela 2019—implications for public health and travel medicine. *Rev. Panam. Enferm. Infecc.* 1, 73–93. doi: 10.13140/RG.2.2.13082.90562/1

Tran, X. H., Le, T. T. P., Nguyen, Q. H., Do, T. T., Nguyen, V. D., Gay, C. G., et al. (2021). African swine fever virus vaccine candidate ASFV-G-DeltaI177L efficiently protects European and native pig breeds against circulating Vietnamese field strain. *Transbound. Emerg. Dis.*69, e497–e504. doi: 10.1111/tbed.14329

Tran, X. H., Phuong, L. T. T., Huy, N. Q., Thuy, D. T., Nguyen, V. D., Quang, P. H., et al. (2022). Evaluation of the safety profile of the ASFV vaccine candidate ASFV-G-andDelta;I177L. *Viruses* 14:896. doi: 10.3390/v14050896

Tulman, E. R., Delhon, G. A., Ku, B. K., Rock, D. L. (2009). African swine fever virus. *Curr. Top. Microbiol. Immunol.* 328, 43–87. doi: 10.1007/978-3-540-68618-7_2

USDA (2021). *USDA Statement on Confirmation of African Swine Fever in the Dominican Republic*. USDOA Animal and Plant Health Inspection Service, USDA.

Uwishema, O., Chalhoub, E., Zahabioun, A., David, S. C., Khoury, C., Al-Saraireh, T. H., et al. (2021). The rising incidence of African swine fever during the COVID-19 pandemic in Africa: efforts, challenges and recommendations. *Int. J. Health Plann. Manage.* 37, 561–567. doi: 10.1002/hpm.3357

Velazquez-Salinas, L., Ramirez-Medina, E., Rai, A., Pruitt, S., Vuono, E. A., Espinoza, N., et al. (2021). Development real-time PCR assays to genetically differentiate vaccinated pigs from infected pigs with the Eurasian strain of African swine fever virus. *Front. Vet. Sci.* 8:768869. doi: 10.3389/fvets.2021.768869

Vilem, A., Nurmoja, I., Niine, T., Riit, T., Nieto, R., Viltrop, A., et al. (2020). Molecular characterization of African swine fever virus isolates in Estonia in 2014–2019. *Pathogens* 9:582. doi: 10.3390/pathogens9070582

Wang, W.-H., Lin, C.-Y., Chang Ishcol, M. R., Urbina, A. N., Assavalapsakul, W., Thitithanyanont, A., et al. (2019). Detection of African swine fever virus in pork products brought to Taiwan by travellers. *Emerg. Microb. Infect.* 8, 1000–1002. doi: 10.1080/22221751.2019.1636615

WOAH (2021a). *Follow-up Report 1. African Swine Fever Virus (Inf. with), Dominican (Rep.)—REPORT ID FUR_151044*. O. World Organization for Animal Health.

WOAH (2021b). *Follow-up Report 1. African Swine Fever Virus (Inf. with), Haiti—REPORT ID FUR_151855*. O. World Organization for Animal Health.

WOAH (2021c). *Immediate Notification. African Swine Fever Virus (Inf. with), Dominican (Rep.)—REPORT ID IN_150921*. O. World Organization for Animal Health.

WOAH (2021d). *Immediate Notification. African Swine Fever Virus (Inf. with), Haiti—REPORT ID IN_151732*. O. World Organization for Animal Health.

WOAH (2021e). *RESOLUTION No. 20. Recognition of the Classical Swine Fever Status of Members*. Oie: Paris, France.

Wormington, J. D., Golnar, A., Poh, K. C., Kading, R. C., Martin, E., Hamer, S. A., et al. (2019). Risk of African swine fever virus sylvatic establishment and spillover to domestic swine in the United States. *Vector Borne Zoonotic Dis.* 19, 506–511. doi: 10.1089/vbz.2018.2386

Zani, L., Forth, J. H., Forth, L., Nurmoja, I., Leidenberger, S., Henke, J., et al. (2018). Deletion at the 5'-end of Estonian ASFV strains associated with an attenuated phenotype. *Sci. Rep.* 8:6510. doi: 10.1038/s41598-018-24740-1

Zhou, X., Li, N., Luo, Y., Liu, Y., Miao, F., Chen, T., et al. (2018). Emergence of African swine fever in China, 2018. *Transbound. Emerg. Dis.* 65, 1482–1484. doi: 10.1111/tbed.12989

frontiers | Frontiers in Microbiology

TYPE Original Research
PUBLISHED 21 October 2022
DOI 10.3389/fmicb.2022.944679

OPEN ACCESS

EDITED BY
Lin Deng,
Kobe University, Japan

REVIEWED BY
Hongzhuan Wu,
Alabama State University, United States
Dongbo Sun,
Heilongjiang Bayi Agricultural University, China

*CORRESPONDENCE
Huansheng Wu
huanswu@jxau.edu.cn

†These authors have contributed equally to this work

SPECIALTY SECTION
This article was submitted to Virology, a section of the journal Frontiers in Microbiology

RECEIVED 15 May 2022
ACCEPTED 04 July 2022
PUBLISHED 21 October 2022

CITATION
Hu X, Ding Z, Li Y, Chen Z and Wu H (2022) Serum investigation of antibodies against porcine circovirus 4 Rep and Cap protein in Jiangxi Province, China.
Front. Microbiol. 13:944679.
doi: 10.3389/fmicb.2022.944679

Serum investigation of antibodies against porcine circovirus 4 Rep and Cap protein in Jiangxi Province, China

Xifeng Hu[1,2†], Zhen Ding[1,2†], Yu Li[1,2], Zheng Chen[1,2] and Huansheng Wu[1,2*]

[1]Department of Preventive Veterinary Medicine, College of Animal Science and Technology, Jiangxi Agricultural University, Nanchang, China, [2]Department of Veterinary Microbiology, Jiangxi Provincial Key Laboratory for Animal Science and Technology, College of Animal Science and Technology, Jiangxi Agricultural University, Nanchang, China

In 2019, a novel porcine circovirus 4 (PCV4) was first identified in Hunan Province, China. The circular PCV4 DNA was detected in both diseased and healthy pigs. Recently, PCV4 prevalence surveys have been analyzed in many provinces in both China and South Korea with low positive rates. However, no serological data has been conducted to investigate the prevalence of PCV4 in pigs from Jiangxi Province. To address this issue, an indirect anti-PCV4 antibody enzyme-linked immunosorbent assay (ELISA) based on Cap and Rep protein as a coating antigen was established and applied to study the serum epidemiology of PCV4 in Jiangxi Province. Purified PCV4-His-tagged Cap and Rep were used as the coating antigen to develop an ELISA detection kit. There was no cross-reaction of the Cap/Rep-based ELISA with antisera against PCV2, TGEV and PRRSV, indicating a high specificity of this ELISA assay. The intra-assay coefficient variations (CVs) of Cap-based were 1.239%–9.796%, Rep-based 1.288%–5.011%, and inter-assay CVs of 1.167%–4.694% and 1.621%–8.979%, respectively, indicating a good repeatability. Finally, a total number of 507 serum samples were collected from Jiangxi Province to test for antibody prevalence of PCV4, and 17 (3.35%) and 36 (7.10%) of the samples were Cap and Rep antibody positive, respectively. In summary, our established ELISA kit could be used to detect PCV4 antibodies in serum with good repeatability and high specificity. In addition, field samples detection results showed that the antibody of PCV4 was poorly distributed in intensive pig farms in Jiangxi Province, China.

KEYWORDS

porcine circovirus 4, ELISA, Cap protein, Rep protein, antibody, serum epidemiology

Introduction

Porcine circovirus (PCV) is a member of genus Circovirus that belongs to the Circoviridae family (Lefkowitz et al., 2018). The virion of PCV is a small, icosahedral and non-enveloped virus containing a single-stranded, closed-circular DNA (ssDNA) (Tischer et al., 1982; Reuter et al., 2014). The length of genome of PCVs is about

1.7–2.0 kb (Tischer et al., 1974). To date, four genotypes of PCVs, PCV1, PCV2, PCV3, and PCV4 have been identified and isolated (Zhang H. H. et al., 2020; Hou et al., 2022). PCV1 was first isolated in cultured porcine kidney (PK-15) cell lines without pathogens (Kim and Chae, 2002; Hirai et al., 2006). Unlike PCV1, PCV2 still poses a threat to the intensive swine industry because PCV2 is the main pathogenic virus causing porcine circovirus-related diseases (PCVAD) (Saporiti et al., 2020; Sibila et al., 2021). PCV3 has been identified in both diseased and healthy pigs (Jiang et al., 2019). In addition, PCV3 has been reported to be associated with porcine dermatitis and nephropathy syndrome (PDNS) (Jiang et al., 2019). From 2019 to 2021, PCV4 was identified as a distinct circovirus species and associated with severe clinical disease with respiratory PDNS via conventional PCR or qPCR in both China and South Korea with low positive rates (Franzo et al., 2020; Ha et al., 2021; Sun R. et al., 2021; Tian et al., 2021; Hou et al., 2022; Kim et al., 2022; Nguyen et al., 2022). Genetically, PCV4 shared the closest relationship and similarity to a mink circovirus with 67% genomic identity, which is higher than PCV1–PCV3 with 52% genomic identity (Zhang H. H. et al., 2020).

Similar to other PCVs, the genome of PCV4 is a 1,770 nt circular single-stranded DNA containing two large open reading frames (ORFs): ORF1 is 891 nt encoding the putative replicase protein (Rep); ORF2 is 687 nt encoding the putative capsid protein (Cap) (Kim et al., 2022). According to a previous report on PCV2, the Cap protein is an important viral affect involved in host cell entry (Cao et al., 2015). The Cap protein mediates the binding of the virus to the cell surface during the invasion process (Ren et al., 2016; Zhang Y. et al., 2020; Sun W. et al., 2021). The literature has shown that the Cap protein plays a crucial biological role in the process of entering host cells via binding to the receptors (Khayat et al., 2011). In addition, the Cap protein is an antigenic epitope that supports the formation of antibodies in the host, thereby stimulating the host to recognize invasive viruses (Kekarainen and Segales, 2015; Park et al., 2021). The Rep protein of PCVs is the major protein that replicates the viral genome and is included in mature virions. The Rep protein is highly expressed during the process of PCV replication, which could promote the production of specific antibodies in the infected host (Hu et al., 2019).

As we all know, a reliable, widely available and highly sensitive and specific serological test for PCV4 specific antibodies could be useful to assess the serological status of pigs, which will provide comprehensive information on the spread and transmission of PCV4. Recently, a variety of methods for the PCV4 Cap protein-based antibody test have been reported and further applied to detect the prevalence of Cap antibodies in Jiangsu Province, China (Lian et al., 2021). Antibody detection of Rep or Cap could help diagnose PCV infection or study the effect of PCV vaccines. Compared to whole virus-based antibody detection methods, purified recombinant protein was used as an envelope antigen to determine the indirect ELISA results to reduce cross-reactivity and improve the accuracy of detection (Lin et al., 2020; Lian et al., 2021). Therefore, both Cap and Rep proteins are one of the most important target proteins for engineered vaccines and detection technologies. In this study, the purified His-Cap or His-Rep proteins were selected as the coating antigens to develop an indirect ELISA to detect PCV4 antibodies. Furthermore, we evaluated the repeatability, sensitivity, and specificity of this indirect ELISA, which was further used to analyze PCV4 antibody levels in intensive pig farms in Jiangxi Province, China. In summary, our study attempted to develop a serological diagnostic method to detect PCV4 infection or to assess vaccine-induced antibody levels in future research.

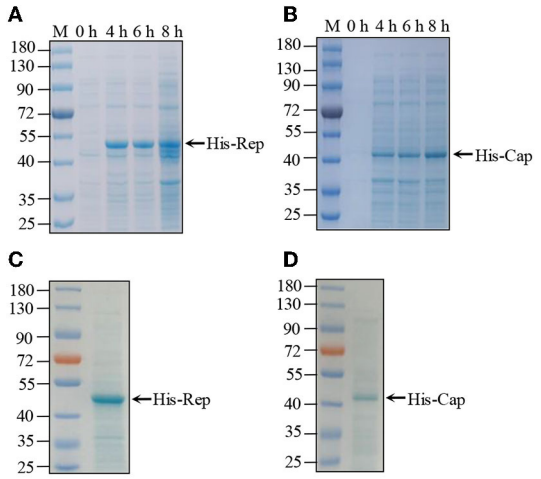

FIGURE 1
Purification of PCV4 Rep and Cap protein. **(A,B)** His-tagged recombinant protein expression and purification. pET-32a-Rep **(A)** and pET-32a-Cap **(B)** recombinant plasmid individually transferred into BL21pLyss *Escherichia coli* were induced expression by IPTG at different times. Induced protein samples were subjected to SDS–PAGE and Coomassie brilliant blue staining. **(C,D)** Subsequently, expressed His-tagged Rep **(C)** and Cap **(D)** recombinant proteins were purified by Ni-NT assay, which were further analyzed by SDS–PAGE and Coomassie brilliant blue staining.

Results

PCV4 Rep and Cap recombinant purification

The complete genome of PCV4 is 1,770 bp that contains two major ORFs, which encodes Rep (891 bp) and Cap (687 bp) proteins (Franzo et al., 2020). Both the Rep and Cap genes were amplified from wild boar samples,

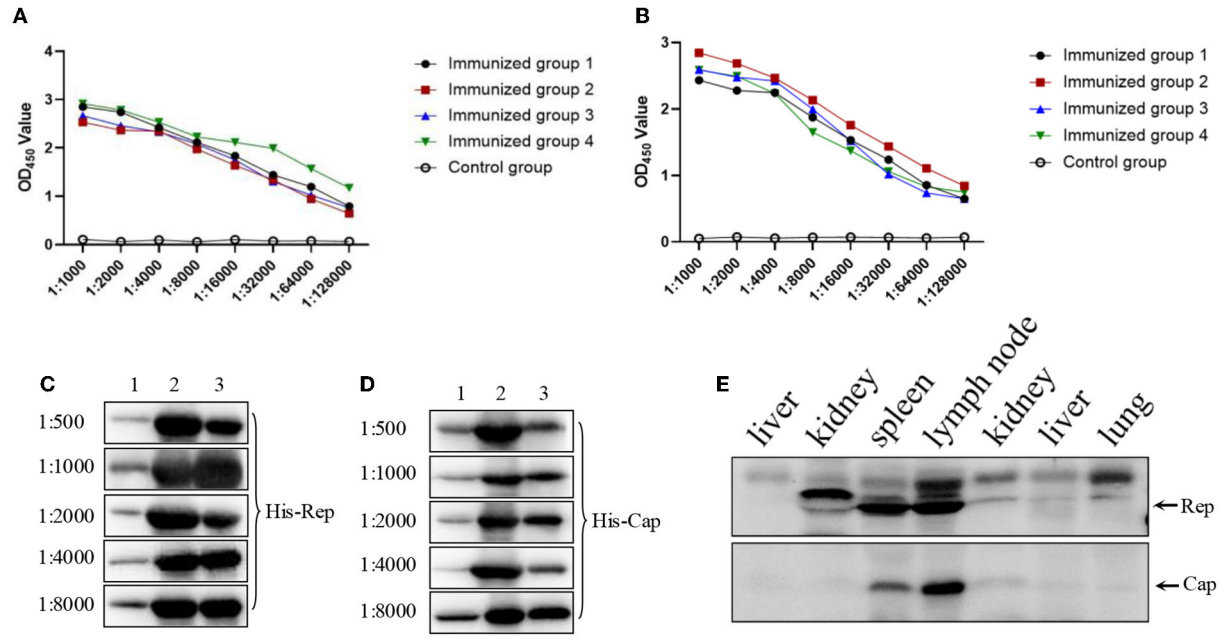

FIGURE 2
Immunogenicity examination of both Rep and Cap protein. **(A,B)** Four mice antibody titers against Rep **(A)** or Cap **(B)** after third round immunizations. The data were analyzed using Graphpad Prism software 5.0. OD_{450}: optical density 450 nm. **(C,D)** Different antibodies against Rep protein **(C)** or Cap protein **(D)** through 1:500 to 1:8,000 were used to react with indicated proteins. The three lanes were as follows: 1, protein expression before induced; 2, protein expression after induced; 3, proteins after purification. **(E)** Both Rep and Cap antibody (1:1,000) were used to detect the endogenous corresponding protein derived from wild boars' tissues including liver, kidney, spleen, lymph node, and lung.

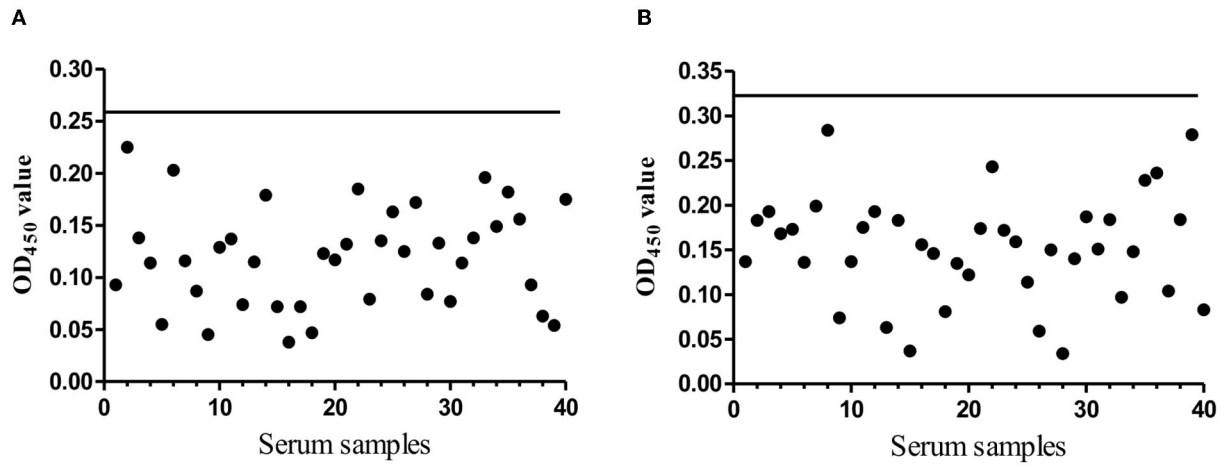

FIGURE 3
The cut-off value determination. **(A)** The evaluation of the cut-off OD_{450} value of the indirect Rep based ELISA. The black solid line presents the OD_{450} cut-off value (0.262). **(B)** The evaluation of the cut-off OD_{450} value of the indirect Cap based ELISA. The black solid line presents the OD_{450} cut-off value (0.327).

which were subsequently cloned into the pET32a vector for induced expression. Recombinant plasmids were transferred into BL21pLyss *Escherichia coli*. The expression of His-Rep and His-Cap proteins was induced expression in the control by IPTG at different times (4, 6, and 12 h). The results shown in Figures 1A,B revealed that both His-Rep and

His-Cap were successfully expressed at ∼50 and 43 kDa, respectively. Then both His-Rep and His-Cap proteins were further purified by the Ni-NTA method with no obvious non-specific protein determined by Coomassie brilliant blue staining (Figures 1C,D).

Immunogenicity examination of both Rep and Cap protein

Recombinant His-Cap and His-Rep proteins supplemented with Freund's complete adjuvant were injected individually into four different mice to produce antibodies against Cap and Rep proteins. After the third round of immunization, serums were collected for detection using the established indirect ELISA. Serum antibody titers of Rep and Cap proteins were up to 1:128,000 and 1:64,000, respectively (Figures 2A,B) and were significantly higher than that of control mice. Then the specific antibodies were used to detect the corresponding protein by western blotting with different dilutions. As shown in Figures 2C,D, we found that the 1:8,000 serum dilutions could still react with purified His-Rep and His-Cap proteins. In addition, the positive wild boar samples were additionally detected by Rep and Cap antibodies. We found that both the Rep and Cap antibodies could efficiently react with endogenous viral protein, indicating that the antibody produced could be used for western blotting (Figure 2E), and both Rep and Cap possess good immunogenicity.

Cut-off value determination of Rep and Cap based ELISA kit

An excellent ELISA kit should have an appropriate cut-off value to characterize the positive or negative sample. To address this issue, the 40 negative serum samples were used to determine the cut-off value. After three independent experiments, both the mean average value (χ) and the standard deviations (SDs) were determined. For Rep-based, ELISA was 0.121 and SD was 0.047. For Cap-based, ELISA was 0.153 and SD was 0.058. The OD_{450} cut-off value was calculated based on the formula $OD450 = \chi + 3SD$, suggesting that the OD_{450} value 0.262 of the samples was recoded as Rep antibody positive; the OD_{450} value 0.327 of the samples as Cap antibody positive was recorded. If not, the serum was considered negative (Figures 3A,B).

Repeatability of the ELISA kit

In general, an established indirect ELISA kit, such as the commercial ELISA kit, needs a well detectable repeatability. To assess this, we next performed the repeatability determination.

TABLE 1 Determination of Rep based ELISA coefficient of variation (CV) from eight serums (1–4: positive serum; 5–8: negative serum).

	Sample	χ	SD	CV%
Intra-assay	1	1.418	0.018	1.288
	2	0.995	0.014	1.388
	3	1.299	0.019	1.472
	4	1.309	0.026	1.980
	5	0.070	0.003	4.165
	6	0.052	0.003	4.997
	7	0.067	0.003	5.011
	8	0.082	0.002	2.899
Inter-assay	1	1.329	0.023	1.740
	2	1.731	0.028	1.621
	3	1.071	0.029	2.797
	4	1.520	0.028	1.861
	5	0.037	0.003	8.979
	6	0.059	0.005	8.711
	7	0.045	0.003	6.647
	8	0.052	0.003	6.257

TABLE 2 Determination of Cap based ELISA coefficient of variation (CV) from eight negative serums (1–4: positive serum; 5–8: negative serum).

	Sample	χ	SD	CV%
Intra-assay	1	1.809	0.022	1.239
	2	1.500	0.068	4.521
	3	1.166	0.029	2.530
	4	1.007	0.027	2.679
	5	0.069	0.007	9.796
	6	0.058	0.002	4.129
	7	0.059	0.004	6.357
	8	0.063	0.003	5.209
Inter-assay	1	1.145	0.054	4.694
	2	1.208	0.052	4.321
	3	1.448	0.024	1.647
	4	1.720	0.020	1.167
	5	0.199	0.004	1.859
	6	0.059	0.002	3.556
	7	0.124	0.005	3.863
	8	0.124	0.002	2.250

Eight negative serum samples were used to examine intra-assay and inter-assay repeatability. As shown in Table 1 (Rep), intra-assay coefficient of variations (CVs) were 1.288%−5.011%, and inter-assay CVs were 1.621%−8.979%. And, as showed in Table 2 (Cap), the intra-assay CVs were 1.239%−9.796%, and the inter-assay CVs were 1.167%−4.694%. Both CVs of the Rep and Cap based ELISA indicate that this indirect ELISA could

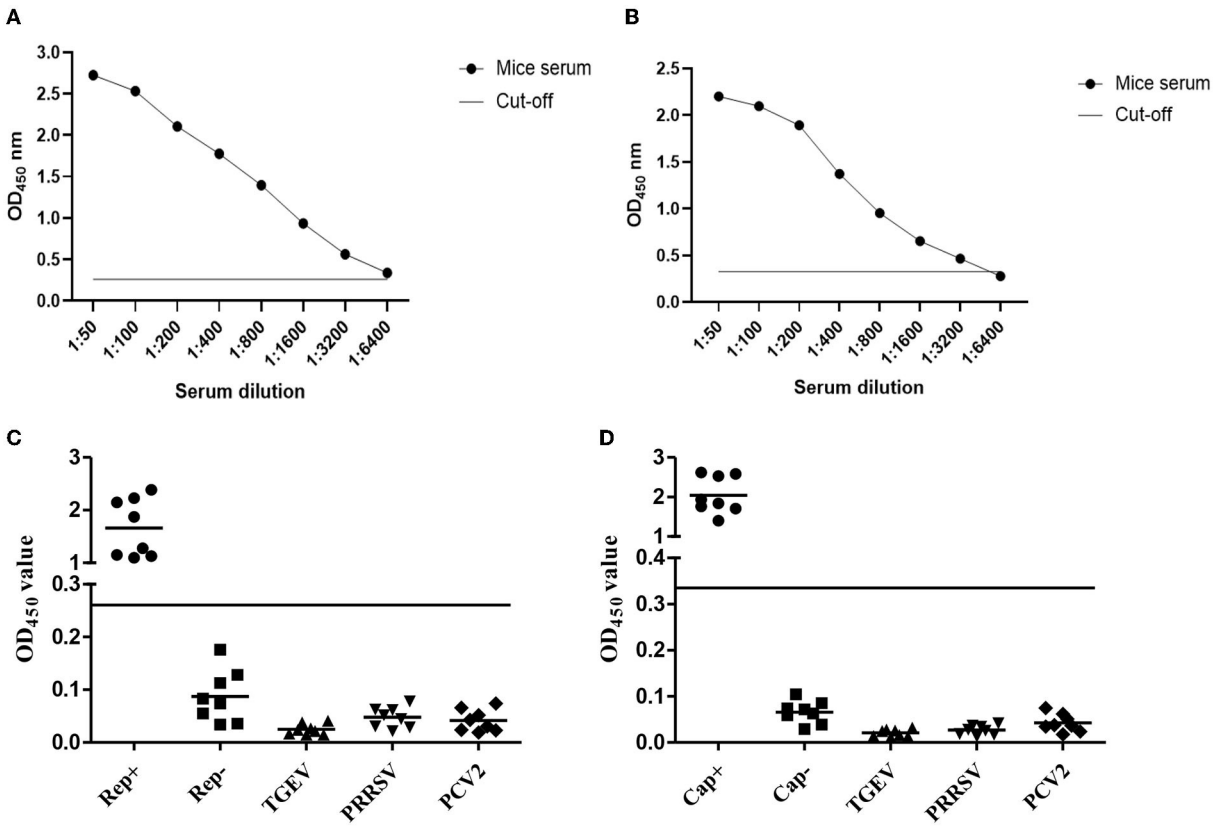

FIGURE 4
Sensitivity and specificity analyzing of the indirect ELISA. **(A,B)** Antibody against Rep protein **(A)** or against Cap protein **(B)** diluted from 1:50 to 1:6,400 was individually used to test the sensitivity of ELISA. **(C,D)** Eight indicated serum samples were used to analyze the specificity of Rep-based **(C)** and Cap-based **(D)** ELISA. The OD_{450} value higher than the value of black line was recorded as positive, if not, negative.

work very well with excellent repeatability, since CV% values of less than 10% were often recorded as good repeatability.

Sensitivity and specificity analyzing of the indirect ELISA

As we all know, a well-functioning, well-established indirect ELISA kit must be free of non-specific reactions as well as being highly sensitive. To determine the sensitivity of the Rep- or Cap-based ELISA method, the dilutions of Rep antibody from 1:50 to 1:6,400, of Cap antibody from 1:50 to 1:32,00 were used to determine the Rep- Detect protein or the Cap protein. The Rep OD_{450} value of 1:6,400 is 0.285 (Figure 4A) and the Cap OD_{450} value of 1:3,200 is 0.298 (Figure 4B). 1:3,200 serum dilutions are sensitive to Rep- or Cap-based ELISA detection. To address this problem of non-specific reactions, eight serum samples each positive for Rep or Cap, negative for Rep or Cap, TGEV, PRRSV, and PCV2 were used to analyze the specificity of this indirect ELISA. The results showed in Figures 4C,D suggest that indirect ELISA cannot cross-react with antisera to other pathogens or PCV4-negative serum samples.

Application of ELISA in testing antibodies in field samples

Finally, the ELISA kit should be used to detect the antibodies against PCV4 Rep and Cap protein in field samples. A total number of 507 field serum samples collected from intensive pig farms in Jiangxi Province were used to detect the antibodies. The results shown in Tables 3, 4 showed that 36 (7.10%) of the samples were positive for Rep antibody and 17 (3.35%) of the samples were positive for Cap antibody. Among the serum samples, 12 (11.76%) of the samples were positive for Rep antibody from JiAn, which was higher than those from other pig farms including Nanchang (7.92%), Shangrao (2.97%), Yichun (7.92%) and Ganzhou (4.90%), indicating that the rate of Rep antibodies was low in positive mice. The low Rep antibody positive rate was remarkably lower than the 43.97% positive rate reported in previous data. However, the low

TABLE 3 The Rep antibody detection results by the ELISA from 507 serum samples.

	Samples (*n*)	Positive (*n*)	Negative (*n*)	Positive rate (%)
NanChang	101	8	96	7.92
ShangRao	101	3	98	2.97
JiAn	102	12	90	11.76
YiChun	101	8	93	7.92
GanZhou	102	5	97	4.90
Total	507	36	471	7.10

TABLE 4 The Cap antibody detection results by the ELISA from 507 serum samples.

	Samples (*n*)	Positive (*n*)	Negative (*n*)	Positive rate (%)
NanChang	101	5	96	4.95
ShangRao	101	3	98	2.97
JiAn	102	1	101	0.98
YiChun	101	6	95	5.94
GanZhou	102	2	100	1.96
Total	507	17	490	3.35

Cap antibody positive rate in this study was almost equal to that in Jiangsu Province (3.44%). Thus, field serum samples detected by established Rep-based and Cap-based ELISA showed that both Rep and Cap antibodies were distributed at low rates in Jiangxi province. Nevertheless, our limited serum samples may not reflect the average antibody distribution in our country, necessitating extensive studies of PCV4 serum epidemiology.

Discussion

Recently, porcine circovirus 4 (PCV4) has been identified in several provinces in China, including Jiangsu, Henan, Hunan, Guangxi, Fujian, Anhui and Shanxi, and in South Korea (Lian et al., 2021). The total length of the PCV4 genome is 1,770 bp. Although a Taq-Man based qPCR assay could be used to detect PCV4 infection, there is no suitable method to detect PCV4 antibodies. In addition, there is no serological epidemiology of PCV4 in Jiangxi Province. Therefore, in this study, we developed an indirect ELISA method to analyze antibodies against PCV4 Rep and Cap protein because the ELISA assay is inexpensive, highly specific, and suitable for large-scale detection of serum samples. In addition, it was reported that the sensitivity of Rep-based ELISA was lower than that of Cap-based ELISA for PCV2 detection. And there is little identity of both Rep and Cap proteins between PCV4 and other PCVs, indicating that there may not be any cross-reactivity with other PCVs, consistent with our data in this study.

In this study, both the PCV4 Rep and Cap proteins were delivered to the prokaryotic expression system in *E. coli*. First, we obtained the full length Rep and Cap genes inserted into the expression vector. After induced expression by IPTG purified by Ni-NTA, SDS–PAGE results showed that the expression and purification of His-Rep and His-Cap proteins were as effective as expected. Furthermore, the enhanced immunogenicity after the third round showed that the specific antibodies produced by injected mice could efficiently react with His-Rep and His-Cap proteins but not with TGEV, PRRSV, and PCV2. An excellent ELISA kit must require well-functioning repeatability, high sensitivity, and high specificity. To clarify the characteristics of this ELISA assay, the repeatability evaluation showed that the value of both intra-assay and inter-assay was $<10\%$, suggesting that this Rep-based and Cap-based ELISA kit base with good repeatability worked (Mu et al., 2021).

Usually, the diagnosis of a viral infectious disease requires the detection of antigens (or viral nucleotides) or antibodies, both of which can help characterize the prevalence of pathogens (Han et al., 2021).

At present, there is no PCV4 vaccine application in China, leading to the urgent need to introduce ELISA to detect the antibody level of PCV4. In this study, a total number of 507 serum samples from intensive pig farms in Jiangxi Province were collected for field sample detection. The data showed that 7.10% (36/507) of the samples were PCV4 Rep positive and 3.35% (17/507) of the samples were PCV4 Cap positive, indicating a low prevalence of PCV4 in pigs. This low positive rate of both Rep and Cap antibodies of PCV4 was also found in Jiangsu Province. Still, according to a previous report, there was a high positive rate of 43.97% in 17 provinces in China. The high difference in the positive rate could be due to the different detection method used by different study farms, which needs further investigation. However, there were several limitations in this study. (1) Since the pathogenicity of PCV4 has not been clarified to date, the serum samples taken were not focalized, resulting in the low positive rate of PCV4 antibodies cannot reflect a threat of PCV4 infection; (2) In general, a new indirect ELISA-based detection kit needs to be validated by comparison with the same or a similar commercial ELISA kit. Although the primary application of this novel ELISA kit can potentially be used as a diagnostic test, further comparative analyses of this indirect ELISA still need to be performed. (3) A small number of serum samples from a limited area restricted the application of this novel ELISA kit, the low PCV4 positive rate in Jiangxi province did not reflect the positive rate in our country.

Therefore, large-scale serum antibody studies must continue to be performed.

Materials and methods

Serum samples collection

A total number of 507 pig serum samples were collected from different intensive pig farms located in Nanchang, Shangrao, JiAn, Yichun and Ganzhou in Jiangxi Province, China, between January 2021 and December 2021. The detailed information of serum samples showed in Tables 3, 4. The Committee on the Ethics of Animal Experiments of Jiangxi Agricultural University supervised the serum samples collection.

PCV4 Cap and Rep protein expression

In order to obtain the full-length Cap and Rep gene of PCV4, the complete genome of strain JXWY-2020 (MW988108) was first obtained. The Cap and Rep genes were then inserted into pET-32a-vector after digestion with XhoI and EcoRI and T4 ligation. Finally, the recombinant plasmid was transferred into competent *E. coli* BL21 pLyss cells. Subsequently, both His-Cap and His-Rep proteins were expressed under the control of 2.0 mM IPTG at 37 for 8 h. Expressed recombinant protein was further analyzed by SDS–PAGE and Coomassie brilliant blue staining. Finally, both recombinant proteins were purified through a Ni-NTA affinity chromatography column in non-denaturing state based on the Ni-NT purification kit instructions.

Immunogenicity determination

About 20–25 g, six-week-old BALB/c mice purchased from the Center for Experimental Animals of Jiangxi Traditional Medical University were kept under normal conditions in the animal care facility of Jiangxi Agricultural University. Both purified recombinant His-Cap and His-Rep protein (30 g/mouse) emulsified with Freund's complete adjuvant were injected individually into four different mice (one mouse was used as a negative control). After 1 week, and another 2 weeks later, these mice were immunized a second and third time individually with 30 and 200 g/mouse. After another week, we carried out the fourth immunization with injection of 100 g/mice accompanied by complete Freund's adjuvant. The immunized serum was collected from the caudate artery. Finally, the immunized mice were euthanized in a CO_2 chamber. The antibody of Cap and Rep was determined using the established ELISA in this study to assess antibody titer.

Indirect ELISA for analyzing both anti-Cap and anti-Rep antibodies

According to the guideline of the P/N value, the perfectly suitable conditions of the indirect ELISA have been optimized, such as blocking solution, sera, dose of coated antigen protein, concentrations of HRP-conjugated goat anti-pig IgG and its reaction time. After process optimization, we performed the following best reaction conditions: 1.25 mg/ml His-Rep and 2.5 mg/ml His-Cap were suitable for loading onto the plate. The coated plates were washed three times with PBST, then 100 μl of 1% bovine serum albumin (BSA) was added to each well and incubated at 37°C to block for 1.5 h for Cap protein; 100 μl of 5% milk was added to each well and incubated at 37°C for blocking for 2 h for Rep protein. Fifty liters of serum diluted 1:800 was added to react at 37°C for an additional hour. Finally 100 μl TMB substrate solution and 10 min incubation at room temperature stopped by loading 100 μl ELISA final solution buffer.

The cut-off value determination

To confirm the OD_{450} value, 40 negative serum was used to detect three times. For Rep protein: The standard deviation (SD) was 0.047 and the mean PR value (χ) was 0.121. The cut-off value of OD_{450} is in the conversion based on the following formula: OD_{450} value $= \chi + 3$ SDs $= 0.262$. Finally, the $OD_{450} \geq 0.262$ was recorded as a positive sample, if not, it was negative. For Cap protein: SDs was 0.058, χ was 0.153, and $OD_{450} \geq 0.327$ was recorded as a positive sample, if not, it was negative.

The examination of coefficient of variations

To further assess CVs, four positive and negative serum samples were used to assess both intra-assay and inter-assay variations of Rep and Cap proteins. The value of each sample was displayed as mean, standard deviation, and CVs. Intra-assay CVs were determined from the results of the quadruple detection using the same procedure. In addition, inter-assay CVs were calculated based on the result of four-time analysis on different days within the same assay.

Sensitivity and specificity analyzing of the indirect ELISA

To determine the sensitivity of the Rep- or Cap-based ELISA method, the dilutions of Rep antibody from 1:50 to 1:6,400, and of Cap antibody from 1:50 to 1:3,200, were used to determine the Rep-Detect protein or the Cap protein. The Rep OD_{450} of 1:6,400 is 0.285 and the Cap OD_{450} of 1:3,200 is 0.298, which is closest to the cut-off OD_{450}, indicating that the 1:6,400 or 1:3,200 dilutions of serum most sensitive are Rep or Cap based ELISA detection. In addition, to assess the specificity of the indirect ELISA, eight serum samples each against PCV2, PPRSV, TGEV, and negative serum against PCV4 Rep or Cap were used to assess its specificity within the same ELISA procedure with triplicate experiments and the OD_{450} value was used to characterize whether the sample was positive or negative.

Antibodies of field samples detection

A total number of 507 serum samples were collected from intensive pig farms in Nanchang, Shangrao, JiAn, Yichun and Ganzhou in Jiangxi Province, China. All the serum samples were detected according to the protocols in this indirect ELISA kit. The OD450 value $\geq$0.262 of serum samples was recorded as a positive sample of Rep antibody, if not, it was negative sample. The OD450 value $\geq$0.327 of serum samples was recorded as a positive sample of Cap antibody, if not, it was recorded as negative.

Data availability statement

The original contributions presented in the study are included in the article/supplementary material, further inquiries can be directed to the corresponding author.

Ethics statement

The animal study was reviewed and approved by the Committee on the Ethics of Animal Experiments of Jiangxi Agricultural University.

Author contributions

HW conceived and designed the experiments. XH, ZD, and YL performed the experiments and analyzed the data. HW, ZD, and ZC wrote, reviewed, revised, and edited the manuscript. All authors have read and agreed to the published version of the manuscript.

Funding

This work was supported by grants from the Natural Science Foundation of Jiangxi Province (20202BABL215023) and the Jiangxi Provincial Department of Education (GJJ190213).

Conflict of interest

The authors declare that the research was conducted in the absence of any commercial or financial relationships that could be construed as a potential conflict of interest.

Publisher's note

All claims expressed in this article are solely those of the authors and do not necessarily represent those of their affiliated organizations, or those of the publisher, the editors and the reviewers. Any product that may be evaluated in this article, or claim that may be made by its manufacturer, is not guaranteed or endorsed by the publisher.

References

Cao, J., Lin, C., Wang, H., Wang, L., Zhou, N., Jin, Y., et al. (2015). Circovirus transport proceeds *via* direct interaction of the cytoplasmic dynein IC1 subunit with the viral capsid protein. *J. Virol.* 89, 2777–2791. doi: 10.1128/JVI.03117-14

Franzo, G., Ruiz, A., Grassi, L., Sibila, M., Drigo, M., Segales, J., et al. (2020). Lack of porcine circovirus 4 genome detection in pig samples from Italy and Spain. *Pathogens* 9, 433. doi: 10.3390/pathogens9060433

Ha, Z., Yu, C., Xie, C., Wang, G., Zhang, Y., Hao, P., et al. (2021). Retrospective surveillance of porcine circovirus 4 in pigs in Inner Mongolia, China, from 2016 to 2018. *Arch. Virol.* 166, 1951–1959. doi: 10.1007/s00705-021-05088-w

Han, L., Yuan, G. F., Chen, S. J., Dai, F., Hou, L. S., Fan, J. H., et al. (2021). Porcine circovirus type 2 (PCV2) infection in Hebei Province from 2016 to 2019: a retrospective study. *Arch. Virol.* 166, 2159–2171. doi: 10.1007/s00705-021-05085-z

Hirai, T., Nunoya, T., Ihara, T., Saitoh, T., Shibuya, K., Nakamura, K., et al. (2006). Infectivity of porcine circovirus 1 andcircovirus 2 in primary porcine hepatocyte and kidney cell cultures. *J. Vet. Med. Sci.* 68, 179–182. doi: 10.1292/jvms.68.179

Hou, C. Y., Zhang, L. H., Zhang, Y. H., Cui, J. T., Zhao, L., Zheng, L. L., et al. (2022). Phylogenetic analysis of porcine circovirus 4 in Henan Province of China: a retrospective study from 2011 to 2021. *Transbound. Emerg. Dis.* 69, 1890–1901. doi: 10.1111/tbed.14172

Hu, Y., Cai, X., Zhan, Y., Yuan, X., Liu, T., Tan, L., et al. (2019). Truncated Rep protein of porcine circovirus 2 (PCV2) caused by a naturally occurring mutation reduced virus replication in PK15 cells. *BMC. Vet. Res.* 15, 248. doi: 10.1186/s12917-019-1984-8

Jiang, H., Wang, D., Wang, J., Zhu, S., She, R., Ren, X., et al. (2019). Induction of porcine dermatitis and nephropathy syndrome in piglets by infection with porcine circovirus type 3. *J. Virol.* 93, e02045-18. doi: 10.1128/JVI.02045-18

Kekarainen, T., and Segales, J. (2015). Porcine circovirus 2 immunology and viral evolution. *Porcine Health Manag.* 1, 17. doi: 10.1186/s40813-015-0012-z

Khayat, R., Brunn, N., Speir, J. A., Hardham, J. M., Ankenbauer, R. G., Schneemann, A., et al. (2011). The 2.3-angstrom structure of porcine circovirus 2. *J. Virol.* 85, 7856–7862. doi: 10.1128/JVI.00737-11

Kim, D. Y., Kim, H. R., Park, J. H., Kwon, N. Y., Kim, J. M., Kim, J. K., et al. (2022). Detection of a novel porcine circovirus 4 in Korean pig herds using a loop-mediated isothermal amplification assay. *J. Virol. Methods* 299, 114350. doi: 10.1016/j.jviromet.2021.114350

Kim, J., and Chae, C. (2002). Double in situ hybridization for simultaneous detection and differentiation of porcine circovirus 1 and 2 in pigs with postweaning multisystemic wasting syndrome. *Vet. J.* 164, 247–253. doi: 10.1053/tvjl.2001.0697

Lefkowitz, E. J., Dempsey, D. M., Hendrickson, R. C., Orton, R. J., Siddell, S. G., Smith, D. B., et al. (2018). Virus taxonomy: the database of the International Committee on Taxonomy of Viruses (ICTV). *Nucleic Acids Res.* 46, D708–D717. doi: 10.1093/nar/gkx932

Lian, Z., Liu, J., Liu, P., Zhu, Z., Yao, X., Yuan, L., et al. (2021). Development and application of an indirect ELISA for the detection of antibody to porcine circovirus 4 in pigs. *Transbound. Emerg. Dis.* 68, 2975–2979. doi: 10.1111/tbed.14267

Lin, C. N., Ke, N. J., and Chiou, M. T. (2020). Cross-sectional study on the sero- and viral dynamics of porcine circovirus type 2 in the field. *Vaccines* 8, 339. doi: 10.3390/vaccines8020339

Mu, Y., Jia, C., Zheng, X., Zhu, H., Zhang, X., Xu, H., et al. (2021). A nanobody-horseradish peroxidase fusion protein-based competitive ELISA for rapid detection of antibodies against porcine circovirus type 2. *J. Nanobiotechnol.* 19, 34. doi: 10.1186/s12951-021-00778-8

Nguyen, V. G., Do, H. Q., Huynh, T. M., Park, Y. H., Park, B. K., Chung, H. C., et al. (2022). Molecular-based detection, genetic characterization and phylogenetic analysis of porcine circovirus 4 from Korean domestic swine farms. *Transbound. Emerg. Dis.* 69, 538–548. doi: 10.1111/tbed.14017

Park, Y., Min, K., Kim, N. H., Kim, J. H., Park, M., Kang, H., et al. (2021). Porcine circovirus 2 capsid protein produced in *N. benthamiana* forms virus-like particles that elicit production of virus-neutralizing antibodies in guinea pigs. *N. Biotechnol.* 63, 29–36. doi: 10.1016/j.nbt.2021.02.005

Ren, L., Chen, X., and Ouyang, H. (2016). Interactions of porcinecircovirus 2 with its hosts. *Virus Genes* 52, 437–444. doi: 10.1007/s11262-016-1326-x

Reuter, G., Boros, A., Delwart, E., and Pankovics, P. (2014). Novel circular single-stranded DNA virus from turkey faeces. *Arch. Virol.* 159, 2161–2164. doi: 10.1007/s00705-014-2025-3

Saporiti, V., Huerta, E., Correa-Fiz, F., Grosse, L. B., Duran, O., Segales, J., et al. (2020). Detection and genotyping of porcine circovirus 2 (PCV-2) and detection of porcine circovirus 3 (PCV-3) in sera from fattening pigs of different European countries. *Transbound. Emerg. Dis.* 67, 2521–2531. doi: 10.1111/tbed.13596

Sibila, M., Rocco, C., Franzo, G., Huerta, E., Domingo, M., Nunez, J. I., et al. (2021). Genotyping of porcine circovirus 2 (PCV-2) in vaccinated pigs suffering from PCV-2-systemic disease between 2009 and 2020 in Spain. *Pathogens* 10, 1016. doi: 10.3390/pathogens10081016

Sun, R., Deng, Z., Han, X., Zhang, Y., Zhou, Y., Shan, Y., et al. (2021). Porcine circovirus 2 manipulates the PERK-ERO1alpha axis of the endoplasmic reticulum to favor its replication by derepressing viral DNA from HMGB1 sequestration within nuclei. *J. Virol.* 95, e100921. doi: 10.1128/JVI.01009-21

Sun, W., Du, Q., Han, Z., Bi, J., Lan, T., Wang, W., et al. (2021). Detection and genetic characterization of porcine circovirus 4 (PCV4) in Guangxi, China. *Gene* 773, 145384. doi: 10.1016/j.gene.2020.145384

Tian, R. B., Zhao, Y., Cui, J. T., Zheng, H. H., Xu, T., Hou, C. Y., et al. (2021). Molecular detection and phylogenetic analysis of porcine circovirus 4 in Henan and Shanxi Provinces of China. *Transbound. Emerg. Dis.* 68, 276–282. doi: 10.1111/tbed.13714

Tischer, I., Gelderblom, H., Vettermann, W., and Koch, M. A. (1982). A very small porcine virus with circular single-stranded DNA. *Nature* 295, 64–66. doi: 10.1038/295064a0

Tischer, I., Rasch, R., and Tochtermann, G. (1974). Characterization of papovavirus-and picornavirus-like particles in permanent pig kidney cell lines. *Zentralbl. Bakteriol. Orig. A* 226, 153–167.

Zhang, H. H., Hu, W. Q., Li, J. Y., Liu, T. N., Zhou, J. Y., Opriessnig, T., et al. (2020). Novel circovirus species identified in farmed pigs designated as porcine circovirus 4, Hunan province, China. *Transbound. Emerg. Dis.* 67, 1057–1061. doi: 10.1111/tbed.13446

Zhang, Y., Sun, R., Li, X., and Fang, W. (2020). Porcine circovirus 2 induction of ROS is responsible for mitophagy in PK-15 cells *via* activation of Drp1 phosphorylation. *Viruses* 12, 89. doi: 10.3390/v12030289

frontiers | Frontiers in Microbiology

TYPE Original Research
PUBLISHED 15 November 2022
DOI 10.3389/fmicb.2022.1046894

OPEN ACCESS

EDITED BY
Sha Li,
Jiangxi Agricultural University,
China

REVIEWED BY
Li Ang,
First Affiliated Hospital of Zhengzhou University, China
Jisen Huai,
Xinxiang Medical University,
China

*CORRESPONDENCE
Chuanxin Liu
15222003775@163.com
Jiajia Duan
jane4123@126.com

†These authors have contributed equally to this work and share first authorship

SPECIALTY SECTION
This article was submitted to Virology, a section of the journal Frontiers in Microbiology

RECEIVED 17 September 2022
ACCEPTED 28 October 2022
PUBLISHED 15 November 2022

CITATION
Duan J, Wang W, Jiang T, Bai X and Liu C (2022) Viral metagenomics combined with metabolomics reveals the role of gut viruses in mouse model of depression. *Front. Microbiol.* 13:1046894. doi: 10.3389/fmicb.2022.1046894

Viral metagenomics combined with metabolomics reveals the role of gut viruses in mouse model of depression

Jiajia Duan[1*†], Wei Wang[2†], Tao Jiang[1], Xiaoyang Bai[3] and Chuanxin Liu[4*]

[1]Department of Clinical Laboratory, The First Affiliated Hospital, College of Clinical Medicine of Henan University of Science and Technology, Luoyang, China, [2]Department of Neurology, The Affiliated Hospital of Guizhou Medical University, Guiyang, Guizhou, China, [3]Department of Medical Equipment, The First Affiliated Hospital, College of Clinical Medicine of Henan University of Science and Technology, Luoyang, China, [4]Endocrine and Metabolic Disease Center, Medical Key Laboratory of Hereditary Rare Diseases of Henan, Luoyang Sub-Center of National Clinical Research Center for Metabolic Diseases, The First Affiliated Hospital, and College of Clinical Medicine of Henan University of Science and Technology, Luoyang, China

Depression is a heterogeneous mental disorder that has been linked to disturbances in the gut microbiome. As an essential part of the gut microbiome, gut virome may play critical roles in disease progression and development. However, the relationship between the effect of gut virome on neurotransmitter metabolism and depression is unknown. We evaluated the alterations of gut virome and neurotransmitters in chronic restraint stress (CRS)-induced mouse model of depression based on viral metagenomics and LC–MS/MS metabolomics analyses. The results reveal that the gut virome profile of CRS group differed significantly from CON group. *Microviridae* was the most abundant differential viral family in both groups, followed by *Podoviridae*, while *Siphoviridae* was only enriched in CRS group of the top 100 differential viruses. The differential viruses that predicted to *Enterobacteriaceae* phage, *Gammaproteobacteria* phage and *Campylobacteraceae* phage were enriched in CRS group. Furthermore, 12 differential neurotransmitters primarily involved in the tryptophan metabolism pathway were altered in depressive-like mice. Besides, tryptamine and 5-methoxytryptamine hydrochloride were strongly associated with differential viruses belonging to *Podoviridae* and *Microviridae*. Our findings provide new insight into understanding the potential role of the gut virome and metabolites in depression.

KEYWORDS

gut viruses, viral metagenomics, neurotransmitters, depression, chronic restraint stress

Introduction

Depression is a common psychiatric disorder that imposes an enormous socio-economic loss worldwide. About half of the world's population suffers from depression at some point in time, with an average episode lasting about 6 months (Calliope Holingue, 2018). A prospective epidemiological study reported a lifetime prevalence of major depressive disorder as high as 30–40% (Moffitt et al., 2010). Moreover, depression has been linked to various chronic physical diseases, including cardiovascular diseases, obesity, diabetes, hypertension, cancer, cognitive impairment, chronic respiratory disease, and others (Gold et al., 2020). The most widely accepted pathogenesis of depression includes genetic, psychosocial, and biological factors. Biological factors include theories about monoamine neurotransmitters, neuroplasticity, neurogenesis, inflammation, and circadian rhythm (Peng et al., 2015; Mendoza, 2019). However, the exact biological mechanisms remain unknown.

Recently, multiple studies have shown that the pathogenesis and treatment of depression are inseparable from the gut microbiome (Valles-Colomer et al., 2019; Zheng et al., 2021). Gut microbiota can be influenced by the host's genetic makeup, diet, and environment. Gut bacteria can produce various neuroactive substances, including gamma-aminobutyric acid (GABA) and serotonin, which are involved in the development of various psychiatric disorders through the gut-brain axis (Dalile et al., 2019; Agirman et al., 2021). Furthermore, animal studies have shown that depressed phenotypes can be transferred to non-depressed animals through microbiome transplantation (Zheng et al., 2016; Zhang et al., 2019). As part of the gut microbiome, the potential roles of the gut virome, such as maintaining homeostasis and promoting disease progression, have also been investigated. Although the cause remains unknown, there are evidence for an association between the virome and human diseases, like SARS-CoV-2 infection, human immunodeficiency virus infection, inflammatory bowel disease, diabetes, obesity, and high blood pressure (Bai et al., 2022). Viruses, especially bacteriophages, are gradually gaining researchers' attention. A recent study confirmed that bacteriophage infection of a cytolysin-producing strain of *Enterococcus faecalis* reduced liver disease severity in patients with alcoholic hepatitis (Duan et al., 2019). However, little is known about the association between gut virome and depression. Researchers have previously characterized the signatures of gut bacteriophages using a cross-sectional whole-genome shotgun metagenomics analysis of fecal samples from major depressive disorder patients (Yang et al., 2020b). However, because metagenomics contains the genetic information of an entire microbial community, it is difficult to capture as much virus information as possible.

Viral metagenomics is a new field of study that combines the theory of metagenomics with the existing molecular biology virus detection technology. Viral metagenomic pipeline comprises sample collection, processing, sequencing, and bioinformatics analysis (Rose et al., 2016; Nooij et al., 2018; Cantalupo and Pipas, 2019; Santiago-Rodriguez and Hollister, 2020). The critical step of viral metagenomics is the enrichment of virus-like particles (VLPs) from samples containing a large number of microbial cells. Viral metagenomics provides a more comprehensive understanding of the alterations in virus composition and functions between the disease and the physiological state of the host. Given the high correlation between the gut microbiome and body metabolism, metabolomics has become a powerful tool for studying the impact of virome on host health and disease (Yadav et al., 2016; Yang et al., 2020b). To the best of our knowledge, no study has reported whether the gut virome can affect neurotransmitter metabolism associated with depressive-like behaviors. We developed a mouse model of depression using CRS in this study. We aimed to investigate the association between gut virome and neurotransmitters in a mouse model of depression by combining viral metagenomics and liquid chromatography tandem mass spectrometry (LC–MS/MS) metabolomics analysis. Our findings will provide new insights into the possible role of the gut virome in depression.

Methods and materials

Animal experiments

Male adult C57BL/6J mice aged 6–8 weeks were used in the present study. All mice were housed under relatively stable conditions with a 12 h light–dark cycle, 55 ± 5% humidity, a constant temperature of 23 ± 2°C, and allowed water and food *ad libitum*. The animals were randomly divided into two groups (random number table method). The mice in the control group were housed 3–4 per cage, while those in CRS group were housed individually. The body weights of mice were measured at the baseline and once a week during the experiment. All mice were purchased from Beijing Weitong Lihua Biotechnology Co., Ltd. All animal experiments complied with ethical regulations and were approved by the Animal Care Welfare Committee of the GuiZhou Medical University.

CRS group mice were subjected to the chronic restraint stress protocol for 21 days, 6 h per day. The mice were placed in a 50 ml centrifuge tube used as a restraint tube (the centrifuge tube was scalded in advance with air holes, evenly dispersed on the wall of the centrifuge tube, and there was a small hole in the middle of the lid to allow the mouse's tail to pass through). CRS group mice were deprived of water and food during restraint, while the mice in the control group were housed under relatively stable conditions.

Behavioral assays

Behavioral analyses were performed by individuals blinded to experimental conditions. The experiments were conducted in a soundproof room. The behavior of all animals was recorded and analyzed by SuperFst/Tst Video Tracking Software.

Sucrose preference test

The sucrose preference test includes an adaptation training phase and a testing phase. Mice were housed individually and habituated to water and 1% sucrose solution for 2 days during the adaptation training phase. The bottles were rotated daily to avoid positional preferences. Mice were then deprived of food and water for 12 h. In the testing phase, mice were exposed to two bottles containing 1% sucrose solution and tap water for 12 h in the dark. Two bottles were removed and weighed, the sucrose solution and water consumption were recorded, and the sucrose preference ratio was calculated.

Forced swimming test

The mice were placed in a transparent cylindrical container (pool, 30 cm in height and 15 cm in diameter) with a water depth of 15 cm and temperature of 24 ± 1°C. The time of swimming and immobility state of mice during the 5 min test phase was recorded, and the immobility ratio was calculated. Swimming behavior refers to the mice swimming on and around the pool level, whereas immobility behavior refers to mice having no other behaviors except an upward movement to avoid drowning.

Tail suspension test

The rear one-third of the mouse's tail was taped and hung from a special bracket. The mouse head was 15 cm away from the bottom surface, with a white background creating a stark contrast with the mouse fur. The struggling and immobility states of the mice were recorded and calculated after 5 min. Immobility was defined as the mice moving only their forelimbs and not their hind limbs.

Viral DNA extraction and sequencing

VLPs from fecal samples of mice were enriched and purified. Fecal samples were collected and grounded, and a pre-chilled Extraction Buffer (EB) was added. The precipitates were removed after vortexing and centrifugation. The supernatant was filtered through a 0.45 μm filter membrane to remove cells and fragments and added to Precipitation Buffer (PB). The supernatant was discarded after standing at 4°C for 2 h, and the precipitate was resuspended in 200 μl EB. The enzyme mix buffer, enzyme mix, and stop solution were sequentially added to the reaction mixture and incubated at 65–70°C for 10 min. After centrifuging at 2000 rpm for 5 min, 200 μl supernatant was stored at −20°C for use in subsequent experiments. Viral DNA and RNA were extracted with Magen R6662-02 MagPure Viral DNA/RNA Mini LQ Kit according to the manufacturer's instructions. Whole-genome amplification was performed using Qiagen 150,054 REPLI-g Cell WGA & WTA Kit (Qiagen, Dusseldorf, Germany). Qualified samples were used for library construction using NEB Next® Ultra II™ DNA Library Prep Kit for Illumina (NEB, USA). After quality inspection of the library with the Qubit® dsDNA HS Assay Kit (Life Technologies, USA) and the Agilent 4,200 TapeStation (Agilent, USA), the Illumina Novaseq 6,000 was used for sequencing with 150 bp paired-end mode.

Bioinformatics analysis of the virome

Trimmomatic (v0.36) was used to obtain high-quality data by removing low-quality raw data (Bolger et al., 2014). The clean reads were aligned with the Silva.132 database and the mouse database using the BWA software (Li and Durbin, 2009). The alignments with coverage below 80% of the sequence length were filtered out, and host genomic sequences were eliminated. The clean reads were then aligned with the Virus-NT database for the initial classification. Clean data were assembled using Megahit software (Li et al., 2016). Contigs from all samples were clustered using CDHIT.

The CheckV software (Nayfach et al., 2021) was used to predict the set of potential virus sequences within the assembled sequence. According to the alignment of virus contigs and the virus-NT database blast (v2.9.0+), the best hits with e < 1e-5 were selected for annotation to obtain functional information about the virus. A CRISPR-Cas spacer database was constructed from bacterial genomes in the Refseq database using the CRISPR Recognition Tool (CRT, http://www.room220.com/crt/). The contigs identified above were then aligned by blastn-short (v2.9.0+), satisfying e-value ≤1e-10, alignment similarity ≥95%, and spacer coverage of 80%. The best hit was chosen as possible host information for phage. Only a subset of viral contigs can predict possible hosts due to the limited number of known spacer sequences.

Neurotransmitters analysis by LC–MS/MS

After thawing and crushing the fecal samples, 0.05 g of the sample was mixed with 500 μl of 70% methanol/water. The sample was vortexed at 2500 r/min for 3 min and centrifuged at 12,000 r/min for 10 min at 4°C. About 300 μl of supernatant was transferred to a new centrifuge tube and refrigerated at −20°C for 30 min. The supernatant was then centrifuged at 12,000 r/min for 10 min at 4°C, and 200 μl of supernatant was separated for further LC–MS analysis.

The sample extracts were analyzed using an LC-ESI-MS/MS system (UPLC, ExionLC AD, https://sciex.com.cn/; MS, QTRAP® 6,500+ System, https://sciex.com). The analytical conditions were as follows:

HPLC column, Waters ACQUITY UPLC HSS T3 C18 (100 × 2.1 mm i.d., 1.8 μm); solvent system, water with 0.1% formic acid (A), acetonitrile with 0.1% formic acid (B); the gradient was initiated at 5% B (0 min), increased to 95% B (0–8 min), 95% B (8–9.5 min), and then decreased to 5% B (9.6–12 min); flow rate: 0.35 ml/min; temperature: 40°C; injection volume: 2 μl.

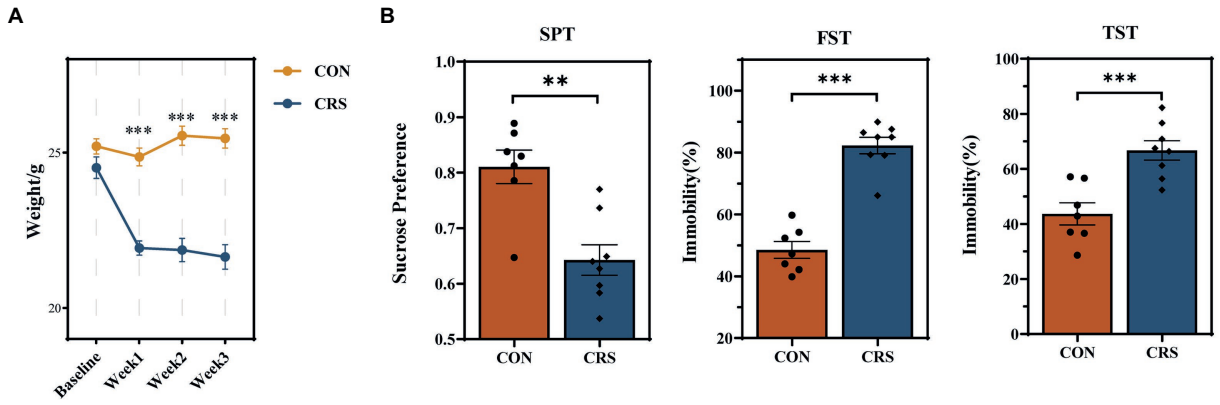

FIGURE 1
Behavioral results and body weight changes in mice during the experiment. **(A)** Weight changes per week from baseline to end of the study. **(B)** Behavioral results of sucrose preference test (SPT), forced swimming test (FST), and tail suspension test (TST). The data are represented as the mean±standard errors of the means (SEM). $^{**}p<0.01$, $^{***}p<0.001$.

AB 6500+ QTRAP® LC–MS/MS System, equipped with an ESI Turbo Ion-Spray interface, operating in positive and negative ion modes, and controlled by Analyst 1.6 software (AB Sciex). The ESI source operation parameters were as follows: an ion source, turbo spray, source temperature 550°C, ion spray voltage (IS) 5,500 V (Positive), −4,500 V (Negative); curtain gas (CUR) was set to 35.0 psi; and DP and CE were further optimized for individual MRM transitions. A specific set of MRM transitions was monitored for each period according to the neurotransmitters eluted during this period.

Statistical analysis

All statistical analyses were performed using R (v3.5.1) and SPSS 26.0. Alpha and beta diversity analysis was performed using the phyloseq package. Beta diversity was analyzed using principal coordinate analysis (PCoA) with Bray-Curtis distance, and the statistical significance of the clustering pattern in ordination plots was evaluated using permutational ANOVA (PERMANOVA). Data from behavioral results and body weight were compared using Student's t-test, while the virome and metabolites data were compared using Wilcoxon rank-sum test. Correlation between relative abundances of differential viruses and between differential viruses and metabolites was determined by spearman correlation analysis. GraphPad Prism 9.3.1, Origin 9.8.0, and Cytoscape 3.8.0 were used for graphing.

Results

CRS-induced depression-like behaviors in mice

In the present study, mice were exposed to CRS for 21 days to induce depression-like behaviors. The depression-like behaviors in mice were evaluated by the sucrose preference test (SPT), forced swimming test (FST), and tail suspension test (TST). The baseline and weekly body weights of mice were measured during the experiment. The body weights of mice in CRS group (N = 8) were considerably lower than those in CON group (N = 7) after 3 weeks of stress ($p < 0.001$, Figure 1A). SPT, TST, and FST were examined at baseline in both groups of mice and no difference between the two groups was observed (Supplementary Table S1). Significant reduction in sucrose consumption in SPT (CON: 0.811 ± 0.030 [mean ± SEM]; CRS: 0.643 ± 0.027 [mean ± SEM]; $p = 0.001$), increase in immobility ratio in FST (CON: 48.487 ± 2.718 [mean ± SEM]; CRS: 82.289 ± 2.672 [mean ± SEM]; $p < 0.001$) and increase in immobility ratio in TST (CON: 43.671 ± 4.028[mean ± SEM]; CRS: 66.709 ± 3.535 [mean ± SEM]; $p < 0.001$) were observed in CRS group compared to the control group (Figure 1B). These results indicated that CRS had induced depression-like behaviors in mice.

Diversity and composition of the virome community between CON and CRS groups

DNA virome in the feces of CRS and CON groups was analyzed. Alpha diversity was analyzed to assess differences in subject-to-subject diversity. The alpha-diversity analysis showed no significant difference in gut virome composition of the two groups (ACE index, $p = 0.536$; Shannon index, $p = 0.694$; Simpson index, $p = 0.121$; Chao1 index, $p = 0.536$; Figure 2A). Meanwhile, Beta diversity was analyzed to measure group-to-group diversity. β-diversity analysis based on PCoA with Bray-Curtis distance showed significant differences between the two groups ($R^2 = 0.132$, $p = 0.025$, PERMANOVA; Figure 2B).

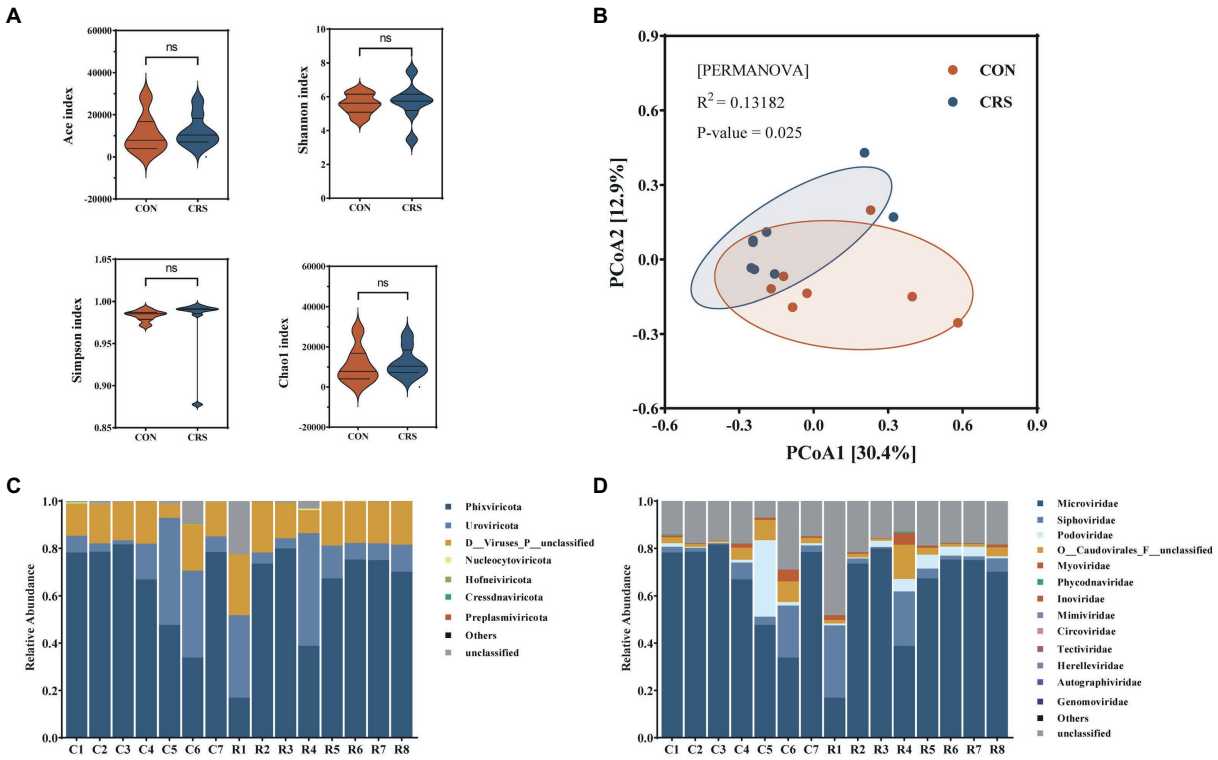

FIGURE 2
Comparison of viral community diversity and composition at contigs level between the two groups. **(A)** Alpha-diversity presented by Ace, Shannon, Simpson, and Chao1 index. No significant differences were detected. **(B)** Beta diversity visualized using a PCoA plot with Bray–Curtis dissimilarity distances. Compositions of the viral communities at the phylum level **(C)** and family level **(D)**.

We identified and taxonomically annotated the viral sequences to clarify the virome characteristics between the two groups. From all samples, 84,108 contigs were obtained. Among them, phage and non-phage viruses accounted for 89.48 and 10.52%, respectively, and the predominant viral genome type is dsDNA (87.64%) (Supplementary Figure S1A). Viral community compositions at the phylum and family levels are shown in Figures 2C,D, and Supplementary Figure S1B. The five most prevalent virome phyla detected in all samples were *Phixviricota*, *Uroviricota*, *Nucleocytoviricota*, *Hofneiviricota*, and *Cressdnaviricota* (Figure 2C). The top 10 virome families were *Microviridae*, *Siphoviridae*, *Podoviridae*, *O__Caudovirales_F__unclassified*, *Myoviridae*, *Phycodnaviridae*, *Inoviridae*, *Mimiviridae*, *Circoviridae*, *Tectiviridae* (Figure 2D). We performed gene set functional enrichment in all samples using KEGG pathway analysis. Genetic information processing was the predominant enrichment pathway in KEGG level 2 and DNA replication proteins in KEGG level 3 (Supplementary Figures S2A,B).

The differential profile and relationship of the virome between two groups

We compared the virome composition at the contigs level to gain a deeper understanding of the differential virome profile between CON and CRS groups. A total of 5,006 contigs were differentially enriched in the two groups. We have analyzed the top 100 viral contigs with the highest relative abundance (Figure 3A). Among the top 100 contigs, 95% (95/100) were enriched in CRS group. *Microviridae* was the most abundant differential family, followed by *Podoviridae* in CON and CRS groups. However, *Siphoviridae* was only enriched in CRS group. Figure 3B shows the comparison of the relative abundance of 20 contigs that were successfully annotated to the family level of the virome and predicted to the possible bacterial hosts between CON and CRS groups. The contigs predicted to be the phages of *Enterobacteriaceae*, *Gammaproteobacteria*, and *Campylobacteraceae* were enriched in CRS group. Furthermore, two contigs, including *Clostridia* and *Proteobacteria* phages, were enriched or partially enriched in CON group. Co-expression network of the differential virome was constructed to determine the relationship within the differential virome ($|r|>0.6$, $p<0.01$; Figure 3C). We discovered that members of *Microviridae* had a strong relationship within the cluster, with the majority exhibiting a positive correlation. R2|contig_16633 served as the link between *Microviridae* cluster and *Siphoviridae*, *Myociridae*, *Podoviridae*, and other unclassified viral clusters. The viruses belonging to *Podoviridae* showed a weak correlation with each other. Notably, C7|contig_43448, *Podoviridae* member with a negative correlation with *Microviridae* cluster.

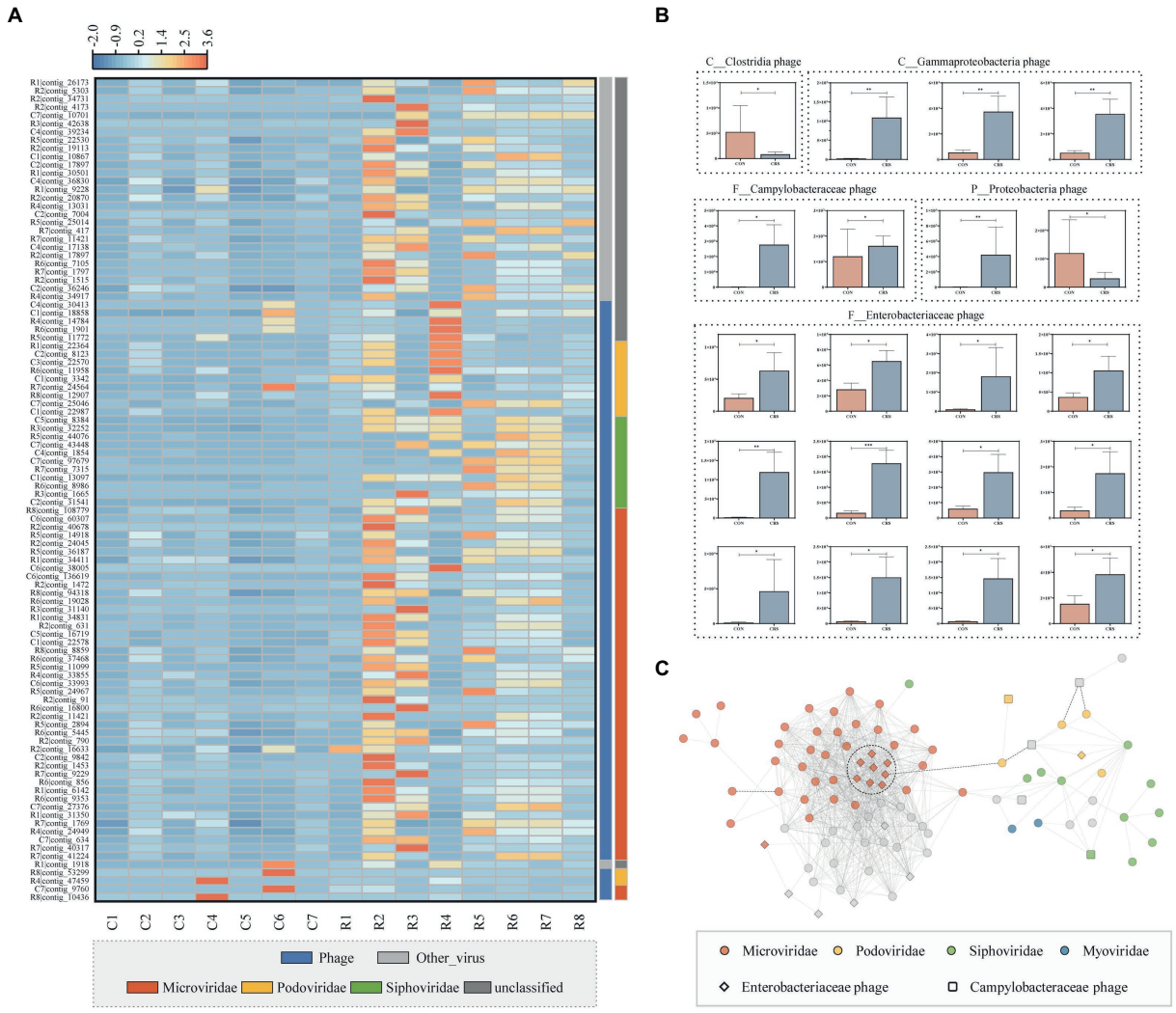

FIGURE 3
Differential viral profile and the correlations between the differential virus contigs of the two groups. **(A)** Heatmap of the differential virus contigs (the top 100 of relative abundance); the color scale bar shows z-score values after z-score row normalization. **(B)** Bar plot of 20 differential viral contigs, of which the potential bacterial hosts were predicted. The data are represented as the mean±standard errors of the means (SEM). *p<0.05, **p<0.01, ***p<0.001. **(C)** The differential virome co-expression network with Spearman's rank correlation coefficient (|r|>0.6, p<0.01). Dots with different colors indicate different families.

Disturbances of fecal metabolic signatures between CON and CRS groups

LC–MS/MS was used to assess the metabolic profiles of CON and CRS fecal samples. A total of 55 neurotransmitter metabolites were identified in the present study. Metabolites with missing values greater than 60% per group were eliminated after data processing, leaving 46 neurotransmitter metabolites for further analysis. Principal component analysis (PCA) was performed to reduce dimension and identify specific metabolic features that drive group separation. One outlier sample was removed for further analysis. PCA score plot showed a significant distinction between the two groups (Figure 4A). A volcano plot with Fold change (FC)>1.5 and value of p <0.05 was applied to identify the specific metabolites differences between the two groups (Figure 4B). The two groups differed in 12 metabolites. The CON-enriched metabolites included tryptamine and 3-hydroxyanthranilic acid. Meanwhile, CRS-enriched metabolites included methionine, phenylalanine, tyrosine, leucine, serine, choline, 3-phenylpyruvic acid, aspartic acid, arginine, and 5-methoxytryptamine hydrochloride. Furthermore, all signatures of 46 neurotransmitter metabolites between the two groups are shown in Figure 4C. Quantitative enrichment analysis (QEA) of differential metabolites was performed using MetaboAnalyst 5.0. Three of differential metabolites were mainly involved in tryptophan metabolism (5-methoxytryptamine hydrochloride, tryptamine, and 3-hydroxyanthranilic acid), and six were involved

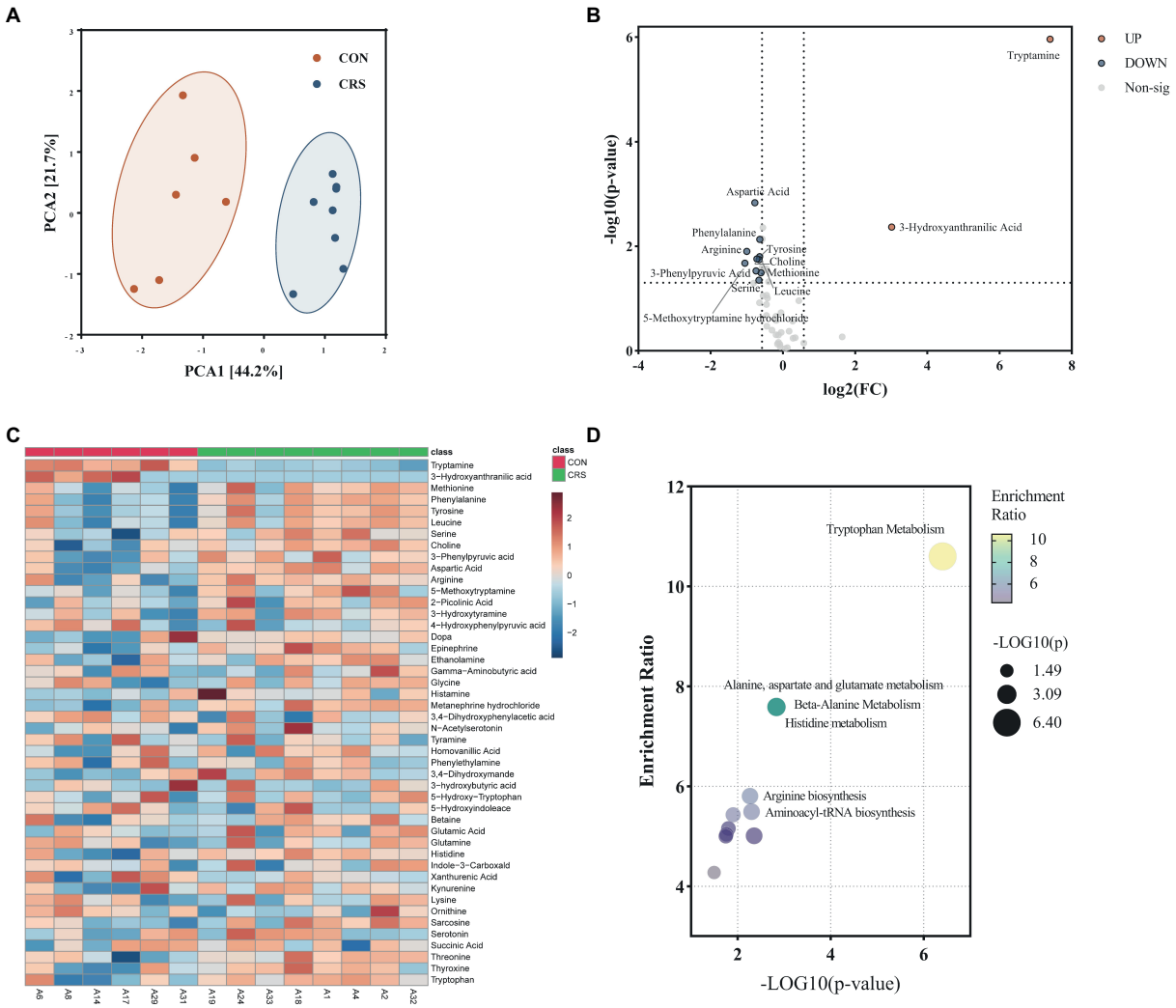

FIGURE 4
Characterization of metabolites profile of neurotransmitters from mice fecal. **(A)** Principal component analysis (PCA) Scores plot between the two groups. The explained variances are shown in brackets. **(B)** Volcano plot for differential metabolites. Significantly regulated metabolites between groups determined by fold change and value of p (FC>|1.5|, p<0.05). Red dots represent increased metabolites in CON group; blue dots represent decreased metabolites in CON group. **(C)** Heatmap of all neurotransmitters; differential metabolites were indicated by an asterisk. **(D)** Pathway enrichment analysis of differential metabolites.

in aminoacyl-tRNA biosynthesis (phenylalanine, arginine, aspartic acid, methionine, leucine, and tyrosine) (Figure 4D). Analyses of neurotransmitter metabolites revealed a divergent profile between the mouse model of depression and controls; tryptophan metabolism and aminoacyl-tRNA biosynthesis might be related to these differences.

Co-occurrence network analysis between the gut virome and neurotransmitter metabolites in CON and CRS groups

A co-occurrence network was performed based on Spearman's rank correlation analysis (|r|>0.6, $p < 0.01$), to explore the association between differential gut virome and neurotransmitter metabolism in mouse models of depression and controls (Figure 5). We discovered that tryptamine, enriched in the tryptophan metabolism pathway, was negatively correlated with three *Podoviridae* viruses. 5-Methoxytryptamine hydrochloride demonstrated a strong positive correlation with 13 *Microviridae* viruses and four *Podoviridae* viruses. A positive correlation was observed between aminoacyl-tRNA biosynthesis pathway metabolites and gut virome. Arginine was positively correlated with two viruses of *Microviridae* and one of *Siphoviridae*, while methionine was positively correlated to one *Siphoviridae* virus. However, two metabolites, phenylalanine and choline showed no significant correlation with the viruses. These results indicate that altered gut virome and neurotransmitter

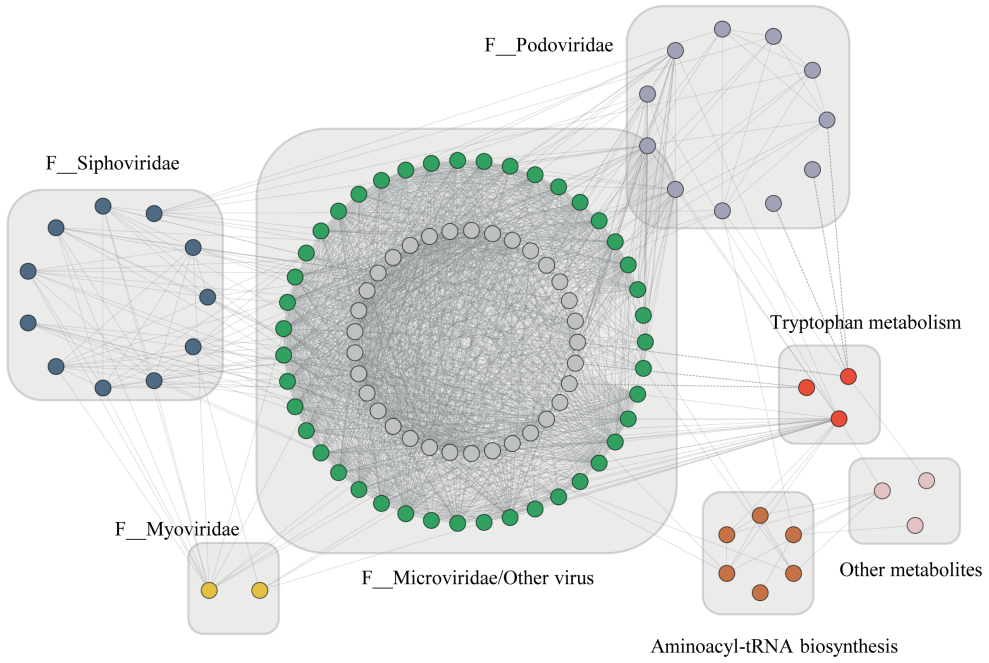

FIGURE 5
Co-occurrence network between the differential virome and metabolites with Spearman's rank correlation coefficient (|r|>0.6, p<0.01). Viruses were shown in blue, green, yellow, purple, and gray dots and metabolites were shown in red, orange, and pink. Solid lines indicate positive correlations, and dashed lines represent negative correlations.

metabolites formed a synergistic and node-related co-occurrence network between CON and CRS groups, in which metabolites enriched in the tryptophan metabolism pathway played a potential role.

Discussion

The microbiome is the microorganisms found in mammalian hosts, including viruses, bacteria, archaea, fungi, and protozoa. Recently, microbiome research has expanded in number and scope. Since the coronavirus disease 2019 (COVID-19) pandemic, researchers' interest in virome has increased tremendously. The gut has been shown to contain a diverse virome. Several studies have summarized the interaction between gut virome and human diseases, such as diabetes mellitus, asthma or pneumonia, and hypertension (Han et al., 2018; Ma et al., 2018; Romero-Espinoza et al., 2018; Cinek et al., 2021). However, it has not been established if the gut virome is involved in neurotransmitter metabolism to mediate the occurrence of depression. We constructed a CRS depression mouse model and investigated the association between gut virome and neurotransmitter metabolites using viral metagenomics and LC–MS/MS methods to provide insights into the role of the gut virome in depression.

In the present study, we found that body weight of mice was reduced after 1 week of CRS. The depressive symptoms, including decreased sucrose preference ratio and increased immobility time in FST and TST, were shown in mice of CRS group. We then combined the α-diversity and β-diversity analyses with species composition to evaluate the diversity and compositional differences of virus communities within the dataset. Analysis of viral α-diversity (Ace, Shannon, Simpson, and Chao1 indices) revealed no significant difference between CRS and CON groups, indicating that the diversity within each fecal sample was relatively stable between the two groups. However, β-diversity analysis based on Bray–Curtis dissimilarity distances showed that CRS group could be distinguished from CON group. The results indicated that CRS could affect the gut virome in mouse models of depression. It contradicted a previous human study that found no significant global alteration of gut virome between major depressive disorder patients and healthy controls (Yang et al., 2020b). This may be attributable to the small sample size of our study or the potential difference between animals and humans.

Moreover, we have described the phylum and family-level virus composition of the two groups. *Phixviricota* was the most abundant phylum in both groups, followed by *Uroviricota*. The top five most abundant families in both groups include *Microviridae*, *Siphoviridae*, *Podoviridae*, *Myoviridae*, and *Phycodnaviridae*. Multiple studies showed that the human gut virome mainly comprises tailed, dsDNA viruses from *Caudovirales* and non-tailed, ssDNA viruses from *Microviridae* (Reyes et al., 2012; Aggarwala et al., 2017; Mirzaei and Maurice, 2017; Shkoporov and Hill, 2019). The most important members of *Caudovirales* include *Myoviridae*, *Podoviridae*, and *Siphoviridae* (Liang and Bushman, 2021), which is consistent with our findings. These results indicate that the major components of the virome in mouse and human

studies are similar. Since mice are not affected by various human-related environmental, dietary, and social factors, they can more accurately reflect changes in the gut virome in response to different situations.

We compared the viral profiles of CON and CRS groups at the contig level to investigate whether a specific virus cluster differed between the two groups. Interestingly, the majority (95%) of the top 100 relative abundant differential virus contigs were enriched in the CRS group. The most enriched differential taxa in the CRS group were *Microviridae*. Some *Microviridae* members have been identified as the prophages of *Bacteroides* and *Parabacteroides* species (Krupovic and Forterre, 2011). Since *Bacteroides* were confirmed to be enriched in the gut microbiome of depressed patients (Yang et al., 2020b), our results suggested that *Microviridae* may be associated with depression by influencing the dysregulation of *Bacteroides*. Moreover, *Microviridae* members exhibit many internal correlations, which may help restore dysregulated community states to healthy homeostasis (Manrique et al., 2017).

Most gut viromes are bacteriophages [32], and their role in gut physiology may be far more important than altering bacterial communities by bacteriophage infection (Miedzybrodzki et al., 2008; Ksendzovsky et al., 2012; Virgin, 2014). Changes in the gut phage community composition may contribute to the relevant transition between health and disease. In our study, the most abundant differential viral taxa between CRS and CON groups were identified, and they all belonged to bacteriophages. Their presumed bacterial hosts were mainly *Enterobacteriaceae*, followed by *Gammaproteobacteria*. Most *Enterobacteriaceae* and *Gammaproteobacteria* phages were enriched in CRS group. A previous study reported an increase in *Enterobacteriaceae* prevalence in patients with the major depressive disorder (Jiang et al., 2015). The *Enterobacteriaceae* family includes several inflammogenic enteric pathogens that could be translocated into the systemic circulation in depressed patients due to the increased permeability of the gut wall (O'Malley et al., 2010). Some gut phages are lytic and can influence the host cell transcription or translation process to produce more phage components before lysing the host cell membrane and releasing the phage particle into the local environment. Most gut phages are lysogenic, implying that they introduce their DNA into the host cell and replicate passively with their host over time without producing virions (Cryan et al., 2019). Research showed that *Enterobacter* phages prevalent in COVID-19 patients may be involved in the host immune response (Zuo et al., 2021). Enrichment of *Enterobacteriaceae* phages in CRS group of our study suggested that this phage might play an important role in depression. However, further research is required to determine whether the phages are lysogenic. If the causal relationship between *Enterobacteriaceae* and depression were clarified by future studies, the enriched *Enterobacteriaceae* phages in mouse models of depression would provide resources and directions for the application of phage therapy.

We then used targeted metabolomics to investigate neurotransmitter differences and the potential relationship between neurotransmitters and gut virome. We discovered 12 metabolites that changed after CRS procedure, most of which were involved in the tryptophan metabolism pathway and the aminoacyl-tRNA biosynthesis pathway. Tryptamine is the indoleamine metabolite of the essential amino acid tryptophan (Jenkins et al., 2016), and multiple studies have revealed that tryptamine can regulate dopaminergic, serotonergic, and glutamatergic systems (Khan and Nawaz, 2016; Berry et al., 2017). Tryptophan in the diet can be converted into tryptamine in the gut by symbiotic bacteria, which further activates 5-HT_4 receptors to regulate gastrointestinal motility (Jenkins et al., 2016; Bhattarai et al., 2018). Furthermore, synthetic modifications of tryptamine can produce serotonin and melatonin. In the current study, we discovered that tryptamine was significantly reduced in CRS group, while 5-methoxytryptamine hydrochloride was increased. Since serotonin is essential for maintaining a normal emotional and psychological state in patients with depression, the decrease in tryptamine indicated a possible serotonin deficiency related to depression-like behaviors in CRS group. Another significant metabolic pathway was aminoacyl-tRNA biosynthesis pathway, which was an important metabolic pathway of protein synthesis. In addition, the aminoacyl-tRNA biosynthesis pathway was also identified in patients with major depressive disorder (Yang et al., 2020a). The depression patients were found to have significant disturbances in amino acid metabolism, such as tryptophan and glutamic acid. The results indicated that the aminoacyl-tRNA biosynthesis pathway might be involved in the development of depression by affecting the synthesis of specific amino acids.

Besides, we studied the association between differential metabolites and gut virome using a co-occurrence network. Metabolites from the tryptophan metabolic pathway showed strong associations with viruses from *Microviridae*. Previous research demonstrated that improvements in the composition and metabolism of gut microbiota could affect peripheral tryptophan availability and central tryptophan levels, resulting in changes in central serotonin metabolism (Gao et al., 2020). Viruses may indirectly affect the pathophysiology of depression by interacting with bacteria, including altering their composition and metabolism. Previous studies have found increased lytic *Lactococcus* phages and decreased *Lactococcus* spp. in patients with Parkinson's disease. The *Lactococcus* spp. is considered capable of producing microbiota-derived neurochemicals (Tetz et al., 2018). Another study reported an indirect link between phages and central nervous system (CNS) disease, revealing that *Lactobacillus phage φadh* was enriched in schizophrenia patients more than in controls, and the primary bacterial host was known to modulate intestinal permeability (Yolken et al., 2015). Therefore, the role of the gut virome in CNS diseases, such as depression, cannot be underestimated, but greater investment and research are required.

It should be mentioned that there are some limitations in this study: (i) Using CRS mouse model cannot fully reproduce the pathophysiology of depressed patients, the assumptions in our study need more experimental data to validate and more supports from clinical data; (ii) The small sample size is also an important

limitation to be addressed in future research; (iii) Alterations in the gut bacteria of mice were not examined in this study. The interaction between gut bacteria and virome is also important to depression, which deserves attention in future studies.

In conclusion, we have demonstrated that CRS can result in gut virome dysregulation. Most of the differential gut virome in the mouse model of depression are *Microviridae*, and the differential metabolites are mainly enriched in the tryptophan metabolic pathway. The results also showed a strong association between the differential gut virome and neurotransmitters. We provide new insights into the role of the virome in depression pathogenesis. Research on gut virome and psychiatric diseases is still preliminary, while gut virome ecology research is primarily in the descriptive stages. In the future, it is more important to go beyond association researches in this field to study the causation of disease further.

Data availability statement

The data presented in the study are deposited in the NCBI repository, accession number PRJNA877780.

Ethics statement

The animal study was reviewed and approved by Animal Care Welfare Committee of the GuiZhou Medical University.

Author contributions

JD, WW, and CL designed the study. JD wrote the manuscript. WW, JD, and XB performed the experiments and analyzed the data. WW, TJ, and CL reviewed the manuscript. All authors contributed to the article and approved the submitted version.

Funding

This work was supported by the Natural Science Foundation Youth Fund Training Program of Affiliated Hospital of Guizhou Medical University (Grant no. gyfynsfc-2021-15).

Conflict of interest

The authors declare that the research was conducted in the absence of any commercial or financial relationships that could be construed as a potential conflict of interest.

Publisher's note

All claims expressed in this article are solely those of the authors and do not necessarily represent those of their affiliated organizations, or those of the publisher, the editors and the reviewers. Any product that may be evaluated in this article, or claim that may be made by its manufacturer, is not guaranteed or endorsed by the publisher.

Supplementary material

The Supplementary material for this article can be found online at: https://www.frontiersin.org/articles/10.3389/fmicb.2022.1046894/full#supplementary-material

References

Aggarwala, V., Liang, G., and Bushman, F. D. (2017). Viral communities of the human gut: metagenomic analysis of composition and dynamics. *Mob. DNA* 8:12. doi: 10.1186/s13100-017-0095-y

Agirman, G., Yu, K. B., and Hsiao, E. Y. (2021). Signaling inflammation across the gut-brain axis. *Science* 374, 1087–1092. doi: 10.1126/science.abi6087

Bai, G. H., Lin, S. C., Hsu, Y. H., and Chen, S. Y. (2022). The human virome: viral metagenomics, relations with human diseases, and therapeutic applications. *Viruses* 14, 278–306. doi: 10.3390/v14020278

Berry, M. D., Gainetdinov, R. R., Hoener, M. C., and Shahid, M. (2017). Pharmacology of human trace amine-associated receptors: therapeutic opportunities and challenges. *Pharmacol. Ther.* 180, 161–180. doi: 10.1016/j.pharmthera.2017.07.002

Bhattarai, Y., Williams, B. B., Battaglioli, E. J., Whitaker, W. R., Till, L., Grover, M., et al. (2018). Gut microbiota-produced tryptamine activates an epithelial g-protein-coupled receptor to increase colonic secretion. *Cell Host Microbe* 23, 775.e5–785.e5. doi: 10.1016/j.chom.2018.05.004

Bolger, A. M., Lohse, M., and Usadel, B. (2014). Trimmomatic: a flexible trimmer for illumina sequence data. *Bioinformatics* 30, 2114–2120. doi: 10.1093/bioinformatics/btu170

Calliope Holingue, M. P. H. (2018). Mental disorders around the world: facts and figures from the who world mental health surveys. *Am. J. Psychiat.* 175, 911–912. doi: 10.1176/appi.ajp.2018.18050506

Cantalupo, P. G., and Pipas, J. M. (2019). Detecting viral sequences in ngs data. *Curr. Opin. Virol.* 39, 41–48. doi: 10.1016/j.coviro.2019.07.010

Cinek, O., Kramna, L., Odeh, R., Alassaf, A., Ibekwe, M., Ahmadov, G., et al. (2021). Eukaryotic viruses in the fecal virome at the onset of type 1 diabetes: a study from four geographically distant African and Asian countries. *Pediatr. Diabetes* 22, 558–566. doi: 10.1111/pedi.13207

Cryan, J. F., O'Riordan, K. J., Cowan, C., Sandhu, K. V., Bastiaanssen, T., Boehme, M., et al. (2019). The microbiota-gut-brain axis. *Physiol. Rev.* 99, 1877–2013. doi: 10.1152/physrev.00018.2018

Dalile, B., Van Oudenhove, L., Vervliet, B., and Verbeke, K. (2019). The role of short-chain fatty acids in microbiota-gut-brain communication. *Nat. Rev. Gastroenterol. Hepatol.* 16, 461–478. doi: 10.1038/s41575-019-0157-3

Duan, Y., Llorente, C., Lang, S., Brandl, K., Chu, H., Jiang, L., et al. (2019). Bacteriophage targeting of gut bacterium attenuates alcoholic liver disease. *Nature* 575, 505–511. doi: 10.1038/s41586-019-1742-x

Gao, K., Mu, C. L., Farzi, A., and Zhu, W. Y. (2020). Tryptophan metabolism: a link between the gut microbiota and brain. *Adv. Nutr.* 11, 709–723. doi: 10.1093/advances/nmz127

Gold, S. M., Köhler-Forsberg, O., Moss-Morris, R., Mehnert, A., Miranda, J. J., Bullinger, M., et al. (2020). Comorbid depression in medical diseases. *Nat. Rev. Dis. Primers.* 6:69. doi: 10.1038/s41572-020-0200-2

Han, M., Yang, P., Zhong, C., and Ning, K. (2018). The human gut virome in hypertension. *Front. Microbiol.* 9:3150. doi: 10.3389/fmicb.2018.03150

Jenkins, T. A., Nguyen, J. C., Polglaze, K. E., and Bertrand, P. P. (2016). Influence of tryptophan and serotonin on mood and cognition with a possible role of the gut-brain axis. *Nutrients* 8, 56–70. doi: 10.3390/nu8010056

Jiang, H., Ling, Z., Zhang, Y., Mao, H., Ma, Z., Yin, Y., et al. (2015). Altered fecal microbiota composition in patients with major depressive disorder. *Brain Behav. Immun.* 48, 186–194. doi: 10.1016/j.bbi.2015.03.016

Khan, M. Z., and Nawaz, W. (2016). The emerging roles of human trace amines and human trace amine-associated receptors (htaars) in central nervous system. *Biomed. Pharmacother.* 83, 439–449. doi: 10.1016/j.biopha.2016.07.002

Krupovic, M., and Forterre, P. (2011). Microviridae goes temperate: microvirus-related proviruses reside in the genomes of bacteroidetes. *PLoS One* 6:e19893. doi: 10.1371/journal.pone.0019893

Ksendzovsky, A., Walbridge, S., Saunders, R. C., Asthagiri, A. R., Heiss, J. D., and Lonser, R. R. (2012). Convection-enhanced delivery of m13 bacteriophage to the brain. *J. Neurosurg.* 117, 197–203. doi: 10.3171/2012.4.JNS111528

Li, H., and Durbin, R. (2009). Fast and accurate short read alignment with burrows-wheeler transform. *Bioinformatics* 25, 1754–1760. doi: 10.1093/bioinformatics/btp324

Li, D., Luo, R., Liu, C. M., Leung, C. M., Ting, H. F., Sadakane, K., et al. (2016). Megahit v1.0: a fast and scalable metagenome assembler driven by advanced methodologies and community practices. *Methods* 102, 3–11. doi: 10.1016/j.ymeth.2016.02.020

Liang, G., and Bushman, F. D. (2021). The human virome: assembly, composition and host interactions. *Nat. Rev. Microbiol.* 19, 514–527. doi: 10.1038/s41579-021-00536-5

Ma, Y., You, X., Mai, G., Tokuyasu, T., and Liu, C. (2018). A human gut phage catalog correlates the gut phageome with type 2 diabetes. *Microbiome.* 6:24. doi: 10.1186/s40168-018-0410-y

Manrique, P., Dills, M., and Young, M. J. (2017). The human gut phage community and its implications for health and disease. *Viruses* 9, 141–159. doi: 10.3390/v9060141

Mendoza, J. (2019). Circadian insights into the biology of depression: symptoms, treatments and animal models. *Behav. Brain Res.* 376:112186. doi: 10.1016/j.bbr.2019.112186

Miedzybrodzki, R., Switala-Jelen, K., Fortuna, W., Weber-Dabrowska, B., Przerwa, A., Lusiak-Szelachowska, M., et al. (2008). Bacteriophage preparation inhibition of reactive oxygen species generation by endotoxin-stimulated polymorphonuclear leukocytes. *Virus Res.* 131, 233–242. doi: 10.1016/j.virusres.2007.09.013

Mirzaei, M. K., and Maurice, C. F. (2017). Ménage à trois in the human gut: interactions between host, bacteria and phages. *Nat. Rev. Microbiol.* 15, 397–408. doi: 10.1038/nrmicro.2017.30

Moffitt, T. E., Caspi, A., Taylor, A., Kokaua, J., Milne, B. J., Polanczyk, G., et al. (2010). How common are common mental disorders? Evidence that lifetime prevalence rates are doubled by prospective versus retrospective ascertainment. *Psychol. Med.* 40, 899–909. doi: 10.1017/S0033291709991036

Nayfach, S., Camargo, A. P., Schulz, F., Eloe-Fadrosh, E., Roux, S., and Kyrpides, N. C. (2021). Checkv assesses the quality and completeness of metagenome-assembled viral genomes. *Nat. Biotechnol.* 39, 578–585. doi: 10.1038/s41587-020-00774-7

Nooij, S., Schmitz, D., Vennema, H., Kroneman, A., and Koopmans, M. (2018). Overview of virus metagenomic classification methods and their biological applications. *Front. Microbiol.* 9:749. doi: 10.3389/fmicb.2018.00749

O'Malley, D., Julio-Pieper, M., Gibney, S. M., Dinan, T. G., and Cryan, J. F. (2010). Distinct alterations in colonic morphology and physiology in two rat models of enhanced stress-induced anxiety and depression-like behaviour. *Stress* 13, 114–122. doi: 10.3109/10253890903067418

Peng, G. J., Tian, J. S., Gao, X. X., Zhou, Y. Z., and Qin, X. M. (2015). Research on the pathological mechanism and drug treatment mechanism of depression. *Curr. Neuropharmacol.* 13, 514–523. doi: 10.2174/1570159x1304150831120428

Reyes, A., Semenkovich, N. P., Whiteson, K., Rohwer, F., and Gordon, J. I. (2012). Going viral: next-generation sequencing applied to phage populations in the human gut. *Nat. Rev. Microbiol.* 10, 607–617. doi: 10.1038/nrmicro2853

Romero-Espinoza, J. A., Moreno-Valencia, Y., Coronel-Tellez, R. H., Castillejos-Lopez, M., Hernandez, A., Dominguez, A., et al. (2018). Virome and bacteriome characterization of children with pneumonia and asthma in Mexico City during winter seasons 2014 and 2015. *PLoS One* 13:e192878. doi: 10.1371/journal.pone.0192878

Rose, R., Constantinides, B., Tapinos, A., Robertson, D. L., and Prosperi, M. (2016). Challenges in the analysis of viral metagenomes. *Virus Evol.* 2:w22. doi: 10.1093/ve/vew022

Santiago-Rodriguez, T. M., and Hollister, E. B. (2020). Potential applications of human viral metagenomics and reference materials: considerations for current and future viruses. *Appl. Environ. Microbiol.* 86: e01794–20. 1-12. doi: 10.1128/AEM.01794-20

Shkoporov, A. N., and Hill, C. (2019). Bacteriophages of the human gut: the "known unknown," of the microbiome. *Cell Host Microbe* 25, 195–209. doi: 10.1016/j.chom.2019.01.017

Tetz, G., Brown, S. M., Hao, Y., and Tetz, V. (2018). Parkinson's disease and bacteriophages as its overlooked contributors. *Sci. Rep.* 8:10812. doi: 10.1038/s41598-018-29173-4

Valles-Colomer, M., Falony, G., Darzi, Y., Tigchelaar, E. F., Wang, J., Tito, R. Y., et al. (2019). The neuroactive potential of the human gut microbiota in quality of life and depression. *Nat. Microbiol.* 4, 623–632. doi: 10.1038/s41564-018-0337-x

Virgin, H. W. (2014). The virome in mammalian physiology and disease. *Cells* 157, 142–150. doi: 10.1016/j.cell.2014.02.032

Yadav, H., Jain, S., Nagpal, R., and Marotta, F. (2016). Increased fecal viral content associated with obesity in mice. *World J. Diabetes* 7, 316–320. doi: 10.4239/wjd.v7.i15.316

Yang, J., Yan, B., Zhao, B., Fan, Y., He, X., Yang, L., et al. (2020a). Assessing the causal effects of human serum metabolites on 5 major psychiatric disorders. *Schizophr. Bull.* 46, 804–813. doi: 10.1093/schbul/sbz138

Yang, J., Zheng, P., Li, Y., Wu, J., Tan, X., Zhou, J., et al. (2020b). Landscapes of bacterial and metabolic signatures and their interaction in major depressive disorders. *Sci. Adv.* 6: eaba8555. 1-11. doi: 10.1126/sciadv.aba8555

Yolken, R. H., Severance, E. G., Sabunciyan, S., Gressitt, K. L., Chen, O., Stallings, C., et al. (2015). Metagenomic sequencing indicates that the oropharyngeal phageome of individuals with schizophrenia differs from that of controls. *Schizophr. Bull.* 41, 1153–1161. doi: 10.1093/schbul/sbu197

Zhang, Y., Huang, R., Cheng, M., Wang, L., Chao, J., Li, J., et al. (2019). Gut microbiota from nlrp 3-deficient mice ameliorates depressive-like behaviors by regulating astrocyte dysfunction via circhipk 2. *Microbiome* 7:116. doi: 10.1186/s40168-019-0733-3

Zheng, P., Wu, J., Zhang, H., Perry, S. W., Yin, B., Tan, X., et al. (2021). The gut microbiome modulates gut-brain axis glycerophospholipid metabolism in a region-specific manner in a nonhuman primate model of depression. *Mol. Psychiatry* 26, 2380–2392. doi: 10.1038/s41380-020-0744-2

Zheng, P., Zeng, B., Zhou, C., Liu, M., Fang, Z., Xu, X., et al. (2016). Gut microbiome remodeling induces depressive-like behaviors through a pathway mediated by the host's metabolism. *Mol. Psychiatry* 21, 786–796. doi: 10.1038/mp.2016.44

Zuo, T., Liu, Q., Zhang, F., Yeoh, Y. K., Wan, Y., Zhan, H., et al. (2021). Temporal landscape of human gut rna and dna virome in SARS-cov-2 infection and severity. *Microbiome* 9:91. doi: 10.1186/s40168-021-01008-x

Frontiers in Microbiology

Explores the habitable world and the potential of microbial life

The largest and most cited microbiology journal which advances our understanding of the role microbes play in addressing global challenges such as healthcare, food security, and climate change.

Discover the latest Research Topics

See more →

Frontiers

Avenue du Tribunal-Fédéral 34
1005 Lausanne, Switzerland
frontiersin.org

Contact us

+41 (0)21 510 17 00
frontiersin.org/about/contact